Surface Acoustic Waves Nebulisation for Pulmonary Drug Delivery

Xi King

Submitted in fulfilment of the requirements for the
Degree of Doctor of Philosophy

School of Engineering
College of Science and Engineering
University of Glasgow

June 2019

Abstract

Surface Acoustic Waves (SAWs) devices for droplets manipulation have become widespread in the last twenty years for their ability to work at the microscale, focusing their energy on small targets. SAWs, combined with vesicles-based drug carrier systems such as liposomes, offer the opportunity of efficient drug delivery to the lungs. Liposomes are important drug delivery systems due to their structure, able to retain either a hydrophilic drug within their aqueous core, behind a phospholipid barrier, or a hydrophobic drug associated with the membrane's hydrophobic core. They are capable of releasing the drugs in a controlled manner in conjunction with pH or temperature changes, which is a fundamental feature for the treatment of many diseases such as cancer. SAW devices are ideal platforms for liquid manipulation at the micro-scale, due to their low fabrication cost and low power consumption. The main advantage as a nebuliser, for pulmonary drug delivery, lies with their ability to provide control of the aerosolized droplet size. Another advantage, compared to a commercially available nebuliser, is given by the high frequencies (>1MHz) employed during the nebulisation, which avoids denaturation of the delivered molecules by cavitation. The aim of this PhD is the development of a SAW nebulisation device, capable of delivering drug-loaded liposomes in a targeted manner to the deep lung tissues. The creation of a novel SAW nebulisation platform, where liposomes can be formed *in-situ* and drugs (or complex molecules) can be loaded in one single step, will avoid drugs side effects and wastage of expensive drugs.

The project can be divided into three main objectives. The first objective was the design of the SAW platform, studying the SAW interaction with pre-formed liposomes, the effects of the SAW on temperature sensitive-enzyme and the stability of liposomes after the SAW nebulisation. Once the feasibility of using SAW as a method to deliver drugs encapsulated in liposomes, the second objective was focused toward the control of the aerosols size and the liposomes' formation *in-situ* on the same platform. The aerosols size is a key parameter to deliver efficiently drugs and biologics into the lungs and the liposomes are also key to protect the compound from early degradation and guide it in a specific target. After the optimised parameter were controlled, the final objective was to test the platform *in-vitro* on lungs cancer cells, delivering nucleic acids as DNA luciferase plasmid and GAPDH siRNA and showing high transfection performance. I have demonstrated

that this platform has the potential to be an efficient drug delivery system in terms of drug stability, delivering biologics and optimum absorption of the drug in the lungs.

Contents

List of Figures

Thesis Outline

This thesis is divided into seven chapters and a brief description is given.

Chapter 1 is an overview of different drug delivery system, with main attention to the pulmonary route, exploring the use of liposome in drug delivery in the lungs. A literature review on existing inhalers and nebulisers, including SAW-based previous work, highlighting advantages and disadvantages will also be presented in Chapter 1.

Chapter 2 will describe the general material and methods common to each chapter. In particular, Interdigitated Transducer (IDT) microfabrication process is also described. A description of particle size distribution methods is given with particular interest to dynamic light scattering and laser diffraction, which are the most used in this work.

Chapter 3 will be based on testing liposomes to be nebulised with SAW, using enzymatic colorimetric assay (e.g. horseradish peroxide), as an indirect method to test liposomes'stability, and dynamic light scattering for the vesicles size distribution.

Chapter 4 will present a study on unilamellar vesicles formation and on the control of the aerosols size. Using a microfabricated silicon structure, the formation of LUVs was obtained using the SAW. SAW-formed liposomes were characterised using dynamic light scattering, laser diffraction and transmission electron microscopy. A mechanism for the formation of liposomes *in-situ* is proposed.

Chapter 5 will discuss the analysis the lung deposition of SAW nebulised particle, measuring fluorescence intensity and conductivity of the nebulised solution using the Andersen Cascade Impactor to evaluate size distribution. Comparison with the commercial nebuliser Omron MicroAIR U22 was made to check the SAW nebuliser efficiency.

The final experimental chapter, Chapter 6 (carried out at the University of Hong Kong) will be focused on the *in-vitro* study of nucleic acids transfection to lungs cancer cells. DNA luciferase plasmid and GAPDH siRNA were delivered using the SAW platform and SAW formed liposomes complex. Cell transfection was carried out on A549 lung epithelium cell line, comparing SAW transfection method to the standard one.

Finally, Chapter 7 will show future works, including a design of mouse inhalation chamber towards the *in-vivo* testing of SAW nebulisation platform, in a small animal model.

Publications and Conferences

Journal Papers

1. E. Nazarzadeh, R. Wilson, X. King, J. Reboud, M. Tassieri and J.M. Cooper, " Confinement of surface waves at the air-water interface to control aerosol size and dispersity", Physics of Fluids 29, 112105 (2017)

International Conferences

1. X. King, E. Nazarzadeh, R. Wilson, D. Paterson, J. Reboud and J.M. Cooper, " Feasibility of SAW Nebulisation of Liposomes", ICBEB 2017, International Conference on Biomedical Engineering and Biotechnology, Canton, China

2. X. King, E. Nazarzadeh, R. Wilson, D. Paterson, M. Tassieri, J. Reboud and J.M. Cooper, "Surface Acoustic Waves Nebulisation of Liposomes Manufactured *in-situ* for Pulmonary Drug Delivery", ICAA 2018, International Conference on Acoustics and Applications, Copenhagen, Denmark

3. X. King, E. Nazarzadeh, J. Reboud, Y. Qiu, J. Lam and J.M. Cooper, "Surface Acoustic Waves Nebulisation platform for Gene Therapy", MEDDS 2018, Modelling and Experiments in Drug Delivery System, Glasgow, UK

Acknowledgements

First of all, I would like to thank my supervisor, Prof. Jonathan Cooper, for giving me the opportunity of pursuing my PhD in his amazing research group, for providing funding and facilities, but most of all for his guidance, support and wisdom, which were helpful and inspirational.

I would also like to express my gratitude to Dr. Julien Reboud, my second supervisor, which has been always supportive and helpful, whenever I encountered difficulties throughout my PhD. I would like to thank him for his patience and all the constructive discussions we had.

I am also really thankful to Dr Manlio Tassieri, Dr. Rab Wilson and Dr. Andrew Glidle for their help during the past 4 years. I would like to thank the postdocs in the group who helped me a lot: Dr. David Paterson, Dr. Andrejus Demechenko and Dr. Eloise Larson. A particular thanks goes to Dr. Elijah Nazarzadeh, who worked with me during nebulisation experiments. In all cases, when appropriate, work presented in this thesis is referred to our joint publication. Thanks also to Ms. Margaret Mullins for her help with the TEM and Dr. David Bhella for his expertise in cryo-TEM. A big thank you also to the whole research group and my friends, for making weekends spent in the lab less painful, for the lunch and coffee breaks and their support: Alice, Laura, Joe, Arslan, Jono and Han. Level 5 office mates: Chris and Pawel. I would also like to thank my Italian friends in Glasgow: my first flatmates and best neighbours Marco and Fede, Giulia, my lab soul mate, the last of the Glaswegians (Emanuele and Iacopo), Eugenio, Manuel, Riccardo with whom I shared so many coffee and Kevin, thanks for your support and your understanding. A big thank you to Francesca, Marta and Emmi, for all the nice time spent together. I am grateful to Glasgow Mobility Scholarship 2017 and the Royal Society of Edinburgh, JM Lessells Scholarship 2017, for giving me the opportunity to carry out part of my PhD at the University of Hong Kong. Special thanks to Dr. Lam for her support, expertise and guidance during the three months, spent in Hong Kong and her group. I would like to thank my friends in Rome and l'orrore, friends of a lifetime, thanks for being supportive even from far away. The biggest thank you goes to my family, my mum and dad for their unconditional love and their sacrifices to help me in following my dreams and my brother, who has always been present for me.

Declaration

With the exception of chapters 1 and 2 which contain introductory material, all work in this thesis was carried out by the author unless otherwise explicitly stated.

'I declare that, except where explicit reference is made to the contribution of others, this thesis is the result of my own work and has not been submitted for any other degree at the University of Glasgow or any other institution '

Xi King

List of abbreviations

A	Absorbance
ACI	Andersen Cascade Impactor
BPF	Bilayer Phospholipid Fragment
COPD	Chronic Obstructive Pulmonary Disease
DI	Deionised
DLS	Dynamic Light Scattering
DMEM	Dulbecco's Modified Eagle Medium
DNA	Deoxyribonucleic Acid
DOPC	1,2-Dioleoyl-SN-glycero-3-phosphocholine
DOPE	1,2-Dioleoyl-SN-glycero-3-phosphoethanolamine
DOTAP	N-[1-(2,3 Dioleoyloxy)propyl]-N,N,N-trimethylammonium chloride
DOTMA	N-[1-(2,3-silyloxy)propyl]-N,N,N-trimethylammonium chloride
DOX	Doxorubicin
DPI	Dry Powder Inhaler
dsRNA	double-stranded RNA
DUT	Device Under Test
EDTA	Ethylenediaminetetraacetic acid
GUV	Giant Unilamellar Vesicle
HPLC	High Performance Liquid Chromatography
HRP	Horseradish Peroxidase
HS-DNA	Herring Sperm DNA
IDT	Interdigitated Transducer
LPF	Lipofectamine 2000
LSPC	Lysophosphatidylcholine

LUV	Large Unilamellar Vesicle
MDI	Metered-Dose Inhaler
MLV	Multilamellar Vesicle
mRNA	Messenger RNA
MSLI	Multi Stage Liquid Impinger
MW	Molecular Weight
MWCO	Molecular Weight Cut Off
NGI	Next Generation Impactor
OD	Optical Depth
Opti-MEM	Reduced Serum Medium
PBS	Phosphate Buffered Saline
PCR	Polymerase Chain Reaction
PDI	Polydispersity Index
pDNA	Plasmid DNA
RhB	Rhodamine B
RISC	RNA-Induced Silencing Complex
RLU	Relative Light Unit
RNA	Ribonucleic Acid
RNAi	RNA interference
RO	Reverse Osmosis
SAW	Surface Acoustic Wave
SD	Standard Deviation
SDS	Sodium dodecyl sulfate
siRNA	Small Interference RNA
SOP	Standard of Procedure
STD	Standard
SUV	Small Unilamellar Vesicle
TEM	Transmission Electron Microscopy
TMB	Tetramethylbenzidine
WHO	World Health Organisation

Chapter 1

Introduction

1.1 Motivation of Study

The most common respiratory diseases are asthma, chronic obstructive pulmonary disease (COPD), cystic fibrosis and pulmonary hypertension [1]. According to the World Health Organisation (WHO), 235 million people suffer from asthma and more than 3 million people die per year from COPDs, which is an estimated 6% of all deaths worldwide [1]. Pulmonary diseases are typically treated by the inhalation of aerosols [2]. Aerosol delivery introduces drug directly into the lungs, reducing off-target (e.g. toxicity) effects associated with systemic delivery of drugs in the blood [3]. Effective respiratory drug delivery requires a droplet size distribution between 1 and 5 µm, due to the characteristic lung structure made of multiple diameters' airways [4]. Most of the available nebulisers produce aerosols with a wide range of droplet size distribution, limiting their efficiency for high-value drugs [5]. An effective nebuliser delivers the drug in a targeted way, with minimum wastage and at a low-cost [6]. Reported studies from the usage of current nebulisers on the market resulted in a large amount of drug wastage (50% loss) and only 10% of the dose placed in the nebuliser was deposited in lungs [6]. It was shown that 2/3 of the dose placed in the nebulised chamber remain there at the end of nebulisation. This quantity is acceptable for the delivery of bronchodilators, for which only a small dose is necessary to achieve adequate results. However, for the delivery of expensive drugs, it is important that the quantity delivered reaches the target [7]. Jet and ultrasonic nebulisers, for instance, are bulky, relatively expensive with poor delivery efficiency and non-portable [8]. Mesh nebulisers showed improvements compared to the jet and ultrasonic nebulisers [9], such as higher production of particles in the respirable range and portability, but showed also difficulties in the nebulisation of viscous solutions, resulting in a clogged mesh requiring a long cleaning procedure. This is caused mainly to the size of the pores on the mesh, which are around 1-5 µm. Over the last two decades, several groups worked on surface acoustic waves (SAW) nebulisation [10], [11], [12], creating a novel nebuliser, with high

potential. Using SAWs different compounds were successfully delivered, but none of those studies showed a specific control of the nebulised particle size.

1.2 Aim and Objectives

Surface acoustic waves are increasingly used in biomedical engineering applications, such as cell sorting [13], real-time PCR [14], biosensing [15] and nebulisers [10], [16], [17]. The main advantage of using SAW is their portability, as we can create a miniaturised device, which can facilitate for example the analysis of compounds and have a lab-on-a-chip concept [18]. SAWs are also able to manipulate small volumes, which is a great advantage especially when working with blood samples, they required small amount of power, 1-5 W are enough to nebulise and deliver drugs [19]. In particular, regarding SAW nebulisation, specific control of the size of the aerosol has not been shown yet, previous studies reported only the final particle size distribution [16], [11], [20]. The aim of this research is to create a low cost, portable and user-friendly pulmonary drug delivery platform using SAW [21], [10], [22], which can deliver the drug in an efficient way, avoiding wastage and side effects.

Firstly, the aim of this research is to test the feasibility of SAW to deliver intact liposomes and retain the size and structure of the vesicles. The liposomes can help the delivery of a biological compound to cross the cell membrane and at the same time protect it from degradation.

The second objective was to create a functional drug delivery system and integrate into the same platform, both the control of the aerosols size and the formation of liposomes *in-situ*, two fundamental characteristics for an efficient pulmonary drug delivery system. A novel approach was used, which has the advantage of combining time-consuming steps.

The third objective was to give a proof of concept of the SAW platform's capability to deliver nucleic acids *in-vitro* in lung cancer cells. Cell transfection using directly the SAW platform was performed.

1.3 Drug Delivery Systems

For millennia, drugs have been used to improve health and extend life expectancy [23]. Drug delivery systems are engineered technologies capable of targeted delivery and controlled release of therapeutic agents. The drug has to be precisely released in a specific area, improving the effectiveness of the active agent and reducing the toxicity of a therapy [24]. Many drugs possess negative aspects, termed side effects, which mainly occur when non-targeted cells are exposed to a given drug. There are different anatomical routes by which medical drugs can be delivered into the human body. The choice of the path depends on various factors, such as the desired effect and/or the kind of disease. The most

common routes of drug administration are [25]:

- Oral route. This is the most commonly employed route, used for conventional drug delivery, due to the simplicity and the lowest cost of administration. However, the main drawback associated with it is the reduction of the drugs' bioavailability, during the exposure of the given drug to the digestion enzymes in the gastrointestinal system.

- Parenteral route. This route includes intramuscular, intravenous, intra-arterial and subcutaneous injection. It can be used for drugs that are poorly absorbed or ineffective when given orally. Associated drawbacks are potential pain or discomfort of the patient.

- Transdermal route. The medical treatment is applied to the skin. This route of administration transferred directly a given drug to the systematic circulation bypassing the gastrointestinal and the liver metabolism. However, the transdermal route could be unsuitable for drugs that irritate the skin and the drug entry is limited by the skin's permeability.

- Inhalation route. In this type of medical treatment application route, the drug will directly reach the lungs. This route is considered the first choice in respiratory disease treatment because it avoids the systemic effect and it increases the bioavailability of the drug. The lungs have also a large epithelial surface area of 70 m^2 and they are highly permeable to gas. However, the size of the inhaled droplet must be controlled.

1.4 Pulmonary Drug Delivery and Lungs Structure

Among all the drug administration routes, the inhalation one can be employed, not only for respiratory diseases but also as an alternative route for the systemic administration of the drug. As a matter of fact, lungs offer large absorption area which is around 70 m^2 and low enzymatic activities. Studies have shown the advantage of this route over others, for the delivery of biological products, such as insulin [26].

As previously mentioned, there are many advantages associated with the inhalation route. Furthermore, the direct delivery of drugs to the lungs requires lower overall quantities of the therapeutic agent and consequently brings fewer side effects [29]. It is considered to be a less invasive delivery system, compared to the parenteral route. Moreover, many macromolecules cannot be administered orally, as oral delivery exposes drugs to the digestion system: extreme pH conditions (pH 3) and potential enzymes degradation [30]. The pulmonary route bypasses the gastrointestinal tract and the patient metabolic differences that affect gastrointestinal absorption, showing higher suitability in delivering therapeutic

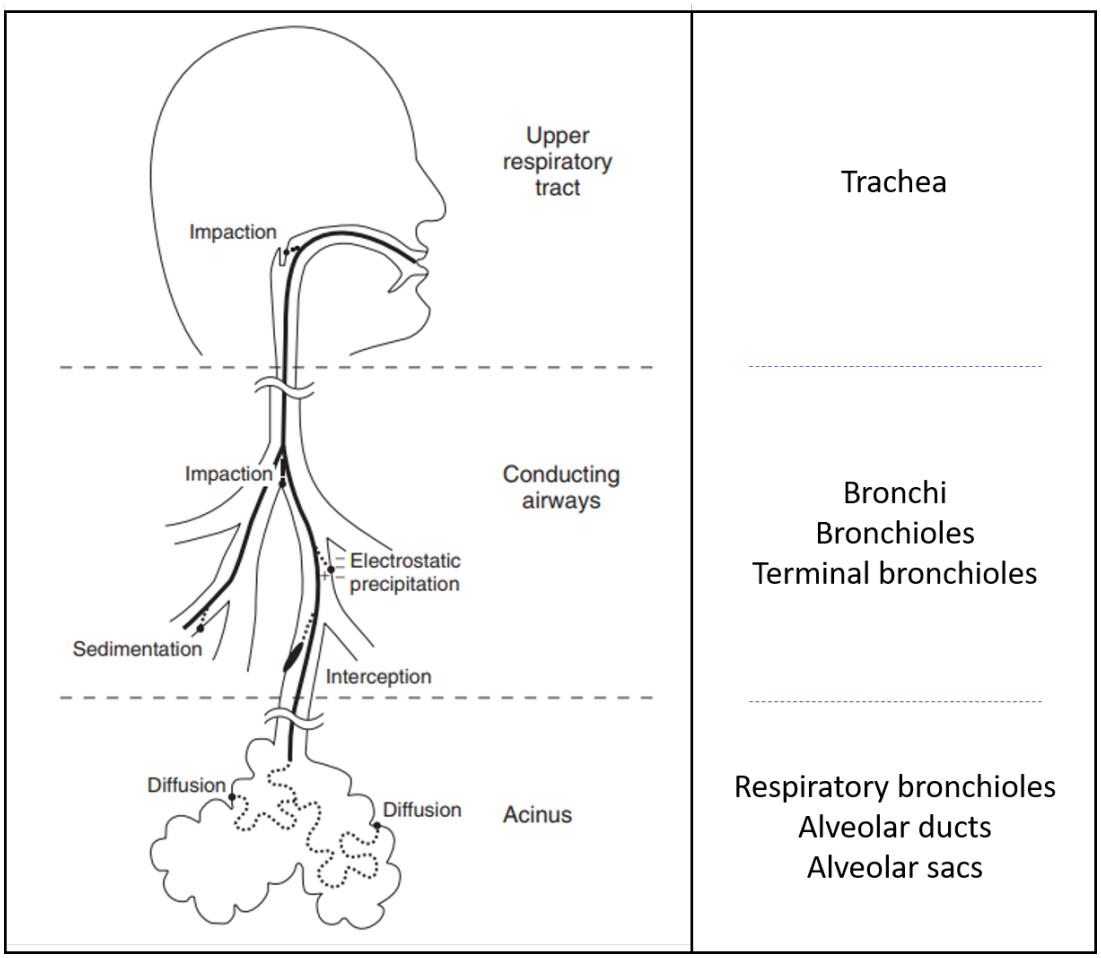

Figure 1.1: Image representing the respiratory tract. Air enters through the mouth or the nose and then arrives in the pharynx and trachea, which divides into two bronchi. In this part of the respiratory tract, inertial impaction is the main deposition mechanism. The two bronchi then divide into several branches, starting the bronchial tree, where different deposition mechanism can be found: impaction, sedimentation, interception and electrostatic precipitation. The final end of the respiratory tract is made of alveolar ducts and sacs, where small particles are characterised by the Brownian diffusion, which is the random motion of small particles suspended in a fluid/gas caused by the collision with fast-speed molecules in the fluid/gas [27]. Figure from [28].

macromolecules [8], [31]. In order to understand the importance of the size of the aerosol in pulmonary drug delivery, the lung structure has to be described. The respiratory tract can be divided anatomically into upper airways, which include the nose, paranasal sinuses, pharynx and lower airways, which include bronchi, bronchioles, alveolar ducts and sacs, and alveoli. It is also divided into conducting and respiratory zone, based on the function of transporting or exchanging gas. As shown in Fig. 1.1, the conducting zone starts with the air enters the respiratory tract through the nose or the mouth. When air passes across the nose, it is humidified and warmed before getting to the pharynx, which is part of both the digestive and respiratory tract. Here, food is channelled to the stomach by the oesoph-

agus, while air goes to the lungs from the trachea [32]. The trachea is divided into two branches called bronchi, starting the bronchial tree. Each time the bronchial tree divides, it forms a new generation. There are 23 generations of airways and the gas exchange is carried out only in the last eight generations [32], which are part of the respiratory zone. Gas exchange is a physical phenomenon, where gases move by diffusion across a surface. In particular, the oxygen in the alveoli passes quickly into the blood in the pulmonary capillaries, similarly, the carbon dioxide moves from the blood into the alveoli and then exhaled. Due to the lung structure, at each division the number of generations and the total cross-sectional area increase, while the diameter of the generations decreases (Fig. 1.1). Therefore, the absorption of the particles within the different respiratory zones depends on the droplet size [3]. The aerosol size affects also the way particles are deposited within the lungs. They can be deposited by inertial impaction, gravitational sedimentation, Brownian diffusion and in some cases, electrostatic precipitation and interception [27].

In the first ten generations of the lungs, from the trachea to the terminal bronchioles, the air velocity is high and the airflow is turbulent. Therefore, it is the area where inertial impaction occurs. [33]. The impaction on airways wall is a consequence of the changing airflow direction and the particle momentum. Gravitational sedimentation predominates in smaller bronchi and bronchioles, in the last five to six airways generation, where the air velocity is low. It occurs when gravitational force equals the opposing resistive force of the air and the particle reaches the settling velocity [27]. Diffusion is predominant in the alveolar region, where the air velocity is negligible, so the movement of a substance will follow its gradient concentration [33]. It results from the random particle motions caused by the collision with gas molecules. Electrostatic precipitation refers to the attraction of charged particles to the airway walls. It contributes to less than 10% of the overall deposition. An interception occurs when elongated particles have one of their ends touching the airway. It is common when the particle size is comparable to the size of the airway [27].

1.5 Carrier Mediated Drug Delivery System

1.5.1 Liposomes: Classification and Formation

Once the delivery route is chosen, it is important to have a drug carrier to guide the compound to a specific target. In order to successfully deliver the drug into the lungs, have better control on the release and protect it from degradation before reaching the target, biological carriers, such as liposomes are often used in drug delivery system. A liposome is a small structure (nm - µm) made up of an aqueous core confined by a lipid bilayer membrane. It can be formed naturally for example during the cellular secretion process

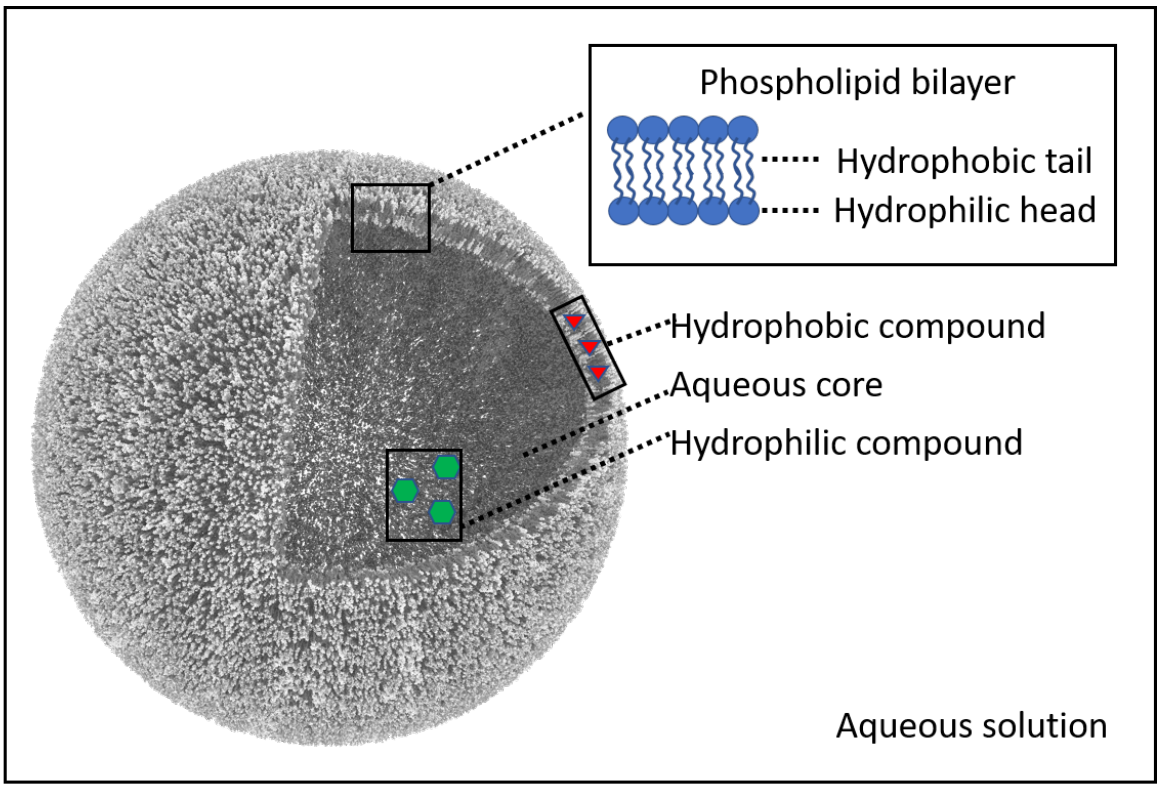

Figure 1.2: Liposome structure, which entraps an aqueous core behind a clearly demarcated phospholipid bilayer structure. Due to the phospholipid structure made of a hydrophilic polar head and a hydrophobic tail, different compounds can be encapsulated. Figure adapted from [34]

(exocytosis) or artificially, creating liposomes. Liposomes consist of an aqueous solution of vesicles, which entrap an aqueous core behind a clearly demarcated phospholipid bilayer structure (Fig. 1.2). They can contain one or more phospholipids bilayers, which are known as lamellae [35]. Liposomes with one bilayer are called unilamellar, while liposomes with multiple layers are called multilamellar [36]. They are largely exploited in drug delivery since they can reach a small size (nanometer scale) and can be used to deliver a different type of drugs. As shown in Fig. 1.2, hydrophilic compounds (green) can be loaded in the aqueous core and hydrophobic drugs (red) are associated with the membrane. In 1961, liposomes were first described and studied by Bangham [37], [38], [39], who noticed that they form spontaneously when phospholipids are dispersed in an aqueous medium.

Bilayer Properties of Liposomes

The bilayer properties of a liposome are due to phospholipids. Phospholipids are amphipathic molecules, containing both a polar head group and a non-polar portion made of two fatty acid chains [40], [41]. In aqueous medium, they align themselves closely to minimise the interaction between the bulk aqueous phase and the long hydrocarbon fatty acid chains, giving rise to characteristic supramolecular arrangements [42]. The tightness

of the phospholipids packing can be modified based on different factors [36], such as increasing the hydrocarbon chain length of the phospholipids or adding cholesterol, results in a tighter film packing. Looser film packing is obtained by increasing the degree of unsaturation of the hydrocarbon chain or increasing the temperature of the system.

Effect of Temperature on Phospholipid Bilayer

Different parameters can modify the structure of the bilayer. A specific temperature, the transition temperature (T_m), has a key role in the fluidity of the phospholipid bilayer [43]. The membrane is subjected to a phase transition around (T_m). Once the phospholipids are assembled together to form a membrane and then a vesicle, the membrane displays different behaviours depending on the temperature of the solution. The T_m is determined by the length and degree of saturation of the hydrocarbon chain, forming the phospholipid tail, and the charge of the phospholipid head. As the length of the hydrocarbon chain increases, the Van der Waals interactions become stronger, requiring more energy to disrupt the ordered packing, and thus the phase transition temperature increases [44]. Above T_m, the membrane is fluid and the phospholipids can diffuse freely inside the bilayer, but the bilayer configuration is conserved thanks to the hydrophobicity of the tail group [45]. Below T_m, the membrane is in a gel phase-the phospholipids are tightly packed and they remain relatively immobile. Around T_m, the two phases can coexist [45] and it can also be modified by higher salt concentration in the solution [45]. Due to their different structure above or below T_m, it is important during the liposome formation to work at a temperature above T_m.

Classification and Lamellarity

As explained, during the liposome's formation it is important to check the T_m, but more important for a drug delivery application is the size of the liposome. To produce smaller liposomes and/or with fewer lamellae, additional energy has to be dispersed in the system, through mechanical (sonication or extrusion) or electrochemical energy (change of pH, ionic strength) [36]. Smaller liposomes and with fewer lamellae may be stable for longer periods [36]. The preparation method influences their physical structure and size; they can be prepared from different kind of phospholipids. Liposomes are also classified based on their lamellarity, as shown in Fig. 1.3. Lamellarity refers to the number of the lipid bilayers that form the liposomes [46]. Based on their size and lipid structural arrangements, different classes of liposomes are produced. In particular, multilamellar vesicles (MLV) with a diameter above 0.5 µm are made of numerous lamellae, unilamellar vesicles (LUV) have a single lamella and can be of different size ranges, based on their diameter they can be classified in a small, large and giant unilamellar vesicle. Finally, multivesicular vesicles are made of several compartments or smaller vesicles encapsulated in a larger one.

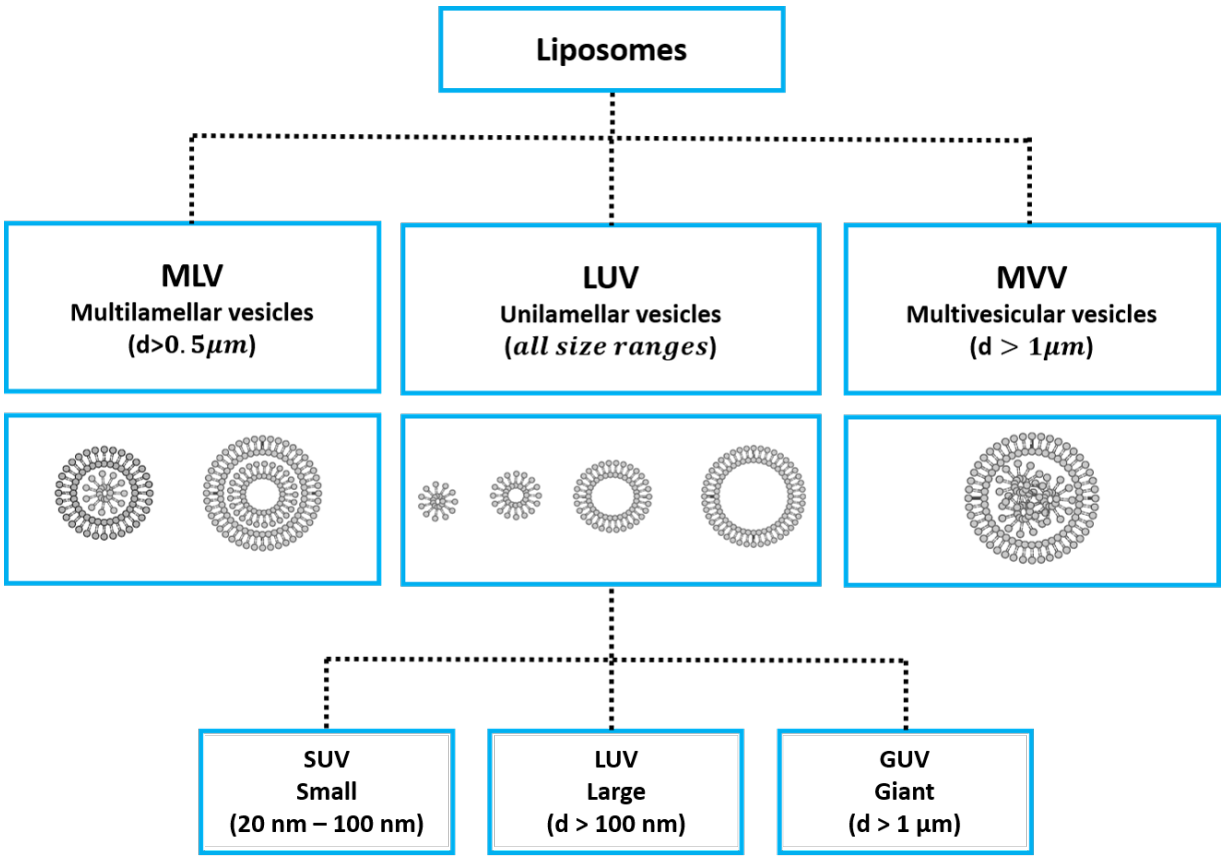

Figure 1.3: Classification of liposomes based on the number of lamellae. Multilamellar vesicles (MLV) have multiple lamellae and the diameter is higher than 0.5 µm, unilamellar vesicles are made of one lamella and multivesicular vesicles are made of a vesicle larger than 1 µm in diameter, which contains several smaller vesicles. Unilamellar vesicles can be of different size ranges and they are divided based on their size into small unilamellar vesicle (SUV, d = 20/100 nm), large unilamellar vesicle (LUV, $d > 100$ nm) and giant unilamellar vesicle (GUV, $d > 1$ µm).

This classification is key in defining which type of liposomes is the most suitable to use in a drug delivery system. LUVs and SUVs are the most common type of vesicles used in drug delivery, due to their small size and because it is easier to control a single layer instead of multiple. The use of MLVs is restricted by many factors: large diameter, low entrapped volume (due to numerous lamellae), wide size distribution and lack of uniformity during preparation [47]. Furthermore, fast degradation (or removal from the bloodstream) in the presence of the mononuclear phagocyte system (MPS) [48] and, most importantly, the lack of control over content release have limited the use of MLVs as a drug carrier [49]. SUVs and LUVs are produced from MLVs, which are formed using the film hydration method. In this work, unilamellar and multilamellar liposomes are mainly used.

Phospholipids Topology and Critical Packing Parameter

In order to form a bilayer, the molecular shape of phospholipids has to be chosen accurately to model the membrane shape that they will form. Depending on their head group and tail group components, they can be in a conical, inverse-conical or cylindrical shape (Fig.1.4). A parameter called the packing parameter was developed, which is useful in determining the size and shape of lipid aggregates [50]. It is described by:

$$S = v/a_0 l \tag{1.1}$$

where v is the hydrocarbon chain volume, a_0 is the area of the head group, and l is the critical length of the hydrophobic chain. The value of S determines the aggregate formed by lipids or any amphiphiles upon hydration. It has been shown that lipids aggregate forms spherical micelles where $S < 1/2$, as in Lysophosphatidylcholine case (LSPC); nonspherical (cylindrical) micelles, where $1/3 < S < 1/2$; bilayers where $1/2 < S < 1$ (DOPC); and reverse micelles or hexagonal phases where $S > 1$, such as 1,2-dioleoyl-sn-glycerol-3-phosphoethanolamine (DOPE).

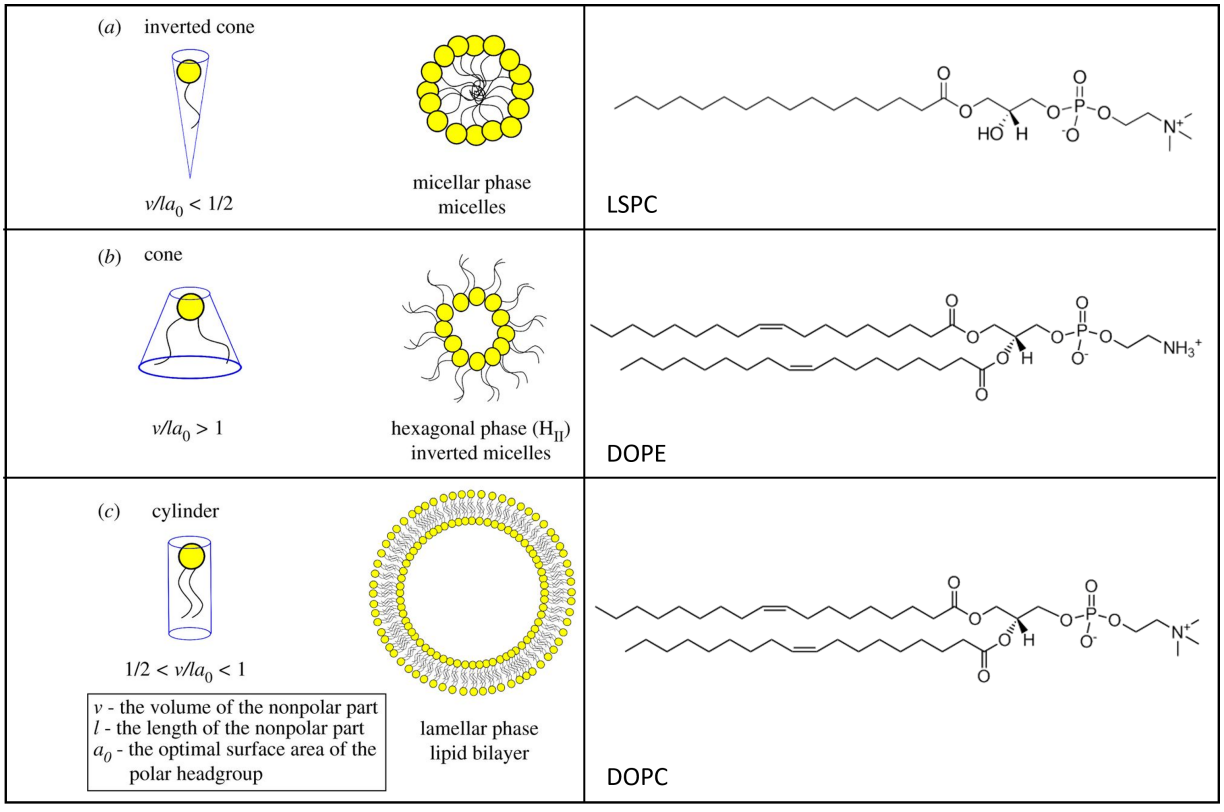

Figure 1.4: Packing parameter of three different phospholipids.(a) Lysophosphatidylcholine has an inverted cone topography. (b) 1,2-dioleoyl-sn-glycero-3- phosphoethanolamine (DOPE) has a cone shape. (c) 1,2-dioleoyl-sn-glycero-3-phosphocholine (DOPC) has a cylinder shape. Fig. adapted from [51]

A stable solution of 1,2-dioleoyl-sn-glycero-3-phosphocholine (DOPC) in PBS, formed

a characteristic cylindrical shape of a bilayer ($S_{DOPC} < 1$), as shown in Appendix A, Fig. A1. Moreover, in heterogeneous phospholipid systems, the packing parameter is additive and the average bulk structure is based on the average packing parameter of the lipid mixture. Phospholipids with an average of $S < 1/2$ forms structure with positive curvature, those with S around 1 form flat non-curved structures, and those with $S > 1$ adopt negatively-curved structures [52].

1.6 Liposomes: Formation and Production

1.6.1 Spontaneous Formation of Multilamellar Vesicles

Multilamellar vesicles are formed spontaneously and can be disrupted to form unilamellar vesicles. Once a dry lipid film comes in contact with water, based on the packing parameter of the phospholipids, MLVs are formed spontaneously upon agitation to help the detachment [38]. Due to the amphipathic nature of phospholipids, the fatty acids tails rearrange their structure to minimise the contact with water, forming bilayers and after shaking, MLVs of 1-15 µm in diameter are generated [53] (Fig. 1.5).

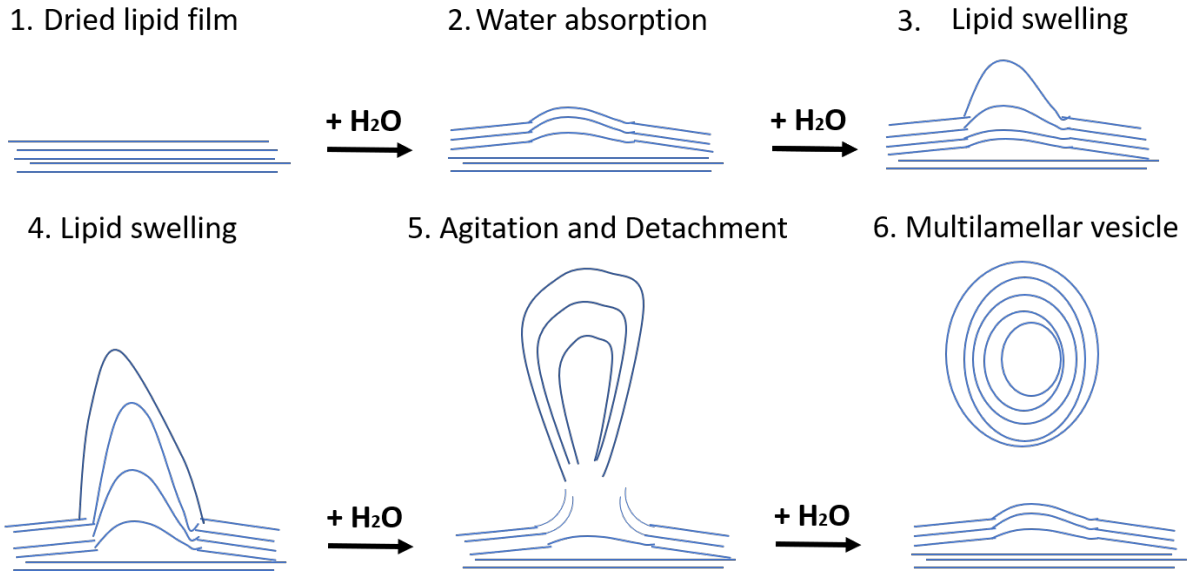

Figure 1.5: MLVs Formation. Polar head of dried phospholipids start to swell in contact of water. The fatty acid rearrange their structure to minimise the contact with water, closing themselves and forming MLVs with sizes between 1-15 µm of diameter. Figure adapted from [54]

In a laboratory setting, this principle is used to generate MLVs via a multistep process. Firstly, a suitable lipid in powder is dissolved in a solvent, once the solvent evaporates and a thin lipid film is created, as shown in Fig. 1.5, the hydration and agitation in an aqueous solution will occur to favour the vesicle self-assembly into MLVs [53]. Despite a large number of studies regarding lipid vesicle formation, the theory behind it is still

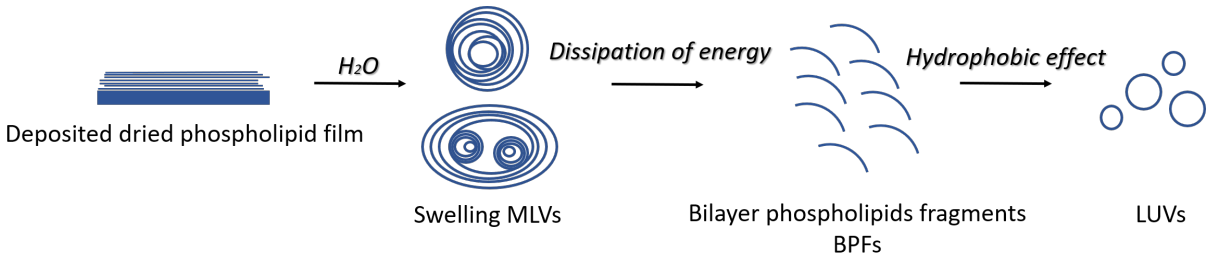

Figure 1.6: Large unilamellar vesicles formation, adding energy to the system, multilamellar vesicles are breaking down into bilayer phospholipid fragment and then due to the hydrophobic effect of the phospholipid fatty chain, the bilayer close themselves.

not completely understood. To form LUVs and SUVs from MLVs, different techniques are followed [36].

One of the main theories on liposomes formation was proposed by Lasic [54]. According to his study, once an MLV dispersion is formed, different methods can be used in order to decrease the size and the lamellarity of the vesicles, by applying energy to the system, usually performed under cavitation, adding pressure or rapidly changing the temperature (e.g. freeze-thaw cycles) [47]. Bilayer phospholipid fragments (BPFs) are formed by adding energy to the MLV mixture [47]. Once BPFs are formed, due to the exposure of hydrophobic chains to water, and depending on the thermodynamic conditions, LUVs can form from BPFs fusion. The liposomes formation process is described in Fig. 1.6. Besides Lasic *et al.*, Talsma [55] proposed the bubble method, where nitrogen gas bubbles are introduced in a solution of water with dried lipids, to promote the formation of phospholipid monolayer at the nitrogen gas/water interface. This theory was subsequently utilised by Feng *et al.*, who demonstrated the formation of a nanoemulsion through bubble bursting at a compound interface [56].

Most common methods for producing SUVs and LUVs from an MLV dispersion, which is obtained using the thin film hydration method, use a mechanical approach, such as extrusion, sonication and freeze-thawing liposomes. Chemical approaches, which can be used to form heterogeneous vesicle sizes, are solvent dispersion method, are detergent depletion and reverse phase evaporation techniques [35]. The vesicles' formation process was described by Lasic *et al.*, [53], [54], [47] and summarised in Fig. 1.7.

1.6.2 Methods of Producing Liposomes

The production of lipid vesicles involves three steps [35]: (1) drying lipids in an evaporated organic solvent to form a lipid film, (2) dispersion of lipids in an appropriate aqueous solution and (3) size reduction and characterisation of liposomes. To dry lipids a rotary evaporator can be used. If the sample volume is lower than 1 mL then a stream of nitrogen can be utilised instead of [57].

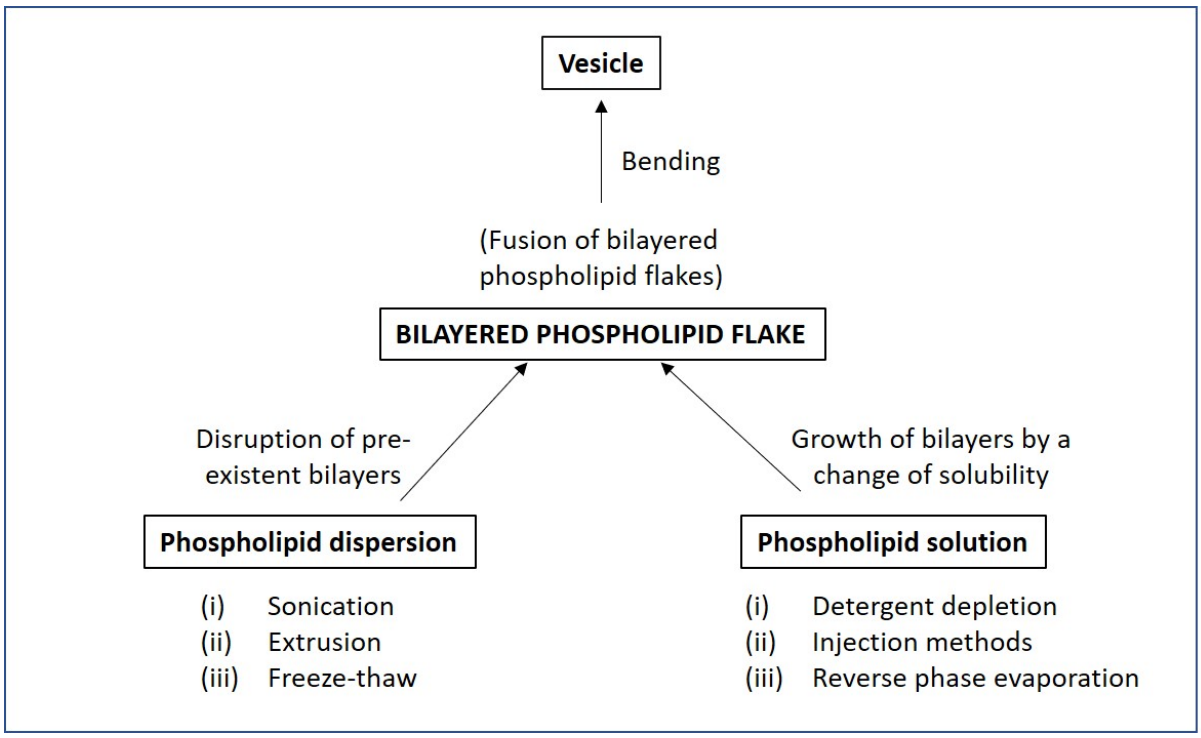

Figure 1.7: Different vesicles preparation methods, according to the mechanism of vesicles formation proposed by Lasic, [54]. Phospholipid solution describes the phospholipid in organic solvent while phospholipid dispersion is a multilamellar vesicles solution. Changing the solubility of the solution and with the disruption of the bilayers in the phospholipid dispersion case, the formation of bilayered phospholipid flakes or fragments (BPFs) will occur. One BPFs are formed, they will fuse and bend in vesicles, due to the hydrophobic effect of the hydrocarbon chains. Figure arranged from [53]

The second step, which involves the hydration of lipids in an aqueous solution, can be achieved using the thin film hydration method (described in Chapter 2) or organic solvent dispersion and detergent dispersion [58].

Mechanical Dispersion: Production of LUVs and SUVs

A thin layer of dried lipids is hydrated in an aqueous solution (thin film hydration method) [59], the head group of the lipids starts to swell and absorb water until the lipid is peeled off to form multilamellar vesicles, while the hydrophobic effect holds the bilayer together. A gentle agitation could help in detaching the MLVs.

Sonication

Sonication uses ultrasonic frequencies (>20 kHz) to disrupt phospholipid membranes and produce unilamellar vesicles from multilamellar vesicles, usually applied using an ultrasonic bath or probe. High energy ultrasound is introduced into a liquid medium, forming alternating cycles of high pressure (compression) and low pressure (rarefaction) [60]. Dur-

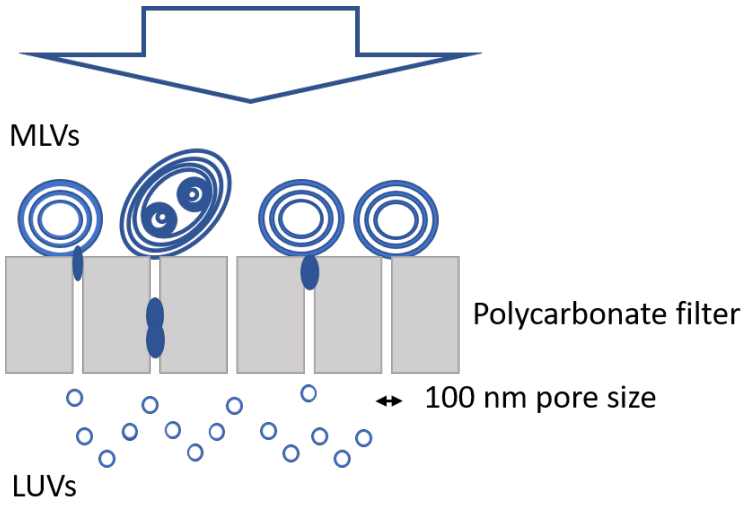

Figure 1.8: Solution of MLVs pushed through a polycarbonate membrane with 100 nm pore diameter.

ing the low-pressure cycle, small vacuum bubbles are created. When the bubbles attain a volume at which they can no longer absorb energy, they collapse violently during a high-pressure cycle. This phenomenon is termed cavitation. During the implosion, high temperatures (approx. 5,000 K) and pressures (approx. 2,000 atm) are reached locally, resulting in liquid jets of up to 280 m/s velocity [60]. The main disadvantages of this method are low volume entrapment, metal pollution from the probe tip, high temperature, which might have a detrimental effect on the structure and stability of encapsulated proteins and multimodal distribution of the produced vesicles. Disruption of MLV suspension using tip ultrasonication typically produces small, unilamellar vesicles with a diameter in the range of 15-50 nm.

Extrusion

The extrusion mechanism involves passing a solution of MLVs through a polycarbonate membrane filter with defined pore size, Fig. 1.8. The solution is sequentially extruded to decrease the size of the vesicles [61]. One of the main advantages of this method is the homogeneous size of the vesicles. However, the resulting produced liposomes are larger than vesicles generated via sonication and the process is time-consuming and labour-intensive.

Freeze-Thawed Liposomes

MLVs are rapidly frozen at -80°C and thawed in a water bath at 37°C. This process is repeated at least 3 cycles. During freeze-thawing, rapidly-forming ice crystal disrupts the structure of MLVs, leading to the formation of liposomes (see Appendix, Fig. C1). However, obtaining a specific size range of vesicles is difficult and using this process biological

material can be damaged due to the exposure to low temperatures.

Organic Solvent Dispersion

Lipids dissolved in ethanol are injected into a huge excess of the buffer. MLVs are rapidly formed, but the techniques produce a heterogeneous population of liposomes and the ethanol removal is challenging [58].

Reverse Phase Evaporation

Reverse phase evaporation is a method based on the formation of inverted micelles. They are formed by sonicating a mixture of the aqueous phase, which contains the molecules to be encapsulated into liposomes, and an organic phase in which the amphiphilic molecules are solubilized [62]. The organic solvents are removed under reduced pressure during continued rotary evaporation and liposomes are formed. The main disadvantage is the exposure of the encapsulated material to an organic solvent and the sonication [58], which can cause DNA damage or protein denaturation.

Detergent Dispersion and Solubilisation

Lipids are solubilised in an aqueous solution through the addition of detergents, which are then removed slowly to help the formation of liposomes [63].

Detergent Depletion

Lipid solubilisation can be obtained using detergents at their critical micelle concentrations (CMC). As the detergent is removed from detergent/lipid-mixed micelles, they increase in numbers and combine to form liposomes [64]. As the detergent needs to be removed via dialysis, the whole process is relatively time-consuming. Additionally, this method results in non-homogeneous populations of liposomes.

1.6.3 Stability of Liposomes

After the description of the main liposomes' formation methods, a explanation of liposomes' stability is made. To deliver a functional compound the liposome has to be stable and intact during the nebulisation. Stability testing is the primary tool used to assess the expiration date of pharmaceutical products under typical storage conditions (shelf-life). Liposome stability is affected by physical, chemical and biological processes. One physical process, such as fusion, affects liposome size, shelf life, and the release of encapsulated material [66]. Chemical degradation, such as hydrolysis of the ester bond linking the fatty acids to the glycerol backbone, also affects liposome stability. Biological stability is

Liposomes production method	Advantages	Disadvantages
Sonication	Fast Small liposomes	High temperature (>80°C) Denaturation of biologics Metal pollution Need MLVs solution [60]
Extrusion	Monodispersity	Time consuming Liposomes diameter ≥100 nm Need MLVs solution [65]
Freeze-Thaw	Easy to operate	Extreme temperatures (-200 °C) Denaturation of biologics Size control Need MLVs solution [36]
Reverse phase evaporation	Fast	Polydispersity Time consuming Exposure to organic solvent Size control [41]
Detergent depletion	Stability	Polydispersity Presence of detergent Size control [40]
SAW nebulisation	Fast Stability Monodispersity Aerosols formation Delivery of biologics	Need MLVs solution (Chapter 4)

Table 1.1: Comparison of different methods to produce liposomes. The advantages of using the SAW nebuliser to produce liposomal aerosols are analysed and studied in Chapter 4.

affected by liposome degradation in the bloodstream. The use of proteins prolongs the circulation time of liposomes by increasing their stability [67].

The stability of liposomal aerosols was previously tested when using jet and ultrasonic nebulisers [68]. Jet nebulisers (Airlife, Respirgard II Filtered Medication Nebuliser) use compressed gas to produce aerosols from an aqueous solution but induce fragmentation of the vesicles during nebulisation due to high shear stress, and design of the nebuliser that allows the recycling of liposome-containing liquid within [5], [69], [70]. Ultrasonic nebulisers are less widely used, both because of the heating that occurs during nebulisation, which denatures proteins, and because of their inability to nebulise liquids of viscosity higher than 6 centipoise [71]. In Taylor's study [70], sodium cromoglycate (SCG), widely used in the prophylactic treatment of asthma, was encapsulated in liposomes, and drug loss was measured using a multi-stage liquid impinger (MLI), which was also employed to evaluate the particle size distribution. Analysis of the solution on the stages of the MLI indicated over 50% loss of the entrapped drug during nebulisation. A decrease in vesicle diameter was also apparent, suggesting that the liposomes were fragmented upon their passage through the nebuliser [72]. To increase the stability of liposomes, they are usually frozen before storage, adding into the freezing solution cryo-protectants, at a concentration below 10% v/v [73], [74]. Whilst this does indeed improve the stability of the liposomes, it is time-consuming. Moreover, it causes the liposomes to shrink and swell, which can cause the encapsulated compound to leak out due to an imbalance in osmotic pressure [75]. The vesicles initially shrink due to the higher concentration of cryoprotectants outside of them and then swell due to the osmotic movement of the cryoprotectant into them [73].

Liposome leakage can be affected by changes in temperature, cholesterol levels and pH [44]. According to experimental results, higher temperatures (compared to room temperature), and pH 1.9 to 5, increase the fluidity of the double bilayer, thereby destabilising the vesicle and increasing leakage. The insertion of cholesterol into a DPPC phospholipid membrane at a molar ratio higher than 0.5:4, in terms of cholesterol: DPPC, decreases leakage [44].

1.6.4 Liposomes in Pulmonary Drug Delivery System

Liposomes were previously used as a pulmonary drug delivery carrier [4], [**Price**], [76]. Many studies have shown the safety of liposomes inhalation [77], [78], [79]. The successful development of an anticancer liposomal formulation for inhalation depends on the inhalation device, which produces the aerosols and the size of the liposomes [80]. Therefore, it is critical to find a suitable device, which can retain the liposomes functionality. Intratracheally instilled liposomes in mice were reported to be uptaken by pulmonary cells [81]. Mainelis outlined the advantages of local intratracheal delivery of Liposomal Doxorubicin (DOX) for the treatment of lung cancer when compared with systemic administration

of the same drug [82]. With the intratracheal delivery of the DOX, a higher peak of the DOX concentration and much longer retention of liposomes was noticed in the lungs of a nude mouse with an orthotopic model of the human lung (A549 non-small cell lung carcinoma). Using a five ports nose-only exposure system for small animal, a greater reduction of the tumour volume after inhalation delivery of liposomal DOX was observed [82]. Therefore, the advantages of administrating intratracheally a combination of liposomes and anticancer drug, such as DOX, were previously demonstrated [83]. Different devices can affect the delivery of liposomal formulation. Pressurised metered-dose inhalers were employed to deliver liposomes by dissolving the phospholipids in CFC propellant, which have been reported to be depleting the ozone layer [84]. Thus, safe alternative propellants are used, but in which phospholipids have low solubility. Main issues encountered are low deposition and stability. The delivery of liposomes using dry powder inhalers resulted in additional freeze-drying step in the liposomes formation procedure and in the insertion of cryo-protectants.

1.7 Liposomes Characterisation

Size measurements are one of the main characterisation methods of dispersion. Direct measurements of particle size are based on microscopy which cannot be used for nano-size dispersion and hard to achieve for aerosols. Confocal microscopy and transmission electron microscopy (TEM) are briefly described, but they were not used to measure the size of the liposomes. Confocal was used to track changes in the liposomes population size and TEM was used to test the structure of the liposomes, but resulted in an expensive and time-consuming method. Therefore, indirect methods, based on light scattering and diffraction are used instead. In this section, a background of light scattering is presented, followed by the dynamic light scattering (DLS) and laser diffraction, which are the principal methods used for characterisation of nano-particles and aerosols in this study.

1.7.1 Light Scattering

Potential interactions of light, when passes through a material are absorption, transmission, fluorescence and scattering. The scattering signal may be analysed by several methods:

- Static: average signal strength
- Dynamic: fluctuations of signal
- Electrophoretic: shift of the signal

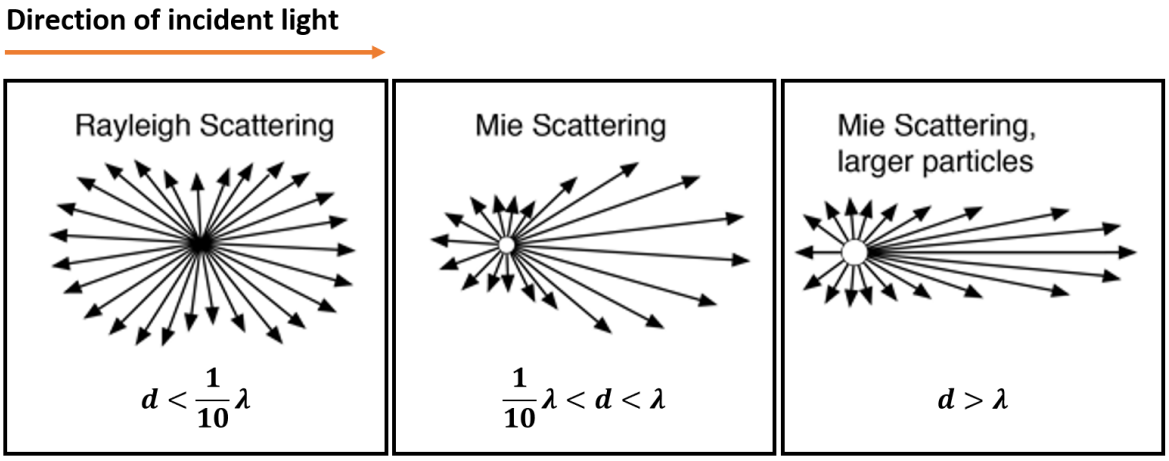

Figure 1.9: Different scattering effects: Rayleigh scattering for small particles which re-radiates the signal with the same phase. Mie scattering is used for particles with a diameter similar to or larger than the wavelength of the incident light and they re-radiated the scattered signal with different phases.

The scattering process can be: (1) elastic, where the wavelength of the scattered light is the same as the incident light (the kinetic energy of the particle is conserved), (2) inelastic, where the emitted radiation has a different wavelength from the incident one (loss of the kinetic energy) and (3) quasi-elastic scattering, where the wavelength of the scattered light has been shifted (small loss of kinetic energy) [85].

Two types of elastic scattering are [86] (Fig.1.9):

- Rayleigh scattering, which is the elastic scattering of light of molecules and particles much smaller than the wavelength of the incident light ($d < \frac{1}{10}\lambda$).
- Mie scattering is a broad class of scattering of light by spherical particles with a diameter similar to or larger than the wavelength of the incident light.

The intensity I of light scattered by any one of the small spheres is [87]:

$$I = I_0(\frac{1 + cos^2\theta}{2R^2})(\frac{2\pi}{\lambda})^4(\frac{n^2 - 1}{n^2 + 2})(\frac{d}{2})^6 \tag{1.2}$$

where I_0 is the laser intensity, θ is the angle from where the scattering is observed, n is the refractive index of the solvent, R is the laser radius and d is the particles diameter.

1.7.2 Dynamic Light Scattering

Dynamic Light Scattering (DLS) is a technique that measures the fluctuations of the light scattered by nano-particles in dispersion, which are moving under Brownian motion. Stokes-Einstein equation describes the diffusion coefficient of a particle under Brownian motion in a quiescent fluid at uniform temperature [88]:

$$D = \frac{kT}{6\pi\eta r} \tag{1.3}$$

where k is the Boltzmann's constant, T is the absolute temperature, η the viscosity of the fluid in which particles are immersed and r is the hydrodynamic radius of the particle.

The sample, which is made of particles dispersed in a solution, is illuminated by a laser. As the laser passes through the medium, it interferes with particles and scatters, resulting in an intensity pattern, which varies as particles move. The intensity fluctuations from the Brownian motion of the particles is analysed by a digital correlator [87]. The correlator compares signals, two different ones or one signal with itself at varying time intervals. At time zero the signal is perfectly correlated with itself, so the correlation is high, over the time as particles diffuse, the correlation will reduce, until there will be no relationship with the original signal and the correlation will be zero. The decay of the correlation is characteristic of the diffusion speed and thus the particles size. The autocorrelation function of the scattered light $g^{(2)}$ for a given delay time τ is described by [89]

$$g^{(2)}(\tau) = \frac{\langle I(t)I(t+\tau)\rangle}{\langle I(t)\rangle^2} \tag{1.4}$$

where $I(t)$ and $I(t+\tau)$ are the intensities of the scattered light at t and $t+\tau$ times, and the angled brackets indicate an averaging over t. The intensity-intensity time autocorrelation function can be also expressed in terms of field-field time autocorrelation function $g^{(1)}(\tau)$ by Siegert relation:

$$g^{(2)}(\tau) = B + \beta[g^{(1)}(\tau)]^2 \tag{1.5}$$

where B (usually $B = 1$), referred as baseline, is the long-time value of $g^{(2)}(\tau)$, β is the geometrical factor and with $g^{(1)}$ individuated by:

$$g^{(1)}(\tau) = \frac{\langle E(t)E^*(t+\tau)\rangle}{\langle E(t)E^*(t)\rangle^2} \tag{1.6}$$

where $E(t)$ and $E(t+\tau)$ are the scattered electric fields at t and $t+\tau$ times. For monodisperse particles in solution the field-correlation function decays exponentially,

$$g^{(1)}(\tau) = exp(-\Gamma\tau) \tag{1.7}$$

with a decay rate of $\gamma = Dq^2$, where D is the diffusion coefficient of the particles and q is the magnitude of the scattering wave vector. The scattering wave vector q is the difference between the incident and the scattered wave vectors and its magnitude is given by:

$$q = \frac{4\pi n}{\lambda_0} sin(\frac{\theta}{2}) \tag{1.8}$$

where n is the refractive index of the solvent, λ_0 is the wavelength of the laser in the vacuum, and θ is the scattering angle. For a polydisperse sample, $g^{(1)}(\tau)$ cannot be represented by a single exponential, but as a sum or an integral over a distribution of decay rates $G(\Gamma)$ by:

$$g^{(1)}(\tau) = \int_0^\infty G(\Gamma) exp(-\Gamma\tau) d\Gamma \tag{1.9}$$

where $G(\Gamma)$ is normalised so that

$$\int_0^\infty G(\Gamma) d\Gamma \tag{1.10}$$

$G(\Gamma)$ using Laplace transform techniques, as $g^{(1)}(\tau)$ is the Laplace transform of $G(\Gamma)$.

Polydispersity Index

The polydispersity index (PDI) is used to characterise the width of the particle size distribution from the DLS measurements [86]. A DLS measurement generates an autocorrelation function, which is evaluated using the cumulant analysis [90], which is a moment expansion that produces different values, such as the polydispersity index [87]. In the cumulants analysis, a single particle size mode is assumed and a single exponential fit is applied to the autocorrelation function [91]. The polydispersity index can be an indicator of the quality of the sample. Values greater than $PDI = 0.7$ indicate that the sample has a very broad size distribution and is probably not suitable for the dynamic light scattering (DLS) technique [90]. PDIs values around 0.1-0.2 indicate high quality, monodisperse sample.

1.7.3 Confocal Microscopy

A laser scanning confocal microscope (Zeiss LSM 5 Live, Jena) was used to check the different population of vesicles, both before and after SAW nebulisation. The main advantages of confocal microscopy are the point-by-point illumination of the sample and the presence of a pinhole which rejects the out-of-focus light, leading to high contrast images [92]. The excitation light is provided by a laser, which encounters a pinhole and becomes the point source of light. The laser light (in this case green, LSM 5 LIVE) reflects off a dichromatic mirror [93], Fig. 1.10. The light is then focused by an objective lens on a desired focal plane in the specimen. The laser excites the DOPE-rhodamine in the lipid samples (MLV mixture, which fluoresces and emits light (red)($\lambda_{abs} = 560$ nm, $\lambda_{em} = 583$ nm). The light emitted by the sample passes through the dichromatic mirror. The second

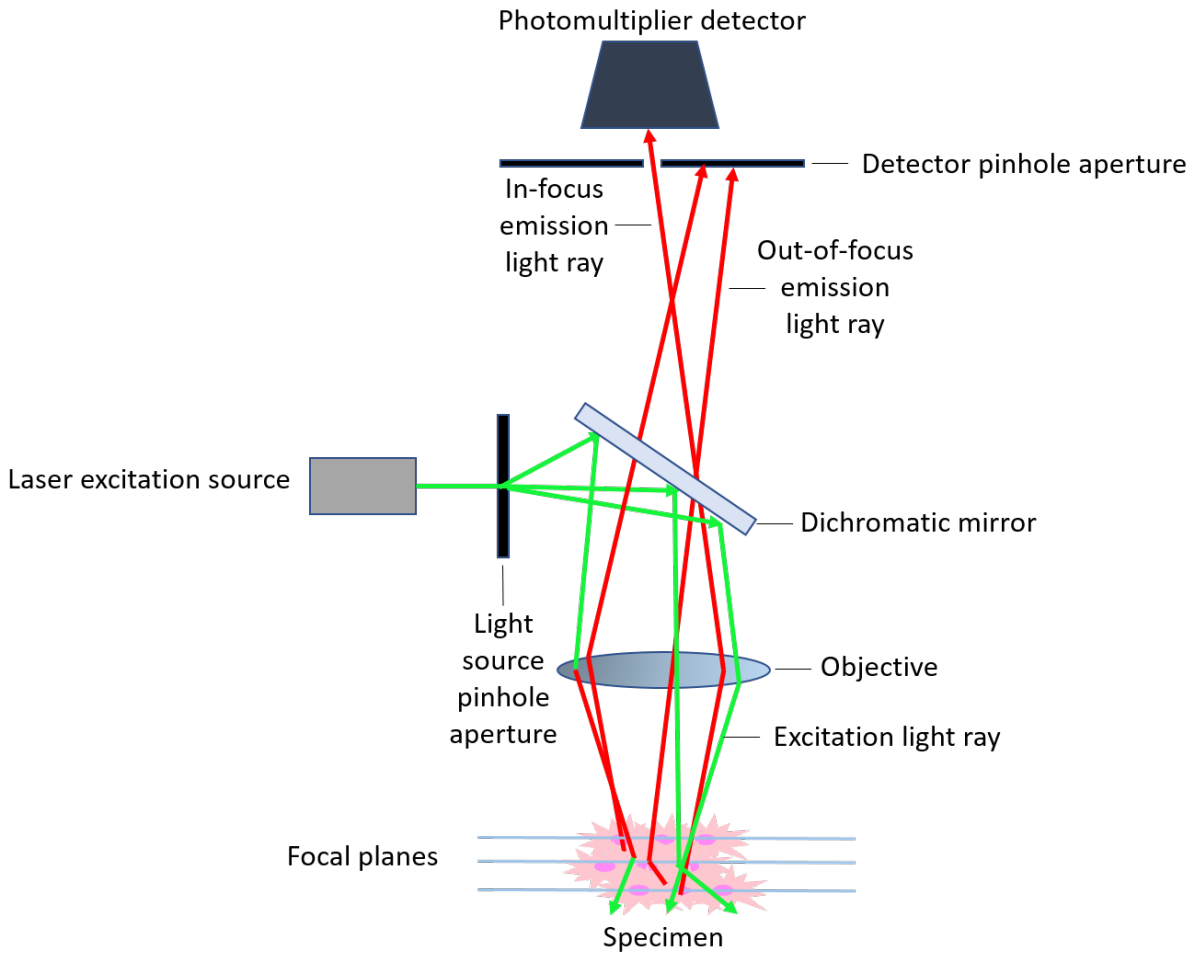

Figure 1.10: Confocal microscope components. A laser, which acts as an excitation source, passes through the first pinhole. The dichromatic mirror reflects the light which is then focused on the specimen by an objective. The dye in the sample fluoresces and emits light which passes through the dichromatic mirror and hits the second pinhole. The second pinhole prevents light from coming from out-of-focus focal planes from reaching the photomultiplier detector [93].

pinhole prevents the light which is coming from a different focal plane from reaching the photomultiplier detector [93].

1.7.4 Trasmission Electron Microscopy: Negative Staining and Cryo-TEM

Resolution in microscopy is limited to about half a wavelength of the illumination source used to image the sample [94], [95]. To overcome this limitation, an illumination source with a shorter wavelength than visible light is needed. LUVs (nanometer order) are below the resolution of a light microscope. Therefore, transmission electron microscopy (TEM) was used in order to visualise SAW-formed vesicles of 100 nm in diameter. Using an accelerated electron beam as a light source, a higher resolution compared to the light

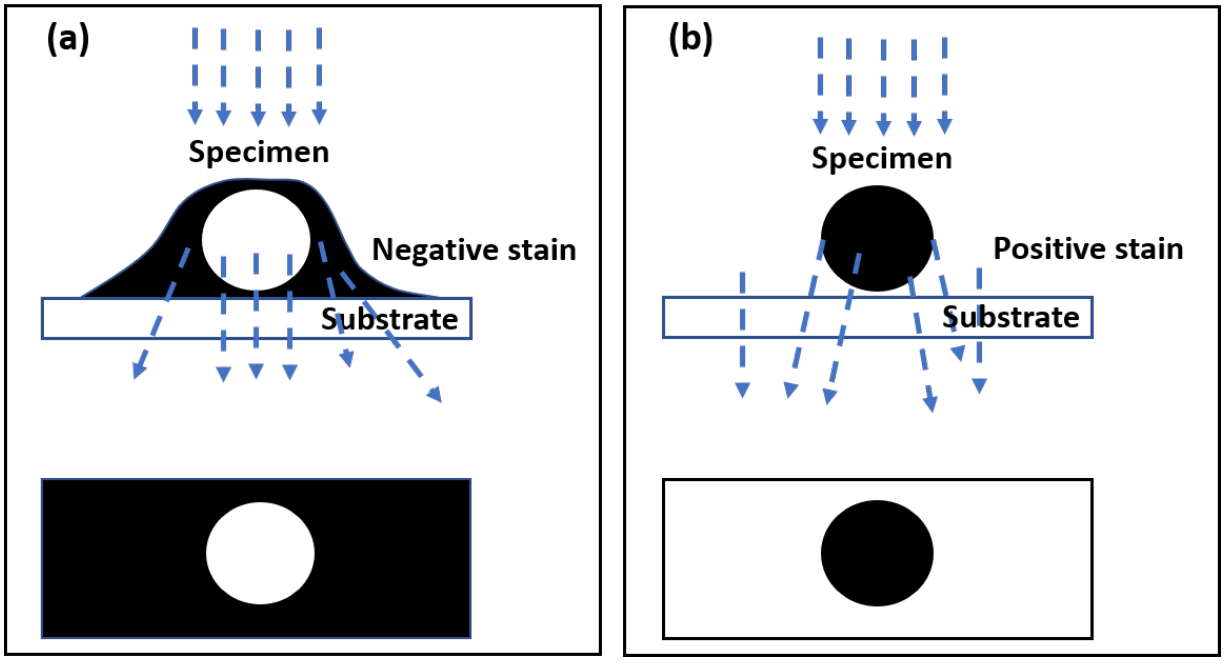

Figure 1.11: Transmission electron microscopy. Differences between negative and positive staining. In negative staining approach, the background is stained while the specimen is not affected [96]. When the electron beam passes through the sample, it will be deflected by its interactions with the sample and the stain. Since the protein sample excludes stain, the deflection of the electron beam through the sample is less than through the stain region. Regarding positive staining, the stain is attached to the surface of the specimen, resulting in a dark image of the sample against a light background [96].

microscope can be obtained and thus, an object of nanometer order can be revealed. Moreover, it is extremely useful for examining different layers of specimens and their structures. When an electron passes through an atom, it encounters three effects, it is so fast that it could pass through the atom and does not interact; it could bounce into the nucleus of the atom, without changing neither the energy or the speed, but only the direction. It is called elastic scattering and it generates the contrast in the image. Finally, the electron could be inelastically scattered and the interaction with electrons in the sample will cause an energy loss of the electrons that will damage the sample. It is called inelastic scattering and it is responsible for the noise in the image. Three problems were highlighted when electron microscopy is used with biological materials [97]. First of all, most biological samples are suspended in aqueous solution thus, if, in contact with a high vacuum, which is needed for the electron beam, their structures will collapse; liposomes, for instance, will burst. Second, elements that are most common to biological (H, N, O, C) have low intrinsic contrast in water and finally, biological samples are radiation sensitive. To solve these problems, two approaches can be applied: negative/positive staining and cryo-TEM [98]. In the negative staining process, heavy metal salts derived from molybdenum, uranium or tungsten can be used to generate high contrast [94]. These

materials readily interact with the electron beam and produce phase contrast, i.e. the light encounters a greater phase shift as it interacts with the stained sample. As shown in Fig. 1.11 stains can be employed for negative and positive staining. In negative staining the stain surrounds the specimen, as it is being excluded from the volume occupied by the sample, producing a clear and detailed image of the sample. In positive staining the stain is attached to the surface of the specimen, resulting in a dark image of the specimen against a light background.

Cryo-TEM has some advantages over negative staining namely, the sample is always in solution and no stain is required. In cryo-TEM, the sample is frozen so fast that water molecules do not have the time to re-organise into ice crystals, thus, it is called vitrified water. Advantages include good preservation of the sample and high resolution, but it is technically demanding and the contrast is limited [99].

1.8 Aerosols Characterisation

1.8.1 Particle Size Distribution and Aerodynamic Diameter

In drug delivery systems, the size of the carrier compound is a key parameter. In order to deliver molecules within the human body is important to have particles of a specific size range, depending on the application [100]. For instance, to pass through the blood-brain barrier, the particle has to be in the range of 15-50 nm, whereas to pass through the endothelium, it has to be smaller than 150 nm [101]. To be able to reach the lungs, the aerosols have to be in the size range of 1-5 µm [102]. The particle size distribution is also crucial to assess the sample quality; if the sample is monodisperse, characterised by particles of uniform size [103], the sample quality is improved and a higher concentration of the drug will reach the desired target. Particles are three-dimensional objects, therefore, to describe them using a single number, a spherical approximation must be used, which is the approach taken by most techniques. For instance, the aerodynamic diameter is used in the inertial impaction method to measure the particle size. It is defined as the equivalent diameter of a spherical particle with a density of 1000 kg/m ^{3} with the same terminal velocity of the particle of interest [104].

1.8.2 Cascade Impactors

Cascade impactors are instruments employed for the characterisation of aerosols, produced by inhalers and nebulisers. The most commonly used cascade impactors are the ACI and the Next Generation Impactor (NGI), both recommended by the US and European Pharmacopeia. The multi-stage liquid impinger (MSLI) was also widespread but was recently substituted by ACI and NGI for the higher resolution in particles diameter. The

Method	Parameter	Size order
Dynamic light scattering (liposomes)	Liposomes size	nm
TEM negative staining (liposomes)	pre-CryoTEM visualisation	nm
Cryo-TEM (liposomes)	Lamellarity of liposomes	nm
Laser diffraction (aerosols)	Aerosols size	µm
Cascade Impactors (aerosols)	Aerosols size	µm

Table 1.2: Summary of liposomes and aerosols' characterisation method, measured parameter and size order.

MSLI has the only advantage compared to the ACI and the NGI that the collection stages are kept moist, avoiding the bouncing effect [105]. The NGI is the improved and more recent version of the ACI. The ACI has a stage size overlap and its use is more time-consuming for the operator, which has to disassemble the impactor at each measurement to recover the deposition on the collection plates [106]. Nevertheless, results from the ACI and the NGI measurements showed comparable values [107], in terms of particle size distribution.

1.8.3 Laser Diffraction

Laser diffraction is an established method to measure the size of the nebulised particles [90]; In this manuscript, a laser diffraction system was used to measure the aerosol produced by the SAW nebuliser. The main advantages of using laser diffraction for aerosol size measurements are: it covers a wide size ranges from submicron to millimetres, reproducibility, easy and rapid measurements [108]. This technique uses the angular variation in the intensity of the light after passing through a particle, to evaluate the particle size distribution. The software analyses the collected angular scattering intensity data, using Mie theory, and provides the measurement based on the given refractive index of particles and medium, assuming a volume-equivalent sphere model. An approximation of the Mie scattering theory, which was used in older laser diffraction instrument is the Fraunhofer diffraction theory can be used when the following conditions are fulfilled: (1) when the particle is 10 times the wavelength and (2) the scattering angle is less than 30°. The two theories are used together in order to ensure that a wide range of particles diameter is covered [109].

1.9 Overview of Inhalers and Nebulisers

In this work, the inhalation route is chosen as the most direct drug delivery route to the lungs. Carrier-mediated drug delivery system were described introducing liposomes and their main characteristics, but an overview of the current available devices is needed to

understand what is the need and what are the problems in order to develop a more efficient nebuliser. Inhalers and nebulisers are largely used to treat pulmonary diseases, by directly delivering drugs to the lungs. They have been employed since the 19th century (Fig. 1.12). There are two primary parameters used to evaluate their performances: the aerosols size distribution and the drug output rate, which depends on several factors, such as, the device type and its design as well as the particular drug delivered [4]. The main difference between inhalers and nebulisers are that first ones need patient's breath-coordination, while second ones operate continuously. Two principal inhalers are currently on the market: metered-dose inhalers (MDI) and dry powder inhalers (DPI). During the activation of a metered-dose inhaler, a pre-measured dose of drug solution is released at high velocity (100 km/h). In order to obtain a clinical efficacy of the treatment, patients need to simultaneously inhale during the drug release. This breath-coordination dependency resulted in difficulties for children and elderly patient [110]. In a dry powder inhaler, the drug is provided in powdered form. Most of the resulting particles are too large to penetrate the lungs, but the turbulent stream created in inhalers during inhalation causes the aggregates to break up into smaller particles [6].

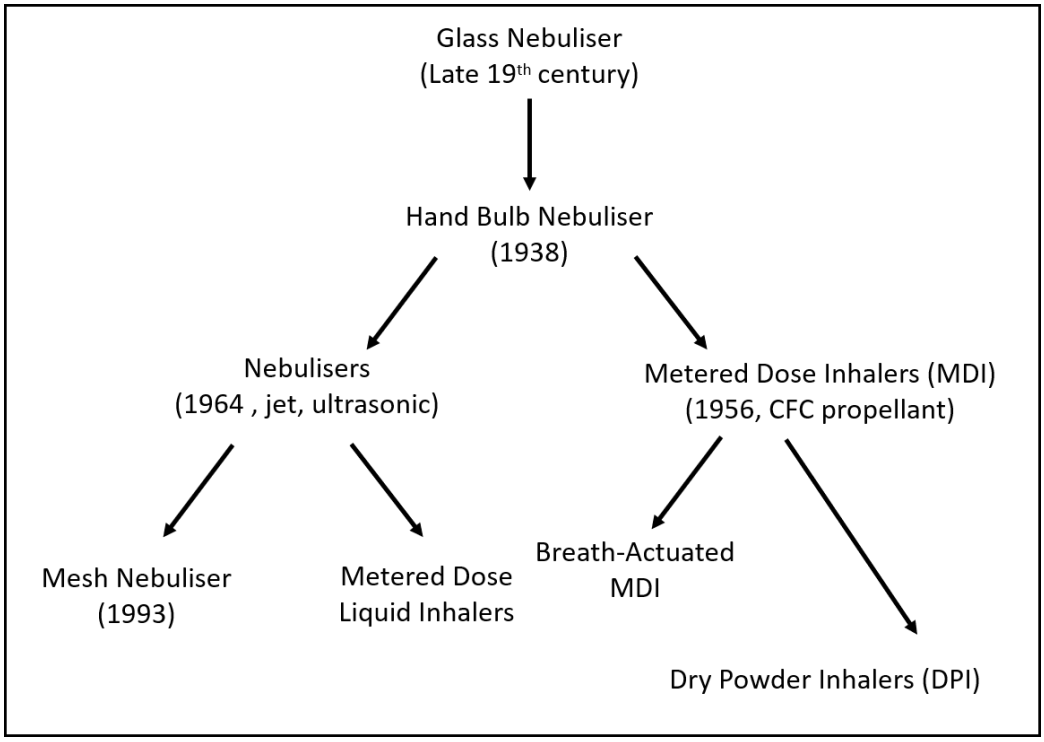

Figure 1.12: A schematic of the evolution of pulmonary drug delivery devices. First developed nebulisers were composed of a liquid reservoir and a pump that was used to spray out a pressurised liquid by hand force. In 1938 a hand-bulb nebuliser was developed, which replace the pump of the previous version [111]. In the early 40s and 50s, metered-dose and dry powder inhalers were manufactured. In 1964, first jet nebuliser and then ultrasonic one was produced and finally, in 1993 the first mesh nebuliser was marketed by Omron [9]. Figure arranged from [33].

Device	Advantages	Disadvantages
Inhalers (MDI, DPI)	Stability of the formulation (dry powder)	Breath-coordination Large aerosols Small volumes Low deposition (7-21%) [113], [110], [107]
Jet nebuliser	Large volumes	Damage of biologics Large aerosols Bulky and noisy High power [5], [113], [6], [114]
Ultrasonic nebuliser	Portability	Damage of biologics Large aerosols Bulky Limitations with suspensions [5], [113], [115], [114]
Mesh nebuliser	Optimum aerosols size	Clogged mesh Small pores (∼1-5 µm) Difficulties in cleaning [5], [9], [66], [116]
SAW nebuliser	Versatile Optimum aerosols size Delivery of biologics Disposable	Small volumes [17], [18], [117], [118]

Table 1.3: Comparison of inhalers and different nebulisers, highlighting advantages and disadvantages. The table shows the numerous advantages of the SAW nebuliser, between them the most important are the size control of the aerosols and the delivery of biologics, which are discussed in Chapter 4 and 6.

The main drawback of using inhalers is that their efficiency, which can be measured in terms of therapeutic effect, depends on the amount of energy that the patient uses to inhale. Nebulisers are capable of delivering a higher drugs quantity compared to inhalers because they operate over a longer period and they do not require coordination skills from patients [110]. The most common forms of nebulisers are jet and ultrasonic nebulisers. Jet nebulisers are based on the Venturi principle, they convert a solution of a drug into a mist of droplets by passing compressed air through a narrow hole [6], [112]. The presence of the constricted section (narrow hole) creates a reduction of fluid pressure, which moves the fluid from the reservoir and breaks it up into droplets by the jet. The main drawback is represented by the nebulisers cumbersomeness due to the compressor size.

The jet of gas expands when exiting the orifice, creating an area of subatmospheric

pressure into which the fluid is moved from the reservoir by the Bernoulli effect and is broken up into droplets by the jet. Droplets are then filtered by baffle structures within the nebuliser. The continuous production of aerosol from the nebuliser during both inspiration and expiration phases causing the production of a large amount of wasted drug. Only 10% of the drug is deposited in the lungs [8]. Ultrasonic nebulisers use a piezoelectric crystal to produce aerosolised particles. Ultrasonic vibrations from the piezoelectric material are transferred into a drug solution, which produces standing waves on the solution surface. Droplets are produced from the crest of the standing waves and are released as a mist [17]. Main advantages of ultrasonic nebulisers are the device portability, which reduces the number of emergency room visits and hospitalisations required and the ease of use compared to inhalers. A significant drawback is the damage of biological compounds and proteins due to the creation of high shear stress from the frequency range used (below MHz order).

Mesh nebulisers are the first choice for inhalation treatment [9], even though they are the latest developed nebulisers on the market (1993). In mesh nebulisers, the liquid drug is forced through multiple apertures [9]. They can be classified into two types: vibrating (active) and static (passive) mesh nebulisers. The drug solution is loaded in a reservoir and in the static mesh nebuliser, a force is applied on the liquid to push it through the mesh [113]. In the vibrating mesh, the mesh vibrates and push the liquid through the pores [5]. Mesh nebulisers, compared to jet and ultrasonic ones, have increased portability and can provide higher drug doses to the patients [5], other advantages are the low shear stress produced and the possibility to produce different aerosols size, based on the manufacturing process of the mesh. Despite all these advantages, different challenges are associated with mesh nebulisers. For instance, the difficulty to deliver a viscous solution and consequently, the clogged mesh pores, which are of few microns order and the high cost of the device.

For all these inhalation therapies the main negative aspect is the low deposition efficiency of the drug in the targeted area [27]. SAW nebulisation technology offers many advantages that will be discussed at the end of the Chapter. Table 1.3 summarises the main inhalation devices on the market with their advantages and disadvantages.

1.10 Surface Acoustic Waves (SAW)

1.10.1 IDT and piezoelectricity

For a better understanding of the advantages of the SAW nebuliser compared to commercially available devices, a brief description of the SAW characteristics and ultrasonic atomisation is made. SAW devices are a relatively new technologies (90s) and still in development. There are many advantages of using SAW for medical purposes, especially in the gene therapy field, which are going to be illustrated in the following Section 1.11.1.

Interdigitated Transducer (IDT) represents the main part of the SAW nebulisation platform, it consists of pairs of gold fingers deposited onto a piezoelectric crystal. In this work Lithium Niobate ($LiNbO_3$) is used as the substrate. Piezoelectricity is the generation of an electrical charge as a result of applied mechanical stress. It is a linear effect and reversible. In the SAW nebuliser the inverse piezoelectric effect is used, where the formation of mechanical stress was caused by the application of an electric field [119]. The effect is caused by the relative motion of ions in the crystal structure, as a consequence of the changed dipole moment [120]. As shown in Fig. 1.13, only crystal without a centre of symmetry can exhibit piezoelectricity [119] because in centre-symmetric materials any motion from an ion is reflected by symmetry to an equal and opposite motion that cancels out the dipole moment [121].

SAWs are mechanical waves that travel along the surface of a piezoelectric material, which can be generated by an interdigitated transducer (IDT) [10], with an amplitude that decays exponentially inside the material [117].
SAWs propagate as Rayleigh waves, first described as a combination of a longitudinal and vertical shear components, Fig.1.14.

When a Rayleigh wave propagates on the surface of the piezoelectric material the particles in the solid move in elliptical paths, with the major axis of the ellipse perpendicular to the surface of the solid. As the wave propagates in depth of the material, the width of the elliptical path decreases [124]. The wave motion attenuates rapidly as the wave moves into the substrate up to 4-5 wavelengths [125]. SAW devices are commonly used as filters, oscillators and transformers that are based on the transduction of acoustic waves. Over the past years, SAW devices have been adopted for micro-scale fluid manipulation, capable of generating range of complex fluid transport phenomena, including mixing, centrifugation, pumping and nebulization [19] through the use of 1-100 MHz acoustic waves. Various microfluidic applications use SAW as a microscale fluid actuation mechanism [126]. The most attractive aspects of SAW employment is the efficient fluid-structural coupling, due to the confinement of the energy adjacent to the surface. The choice of using high frequencies (MHz) compares to lower frequencies (KHz)is due to the advantage of using high accelerations. Friend and Yeo in their review highlighted that for 10MHz frequency vibrations the acceleration of the fluid is over $10^7 m/s^2$, which allows the ejection of droplets from a SAW device [127]. Moreover, a MHz frequency device allows miniaturisation of the device.

1.10.2 Ultrasonic Atomisation and SAW nebuliser

Previous studies on ultrasonic atomisation have shown a correlation between the median diameter of the aerosol droplets, the surface tension of the liquid, the acoustic excitation

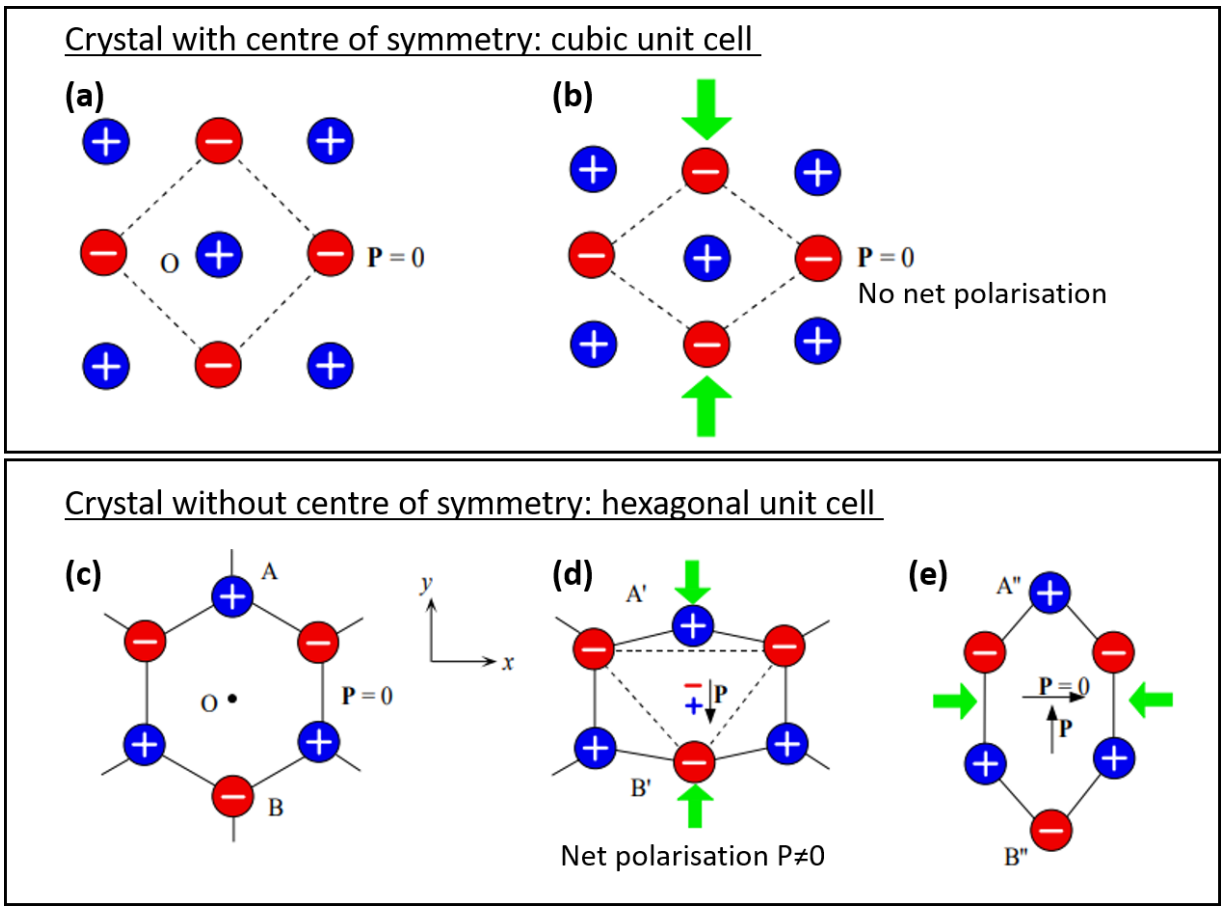

Figure 1.13: (a, b) Representation of a crystal structure with the centre of symmetry. (a) A cubic unit cell with a centre of symmetry is represented and in absence of applied force, the net polarisation is equal to zero. Without applying stress the centre of mass (c.m.) of the positive charges coincides with the c.m. of the negative charges. (b) A force is applied and the total polarisation is still null. Any motion from an ion is reflected by symmetry to an equal and opposite motion that cancels out the dipole moment. (c, d, e) Representation of a crystal structure without the centre of symmetry. (c) The hexagonal unit cell does not have a centre of symmetry, when unstressed the c.m. of the negative charges coincides with the c.m. of the positive charges, thus the net polarisation is null. (d) A force is applied along y, the charged in A and B position move in A' and B' position and their c.m. become shifted. (e) A force is applied in a different direction (x) and gives rise to a polarisation in other crystal directions. Figure adapted from [122].

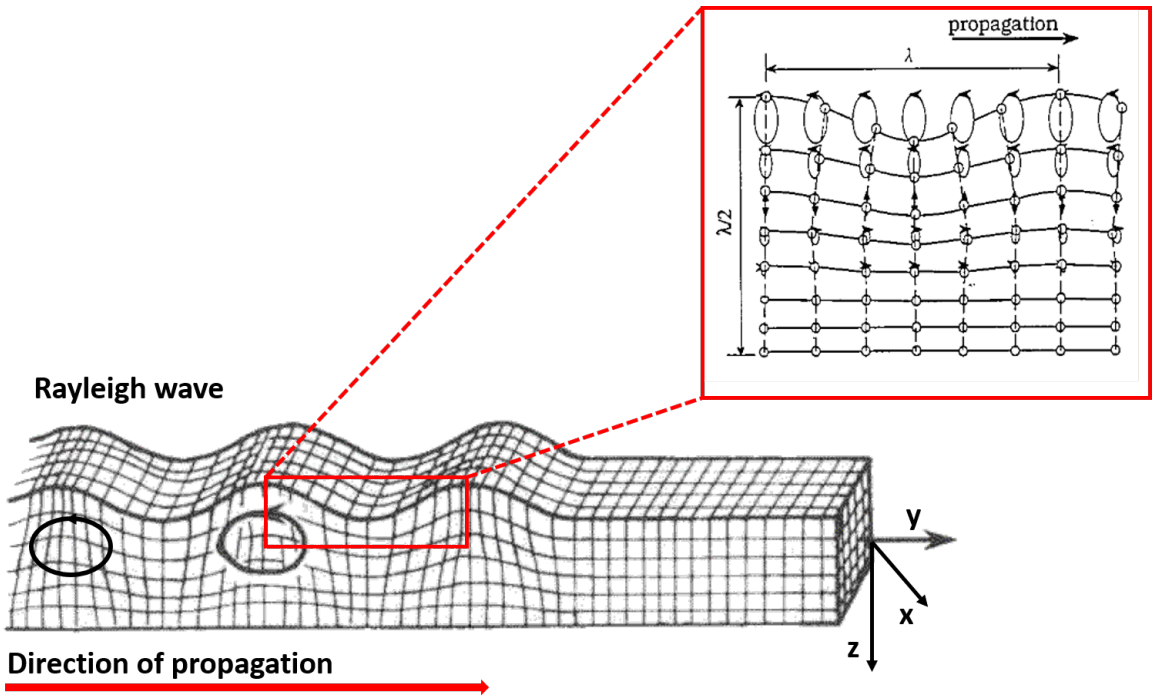

Figure 1.14: Propagation along the y-axis of a Rayleigh wave. Rayleigh waves are a type of surface waves made of longitudinal and vertical shear components, which make the particles in the solid moving in an elliptical motion. Figure adapted from [123], [16]. In the red rectangle a close up of the elliptical motion and the propagation of the surface wave.

frequency and wavelength of the surface waves formed on the liquid surface [128]. These studies used bulk acoustic waves with low ultrasonic frequency (< 1 MHz).

In 1831, Faraday reported the formation of standing waves on the surface of a fluid, when it is placed on a vertically vibrating plate. These small waves on the surface of the fluid are known as capillary waves. Capillary wavelength is described by [129]:

$$\lambda = (\frac{2\pi\sigma}{\rho {f_c}^2})^{1/3} \tag{1.11}$$

where λ is the wavelength, σ is the surface tension, ρ is the liquid density and f_c is the frequency of the surface waves on the surface of the liquid (i.e., capillary waves). Throughout this thesis, a small volume of liquid was used and waves on the surface of fluid are considered as capillary waves.

Based on the assumption that capillary waves are subharmonic Faraday waves [18], it was proposed that the frequency waves on the surface of the liquid are half of the excitation frequency and Lang proposed that equation (1.2) can be rewritten as:

$$D = C\lambda = C(\frac{8\pi\sigma}{\rho F^2})^{1/3} \tag{1.12}$$

where F is the excitation frequency, the relation $f_c = F/2$ was proved by Eisenmenger

[130], indicating that capillary waves oscillate at half of the excitation frequency.

The drop formation is based on the instability mechanism of the capillary waves [16], as their amplitude is growing [130], droplets are ejected into the air [128].

Recent studies suggested that the assumption on the capillary wave frequency (i.e., $f_c = F/2$) is not valid for high frequency excitation (> 1 MHz) [117]. This is explained with the fact that in early studied low frequencies in kHz range were used, which are comparable to the natural oscillation frequency of the liquid [117]. However, the relation between aerosol droplet size and capillary wavelength is well establish in the literature [117], [131], [118], [132].

In 1995, Kurosawa produced for the first time a mist of droplets using a surface acoustic wave transducer, where a mean diameter of the nebulised particles of 19 µm was obtained [16]. As described by Kurosawa, during the nebulisation the fluid was first spreading out into a thin layer and then the nebulisation occurred from the crest of the capillary wave. It was noticed that increasing power, the atomising rate increased. Also, an increase in frequency would induce a smaller device size and a decrease in the atomising rate [16]. Using a 10 MHz transducer, the overall generated droplet size distribution had two peaks, one at 40 µm and the other at 3 µm [16]. A transducer of 48 MHz was also employed, showing the same droplet size distribution with two peaks, but one at 11 µm and the other at 3 µm. A reduction of the largest peak from 40 µm to 11 µm was obtained, where the smallest group of droplets (3 µm) retained their size [133]. Therefore by using a higher frequency transducer, (i.e. 48 MHz instead of 10 MHz), did not bring advantages in terms of droplet size. A reduction of size from 40 µm to 11µm was noticed, but not enough for the particle to be within the clinically validated size range for pulmonary drug delivery. Moreover, the nebulisation rate was lower, reducing the delivered amount of liquid. If the liquid is loaded on the SAW propagating path, the SAW radiates its energy into the liquid [117]. From Giovannini *et al.*, the energy (W) required to disperse a volume of liquid into smaller droplets is [134]:

$$W = (\sigma N)(4\pi r^2) = \sigma(\frac{V}{4/3\pi r^3})(4\pi r^2) \tag{1.13}$$

where, V is the volume of the atomised liquid, r is the radius of the droplets, N is the number of droplets and σ is the liquid surface tension.

Chono *et al.* in 2004, used a filter paper to obtain a stable nebulisation, in order to keep a thin liquid film. Experimental results showed that the angle and the height of the mist depend on the SAW input power. As shown in Fig. 1.15, due to the different propagation speed of the SAW in the two medium, water and lithium niobate, once the wave reached the liquid, it refracts into the droplet of liquid, following a specific angle,

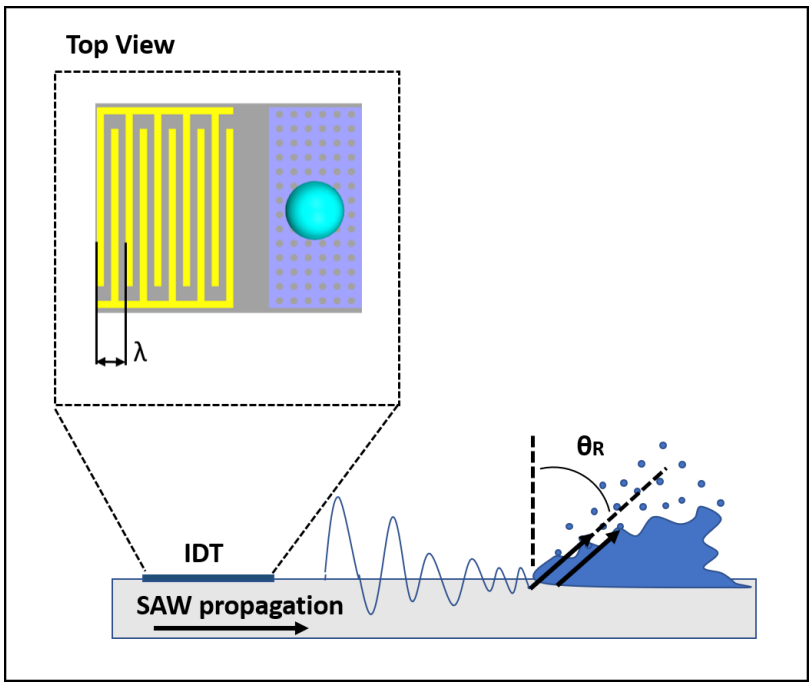

Figure 1.15: SAW propagation into a droplet of liquid. SAW diffracts into the droplet of liquid, following a specific angle, called Rayleigh angle [131]

called Rayleigh angle:

$$\theta_R = sin^{-}1(c_w/c_s) \tag{1.14}$$

where $c_w = 1485$ m/s is the speed of sound in water and $c_s = 3965$ m/s is the speed of sound in lithium niobate.

Further studies were made by Qi *et al.*, where experimental results values showed a weak dependency between droplet size and frequency, especially for frequency above 10 MHz [135]. The droplet size appeared to be related to a balance between the capillary stress, which tends to pull the droplets out from the liquid bulk and the viscous force [135], which represents the fluid resistance to the flow. The explanation of the independence of the droplet size and the driving frequency as previously claimed [16], [133], [20], relies on the fact that SAW nebulisation uses much higher frequency ($F > 10$ MHz) compared to the ultrasonic nebuliser ($F < 1$ MHz), for which the Kelvin's and Lang's equations were formulated. The capillary destabilisation and breaking up process depends on the capillary-viscous resonance [135]:

$$f_c \sim \frac{\sigma}{\mu R} \tag{1.15}$$

where f_c is the resonant frequency of the capillary waves, μ the viscosity of the liquid and R is the radius of the droplets. As a consequence of the capillary-viscous resonance, the capillary wavelength, which determines the size of the aerosols, depends on the properties of the liquid. Different liquid with various surface tensions and viscosities produced different size distributions [117]. The efficacy of SAW nebuliser has been demonstrated

for proteins [136], nucleic acids [137] and pulmonary stem cell delivery [138]. Cortez-Jugo at al. [139] delivered monoclonal antibody to A549 cells, by incubating the cell suspension with a nebulised solution of the antibody. Rajapaksa *et al.* [137], nebulised a 75 µg of DNA plasmid tagged with a fluorescence label solution and added it to lungs tissue. Results showed a low intensity of the fluorescent plasmid after the incubation and the demonstration of the DNA entry in the cell's nucleus was not proven [137]. Alhasan *et al.* [138], used SAW to nebulise stem cells, they demonstrated that SAW does not have a deleterious effect on the cells, the effective delivery was not shown, having also the size of the cells larger than the optimal size range for lungs absorption, between 1-5 µm in diameter [102].

To summarise, the main advantages of using a SAW platform, as a nebuliser for pulmonary drug delivery system, are the low-cost fabrication, made it possible with the use of silicon superstrates over piezoelectric materials [22], the relatively low power consumption (1-2 W), the reduced quantity of the sample (µl) and the control over the aerosol droplet size [132].

1.11 SAW Nebuliser in Gene Therapy

1.11.1 Nucleic Acids and Gene Therapy

Nucleic acids are important macromolecules for the storage, transmission and expression of genetic information [140]. Over the past two decades, nucleic acids have been used in biomedical research for the development of gene-targeted therapies, for their ability to modulate gene expression both at the transcriptional and post-transcriptional levels, in the form of DNA sequences or small interference RNAs respectively [141], [142]. The introduction of nucleic acids into cells can target defective genes responsible for numerous diseases [143], [144]. Individual genes code for specific proteins that perform functions as widespread as the regulation of body's muscle and organ tissue, receptors and enzymes [145]. Gene therapy represents a promising potential treatment for numerous diseases including immuno-deficiencies, haemophilia, Parkinson's disease, cancer and even some viral infections such as those with HIV [146]. There are more than 1800 monogenic hereditary disorders that could be addressed by the replacement of a missing or defective gene [147]. The first attempt to correct a hereditary disorder (in this case, adenosine deaminase deficiency) was undertaken in 1990 by Blaese and Anderson using a gene transfer method [143], [148]. Since then, there have been 95 approved trials of gene transfer therapy. Currently, gene therapy is mainly considered for diseases for which alternative modes of treatment are unknown [149]. Although it is still considered experimental [150], further research will develop gene therapy into a new effective tool for modern medicine. The main advantages of using nucleic acids as therapeutics are their high specificity, versatility,

low toxicity, and low molecular weight, which facilitates their cellular uptake [151], [152]. Nucleic acid therapy includes the use of antisense nucleotides, aptamers and small interfering RNAs (siRNAs), [153]. Antisense nucleotides are either DNA or RNA sequences. An antisense oligonucleotide-based therapeutic agent for the treatment of cytomegalovirus retinitis (CMV) has been approved by the FDA and is the first of its kind. CMV causes an inflammatory viral infection of the eye and belongs to the same family as the herpesvirus [154]. It often infects immunocompromised patients, causing serious diseases like retinitis, hepatitis, colitis and pneumonia [155]. The oligonucleotide, Fomivirsen (Vitravene), has a specific sequence that is complementary to that of the viral mRNA, which is transcribed from the main transcriptional unit of CMV. Thereby, it blocks the expression of the virus in CMV-infected cells [141], [156]. Aptamers are short sequences of nucleic acid that are 15-80 nucleotides in length. Their ability to target molecules with high specificity and affinity is attributable to their unique 3D structures. Recently, they have been studied for targeted delivery into various types of cell, in combination with siRNAs [157]. An siRNA is a double-stranded RNA molecule consisting of 20-25 base pairs, that functions via the RNA interference pathway.

1.11.2 Mechanism of Small Interfering siRNA Activity

RNA has a similar structure to DNA, except for the presence of a ribose sugar residue instead of deoxyribose. It also differs from DNA in that it is typically single-stranded and does not contain thymine, which is replaced by the base uracil [152]. In order to explain the mechanism by which siRNAs exert their activity, the process of gene expression consisting of transcription and translation is now described. A gene encodes for a specific protein, which has a specific function in cells. Firstly, RNA is synthesised from the DNA sequence (transcription) [158]. This process catalysed by RNA polymerase and consists of three steps: initiation, elongation and termination. [159].

RNA polymerase binds with the promoter sites on the DNA sequences, which are generally towards the 5' end, and then separates the double-stranded DNA to produce a single-stranded template for gene transcription. An RNA strand of a sequence complementary to that of the DNA template is formed (elongation); this is the messenger RNA (mRNA) [160]. During elongation, the RNA polymerase selects the correct ribonucleoside triphosphate and catalyses the formation of a phosphodiester bond, building an RNA molecule from bases complementary to those of the DNA template. The RNA polymerase keeps building the RNA transcript until the termination sequence in the gene is detected, as showed in Fig. 1.16. The mRNA strand is then detached from the DNA template.

Once the mRNA is detached from the DNA, translation can begin. The sequence of an mRNA code for a specific protein. The mRNA is translated at ribosomes into a sequence of amino acids (polypeptides), which then folds into an active protein and

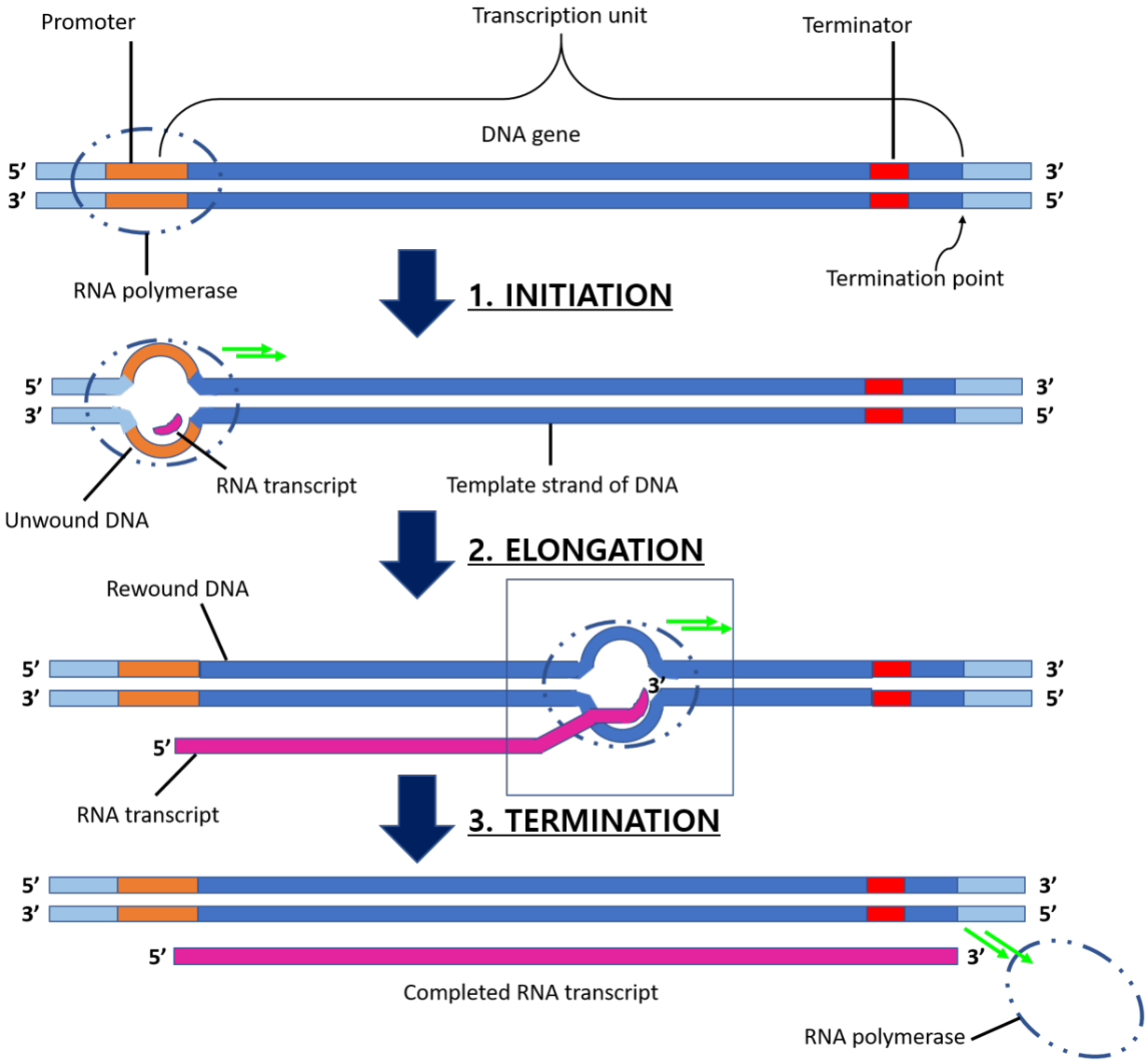

Figure 1.16: RNA synthesis. The process consists of three steps: initiation, elongation and termination. During the initiation process, RNA polymerase binds with the promoter sequence and unwinds the double-stranded DNA. In the following elongation phase, an RNA molecule of a sequence complementary to that of the single-stranded DNA template is formed, the mRNA. Elongation continues until the RNA polymerase detects the termination sequence.

performs its functions in the cell [161]. The mRNA is read based on the genetic code, in which 3 bases constitutes a codon and each codon codes for a specific amino acid. There are also non-coding RNAs: functional RNA molecules that are transcribed from DNA, but not translated into a protein. An example is small interfering RNA (siRNA)[162]. siRNAs are short double-stranded RNAs that are 20-25 base pairs in length, and that have been extensively researched in recent years [163], [164], [152], due to their high specificity in inhibiting the expression of specific mRNAs. They do this by inducing the RNA interference (RNAi) pathway, which prevents protein translation [165]. RNAi is a natural mechanism of sequence-specific gene silencing, playing an important role in gene regulation [166]. Cells use short double-stranded RNA (siRNA) to recognise mRNAs that are then destroyed and unable to be translated into proteins [167]. Specifically, a double-stranded RNA (dsRNA) is processed into an siRNA by the RNase II enzyme Dicer [168], as shown in Fig. 1.17. The siRNA is then loaded into an RNA-induced silencing complex (RISC) [169]. Part of the RISC is the endonuclease AGO2, which cleaves the sense strand (passenger strand) of the siRNA while the antisense strand (guide strand) remains associated with the RISC [168]. The guide strand, as part of the RISC, can scan and bind with complementary mRNA. AGO2 then cleaves the bound complementary mRNA. Since the cleaved mRNA is no longer recognised by the cells, it is degraded. Thereby, the gene from which that mRNA was transcribed is silenced [168] [163].

siRNA has huge potential for use as therapeutic agents, but getting them into cells remains a significant challenge. As mentioned previously, nucleic acids are negatively charged, and so they cannot easily pass through the cell membrane unless a carrier is used [168]. Nanoparticles and liposomes are commonly used as carriers since both are able to efficiently deliver siRNAs whilst protecting them from degradation [170].

siRNA Delivery: Extracellular and Intracellular Barriers

Fifteen years after the discovery of the RNAi pathway, research to determine the best way to deliver siRNA into cells is still ongoing [171]. An ideal siRNA carrier should overcome extracellular and intracellular barriers, be biodegradable and biocompatible, and be neither cytotoxic nor immunogenic [172]. It must also protect the nucleic acid from degradation by nucleases, evade degradation by macrophages, and be reversibly bound so that the siRNA can be released at the target area. [151]. It should also facilitate cellular uptake and promote endosomal escape [168]. To be effective, siRNAs should be delivered into the cytoplasm. The barriers to the delivery of the nucleic acids depend on the type of cell targeted, and the route of administration. Systemic administration of an siRNA is most common, but the siRNA is thereafter degraded by nucleases and excreted through the kidneys, limiting its bioavailability [173]. Local delivery of siRNA to lung cells can be non-invasive and avoids interaction with the serum and consequent degradation [171].

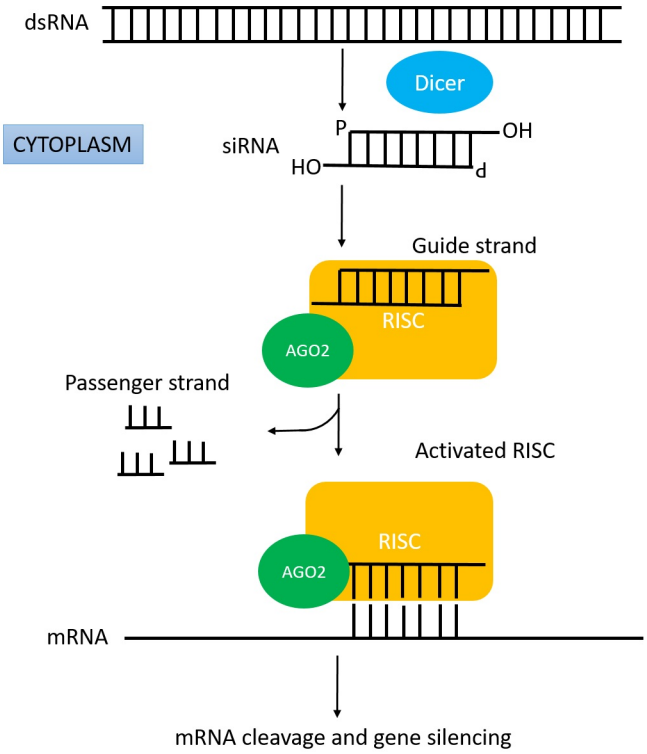

Figure 1.17: Double stranded RNA is processed into an siRNA by the RNase II enzyme Dicer. The siRNA is loaded into the RISC. The endonuclease AGO2 cleaves the sense strand of the siRNA, while the antisense strand remains associated with the RISC. The antisense strand then binds with complementary mRNA, then AGO2 cleaves the bound complementary mRNA.

Pulmonary epithelial cells are the key target for gene knockdown therapies against diseases such as cystic fibrosis, COPD, and asthma [174], in which direct access to the lungs and pulmonary circulation is important [175]. In the lungs, alveolar macrophages represent the main barrier to siRNA delivery. When siRNA/carrier complexes reach the cell they have to pass through the cell membrane, overcoming the extracellular barrier primarily through endocytosis. Once within the cell, they have to escape the endosomal compartment before being degraded by lysosomes [176]. Different means of facilitating endosome escape can be adopted, including membrane fusion, proton sponges, and inserting fusogenic peptides. [176].

Phospholipid and Nucleic Acid Complexes

Lipoplex, which is a complex of nucleic acid and lipids [177], can promote endosomal escape owing to its ability to fuse with the endosomal membrane [178]. It is also proposed that the phospholipid DOPE can aid release due to transforming the bilayer into an inverted hexagonal structure [179]. As discussed previously (Chapter 4), lipids adopt different topologies based on their head groups, fatty acid chains and saturation [34]. Before they can enter the cells and promote endosomal escape, the particles or siRNA/carrier com-

plexes have to first of all actually reach the target cells deep in the lungs and be deposited around them. Deposition of siRNA complexes in the lungs depends on the aerodynamic diameter of the particles in which the siRNAs are formulated, as described in Chapter 1. Only particles between 1 and 5 µm in size can be effectively absorbed in the lungs [102]. The ability to control aerosol size is a major advantage of using surface acoustic waves for nebulisation. The production *in situ* of nucleic acids' carriers within the optimal size range is a promising development in the progress towards making a targeted pulmonary drug delivery platform capable of delivering nucleic acids to target cells.

1.11.3 Nucleic Acid Carriers

The cell phospholipidic membrane is relatively hydrophobic, and its amphipathic structure restricts the entry of large and charged molecules [180]. A nucleic acid is hydrophilic and negatively charged due to the phosphate group backbone. To be able to cross the cell membrane, they, therefore, need a carrier [178]. These carriers (or vectors) are divided into two main categories: viral and non-viral vectors.

Viral Vectors

Viral vectors are highly efficient in the delivery of nucleic acids to specific types of cell. The main challenges they present are avoiding a response by the body's immune system and eliminating the pathogenicity of the virus [181]. Different type of virus is used for various applications, such as retroviruses and adenoviruses. However, even if the viruses are modified to remove their pathogenicity, there remain some risks associated with their use as vectors. The administration of a modified virus can cause the body to develop an immune response if it is seen as a foreign invader. An example of the failed employment of viruses in gene therapy was the clinical trial of Jesse Gelsinger in 1999 [150], which increased ongoing concerns about the safety and ethical issues surrounding this approach.

Non-Viral Vectors

Non-viral vectors, although less efficient than viral vectors, present several advantages, including lower pathogenicity, lower risk of insertional mutagenesis, a DNA mutation caused by the insertion of base pairs, as well as lower cost and easier production [182]. Non-viral methods of delivery can be divided into two groups: physical methods, or multicomponent carriers such as positively charged phospholipids and polymers [183]. Among physical methods, electroporation is the most commonly employed. Its concept relies on the use of electric pulses to temporarily create pores in the cell membrane [183]. Other methods like sonoporation (ultrasound) and hydrodynamic (pressure) delivery are less common because cell targeting needs to be specific [184]. Specific ligands and receptors can be added into

the formulation in order that the complex may be delivered only to specific cells, but this increases the difficulty of the process. Liposomes, which can either encapsulate nucleic acids or bind to them via electrostatic interaction, are one of the oldest nanocarriers used in gene therapy [185]. In the work detailed in this chapter, cationic liposomes were used as a carrier to deliver DNA luciferase plasmids and GAPDH siRNA into the A549 cell line.

1.11.4 Cationic Lipid-Nucleic Acid Complexes and Cellular Uptake

Cationic lipids are one of the most commonly used non-viral nucleic acid carriers, because of their non-immunogenicity, low toxicity, ease of production and their ability to carry nucleic acids into cells [186]. They are used for both gene delivery (DNA) and gene silencing (siRNA), despite their transfection efficiencies remaining low compared to viral vectors [186]. It is known that charged molecules are not able to cross the membrane, due to its hydrophobic core. Nucleic acids thus need a carrier to balance the charge, in order to enter into a cell's nucleus or cytoplasm [180]. Cationic liposomes consist of at least one positively charged phospholipid, which forms a complex with negatively charged nucleic acids through electrostatic interactions, forming a lipoplex. Electrostatic interaction is attractive or repulsive interactions between molecules having different charges. It is a non-covalent interaction, meaning that it does not involve the sharing of electrons. It is critical in maintaining the three-dimensional structure of molecules such as proteins and nucleic acids [187]. The most commonly used cationic phospholipids are N-[1-(2,3-silyloxy)propyl]-N,N,N-trimethylammonium chloride (DOTMA) and N-[1-(2,3 Dioleoyloxy)propyl]-N,N,N-trimethylammonium chloride (DOTAP). For a successful delivery, it is also important to optimise the ratio of lipids to DNA/RNA. It is suggested that an excess of lipids can entrap the nucleic acids between the liposomes' lamellae [185], while increasing the amount of free DNA for example, plasmids were found close to the lipids' vesicles. In order to find the optimal ratio between nucleic acids and carriers, agarose gel electrophoresis was employed. For cationic liposomes, both endocytosis and fusion were proposed as nucleic acid uptake mechanisms. Understanding of the mechanism of transfection and the interaction between the nucleic acid complexes and cell components are still lacking. The endocytic pathway is known to be a major mechanism by which biological agents such as DNA and siRNA are taken up by cells. Nucleic acid-lipid complexes are trapped in endosomes and then degraded by specific enzymes in the lysosome [176]. Part of the cellular membrane starts to bend inside the cell in order to form an endocytic vesicle, containing the substance to be internalised such as an siRNA/DNA complex. Once the endosome is formed inside the cell, the contents have to achieve endosomal escape in order to reach the cytoplasm or nucleus [188]. The size of the carrier is a key parameter in the endosomal escape. Carriers of diameter $d \leq 100$ µm have been reported to accumulate better in tumours, hepatocytes

and inflamed tissues, whereas larger particles are taken up by the reticuloendothelial system [188].

1.11.5 SAW Nebulisation of Nucleic Acids

Jet and ultrasonic nebulisers do not facilitate efficient nucleic acid delivery. They do not allow tight control over the size of the aerosolised droplets, and the high shear stress generated during nebulisation can damage the RNA/DNA material [116]. Yeo's group has been working on SAW drug delivery in the lungs, testing the nebulisation of plasmid vaccines in a large animal model [137]. In their experiments, 300 µg/mL of DNA plasmid bound with yellow fluorescent protein were delivered through SAW nebulisation. Images from confocal microscopy showed that the pDNA was successfully delivered, thus proving the suitability of SAW. However, they found that the efficiency of delivery could be increased by using a vector. As previously mentioned, a positively charged carrier would be a good approach to helping the DNA to enter the cell's nucleus. In the results section, Fig. 6.8, it is shown that naked DNA (without the presence of a carrier) is less efficiently transfected than that within a lipoplex. Here lies the necessity of creating a unique platform which will not damage the compound to deliver and at the same time can form the drug carrier to guide the compound inside the cell.

Chapter 2

Materials and Methods

This Chapter describes the materials, the methods and the different experimental setup used throughout the entire thesis. Microfabrication processes to produce the SAW nebuliser were carried out at the James Watt Nanofabrication Center (JWNC). Gel electrophoresis, western blot and cell culture (methods used in Chapter 6) were carried out at the University of Hong Kong.

2.1 Materials

General chemicals, phospholipids and kits were obtained from Sigma-Aldrich (Merck Group) unless otherwise stated. $1,2-dioleoyl-sn-glycero-3-phosphoethanolamine-N-lissamine$ rhodamine B sulfonyl (DOPE-RhB) was purchased from Avanti Polar Lipids, Inc. (USA) and used without further purification. Herring Sperm DNA and Luciferase assay system were purchased from Promega For *in-vitro* gene expression, DNA luciferase plasmid was purchased from Aldevron (USA). 30% Acrylamide/Bis Solution 29:1 and dye reagent concentration for protein assay were purchased from Bio-Rad (USA) Lipofectamine 2000 was purchased from Invitrogen (USA) and used as a transfection carrier control. Silencer GAPDH siRNA Human and Silencer select negative control siRNA were obtained from Ambion. Gel loading capillaries of 25 mm length were obtained from Labcon (USA) The A549 cell line was purchased from ATCC (Manassas, VA, USA). Cells were grown in the cell culture medium DMEM (Dulbecco's Modified Eagle's medium, Gibco, ThermoFisher Scientific), supplemented with 10% (v/v) FBS and 1% (v/v) antibiotic-antimycotic (ThermoFisher Scientific). A549 cells were seeded in 24 well-plates (Corning Costar TC-Treated Multiple Well Plates, $d = 15.6$ mm) at a concentration of $0.5 \times (10)^5$ cells/mL in 1 mL medium, and in single well-plates (Nunc Cell Culture/Petri Dishes, $d = 35$ mm) at a concentration of $0.8 \times (10)^5$ cells/mL in 2 mL medium. Conductive paint, Electrodag 1415, was purchased from Agar Scientific (UK). 4-inch wafers of Lithium Niobate 127.8° Y-cut X-propagation to produce the IDT and silicon wafers of 200, 270

and 500 µm were obtained from University Wafers (USA).

2.1.1 Buffer Solutions

All stock solutions and subsequent buffers can be found in Table 2.1 and were made using deionised (DI) water and autoclaved before use. A TAE buffer solution made up of Tris base, acetic acid and EDTA was employed for running gel electrophoresis. It is commonly used for this purpose due to its low ionic strength and buffering capacity. A solution with high ionic strength can reduce the current carried by the sample, thus decreasing the rate of migration. Buffering is important because pH can also affect the migration rate [189].

2.2 Microfabrication of Interdigitated Transducer

2.2.1 L-Edit IDT Design

As mentioned in the Introduction, the IDT is the main part of a SAw nebuliser, which needs to be designed to work at a specific resonant frequency. The Tanner L-Edit IC Layout (Mentor Graphics, US) software was used to design IDTs for this study, as represented in Fig. 2.1. An IDT is made of two interlocking comb-shape arrays of metallic electrodes. The resonant frequency of the IDT is determined by the distance between fingers and speed of sound in the substrate. The IDT was designed to have a resonance frequency at 9.7 MHz with 20 pairs of fingers, composed of 10 nm of titanium and 70 nm of gold deposited onto the substrate. By using the following equation:

$$\lambda = 4d = \frac{c}{f} \tag{2.1}$$

where d is the spacing between the metal fingers of the IDT, c is the speed of sound in the substrate (Lithium Niobate, $c = 3980$ m/s) and f is the resonant frequency of the IDT. IDTs with different resonant frequencies were designed by varying the wavelength from 800 µm, 400 µm and 200 µm with resonant frequencies of 4.9, 9.9 and 19.9 MHz, respectively. Highest nebulisation rate was obtained by the IDT with a resonant frequency of around 9.7 MHz, which was used as a reference in all the experiments in this thesis. Higher frequency IDT dispersed power through heat (IDT is subjected to high temperature), while lower frequency IDT needed a higher power to obtain an effective nebulisation rate.

2.2.2 Photolitography

Lithium Niobate 127.8° Y-cut X-propagation, a piezoelectric non-symmetric crystal, was used as a substrate, due to its high electromechanical coupling efficiency [121]. The mi-

Buffer Name	Composition
SDS-Page Lower Buffer (1.5M Tris/HCl, 0.4% SDS)	18.16 g Tris base 0.4 g SDS pH to 8.8 with HCl. Final volume of 100 ml with DIW The solution was filtered and stored at 4C
SDS-Page Upper Buffer (1.5M Tris/HCl, 0.4% SDS)	6.06 g Tris base 0.4 g SDS pH to 6.8 with HCl. Final volume of 100 ml with DIW The solution was filtered and stored at 4C
SDS-Page Running Buffer (10x)	30.30 g Tris base 144 g Glycine 10 g SDS pH should be around 8.3 Final volume of 1000 ml with DIW.
Blotting Buffer (1x)	100 ml 10x blotting buffer 700 ml DIW 200 ml methanol
Tris Buffered Saline, TBS (10x)	24.22 g Tris (0.2 M) 87.83 g NaCl (1.5 M) pH to 7.4. Final volume of 1000 ml with DIW.
Lower Gel (10%)	3.4 ml of 30% Acrylamide Bis 2.5 ml of SDS-Page lower buffer 4.1 ml DIW 0.1 ml of 10% APS 0.01 ml of TEMED.
Upper Gel	0.65 ml of 30% Acrylamide Bis 1.25 ml of SDS-Page upper buffer 3 ml DIW 0.03 ml of 10% APS 0.02 ml of TEMED.
Gel loading dye	0.2 g bromophenol blue 6 ml of 50% glycerol 4 ml of DIW

Table 2.1: List and compositions of buffers used mainly to make gel electrophoresis and western blot. Protocols used were rearranged from Dr. Michael Chow, the University of Hong Kong.

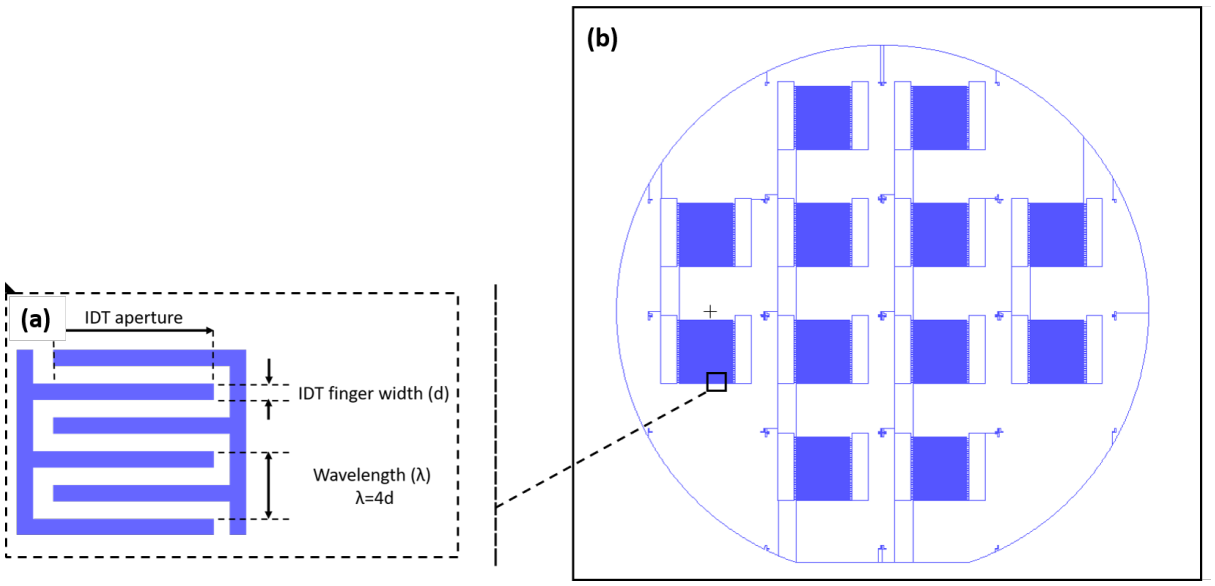

Figure 2.1: (a) Zoom in of the fingers structure of an IDT. The main parameters are shown in the image: IDT aperture, IDT finger width (d) and the wavelength (λ) of the surface wave. (b) Mask designed on L-Edit for IDTs. After cleaning the substrate and spinning of the photoresist, the mask is placed on the substrate. The mask alignment and then UV hard exposure (nitrogen pressure under the substrate) for 4 s, were carried out to lithographically define the electrode pattern.

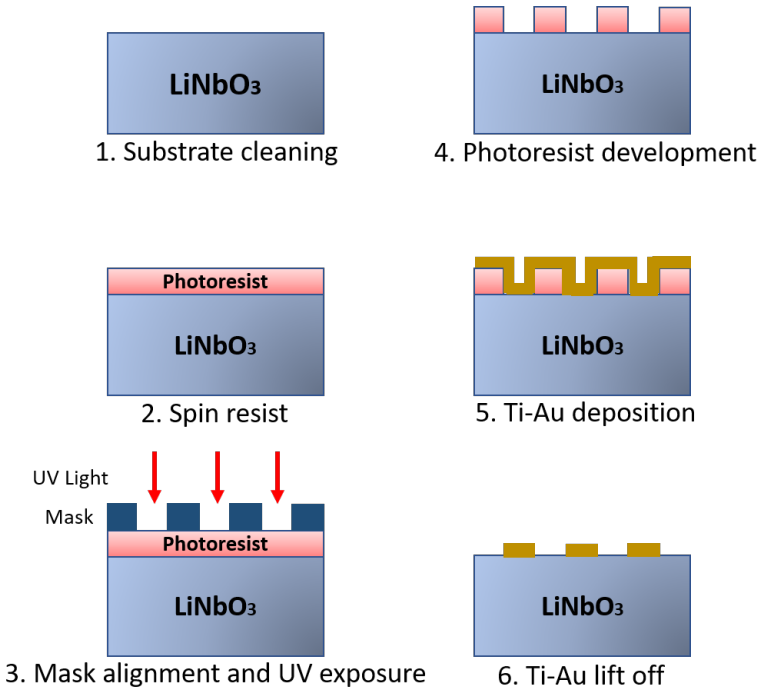

Figure 2.2: IDT Microfabrication processes: 1. $LiNbO_3$ cleaning, 2. Photoresist spinning on $LiNbO_3$, 3. Mask alignment and UV exposure to remove the photoresist exposed to light, 4. Photoresist development, 5. Metal evaporation and deposition, 6. Metal lift-off.

crofabrication process, carried out in James Watt Nanofabrication Center (JWNC), is depicted in Fig. 2.2 and a 4-inch wafer of $LiNbO_3$ was processed as described below:

1. Substrate was cleaned in three steps of 5 minutes inside an ultrasonic bath with Opticlear, acetone, and methanol. The cleaned substrate was consequently rinsed with RO water and dried with nitrogen.

2. Positive photoresist S1818 was spun on the cleaned substrate at spinning speed of 4000 rpm for 30 s, forming a 1.8 µm thick photoresist layer. The sample was then baked at $T = 100°C$ for 3 minutes.

3. The coated substrate is then patterned using an MA6 Mask Aligner(Karl Suss). The substrate was exposed to UV light for 4 s using the designed mask (Fig. 2.1) as shown in Fig. 2.2, stage 3.

4. The exposed substrate is developed with the recommended developer for S1818 (Microposit MF-319) for 75 s. The sample was then subjected to the plasma asher, to remove the traces of resist on the substrate.

5. Metal deposition of 10 nm of Titanium and 70 nm of Gold was completed with Plassys IV (electron beam evaporation).

6. The final stage is the photoresist lift-off (Fig. 2.2, stage 6), that was completed by leaving the substrate in acetone for 1 hour followed by rinsing with reverse osmosis (RO) water and drying with a nitrogen gun.

Gold is selected for IDTs as a preferred metal due to its higher conductivity and corrosion resistance and a thin layer of titanium provides better adhesion between substrate and gold.

2.2.3 Characterisation of IDTs

To check the IDTs' reflection and the working frequency, a network analyser was used. In order to understand the concept of high-frequency network analysis, which involves incident, reflected and transmitted waves travelling along a transmission line, a comparison with a light wave, that travels through an optical lens can be made [190].

When the light hits the lens, part of it can be reflected, part continues to travel through the lens and part can be absorbed, if the lens is made of a lossy material, the same can occur in a transmission line [191]. The resonant frequency of IDTs was found using a network analyser (Agilent Technologies E5071C ENA series, USA).

A network analyser measures parameters of electrical networks, which can be seen as a black box interacting with other circuits through ports. It is usually composed of

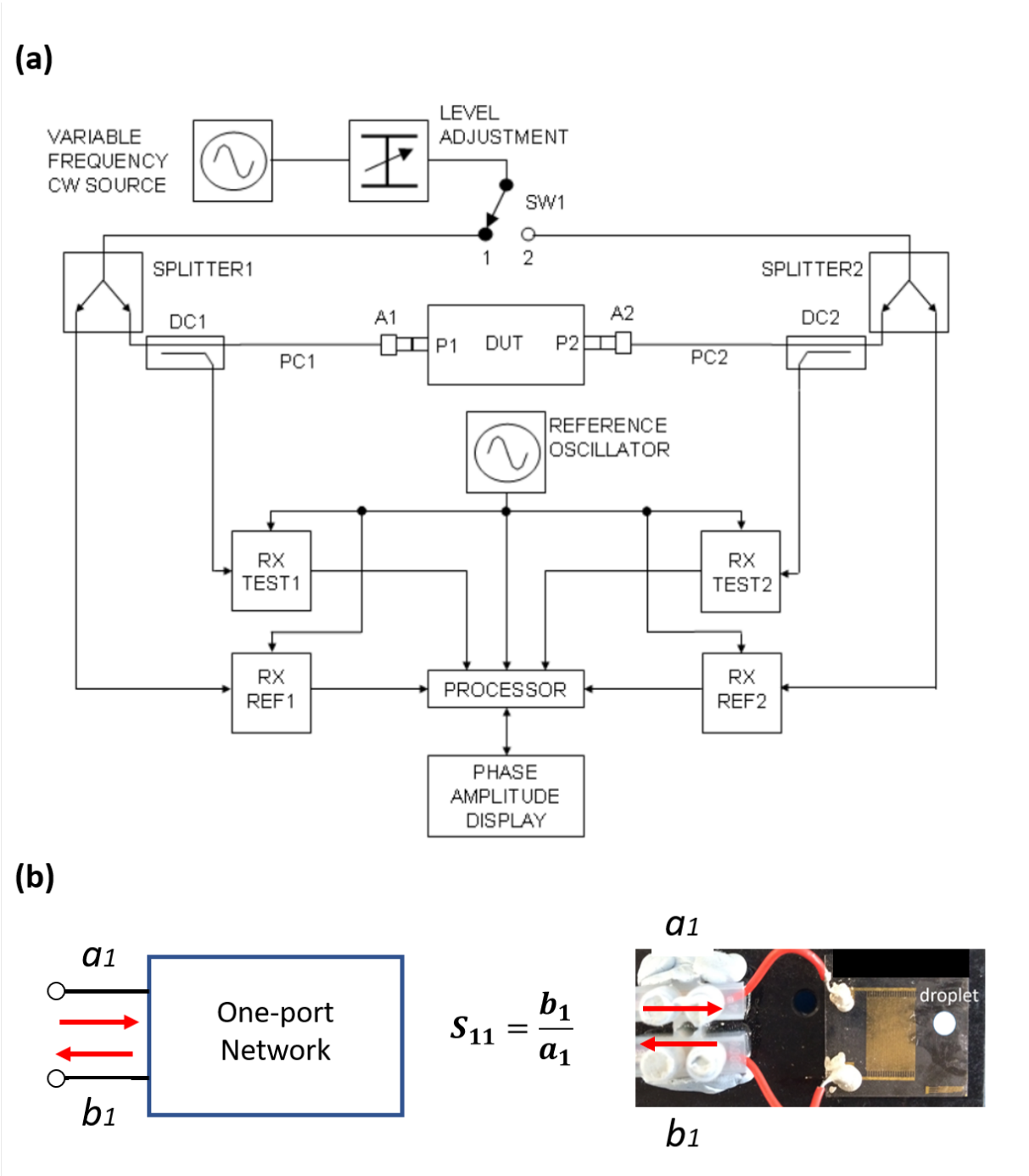

Figure 2.3: (a) Block diagram of a 2-port network analyser, showing the main components. The 2 ports of the DUT are denoted as P1 and P2. The switch SW1 indicates the direction where the signal will pass, in this case, will go through the port 1 of the DUT, and the parameters S_{11} and S_{21} can be measured. (b) The IDT results as a one-port network, where a network analyser was used to send a signal to the one-port network and evaluating the reflected signal, the S_{11} parameter can be evaluated.

a test set, which routes the output from the signal generator to the device under test (DUT), a signal generator, a receiver and a display. The circuit in Fig. 2.3 shows the main components of a 2-port network analyser. P_1 and P_2 are the 2 ports of the DUT. In Fig. 2.3 the switch (SW1) directs the test signal to the port P_1. From SW1 the signal goes to a splitter, which is dividing the signal to a reference channel and to P_1through a directional coupler DC1.

Directional couplers are most frequently constructed from two coupled transmission lines set close enough together such that energy passing through one is coupled to the other.

To characterise a device, the network analyser sends a signal with an amplitude and phase to the DUT and measures the amplitude and phase of the reflected signal and the output signal. Using the ratio between the incident, the transmitted and the reflected signal, the scattering parameter can be evaluated.

Scattering parameters (S parameters) describe the electrical behaviour of linear electrical networks when travelling currents and voltages in a transmission line encounter a discontinuity, caused by the insertion of a network in a transmission line.

The network is then characterised by a signal matrix which can be used to calculate its response to the signal applied to the ports. For an N-ports network, a matrix of N-dimensions and N^2 elements can be built. In the case of IDTs, only one port is present, therefore the parameter of interest is only one, S_{11}, which is also called input port voltage reflection coefficient (Fig. 2.3). As from Fig.2.4, when the amplitude is zero ($S_{11} = 0$) then all the power is reflected and nothing goes through the IDT, and the resonance frequency can be found for the lowest value of S_{11}.

A parameter that can be also evaluated using the network analyser is the characteristic impedance of a transmission line (Z_0), connecting devices with same impedance reduces the signal reflection and maximise the power transfer from the device to the IDT. Therefore, a frequency with an impedance of $50 \pm 0.5\ \Omega$ was chosen as optimal frequency. The Smith Chart on the network analyser was used to check the impedance at specific frequencies.

2.3 Microfabrication of the Silicon Chip

Cylindrical cavities were produced on a silicon wafer of 270 µm thickness. The choice of the thickness was made, after trying out a 500 µm thickness wafer, which was dumping the power and was too thick to be etched, and a 200 µm thickness one. The latter was too thin and during the etching process, all the material was removed, leaving only some part of the chip. A dry etch process was carried out to remove the material to form cylindrical cavities of diameters: 100, 200, 400, 600, 800 and 1500 µm.

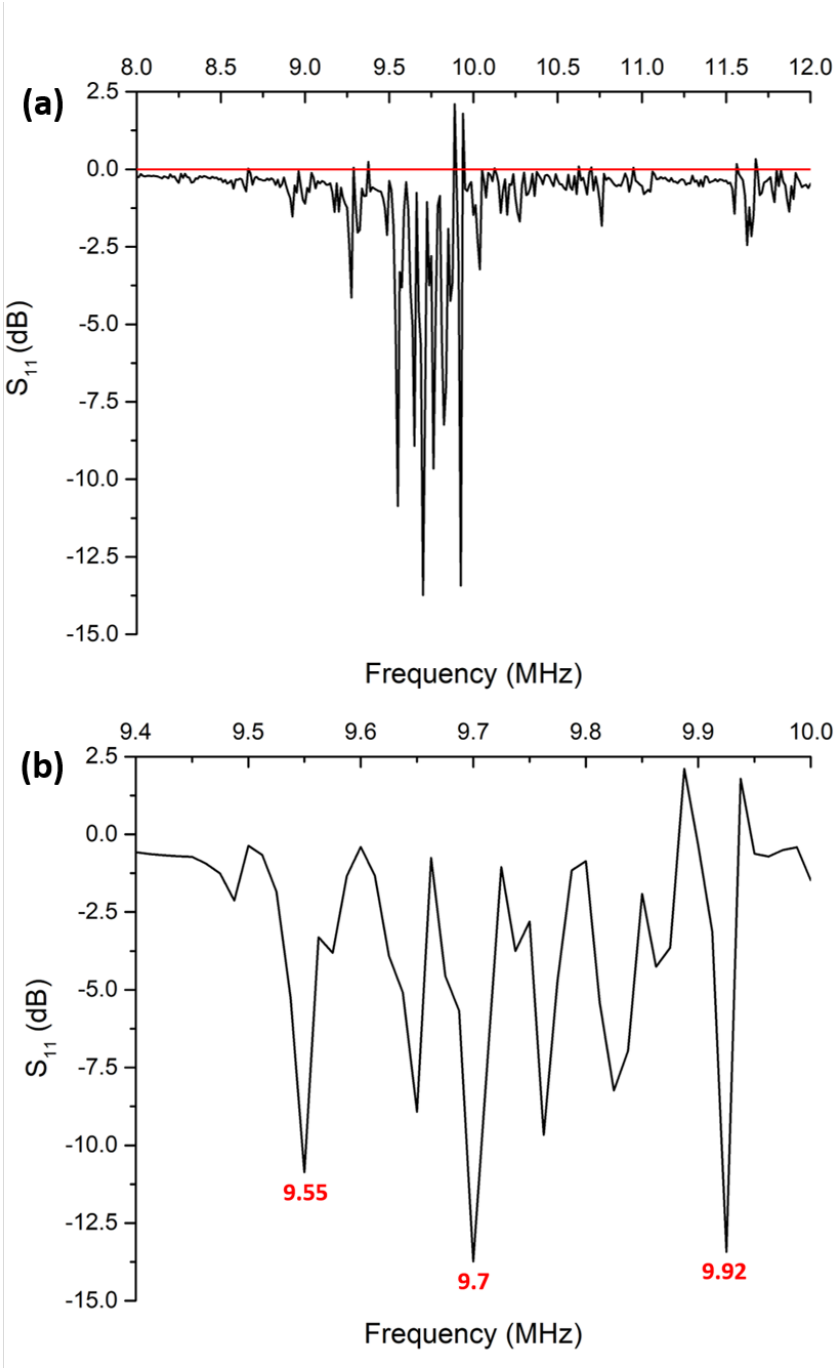

Figure 2.4: From the network analyser (a), (b), the evaluation of S_{11} was made, finding out that for the specific IDT design, the resonance frequency was of 9.7 MHz. Where the amplitude is zero, the test signal sent from the network analyser to the IDT is completely reflected. Oscillations are due to the noise of the environment. (a) Frequency range from 8 to 12 MHz. (b) Zoom in, frequency range from 9.4 to 10 MHz, the maximum amplitude is found around 9.7 MHz.

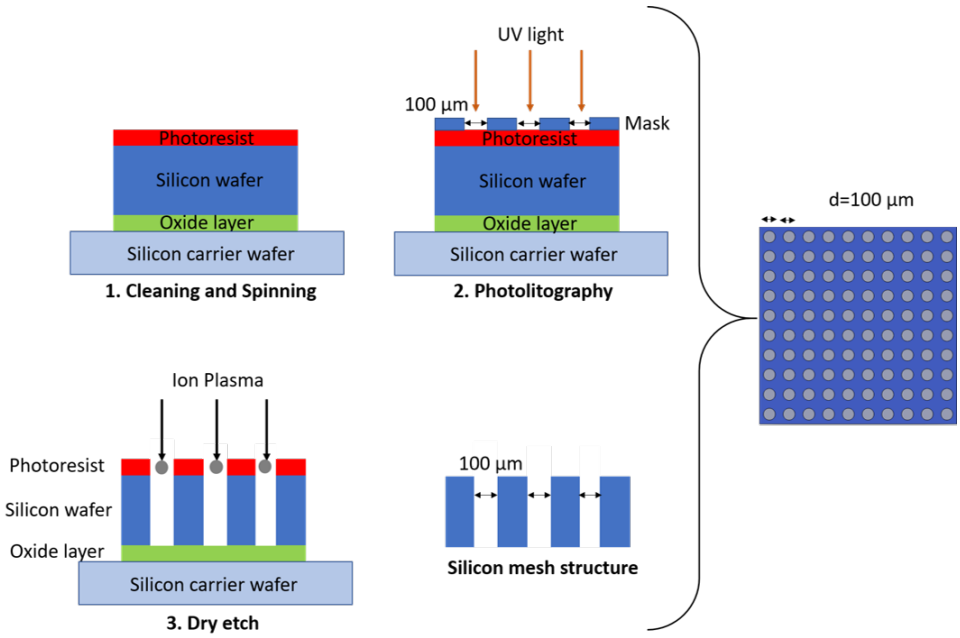

Figure 2.5: Dry etching process. The first step involves cleaning and spinning of the positive photoresist AZ4562 on the silicon wafer. In the second step, the mask alignment is employed to expose the wafer for 24 s to UV light. The third step was carried out by a JWNC technician, using the PlasmaPro 100 Estrelas Deep Silicon Etch System for 60 minutes. Finally, the samples were treated with piranha solution for 60 s and then plasma-ashed for 120 s at 100 W to create a hydrophilic surface.

Cleaning Substrate and Spinning

A 4-inch silicon wafer of 270 µm thickness was subjected to organic solvent cleaning. Opticlear, acetone and methanol were used for 5 min each in an ultrasonic bath to remove any dirt. Then, RO water was used to rinse and a nitrogen gun was employed to dry quickly the wafer. A positive photoresist (AZ4562) was then spun at 200 rpm (thickness around 3 µm, Photoresists MicroChemical GmbH). The procedure is shown in Fig. 2.5, step (1). Pre-baking steps were employed at 60°C for 3 min and at 110 °C for 10 minutes.

Photolithography

In order to create a pattern of cylindrical cavities pattern, designed using L-Edit, a photolithography process was employed with a mask aligner (Karl Suss MA6 Mask Aligner) through a UV hard exposure for 24 s, Fig. 2.5, step (2).

Development and Dry Etch

Photoresist exposed to UV light becomes soluble to a photoresist developer, while the parts covered by the mask remained insoluble. AZ 400K developer was diluted 4 times in deionised (DI) water before the samples were agitated in the developer for 4 minutes. After the development, the samples were loaded on a carrier wafer and dry-etched for 60 minutes

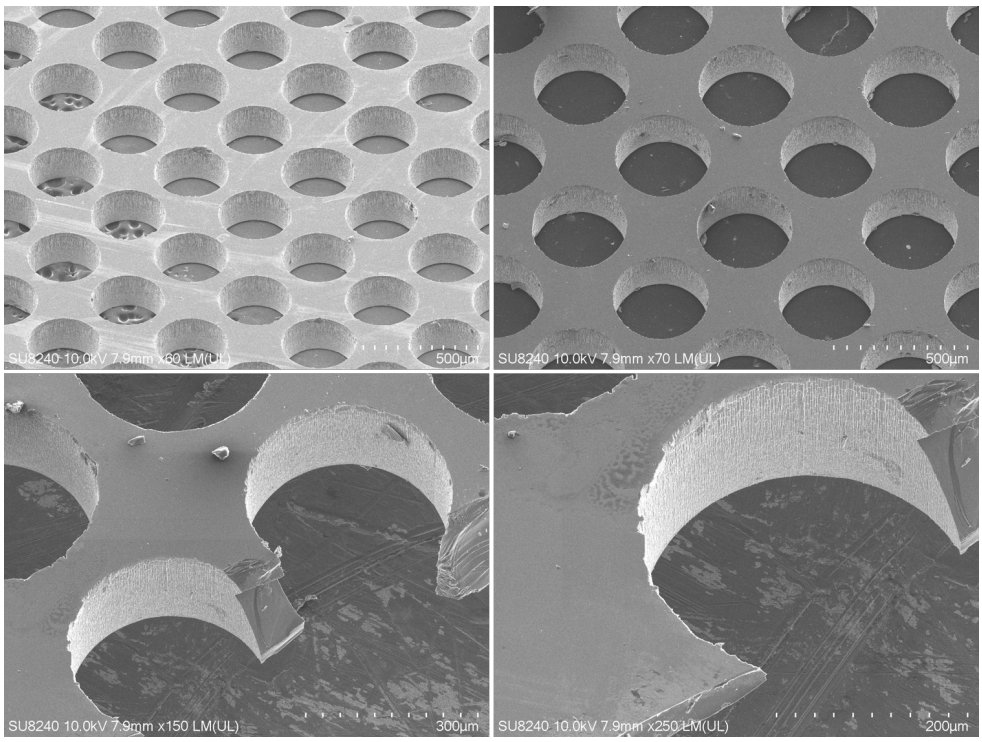

Figure 2.6: SEM SU8240 images of the dry-etched silicon chip, after photolithography process to create the cylindrical cavities pattern.

in order to remove the material inside the cylindrical cavities (Fig. 2.5, step (3) and Fig. 2.6), using Oxford Instruments Estelas 100 ICP RIE Deep Silicon Etch Tool. A squared design was also fabricated (see Appendix B, Fig. B1) Dry etch consists of the removal of material from a patterned sample using a plasma of the gases: sulfur hexafluoride (SF_6), octafluorocyclobutane (C_4F_8), nitrogen (N_2), argon (Ar), helium (He) and oxygen (O_2). The samples are subjected to a bombardment of ions which etch the cylindrical cavities directionally [192].

2.4 Lipid Mixtures

2.4.1 Film Hydration Method

In this work, the phospholipid suspensions were made using the thin film hydration method, which is one of the simplest methods to prepare a multilamellar vesicles mixture and to encapsulate various compounds within the vesicles [59]. A lipid film was produced by depositing the lipids within a clean glass vial, drying under a stream of dry nitrogen, followed by chloroform evaporation through desiccation of the solution for 90 min. The dried lipid layer was rehydrated by addition of 1 ml of phosphate-buffered saline (PBS) or DI water, forming a multilamellar vesicles (MLV) mixture, unless otherwise stated. Gentle hydration of the lipids followed by swelling in excess water yields an ensemble of vesicles

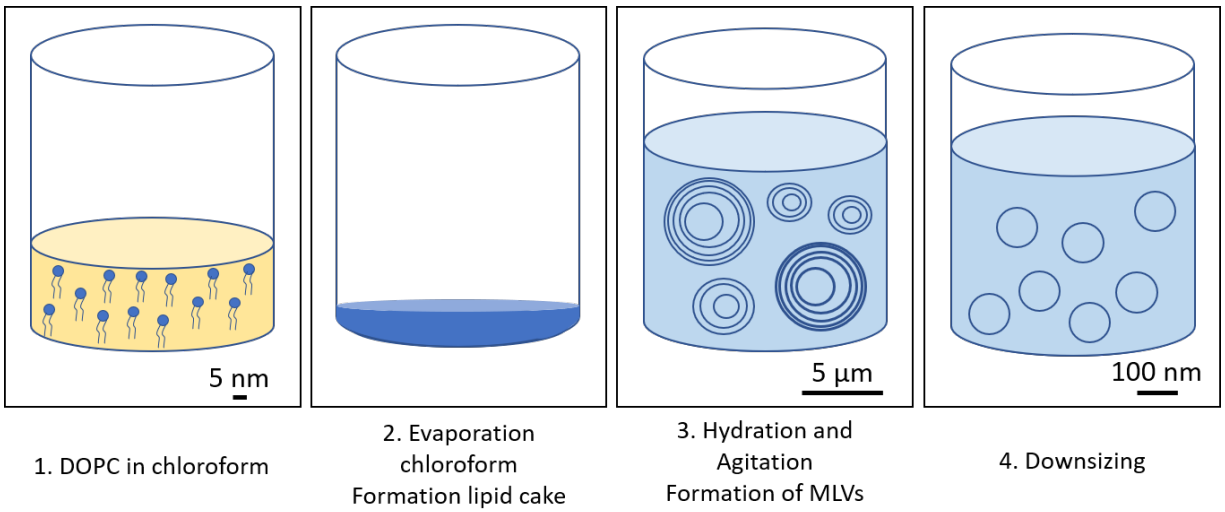

Figure 2.7: Thin film hydration technique was used to form unilamellar vesicles. (1). Phospholipids, which were chosen based on the experiment, are firstly dissolved in an organic solvent as chloroform. (2). A lipid film was produced by spreading the lipid/chloroform solution with a dry nitrogen gun for a small amount of volume, for volume higher than 1 mL, the rotary evaporator technique has to be used. The sample was left in vacuum for 90 min to allow the chloroform to evaporate. (3). Hydration of the lipid cake and agitation were applied in order to have the formation of multilamellar vesicles MLVs. (4.) Downsizing that can be applied through a different method such as extrusion, sonication or chemical methods (See Chapter 1).

with a broad size distribution [35]. A high polydisperse sample ($PDI > 1$) is obtained with vesicles larger than 5µm, which are not suitable for drug delivery.

Different techniques were used to downsize the vesicles and to increase the stability of the vesicles [36]. Freeze-thaw cycles and probe tip ultrasonication (Hielscher Ultrasonic Technology) were used to rupture and reform MLVs.

Fluorescent Liposomes

Different MLV mixtures were made using 1.00 mg/ml, 5.00 mg/ml and 10.00 mg/ml of $1,2-dioleoyl-sn-glycero-3-phosphocholine$ (DOPC) concentration and 0.1%mol of $1,2-dioleoyl-sn-glycero-3-phosphoethanolamine-N-lissamine$ rhodamine B sulfonyl (DOPE-RhB) in DI water, Fig. 2.9. Phospholipids were dried at the bottom of a clean glass vial. A lipid film was produced by using a stream of nitrogen (phospholipids were stored in chloroform). The sample was left in vacuum for at least 1 hour to allow the chloroform to evaporate. To hydrate the lipid layers and create an MLV mixture, 2 ml of DI water were added to each sample. Fig. 2.9 shows a confocal microscopy image of the MLVs population, the red colour is due to DOPE-RhB, which, together with DOPC, is forming the lipid membrane.

This type of mixture was used to check the vesicles population prior to the SAW nebuli-

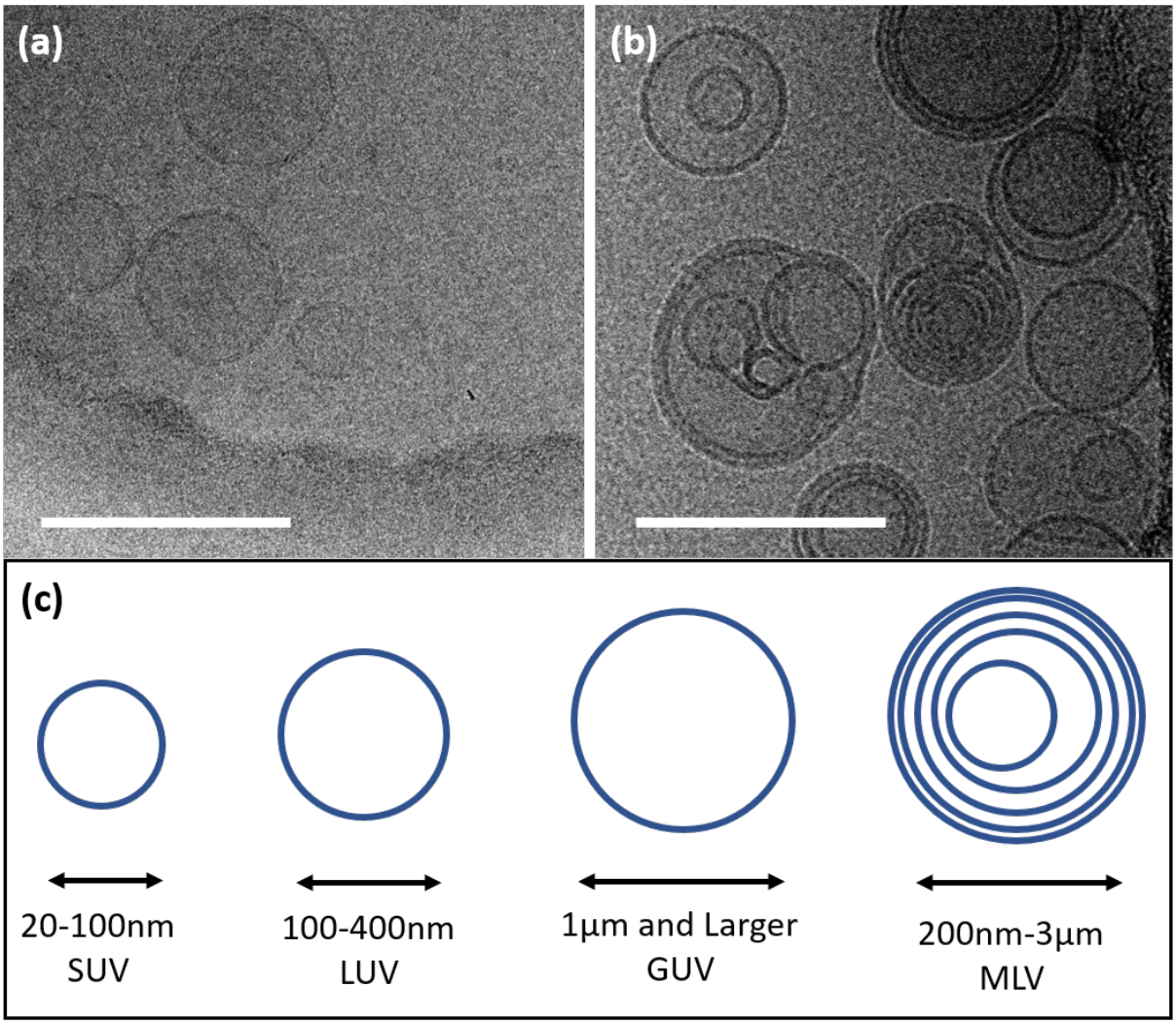

Figure 2.8: (a-b) Cryo-TEM image of unilamellar vesicles on the left and multilamellar vesicles on the right. Scale bar: 200 nm. (c) Classification of liposomes based on the lamellarity and size. From the left: small unilamellar vesicle (SUV), large unilamellar vesicle (LUV), giant unilamellar vesicle (GUV) and multilamellar large vesicle (MLV).

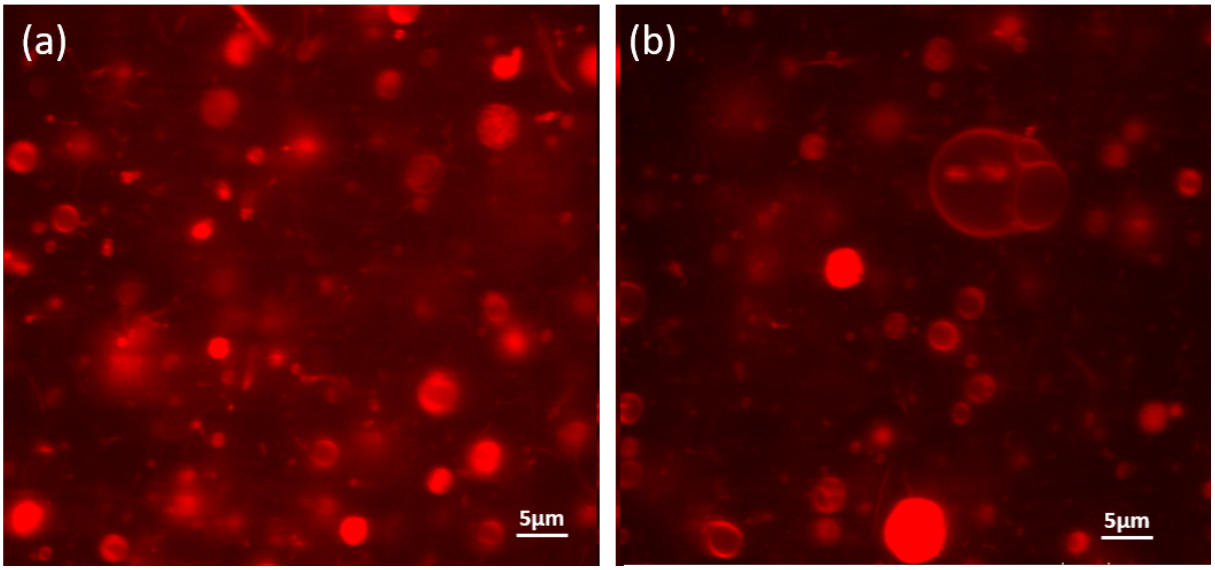

Figure 2.9: (a-b) Confocal microscopy image of MLV mixture, (100x magnification, $\lambda_{exc} = 560$ nm, $\lambda_{em} = 583$ nm). The solution was made using 2.00 mg/ml of DOPC and 0.1% mol of DOPE-RhB. Multilamellar vesicles of different size are visible.

sation and during the nebulisation step, as described in Chapter 4.

Enzyme-Encapsulated Liposomes

In order to encapsulate a hydrophilic enzyme within the liposomes, DOPC at 1.00 mg/ml was dried and left under vacuum and Horseradish Peroxidase (HRP) was chosen as an enzyme model and dissolved in DI water at a concentration of 20 nM using the thin film hydration method [37]. The concentration of HRP was tested using a calibration curve (Results Chapter 3).

This method is a quick and easy way of encapsulating the compound in the liposomes but has the disadvantage that a large amount of drug remains in the external medium.

Cationic Liposomes

Lipid mixtures of DOTAP/cholesterol were made at ratios of 2:1 and 4:1, to a total concentration of 2.4 mg/mL. Mixing only DOTAP and cholesterol in DI water did not lead to the formation of a bilayer system. Lipids have many topographies that depend on their head groups and tail group chemical bonds and can be described as conical, inverse-conical and cylindrical [34]. Both DOTAP and cholesterol are geometrically conical lipids, meaning that they cannot form a bilayer by themselves (Chapter 4). Therefore, a solution of 5% sucrose was used to hydrate the lipid film in order to enable the formation of a bilayer between DOTAP and cholesterol. Sucrose occupies head group volume, such as to overcome the negative curvature of DOTAP and cholesterol, which would otherwise result in the formation of only inverted micelle structures.

Cationic liposomes were used as a carrier for the transfection of both DNA plasmid luciferase and GAPDH siRNA (Chapter 6). Comparison of transfection efficiency (in terms of relative light units (RLU)/mg protein) between extruded liposomes and SAW-formed liposomes was performed. Two terms will be used in this chapter to refer to different methods of transfection: standard transfection, where the solution is added directly to the cell culture dish, and SAW transfection, where the transfection solution is nebulised by SAW.

2.4.2 Downsizing of Multilamellar Vesicles

Large unilamellar vesicles (LUVs) of defined size and homogeneity were obtained by a sequential extrusion (Avanti Polar Lipids, Alabaster, U.S) through a polycarbonate membrane with fixed pores of 200 nm in diameter [43] at a temperature above T_m of DOPC ($T_m = -17°C$).

2.4.3 Extrusion

The extrusion process is based on pinching off part of the liposomes, as it is pressed through a pore of a diameter smaller than its own. The vesicle can deform to a certain extent, but it reaches a point where the pressure differential on the opposite sides of the pore causes the bilayers to rupture. The ruptured bilayers would anneal immediately, forming smaller vesicles, which can eventually all pass through the pore. The extrusion process was carried out using the Mini-Extruder (Avanti Polar Lipids, USA). The extrusion protocol from Avanti Polar Lipids [193] is described, which was used to form unilamellar vesicles of 100 and 200 nm in diameter.

MLVs were initially subjected to 5 cycles of freeze-thaw by immersing an Eppendorf vial containing 1 ml of MLVs in liquid nitrogen (-210°C/-195°C) and then in a water bath at 37°C. The reduced size MLVs were then extruded through a membrane with a pore size of 100 nm. Firstly, a syringe full of the buffer is passed through the extruder in order to pre-wet the polycarbonate membrane and to reduce the dead volume. After discarding the buffer, the sample is loaded into the syringes and place in one end of the Mini-Extruder, making sure the empty syringe plunger is set to zero. The extruder is then inserted into the heating block, so it will guide the pushing of the lipid dispersion. The lipid mixture is pushed 11 times between syringes. An odd number of pushes is important, so that the final extrusion step fills the initial empty syringe, avoiding contamination with remaining large particles in the first syringe. Finally, the mixture is collected in a clean vial and the extruder is cleaned.

A change in the turbidity of the vesicles mixture through the extrusion process indicates the breakdown of larger vesicles into smaller ones. The large size and the several lamellae

of initial MLVs in the buffer makes the mixture turbid, as it passes through the membrane [194], the size of vesicles reduces, reducing the turbidity. The vesicles final size is measured to be in the range of 100 nm (see Chapter 3).

2.4.4 Sonication

A probe sonication (UP200S, Hielscher, Germany) was used to downsize the multilamellar vesicles suspension. To estimate if the power employed by the SAW nebuliser was high enough to determined the break up of MLVs in smaller liposomes, a comparison of the power used in the probe sonication method with the SAW nebuliser was made. During the sonication process, a power of 200 W was utilised for 30, 20 and 10 seconds, while the SAW device was using a power of 5 W. Results are shown in Chapter 4. From Giovannini *et al.* [134], a power of 3 mW was estimated to disperse a volume of liquid into smaller droplets, but data regarding the power necessary to break down liposomes are not present in the literature.

2.5 Liposomes Characterisation

2.5.1 Dynamic Light Scattering

Particle Sizing and Correlation Curve

From the DLS measurements, the software from Zetasizer 90 calculated a correlation curve, which has to be smooth and a single exponential decay function, for a monodisperse sample. If an exponential function is used to fit the correlation function, the diffusion coefficient (D) can be calculated and using the Stokes-Einstein equation the hydrodynamic diameter can be evaluated [90]. In this work, a representation of the particles size is made using the intensity distribution, which is the most sensitive representation, compared to the volume and number distributions, to the presence of larger particles in a sample ($I \propto d^6$). It could indicate an early sign of the instability of the sample, which is an important parameter to test the quality of the sample.

2.5.2 Zetasizer Nano ZS90

For dynamic light scattering measurements, Zetasizer ZS90 (Malvern Panalytical, UK) was used. It is composed of six main components. A Helium-Neon laser with a wavelength of $\lambda = 633$ nm is used to illuminate the dispersion loaded into the cell, where some light will pass through the dispersion and some will be scattered by the particles in the solution. An attenuator is used to reduce the intensity of the laser since the detector is sensitive and it can saturate if too much light is detected. In this particular model, the detector

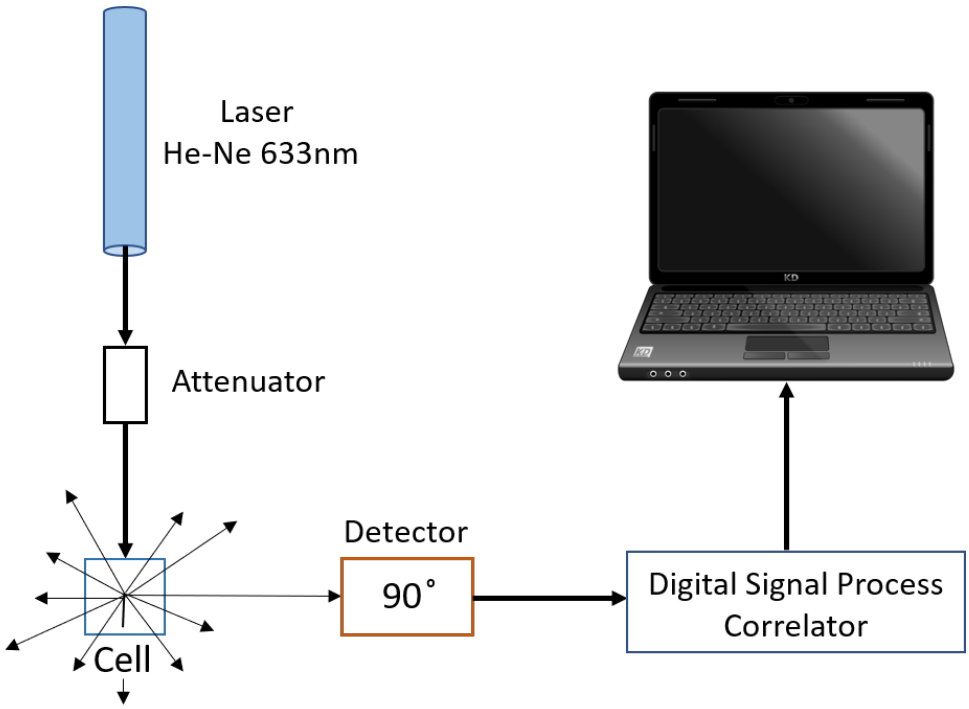

Figure 2.10: Main components of the Zetasizer Nano ZS90. A He-Ne laser 633 nm, passes first through an attenuator, which ensures that the detector will not be saturated. The light then hits the cell with the nanoparticles in the solution and a detector at 90°measure the intensity of the scattered light. From the detector, the signal is processed by a correlator.

is at 90°to measure the intensity of the scattered light. From the detector, the scattered signal goes through a digital signal processor called correlator. The correlator compares the scattering intensity at consecutive time intervals and then the data is passed to a computer, which will analyse it and derive size information.

2.5.3 TEM negative staining and Cryo-TEM

TEM negative staining was used with 2% methylcellulose/uranyl acetate (pH 7) as a negative stain, pictures were taken at the Dept. of Chemistry, the University of Glasgow. A small drop of the sample was placed on the carbon-coated grid, allowed to settle for 1 minute and blotted dry with a filter paper. Then, the sample was covered with a small drop of stain and blotted dry after, to wick away the stain. Some of the major drawbacks of this technique are artefacts, which are frequently observed when the stain is uneven, and the sample distortion during the sample drying, which can cause a collapse of its structure. In order to check the size and lamellarity of SAW produced vesicles, Cryo-TEM (JEM-220FS) pictures were taken at the Centre for Virus Research at the University of Glasgow. To convert a naturally-hydrophobic carbon-coated layer of the grid into hydrophilic, the grid was subjected to a glow discharge, which allowed the sample to spread on the grid

[195]. Then, Vitrobot (the University of Glasgow, Centre for Virus Research) a completely automatised vitrification process, was used to vitrify the sample. Two blotting papers on either side of the sample were pressed against the grid, leaving a thin layer of the sample. The sample was then plunged into liquid ethane, and, finally, the grid containing frozen vesicles was loaded into the electron microscope.

2.6 Aerosol Characterisation

2.6.1 Laser Diffraction: Spraytec

A standard procedure operation (SOP) was made for different experiments, in order to obtain a precise measurement. In the case of nebulisation of a lipid dispersion, a refractive index of $n = 1.38$ was set for DOPC. During the measurements, a single event of 4s was considered and the trigger signal was set for a signal transmission below 99%. The data collection was set for 400 ms before the trigger. The volume intensity (%) was evaluated and obtain through an average of the scattered data. The software provides different average size measurements (e.g. D_{23}, D_{34}); in this work, the median droplet size (D_{50}) is reported as the standard value in pulmonary drug delivery literature.

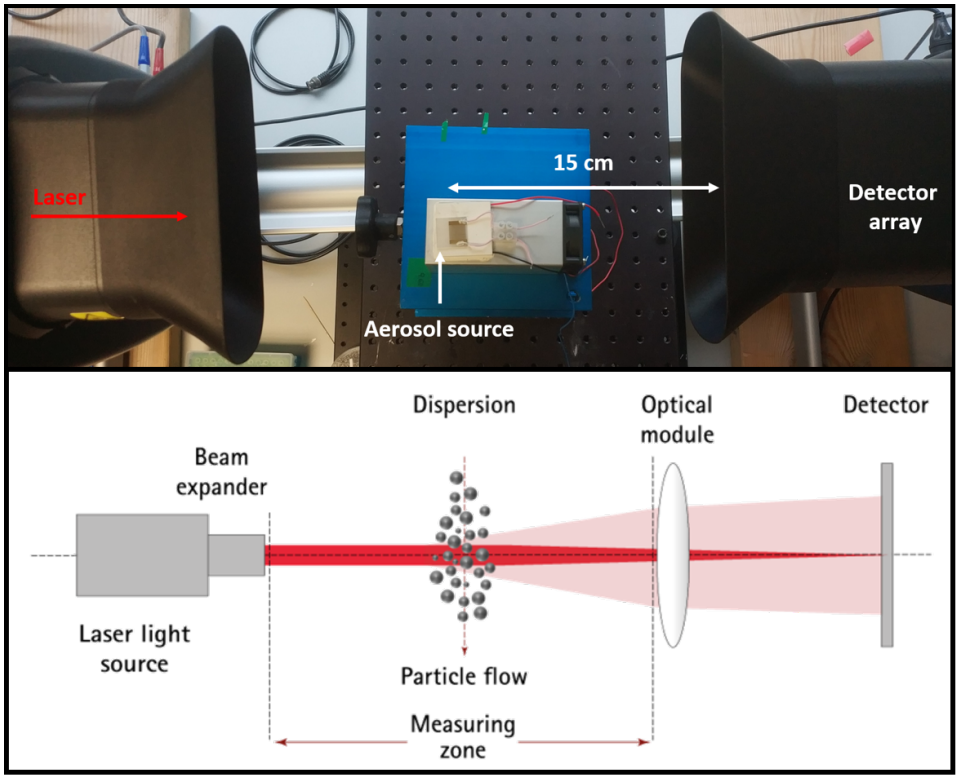

Figure 2.11: Instrumentation for aerosol size distribution measurement using laser diffraction (Spraytec). The image shows that the aerosol has to be at 15 cm from the detector array. The laser hits the aerosol and the light is scattered at different angles based on their sizes. The scattered light is then collected by the detectors.

2.6.2 Andersen Cascade Impactor and Inertial Impaction

The ACI is composed of 8 stages and each of them is made of a collection plate and a specific nozzles arrangement. Each stage is designed to trap particles of decreasing aerodynamic diameter [106]. A pump is connected at the bottom of the cascade impactor to aspirate the airflow from the nebuliser and conduct it into the ACI. The inertial impaction method is used to separate particles based on their inertia, which depends on the size and velocity. Particles that pass through the nozzle will remain in the air stream, which is directed through a right angle at the exit. Particles that impact on the collection plate will remain on the surface and will not follow the airstream [105].

The particle with sufficient inertia will pass through the next stage. Ideally, each stage is associated with a cut-off diameter, for which [104] particles larger than a certain aerodynamic diameter will be collected, while particles smaller than a certain aerodynamic diameter will pass through the next stage.

The ACI used in this work was designed to operate at an air flow of 28.3 L/min, as recommended by the manufacturer. For a flow of 28.3 L/min, the cut-off diameters for each stage are shown in Fig. 2.12. The primary advantage of cascade impactors is the direct measurement of the aerodynamic diameter, which represents the best approximation of particles behaviour during inhalation [106]. Moreover, the ACI produces the required resolution for inhalation products: 0.5 to 5 µm [106]. However, there are some limitations to the use of the impactors. Solid particles could bounce instead of being deposited, and under normal atmospheric conditions it is hard to collect particles smaller than 0.2 µm [104]. Systematic errors can be produced, for instance, particle bounces favour smaller particles in the size distribution [197]. Increase humidity in the environment, to reproduce lungs condition, could lead to an increase of the collected particles.

2.7 Experimental Setup

2.7.1 Pre-SAW Nebulisation

Membrane Dialysis

Once the enzyme or protein has been internalised in the liposome, in order to have the HRP solely in the internal compartment of the liposomes, the remaining non-encapsulated drug was removed by dialysis. Dialysis refers to a technique used to separate molecules based on their differing abilities to diffuse through a semi-permeable membrane [198].

In dialysis, a sample and a buffer solution (called the dialysate) are separated by a semi-permeable membrane [198]. Due to the pore size of the membrane, large molecules in the sample cannot pass through, thereby preventing their diffusion from the sample

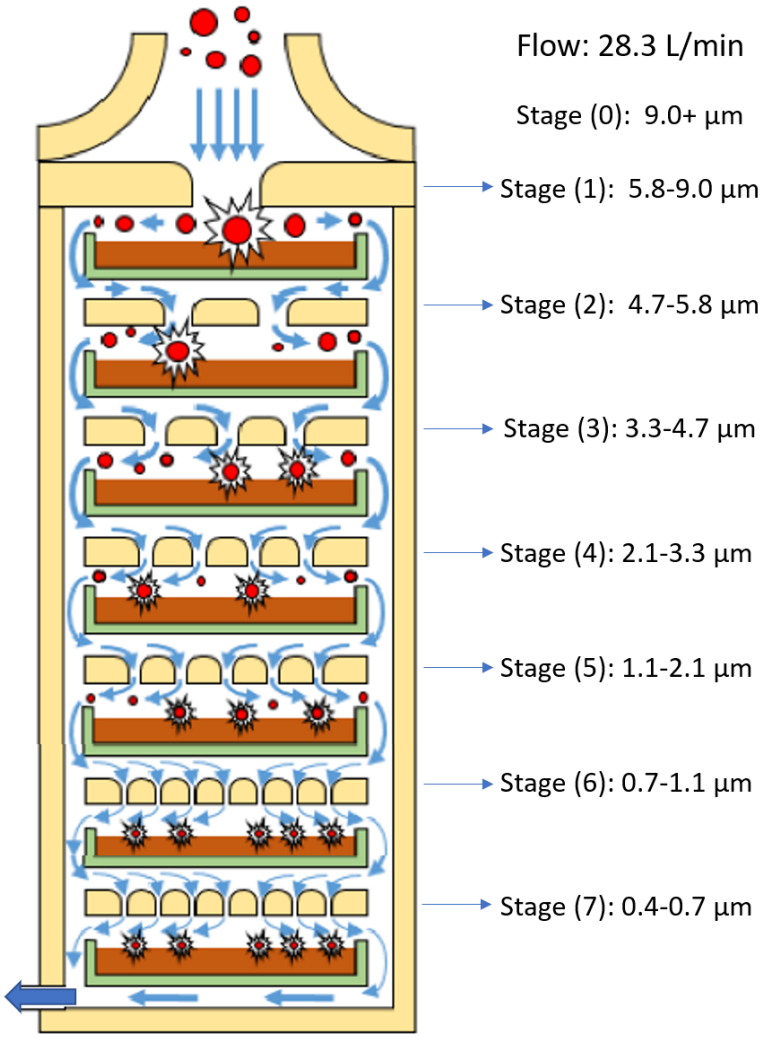

Figure 2.12: Andersen cascade impactor structure. A cross section of the Andersen cascade impactor with a separation in 7 stages, where nozzles of different sizes are present. The particles deposit onto the collection plate or continue to follow the air stream based on their inertia. Larger particles will be cut-off at the upper stages of the cascade. After the nebulisation ended, the collection plates were washed to analyse the quantity deposits on each stage. Picture rearranged from [196].

chamber [198]. By contrast, small molecules will freely diffuse across the membrane to establish an osmotic equilibrium across the entire solution volume. The volume of the sample is 1 ml and it is immersed in the dialysate solution, which is usually 10 times larger [199]. An important property of the membrane is the Molecular Weight Cut Off (MWCO), which needs to be chosen depending on the size of the molecules within the sample. It is an indirect measure of retention, and more precisely is the lowest molecular weight of solute (in daltons) at which 90% of the solute is prevented from passing across the membrane [199]. Since a solute's permeability is also dependent on molecular shape, degree of hydration, ionic charge and polarity, it is usually recommended to select an MWCO that is half of the molecular weight (MW) of the species to be retained, and at least 20 times the molecular weight of the species that should pass through [199]. A dialysis Ultra-pure Biotech Cellulose Ester (CE) Membrane (Spectra/Por Float-A-Lyzer G2) with an MWCO of 300 kDa was used; its pores were 35 nm in size [200]. The membrane was soaked in 10% ethanol for 10 min, and then rinsed and soaked for 5 min in DI water. The sample was then loaded into the device, which was floating in a beaker containing the same buffer as the loaded sample, and a stir bar. The sample was dialysed under rotation at room temperature overnight (12-20 hours), to remove the HRP (MW=44 kDa) from solution, with 3 complete buffer changes after 2, 6 and 10 hours.[201].

SAW Nebulisation of HRP-Encapsulated Liposomes

The dialysed solution was then nebulised and collected in a TMB solution. Triton X-100 was added to release the encapsulated HRP and allow the HRP-TMB reaction. Absorbance was measured both before and after nebulisation. Only intact liposomes protect TMB from HRP. If there are enough intact vesicles, then an increase in signal (O.D.) following the addition of Triton X-100 is observed. Without the addition of the detergent, the O.D. will come solely from any HRP remaining in the outer solution (after dialysis) and should be low.

Temperature Effects in SAW Nebulisation

Enzymes and proteins are temperatures sensitive [202]; they maintain their functional properties only if kept below a certain temperature. One of the main concerns in delivering an active compound is the possibility of protein denaturation during nebulisation, due to increases in temperature. This could be prevented using a cooling system, but such has been shown to reduce ultrasonic nebuliser output [203]. Under SAW nebulisation, a temperature test was carried out, exploiting the HRP-TMB reaction to assess the retention of enzyme activity. A solution of 200 nM HRP was nebulised using an IDT with a resonance frequency of 9.5 MHz, which was supplied with -6 dBm input power, and a syringe pump (World Instruments, Aladdin) to dispense the solution at 60 µl/min. A Peltier module

(I=1.3 A, 20 x 20 mm) was used to fix the temperature at 20°C, 65°C or 100°C. Once the IDT reached a uniform temperature, SAW nebulisation was initiated, and nebulised liposomes were collected. The HRP assay was carried out on the collected samples, and the optical depths were measured.

2.7.2 SAW Nebulisation Setup

The IDT was connected through a conductive silver paint, Electrodag 1415, to the high power amplifier ZHL-5W-1 (Gain=40 dB, 50Ω, 5 to 500 MHz), which was obtained from Mini Circuit (USA) and used throughout the thesis for every SAW nebulisation setup. The signal generator N5181A MXG Analog was used in conjunction with the amplifier, as showed in Fig. 2.13, (b). The same configuration without the application of the silicon chip was used in Chapter 3, where only the feasibility of SAW to nebulise pre-formed liposomes was tested. In order to remove the heat from the hot side of the Peltier, a thermal paste was used between the Peltier and the heat sink. A thin layer of the ultrasound transmission gel(Aquasonic 100, Parker Laboratories, USA) was used to fix the silicon chip on top of the IDT.

SAW Nebulisation of MLVs

In order to transfer energy to the system and obtain smaller, unilamellar vesicles, IDTs with silicon chip was used to nebulise the MLV dispersion. The IDT resonance frequency was 9.6 MHz and an input power of -6 dBm was employed and amplified by 40 dB, obtaining a total power of 2.5 W. The IDT was placed on top of a Peltier module (I=1.3 A, 20 x 20 mm), to keep the temperature constant and avoid thermal stresses within the lithium niobate. As shown in Fig. 2.14, the Peltier module was located on top of a fan-integrated heat sink (dimension 100 x 50 x 50 mm, Fischer Elektronik) to remove the heat from a hot side of the module. The nebulisation flow was collected using 25 µl of the same solution which MLVs were made in and the droplet was placed in front of the nebulisation flow to collect the vesicles produced during the SAW nebulisation. The process was repeated 6 times in order to retrieve at least 100 µl of volume, which is the minimum volume of the sample to be measured by dynamic light scattering.

The same sample was simultaneously measured with laser diffraction to determine the aerosol size and then collected to be analysed with dynamic light scattering to check the vesicle size distribution.

SAW Nebulisation from Lipid-Coated IDT

A uniform layer of 10.00 mg/ml DOPC in chloroform was spun on the IDT (400 rpm, 10 s). The IDT parameters used were: 9.552 MHz with an input power of -6 dBm. IDTs

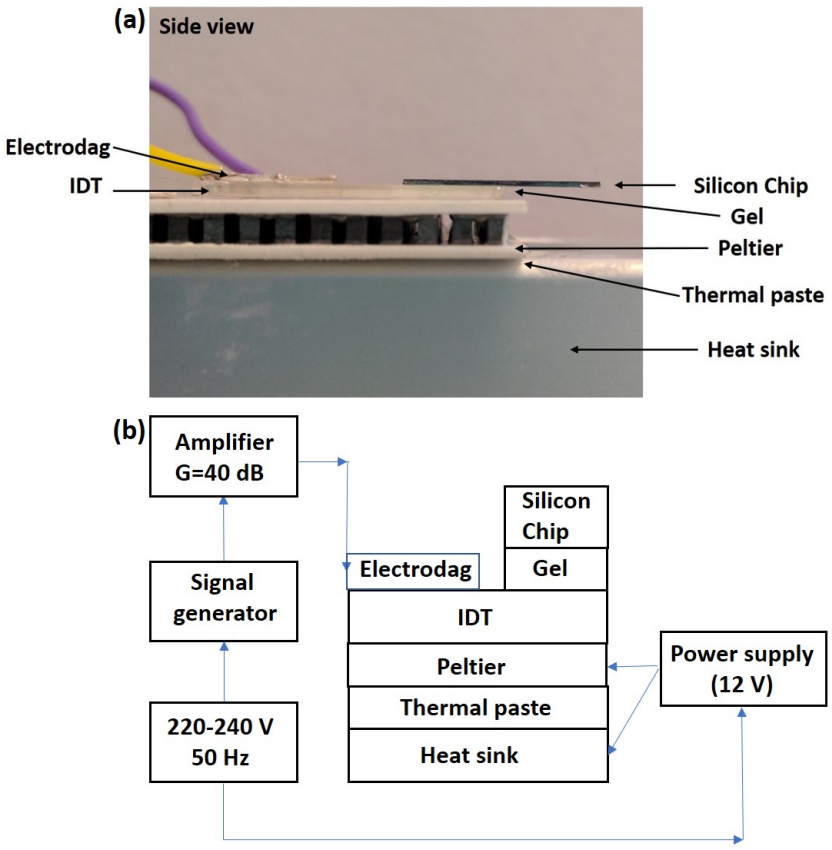

Figure 2.13: (a) Side view of the SAW nebulisation setup. From the bottom, the heat sink is in contact with the Peltier to remove the heat from the hot side. The cold side of the Peltier is in contact with the IDT to keep the temperature constant and avoid thermal stresses within the lithium niobate. On top of the IDT, a thin layer of ultrasound transmission gel was added to fix the silicon chip on top of it. (b) Schematic of the SAW nebulisation setup, where the different layers are shown. From the bottom, the heat sink is connected with a power supply to activate the fan, which removes the heat from the Peltier. A thermal paste, which is thermally conductive, is applied between the heat sink and the hot side of the Peltier. The cold side of the Peltier is in contact with the IDT, which is connected through a metal conductive paste (ELectrodag) and two wires to an amplifier. The latter is amplifying a sinusoidal signal at a resonant frequency.

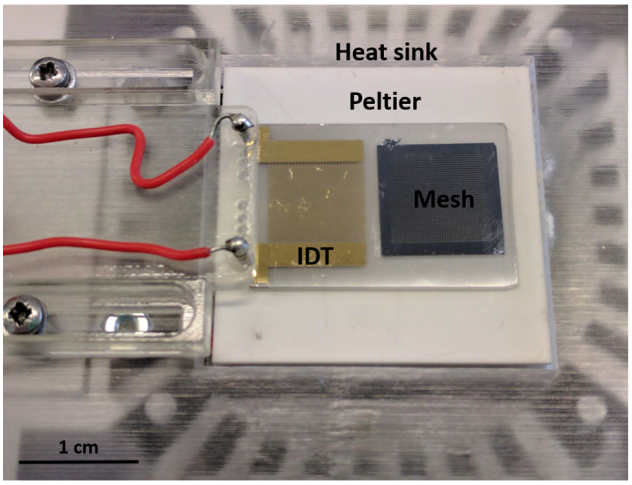

Figure 2.14: SAW Nebulisation equipment. The SAW nebuliser, placed on top of a Peltier module and a heat sink, to keep a uniform temperature. 100 µl of MLV mixture was nebulised and 100 µl of collection buffer was placed on top of the nebulised flow to allow collection of sufficient volume for particle sizing.

were left in vacuum for 90 minutes in order to let the chloroform to fully evaporate. Once the chloroform evaporated, a silicon chip with a pore size of 300 µm was placed above the IDT. Deionised water was added on top of the silicon chip and left to incubate for 5 minutes to allow water absorption by phospholipid head. After incubation, SAWs travelled on the surface of the lithium niobate and then on top of the silicon chip (coupled with IDT), causing the droplets to be pulled out from the surface of the volume confined into the cavity of the silicon chip. Nebulised vesicles were collected on an upside-down glass slide into a droplet of water. Finally, 100 µl of the collected solution was measured on the Zetasizer Nano ZS90 to evaluate the size distribution of the nebulised vesicles.

2.7.3 Post-SAW Nebulisation

Lipid Bilayer Solubilisation by Surfactant

To evaluate the integrity of liposomes and the activity of their encapsulated enzymes after SAW nebulisation, liposomes were intentionally broken down by lipid bilayer solubilisation. For this purpose, different groups have previously used surfactants [204]. Surfactants are amphiphilic molecules that lower the surface tension of the liquid into which they are added [205]. In this work, Triton X-100 was chosen for its property of lysing cells. It is frequently used to extract proteins from cells [206]. Surfactants are molecules that interact with phospholipid bilayers. They are used to solubilise liposomes and release their encapsulated compounds. As stated by Helenius and Simons [207], a three-stage model explains how solubilisation occurs (Fig. 2.15). Firstly, the surfactant molecule inserts itself into the outer layer of the phospholipid bilayer (stage I), resulting in the solubilisation of the bilayer and the consequent formation of lipid-detergent mixed micelles

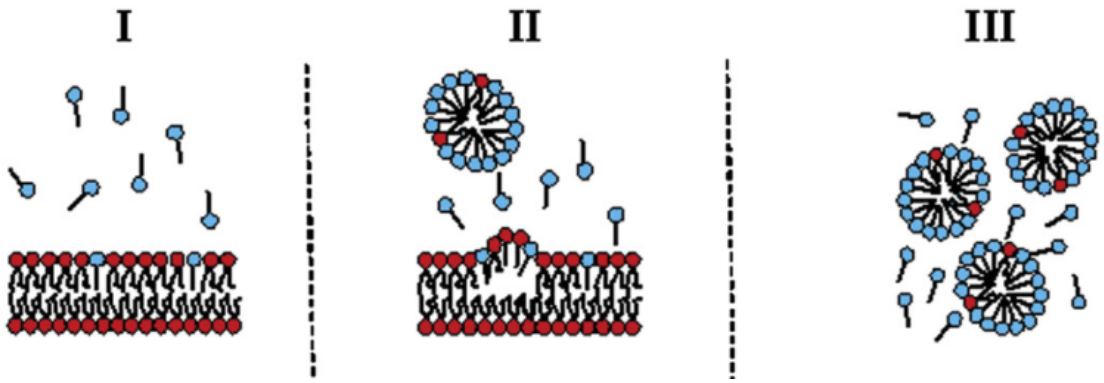

Figure 2.15: Three stage model of lipid bilayer solubilisation by Helenius and Simons. (I) Detergent monomers (blue) insert into the outer bilayer (red), (II)Formation of lipid-detergent mixed micelles and (III) mixed micelles become further enriched in detergent. Picture taken from [208].

(stage II). Thereby, the encapsulated compound is released. Finally, the mixed micelles become smaller and further enriched in detergent (stage III) [208], [209].

Collection of SAW Nebulised Particles

With the purpose of measuring the nebulised nanoparticles in the solution, the following setup was used. A glass slide was placed in front of the nebulised flow. 25 µl of DI water or same buffer used to prepare the solution to nebulise, was placed on the glass slide upside-down. The nebulised particles were collected in the droplet and in the case of liposomes a decrease in surface tension was noticed during the collection. As the liposomes were entering the collection droplet, the droplet spread. This was repeated 5 times in order to retrieve 100 µl volume, which is the minimum amount required from the DLS device. For each collection droplet of 25 µl, 100 µl of the sample was nebulised. This procedure was used for the collection of the HRP encapsulated liposomes in Chapter 3 and the SAW-formed liposomes in Chapter 4.

Recovery of Liposomes from Andersen Cascade Impactor

Liposomes were nebulised in order to test the size stability on the collection plate of each stage. Each stage was covered with 1 mL of the same buffer used to extrude the liposomes to avoid the breakage of nebulised liposome on the collection plate. A volume of 1 mL of the LUVs dispersion was nebulised. From Fig. 2.16, a syringe pump (World Instrument, Aladin) was employed to load the mixture at 300 µl/min. An IDT with a resonance frequency of 9.58 MHz and a silicon chip with 100 µm cavities were employed.

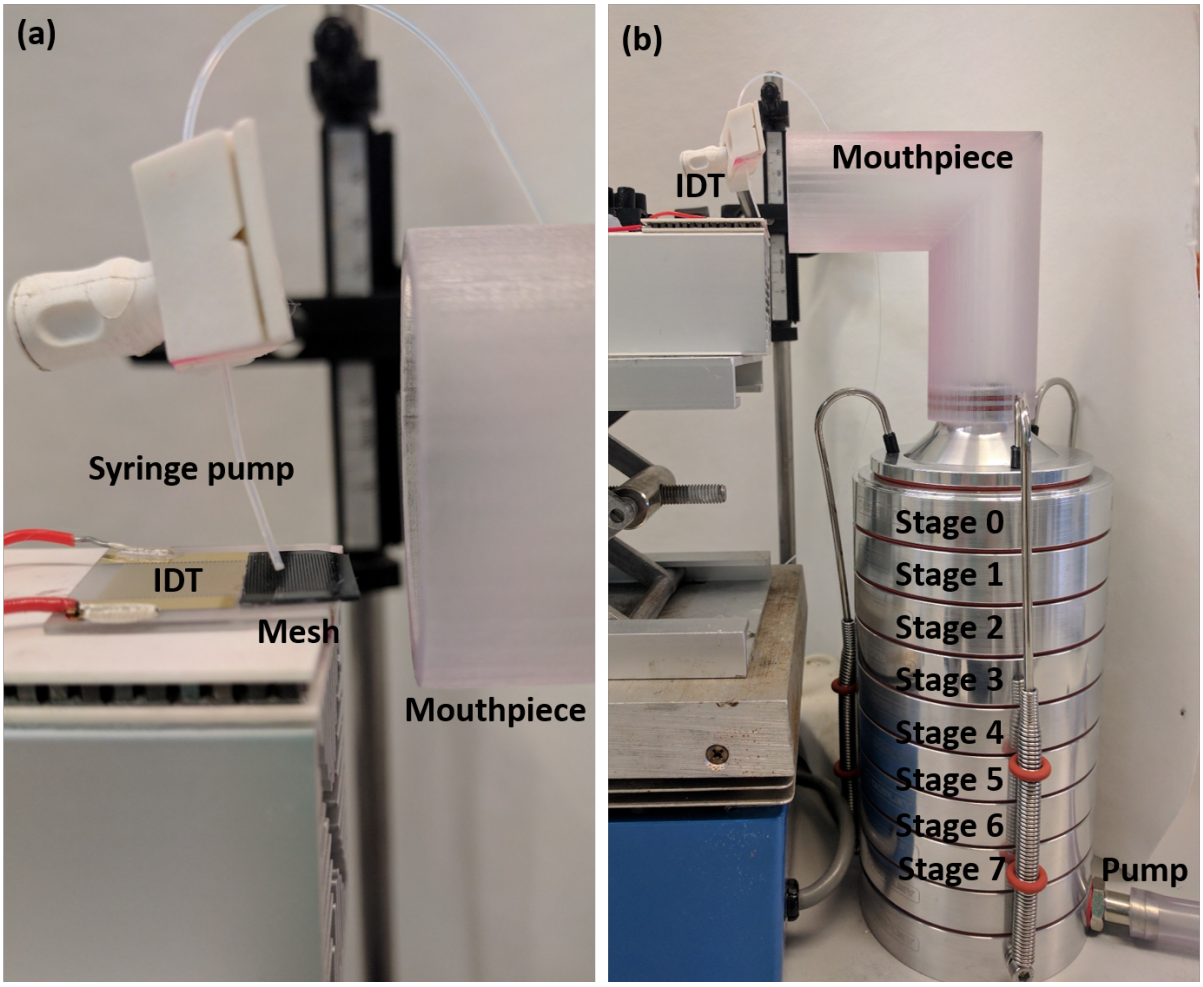

Figure 2.16: Andersen cascade impactor instrumentation. (a) A silicon chip with cavities size of 100 µm was placed on top of the IDT. A syringe pump was loading the LUVs dispersion at 200 µl/min flow. (b) At the bottom of the cascade impactor, a pump was connected in order to create an air flow of 28.3 L/min. The air flow was measured using a flow meter (Platon NGX, Roxspur, UK).

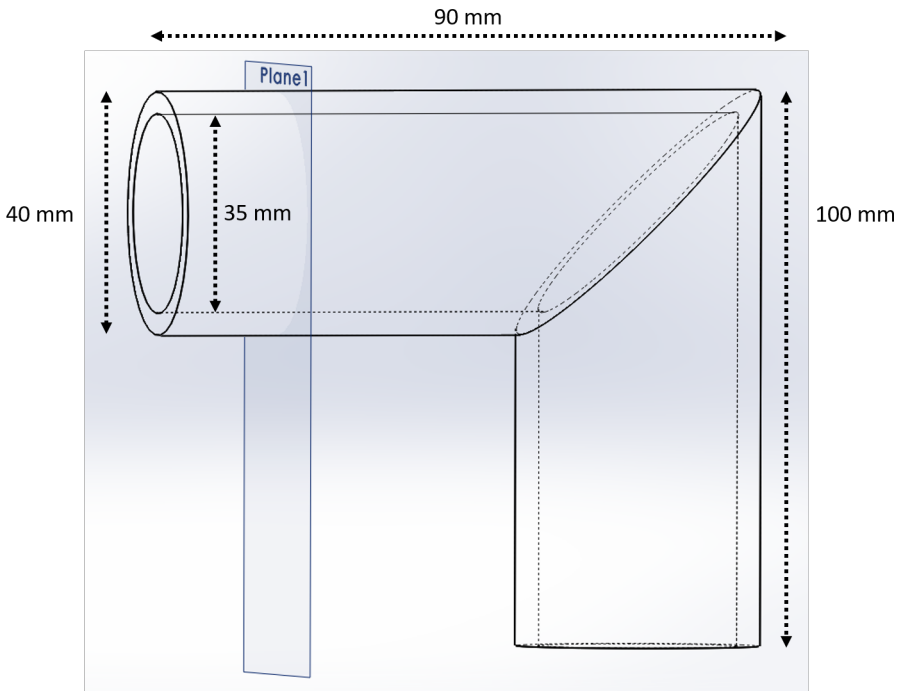

Figure 2.17: Mouthpiece design. SolidWorks draft of the mouthpiece, which collects the aerosolised particles from the SAW nebuliser into the cascade impactor. The simple geometry has an internal diameter, set by the size of the impactor and the length was chosen in order to have enough space to form a 90°angle.

Mouthpiece Design

In order to collect the aerosolised particles from the SAW nebuliser and guide them through the cascade impactor, an L-shape mouthpiece was designed using SolidWorks (Dassault Systemes, France) and then 3D-printed. The internal diameter of 35 mm was dictated by the cascade impactor geometry, Fig. 2.17. It represents a simplified model of the mouth-pharynx-trachea system. The geometry of the mouthpiece could be optimised to increased the volume fraction (%) in the impactor.

2.8 Biochemical Assays

2.8.1 HRP Assay

Horseradish Peroxidase

Horseradish Peroxidase (HRP) is an enzyme found in horseradish roots. It is commonly used in biochemistry for its ability to improve the detection of target molecules by amplifying weak signals. Using Tetramethylbenzidine (TMB) as a substrate, a colourimetric HRP assay was carried out, utilising hydrogen peroxide H_2O_2, to yield a colour change that can be detected by a spectrophotometer. HRP catalyses the conversion of the chro-

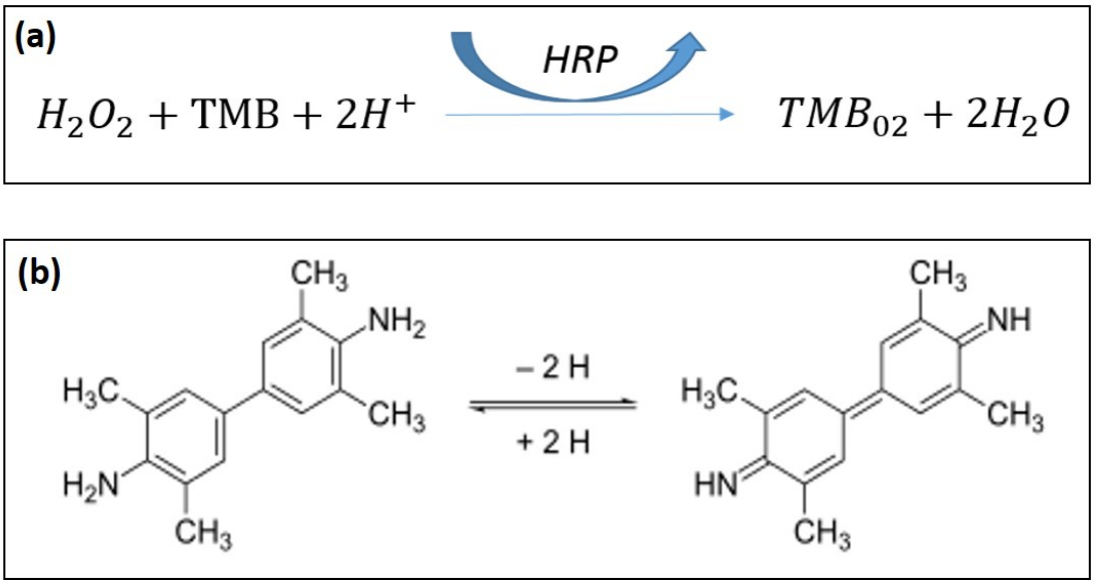

Figure 2.18: HRP-TMB reaction. (a) TMB acts as an electron donor for the reduction of H_2O_2 to H_2O, and the reaction is catalysed by HRP. After H_2O_2 and TMB react with HRP, (b) the Tetramethylbenzidine (TMB) is oxidised to form Tetramethylbenzidine diimine, resulting in a blue colour

mogenic substrate TMB into coloured products. TMB acts as an electron donor for the reduction of H_2O_2 to H_2O by HRP. Fig. 2.18(a) shows the reaction

When the H_2O_2 and TMB react with HRP, the Tetramethylbenzidine (TMB) is oxidised to form Tetramethylbenzidine diimine Fig. 2.18(b), resulting in a blue colour that can be measured with a spectrophotometer at $\lambda = 650$ nm, Fig. 2.18 shows TMB oxidation. In this work, the HRP assay was used as an indirect method to test liposome stability during SAW nebulisation. The reaction of HRP with hydrogen peroxide and TMB was exploited to assess the integrity of LUVs. HRP and TMB were purchased from Sigma Aldrich Company Ltd. (Dorset, U.K.). The HRP assay was carried out according to the following procedure. Firstly, HRP was encapsulated in LUVs using the thin film hydration method, using this method HRP is present both in the inner core of the liposomes and in the outer solution. Therefore, the removal of the HRP from the outer solution was carried out by using a dialysis membrane (described in detail in the next Section). Then, SAW nebulisation of HRP encapsulated in LUVs was performed and the nebulised solution was collected. Triton X-100 was added in the collected solution in order to solubilise the lipid bilayer and release the encapsulated HRP. TMB containing was then added into the collected solution to react with HRP and the reaction was stopped by using 1M sulfuric acid solution. The solution acquired a yellow colour that was detected by a micro-well plate reader at $\lambda = 450$ nm.

Absorbance Measurements

The absorbance of a solution is its capacity to absorb light at a specified wavelength. It is measured by optical depth ($O.D.$), which indicates the opacity of a medium and is defined by:

$$O.D. = ln(\phi^{\mathrm{i}}/\phi^{\mathrm{t}}) \tag{2.2}$$

where ϕ^{i} is the radiant flux received by the material and ϕ^{t} is the radiant flux transmitted by the material. From Eq. (3.1) the absorbance is represented by:

$$A = O.D./ln(10) \tag{2.3}$$

After adding sulfuric acid to samples to stop the reaction, a microplate reader (Synergy HTX, Biotek) was used for measuring the optical depth at the wavelength of $\lambda = 450$ nm.

2.8.2 Luciferase Assay

To test the transfection method and the efficiency with which the cationic liposomes were transfected, a luciferase assay was performed. If the DNA luciferase plasmid successfully enters the nucleus of the cell, then its luciferase enzyme is expressed, which acts on luciferin to produce luminescence. DNA plasmid luciferase was chosen for its high sensitivity and low background. [210]. Luciferases are a class of oxidative enzymes found in different species, that allow the organism to emit light. A typical example is firefly luciferase. Fireflies emit light in a reaction in which luciferin is converted to oxyluciferin by the luciferase enzyme. Energy is released from the reaction in the form of light [211]. This phenomenon is called bioluminescence and differs from fluorescence by the fact that the excitation energy is supplied by the luciferase enzyme. Eukaryotes do not otherwise produce light, and the background light from the sample is very low. Therefore, it is not necessary to filter out light from the sample, and the luminometer collects light from the entire visible spectrum [212]. The luciferase assay is usually used as a reporter assay, where the gene of interest can be cloned and fused to form a vector containing both it and the luciferase gene [210]. The vector and luciferin need to first be introduced into the cells, and their endosome lysed so that their contents are released. Once the luciferin is added, the luminescent signal is measured using a luminometer, which can quantitatively measure the emitted light. Since the gene of interest is fused with the luciferase reporter, its expression can be inferred from the intensity of the emitted light.

Complexes of DOTAP/cholesterol vesicles (at a 4:1 ratio) and DNA were formed by mixing at different ratios, with each well containing 1 µg of luciferase plasmid.

DOTAP/cholesterol liposomes were made by extrusion. In order to determine the

optimal amount of DNA to be bound with liposomes for cellular uptake, complexes were prepared using 6:1, 10:1, 20:1, 30:1 and 40:1 lipid-DNA ratios in Opti-MEM, with two different ratios of DOTAP to cholesterol: 2:1 and 4:1. After 30 min of incubation, the complexes were added to the cells. After 4 h, the Opti-MEM was substituted with serum-supplemented cell culture medium. At 24 h post-transfection, the cells were rinsed with PBS and lysed in 100 µl of reporter lysis buffer. 20 µl of each sample was transferred to a white opaque 96 well-plate and analysed using a Luminometer (Spectramax L, Molecular Devices). The results were expressed as RLU/mg (relative light unit per mg of protein). Protein concentrations were determined using the Bradford assay.

Luciferase Assay Calibration - DNA Quantification

In order to quantify the DNA delivered using the SAW platform, an indirect method was employed. A calibration curve of relative light units (RLU)/mg of protein against the concentration of DNA transfected to the A549 cells was generated. Standard transfection with extruded liposomes (d = 100 nm) was compared with SAW transfection. A lipid solution as made using the hydration method with 4:1 DOTAP:chol at a concentration of 2.4 mg/m. Cells were seeded at a concentration of $0.8 \times (10)^5$ cells/mL in single well plates (d = 35 mm), each well containing 2 mL ($1.6 \times (10)^5$ cells per well). In order to check if there was a linear relationship between the concentration of the transfected DNA and the amount of light emitted, different concentrations of DNA were added to the wells: 0, 0.25, 0.50, 0.75, 1.00, 1.50, 2.00 and 2.50 µg/mL. Samples were made in triplicate.

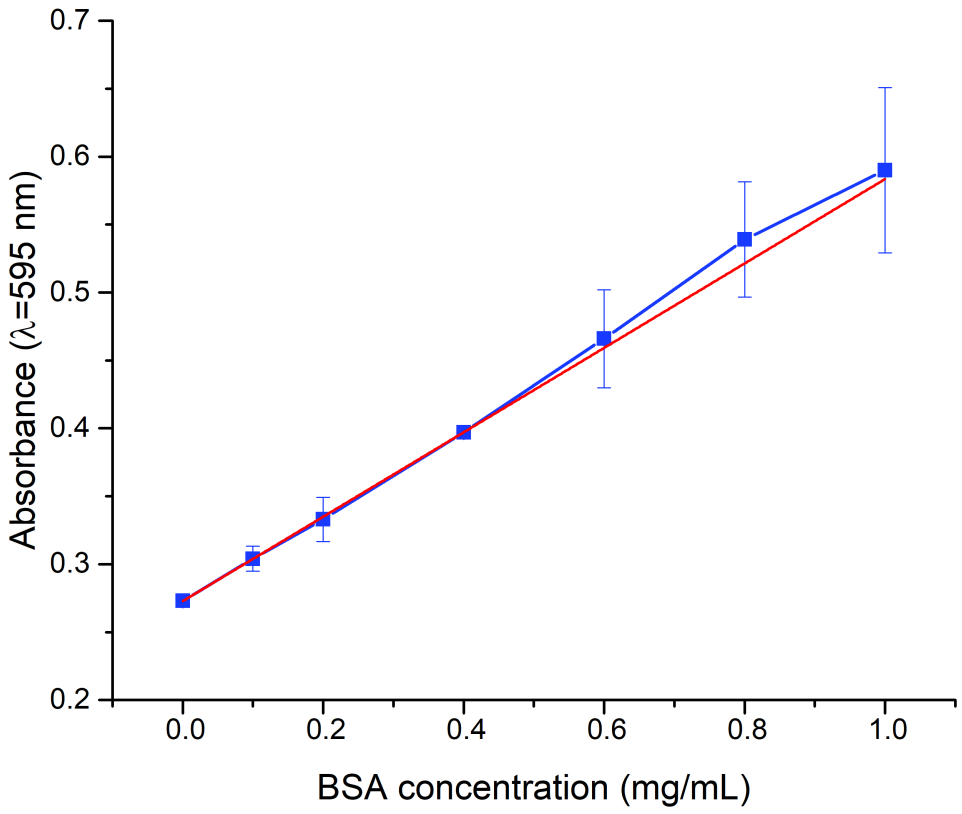

Figure 2.19: A calibration curve for the Bradford assay was obtained using bovine serum albumin, starting from a stock solution of 1 mg/mL. Absorbance measurements at λ = 595nm were made for BSA concentrations of: 1, 0.8, 0.6, 0.4, 0.2, 0.1 and 0 mg/mL.

2.8.3 Bradford Protein Assay

The Bradford protein assay is a method to determine the total concentration of proteins in a solution [213]. It is based on the binding between the Coomassie Brilliant Blue G dye and the proteins in the solution. The binding of the dye to proteins causes a shift in the maximum absorbance of the dye from 465 nm to 595 nm, which is measurable by a spectrophotometer or plate reader. The amount of absorption is proportional to the amount of protein [214]. In order to evaluate the protein concentration in each DNA luciferase plasmid transfection reaction, a calibration curve was generated. The following equation was acquired by linear fitting, with a coefficient of determination R^2=0.99

$$y = 0.323x + 0.271 \tag{2.4}$$

By reversing the equation and substituting the absorbance of the samples, the protein concentration in each sample was calculated. Then the luminescence readings were normalised to the protein concentrations in each sample.

2.8.4 Gel Retardation Assay

In all cases, representative gels were chosen. In some figures, gels have been cropped, although the raw images are shown in the Appendix, Fig. E1 and E3.

The gel is typically made of polyacrylamide for proteins and small nucleic acids, or agarose for larger nucleic acid fragments (>200 bp). A fluorescent dye, ethidium bromide, is often employed to visualise nucleic acids in the gel. It inserts itself between the bases of the DNA helix with a binding ratio of 1:1 (one molecule of dye to one base) [215] and fluoresces when exposed to UV light. It was commonly used in the past, but for safety reasons has been replaced with an alternative called GelRed, which unlike ethidium bromide cannot pass through the cell membrane [216].

A gel retardation assay was performed to check the integrity of the nucleic acid after SAW nebulisation. Samples were prepared by adding 2 µl of loading gel to the sample and then adding 10 µl of the sample into an agarose gel (2% w/v) stained with GelRed. Gel electrophoresis was run in TAE buffer at 120 V for 25 min and the gel was visualised under UV light. In order to establish the binding affinity of lipids/siRNA complexes, several measurements using the gel retardation assay were carried out. Different ratios of DOTAP and cholesterol were mixed at ratios of 1:2, 1:4, 1:6, 1:10, with equal amounts of DNA. Each solution was extruded and then analysed by the dynamic light scattering approach to measuring the sizes of the complexes.

2.8.5 Western Blot

Western blots are a laboratory technique used to identify a specific protein in a mixture of proteins from a cell extract. It is essentially composed of three steps: gel electrophoresis (separation by size and charge), transfer of the proteins from the gel to a membrane by blotting, and marking the target protein [217]. A western blot was carried out after freezing and thawing the cells three times and performing a Bradford assay to determine the concentration of protein in each sample. Cell extracts containing 20 µg of protein were loaded into a 10% SDS polyacrylamide gel, and electrophoresis was run at 120 V for 120 min. After the proteins were resolved, they were transferred onto a nitrocellulose membrane, which was then blocked in 5% nonfat dry milk for 2 h with shaking, to reduce background from non-specific binding. The membrane was washed twice with TBST (Tris-buffered saline with Tween 20) and once with TBS, for 10 min each time, and then incubated overnight with primary antibodies specific to the protein of interest, at 4°C

with shaking. After rinsing, the membrane was incubated with anti β-actin antibody, which binds the β-actin used as the internal control. After repeating the washing steps, the membrane was incubated with a horseradish peroxide-conjugated secondary antibody for 2 h at room temperature. The bound secondary antibody was detected using the ECL western blotting detection reagents [218]. GAPDH expression was evaluated by densitometry using the ImageJ software (Version 1.45S), and the results are reported as the mean of three independent repeats. The remaining GAPDH expression was represented as the density of the GAPDH band in the positive control divided by that of the GAPDH band in the negative control, both of which were first normalised to that of the β-actin band in their respective lanes [152].

β-Actin

β-actin is a major constituent of the contractile apparatus and one of the two non-muscular cytoskeletal actins. Actins are proteins involved in cell motility, and the maintenance of structure and integrity [219]. It is used as an internal control in western blots to minimise the effects that come from experimental loading errors - to assess if protein loading is similar across each sample and to adjust for any differences in such. β-actin's molecular weight is around 40 kDa. As a control for good western blot execution, a clean band at 40 kDa should be visible [218].

2.8.6 MTT Cytotoxicity Assay

The MTT assay is a colourimetric assay that is used to measure the cytotoxicity of potentially dangerous agents [220]. It is a reaction based on the reduction of a tetrazolium dye - in this case of MTT 3-(4,5-dimethylthiazol-2-yl)-2,5-diphenyltetrazolium bromide, to an insoluble formazan (purple colour). The reduction of tetrazolium depends on cellular activity, particularly on the presence of NAD(P)H-dependent oxidoreductase, which is an enzyme abundantly produced in the cytoplasm [221]. Rapidly diving cells (with high metabolism) thus exhibit high rates of MTT reduction [220]. A549 cells were seeded in a 96 well plate at a concentration of $(10)^5$ cells/mL, and 200 µl was added per well. Complexes of DOTAP-cholesterol vesicles (4:1) and siRNA were mixed at different ratios. In each well, 10 pmoles of GAPDH siRNA was prepared in Opti-MEM reduced serum. Complexes were added to cells after 30 min of incubation. After 4 h of incubation at 37°C, the transfection medium was carefully replaced with MTT solution (0.8 mg/mL tetrazolium dye). After 2 h, the MTT solution was removed and 200 µl of isopropanol was added, in order to solubilise the formazan crystals formed by the reduction of the tetrazolium. After solubilisation of the formazan, the 96 well-plate was shaken for 15 min, and then the absorbance at $\lambda = 525$ nm was measured. As a control, three wells were subjected to

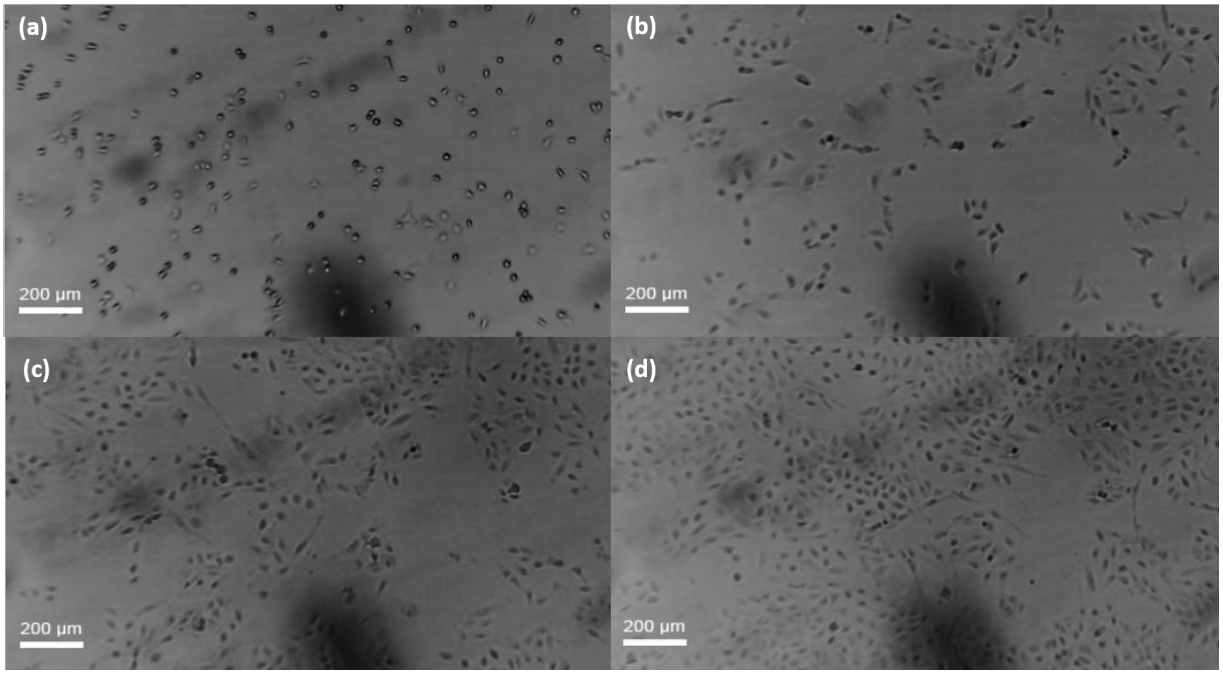

Figure 2.20: Cell division over 3 days. (a) after 2 hours, (b) after 1 day and 5 hours, (c) after 2 days and (d) after 3 days, reaching 70-80% confluence. Images taken using the CytoSMART System, Lonza

the changing of medium without transfection, to account for any loss of cells during the suction of medium. Cell viability was expressed as the absorbance from the cells transfected with the complex relative to that from those subjected to medium changes without transfection [218].

2.9 Cell Culture

Cell coverage was evaluated using the CytoSMART system (Lonza, Switzerland), and a confluence of 70-80% was reached after 3 days (Fig. 2.20 and 2.21). Cells were kept under 5% CO_2 at 37°C, and subcultured according to the ATCC protocol [222].

2.9.1 Cell Transfection

GAPDH siRNA Transfection

GAPDH, glyceraldehyde 3-phosphate dehydrogenase, is an enzyme that catalyses part of the process of glycolysis that breaks down glucose to release energy and carbon. GAPDH siRNA can be used as a control in siRNA experiments to test the transfection procedure [218], due to its stability and the high expression of GAPDH in most cells. The GAPDH siRNA sequence targets the 5' medial region of the GAPDH mRNA. It has been successfully transfected into multiple human cell lines, including A459 cells, *in vitro*, by

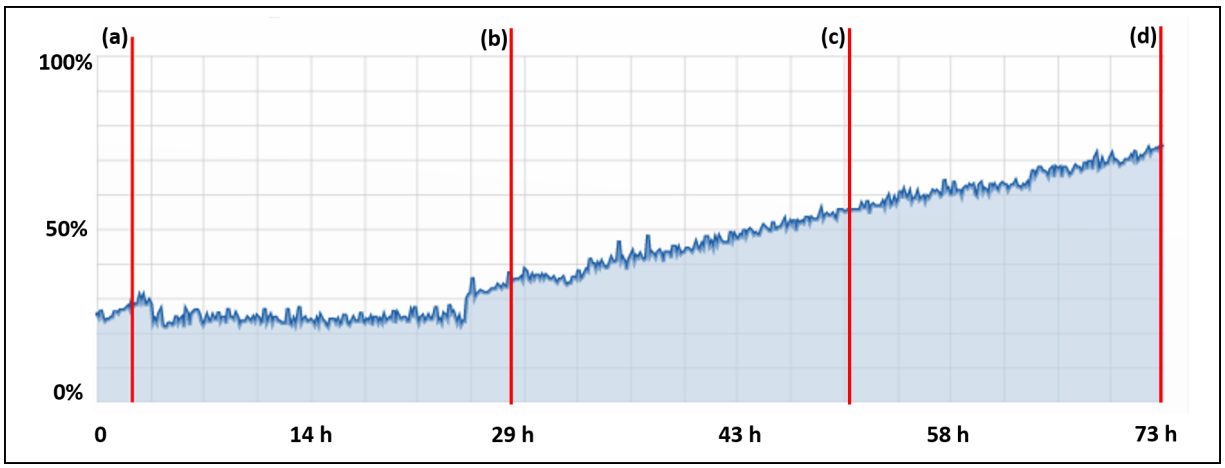

Figure 2.21: Trend of cell coverage over 3 days. (a) after 2 hours, (b) after 1 day and 5 hours, (c) after 2 days and (d) after 3 days, reaching 70-80% confluence

standard transfection methods [223]. A549 cells were seeded in a 6 well-plate at a concentration of $0.8 \times (10)^5$ cells/mL, with 2 mL per well. Complexes of DOTAP-cholesterol (4:1) vesicles and siRNA were formed by mixing at different ratios. DOTAP-cholesterol liposomes were made through extrusion. In each well, 50 pmoles (in 1 mL of Opti-MEM) of GAPDH siRNA and negative control siRNA were prepared. 4 h following the addition of complexes, the Opti-MEM was removed from each well and replaced with cell culture medium. At 72 h post-transfection, cells were washed with PBS and lysed with cell lysis buffer.

2.9.2 DNA and siRNA SAW Transfection

Upright Nebulisation Setup

Standard transfection procedures were performed with materials identical to those used for SAW transfection of DNA and siRNA. In order to deliver the lipoplex to A549 cells, transfection was carried out using the SAW nebuliser. With SAW transfection, the concentration of the DNA solution subjected to nebulisation (3.33 µg/mL) was three times higher than that used in standard transfection (1 µg/mL), in order to account for losses during nebulisation. The ratio of 6:1 lipid-nucleic acid was maintained.

Cells were seeded in single sterile wells of a plate that were placed upside-down on top of the IDT, in order that only the solution inside the desired well was nebulised (Fig. **??**). Cell culture medium (DMEM) was gently removed from the well and two washing steps with PBS were performed. Then a layer of Opti-MEM was added to prevent the cells from drying out. A multilamellar vesicle solution of concentration 2.00 mg/mL with a DNA concentration of 20 µg/mL was released from a syringe pump (World Instrument, Aladin) at a flow rate of 100 µl/min for a total of 2 min. The total amount of DNA/lipid solution nebulised was 200 µl (20 µg/mL of DNA), in a total volume of 1.2 mL of Opti-MEM.

The nebulisation process was carried out for 2 min inside the Microflow Advanced Bio Safety Cabinet (Astec Microflow, Hampshire, UK). After 2 min, 1 mL of Opti-MEM was added and the cells were incubated at 37°C for 72 h for siRNA transfection, and 24 h for DNA plasmid luciferase transfection.
4 h following transfection, the Opti-MEM was removed from the wells, then after incubation, cells were rinsed with PBS. Then 100 µl of cell lysis buffer was added followed and three freeze-thaw cycles were performed.

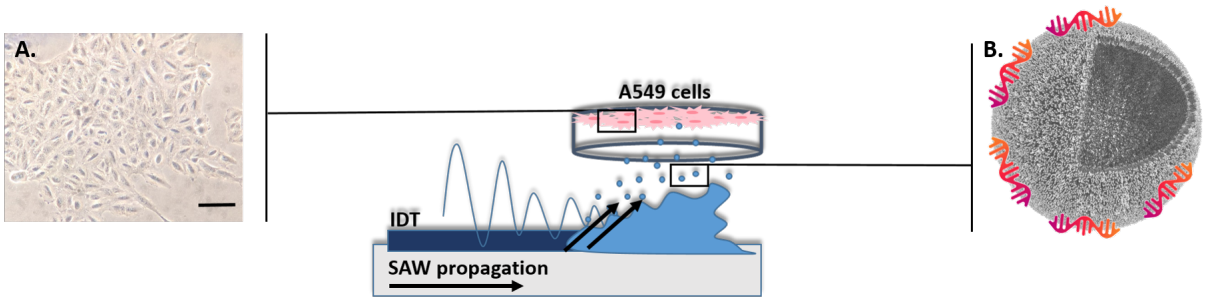

Figure 2.22: SAW transfection upright nebulisation setup. (A.) A549 cells were seeded in a single well and after 24 h the medium was removed. Scale bar 50 µm. Two sets of experiments were carried out: one nebulising a solution of DOTAP: cholesterol with DNA plasmid luciferase and the other with GAPDH siRNA. The solution was nebulised for 2 min, placing the well containing the cells upside-down on top of the nebulised flow. (B.) Image of a lipoplex complex; picture adapted from [34].

Upside-Down Nebulisation Setup

In order to reduce loss during SAW nebulisation whilst keeping the cells in their medium, the setup was optimised. The IDT was placed upside-down, leaving the well containing the cells unchanged. A box was designed using Solidworks and created from laser-cut Polymethylmethacrylate (PMMA) sheets 2.5 mm thick, as shown in Fig. 2.23. The upside-down IDT and petri-dish were fixed inside the box. This increased the transfection efficiency 10-fold. The medium was carefully removed and the wells were rinsed with PBS. 1 mL of Opti-MEM was added and the well was placed below the IDT (Fig. 2.24). Regarding SAW nebulisation, the conditions from the upright nebulisation setup were maintained.

2.9.3 Confocal Live Cell Imaging

A549 cells were seeded in a 35 mm Mattek glass-bottomed culture dish at a concentration of $1.5 \times (10)^5$ cells/mL, with 1 mL medium. MISSION siRNA Fluorescent Universal Negative Control (Sigma Aldrich) conjugated to 6 FAM ($\lambda_{abs} = 495$ nm, $\lambda_{exc} = 520$ nm) was used for visualisation using a fluorescent microscope and assessment of transfection efficiency. A quantity of 150 pmoles of siRNA was used per well (2 µg/well) and the optimised

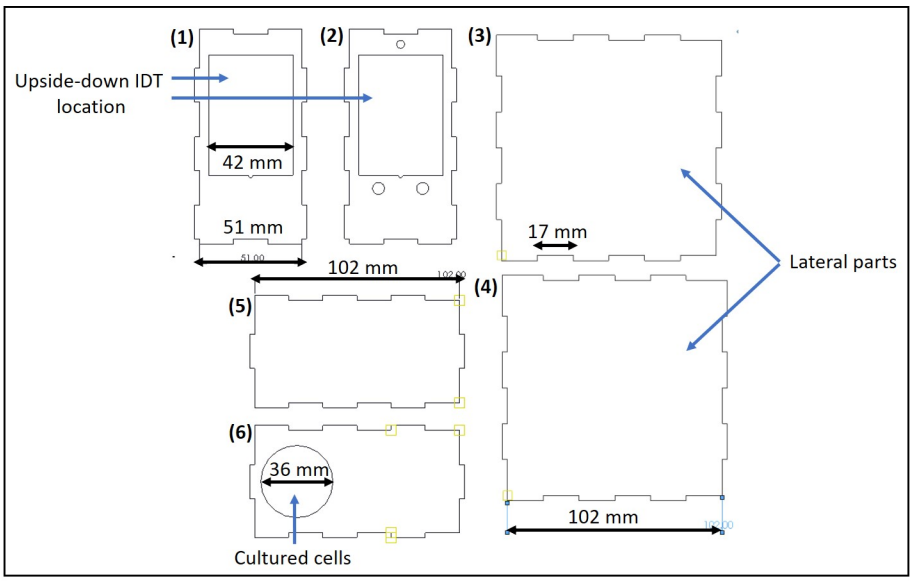

Figure 2.23: Design of the collection box for transfection of A549 cells, using the SAW nebulisation. PMMA sheets were laser-cut and glued together with a solution made of acetone and PMMA. The nebuliser was placed upside-down to leave the cells culture in their medium.

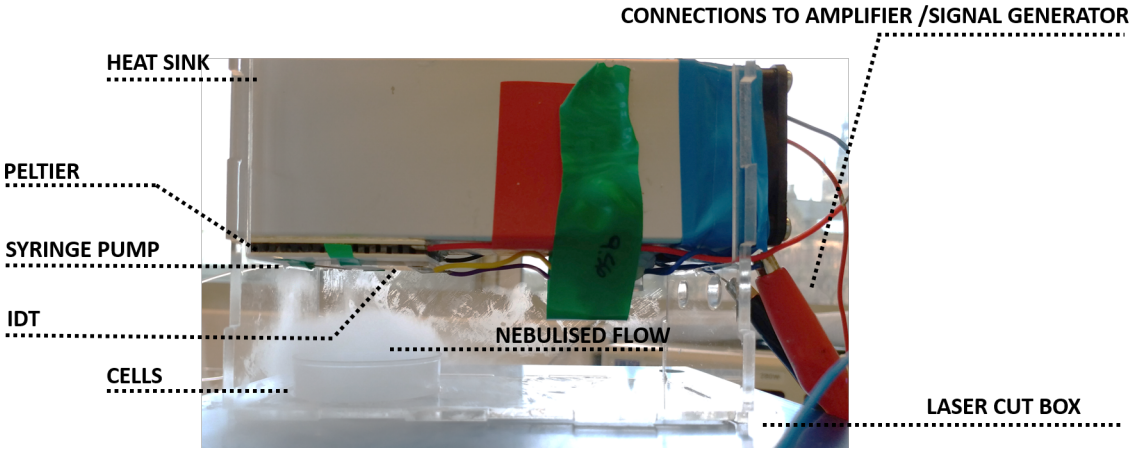

Figure 2.24: Upside-down nebulisation setup for SAW transfection. A549 cells were seeded in a single well. Two sets of experiments were conducted. Solutions of DOTAP:cholesterol with DNA luciferase plasmid and with GAPDH siRNA were nebulised. In order to be able to leave the cells in the medium, the setup was placed upside-down, with the nebulised flow beginning at the top of the well. Nebulised droplets were collected in the well containing the cells.

ratio of lipids to siRNA as determined by the results of standard transfection was used (DOTAP:Chol 4:1, lipids:siRNA 6:1). Nebulisation of the complex by SAW was carried out for 2 minutes as described previously. After 3 h of incubation at 37°C, the transfection medium was replaced with fresh culture medium. Hoechst stain at a concentration of 5 µg/mL was added to each well to stain the nuclei, then cells were incubated for a further 30 min. Prior to visualisation, the wells were washed 10 times with PBS to remove any non-

transfected siRNA. The cells were visualised under a confocal laser scanning microscope (Zeiss LSM 780 inverted microscope, Jena).

2.9.4 Image Analysis

A densitometry assay was performed to analyse the integrity of HS-DNA and the band density in the western blot using ImageJ software (Version 1.45S) and the results were reported as an average of three independent repeats.

2.9.5 Statistical Analysis

The results in this thesis are presented as means ± standard deviation (SD) in triplicate unless otherwise stated. For comparisons between different groups, an ANOVA test followed by a Tukey test was executed. For comparisons between two groups, a t-test has been performed. $p < 0.05$ was considered to be statistically significant. Statistical analyses were performed with the GraphPad Prism 5 (GraphPad Software Inc., La Jolla, USA).

Chapter 3

The Stability of Pre-Formed Liposomes during SAW Nebulisation

3.1 Context and Aim of Result Chapter

Liposomes nebulisation using jet and ultrasonic nebulisers have been studied previously [69]. In 1998 Taylor and Bridges showed that using those nebulisers, a damage to liposomes structures occurred, with a reduction in the measured vesicles sizes [68], [70]. The strong shear forces, exerted on the nebulised particles, resulting in a liposomes damage [69]. In addition, the liquid in the nebuliser was constantly recirculated, leading to the accumulation of stresses during the prolonged nebulisation [224]. The delivery of thermosensitive enzymes such as HRP is also critical in terms of denaturation of the protein. Studies showed that the melting of the HRP's tertiary structure takes place at 45 °C and its functionality is not retained any longer [225].

This chapter focuses on the SAW nebulisation of pre-formed liposomes of a specific size for pulmonary drug delivery. The size stability of liposomes before and after SAW nebulisation was assessed by indirect measurements to test as unlike to jet and ultrasonic, the SAW nebulisation preserved the size of liposomes and the enzyme functionality. Two different techniques were used to characterise liposome stability after SAW nebulisation. The first method was the dynamic light scattering. The second method involved was the horseradish peroxidase (HRP) assay to test the retention of enzyme activity after the SAW nebulisation. An indirect method, such as an enzyme assay technique, was employed to determine LUV stability, as the size of the individual vesicles ($d = 100 - 200$ nm) renders their direct visualisation by conventional fluorescence microscopy unfeasible. Moreover, the assay was chosen due to its capacity to give a high signal to noise ratio (SNR), from small concentrations of both the enzyme and the substrate, and to be quantitative over a wide range.

The SAW nebulisation was proved to be a suitable means of pulmonary drug delivery,

sparing the functionality of enzymes and stability of the liposomes.

3.2 Results

3.2.1 Triton X-100 Calibration

Three different concentrations of Triton X-100 were tested, in order to determine which was the best one for solubilising the liposomes and releasing their contents, as described in Section 2.7.3. Triton X-100 at concentrations of 0.01% v/v, 0.50% v/v and 1% v/v were added into a solution of extruded LUVs (Section 2.4.3), of $100 - 200$ nm diameter (Fig. 3.1 and 3.2). For the lowest concentration (0.01 %v/v) the surfactant was incubated for 20 min, without showing any change in size, thus the concentration was increased to 0.50% v/v and after 1 min a decrease in size appeared. Size measurements before and after adding Triton X-100 showed that 1% v/v is the optimal concentration for bursting liposomes, demonstrating a decrease in peak size from $100 - 200$ nm to 10 nm, indicating solubilisation of the liposomes by the surfactant, and the formation of lipid-detergent mixed micelles. Micelles are usually in the range of $2 - 20$ nm in diameter [191].

Above the critical micelle concentration (CMC), micelles are spontaneously formed, the incubation time required for lipid bilayer solubilisation is inversely proportional to micelle concentration. Triton X-100 was tested to see how it affected the HRP-TMB reaction. A solution of 10 nM HRP was used as described in Section 2.4.1 and different concentrations of Triton X-100 were added: 0.01%, 0.1%, 0.5% and 1.0% v/v. Samples with the detergent, compared to those with water, resulted in a change of O.D. The greatest change in signal was apparent at 1.0% v/v of Triton X-100 (see Section 3.5).

3.2.2 Lipid Bilayer Solubilisation by Triton X-100

In order to prove that the size intensity peak obtained from DLS measurements was due to lipid bilayer vesicles, solubilisation of the bilayer was induced using 1%v/v Triton X-100, as described in Section 2.7.3. Figure 3.3 shows that in the sample collected after SAW nebulisation, adding Triton X-100 reduces vesicle size from 100-200 nm to 10 nm. The change in peak size from 200 nm (red, black line) to 10 nm (blue line) can be explained by the solubilisation of the lipid bilayer and consequent formation of mixed lipid-detergent micelles which are usually 3-50 nm [226] in diameter. The 10 nm peak in Fig. 3.3 results from the range of micelle sizes.

Triton X-100 Negative Control

Triton X-100 was used to solubilise the lipid bilayer of the liposomes and induce the release of the encapsulated compound. In order to check that the increase in optical depth

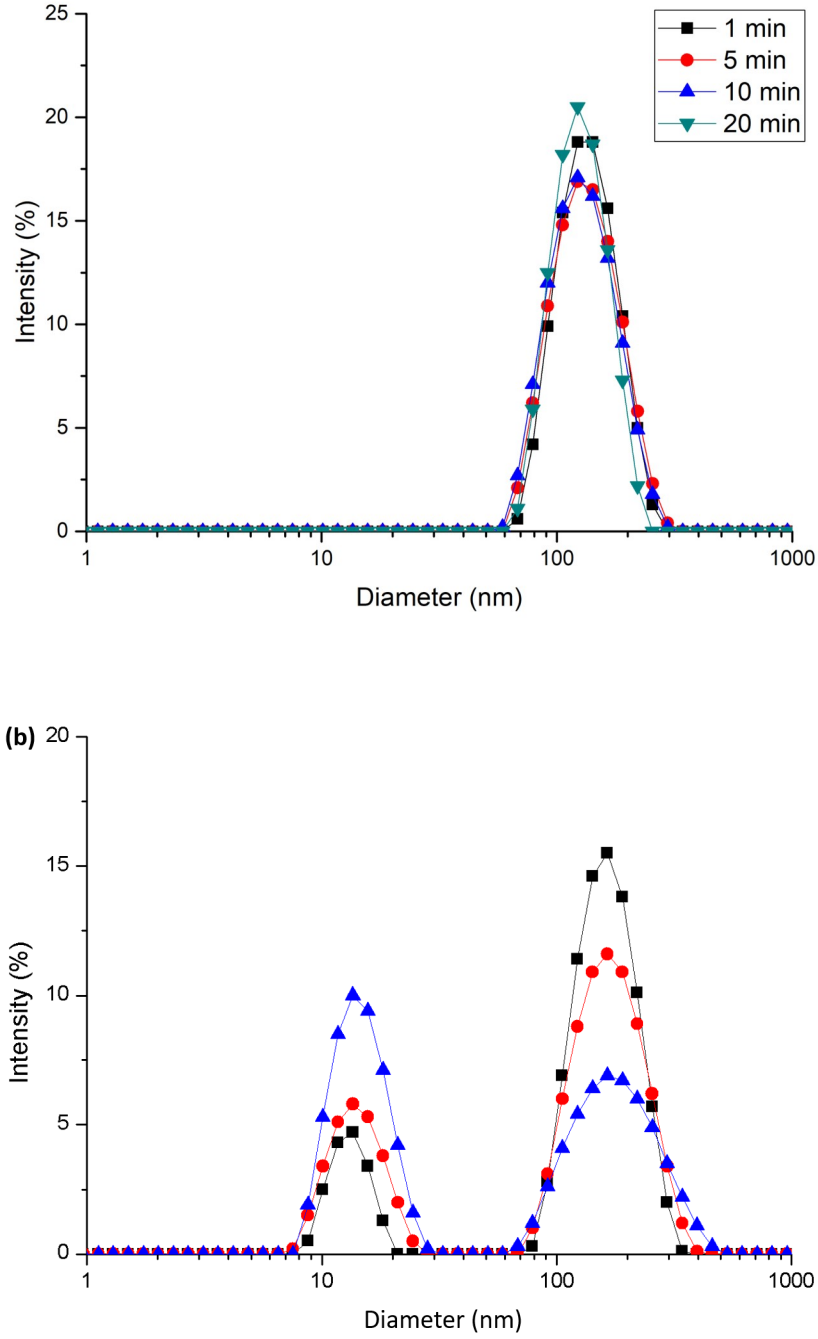

Figure 3.1: Size distribution of extruded liposomes after different incubation times.(a) Solution of 0.01 %v/v of Triton X-100, incubation time of: 1 min (black), 5 min (red), 10 min (blue) and 20 min (green).(b) Solution of 0.50 %v/v of Triton X-100, incubation time of: 1 min (black), 5 min (red) and 10 min (blue). Higher concentrations of Triton X-100 reduced the time taken for the complete solubilisation of the phospholipid bilayer.

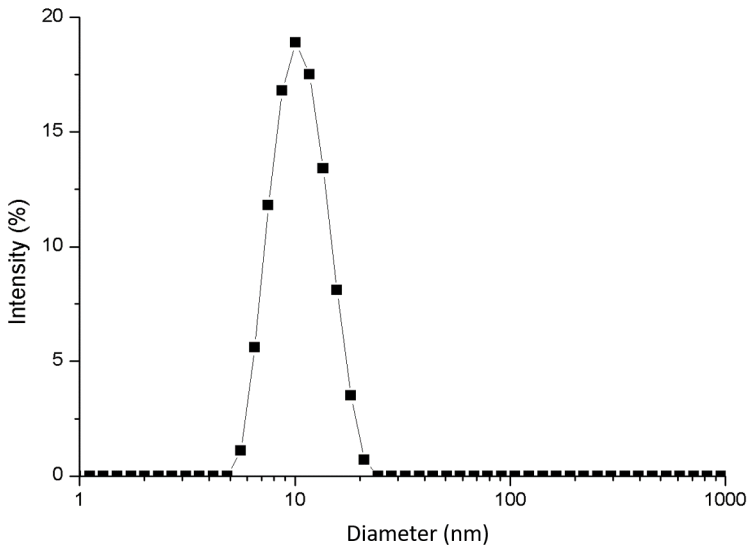

Figure 3.2: Size distribution of extruded liposomes after an incubation time of 1 min with a 1.00 %v/v Triton X-100 solution. With a concentration of 1.00 %v/v of detergent, solubilisation of the membrane was achieved by 1 min.

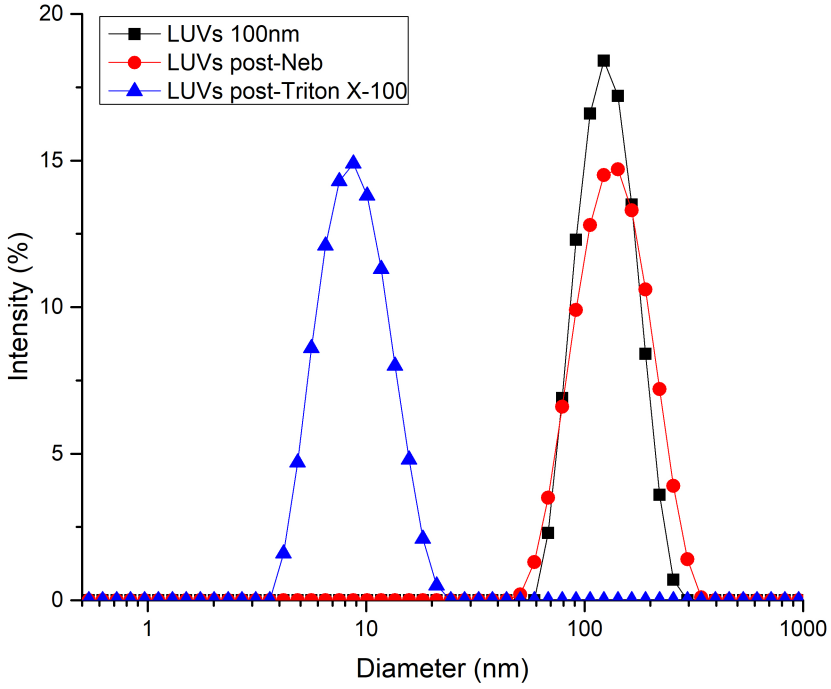

Figure 3.3: Size distribution of extruded liposomes with HRP encapsulated (in black). The same sample was then subjected to SAW nebulisation (in red) and finally, the blue graph shows the size distribution after adding Triton X-100. The results show that Triton X-100 solubilised the liposome bilayer.

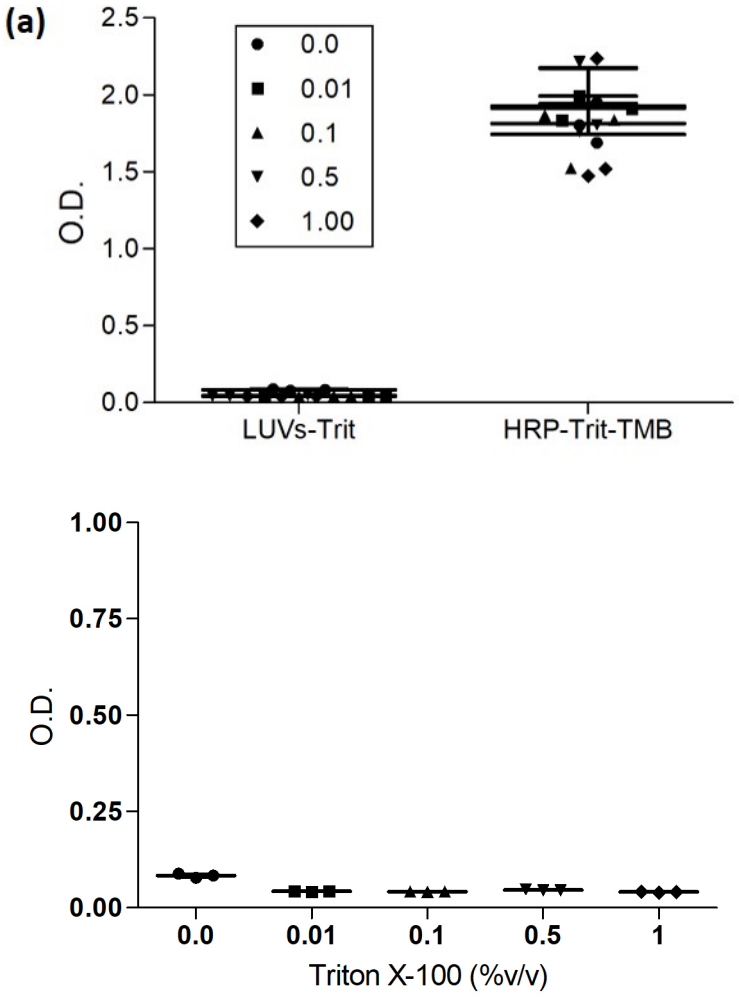

Figure 3.4: A negative control was run to prove that the optical depth signal was due to the sole interaction between the HRP and TMB. (a) Two samples of liposomes (a) without HRP (10 nM) encapsulated and (b) with HRP encapsulated in the liposomes were solubilised to test the optical depth of both samples. As expected, OD from the sample (a) was null.

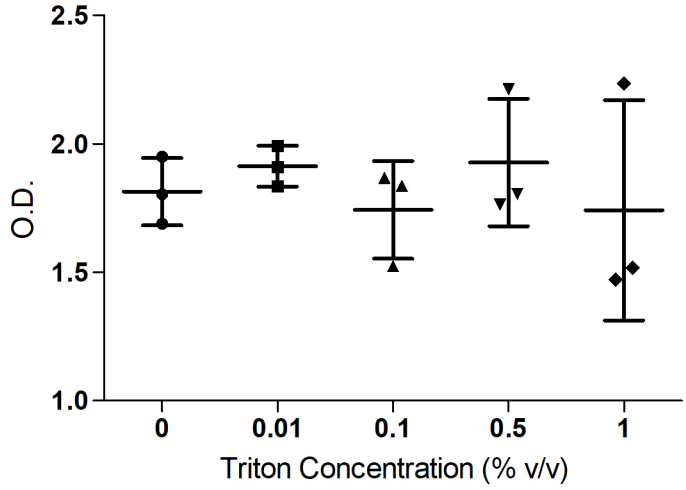

Figure 3.5: Negative control with Triton X-100. 10 nM HRP was used for each sample and different concentrations of Triton X-100 were tested, in order to assess if the detergent was affecting the HRP-TMB reaction. Triton X-100 concentrations of 0.00 %, 0.01%, 0.10%, 0.50% and 1.00% v/v were compared. The P value obtained was higher than 0.05, meaning that no statistically significant differences were found between the samples. Thus, Triton X-100 is suitable for solubilising HRP-containing liposomes, since it does not seem to interfere with the HRP-TMB reaction.

was actually due to increased HRP activity, a negative control was run. Five different concentrations of Triton X-100 were made up in DI water: 0.00 %, 0.01 %, 0.10 %, 0.50 % and 1.00 %v/v and optical depth was measured to test if Triton X-100 alone was increasing the optical depth. Negative control samples were made of: (1) HRP 10 nM, H_2O, TMB, and sulfuric acid to stop the reaction after 60 s and instead of H_2O, (2) 0.01% v/v Triton X-100, (3) 0.10% v/v Triton X-100, (4) 0.50% v/v Triton X-100 and (5) 1.00% v/v Triton X-100. From Fig. 3.5, it is apparent that the O.D. was not significantly different at the various Triton X-100 concentrations compared to in the blank sample (0 % v/v of Triton X-100), with small variations $OD = 1.83 \pm 0.13$. This proved that increased optical depth following the nebulisation of HRP-encapsulated liposomes is due to the release of HRP, rather than from the Triton X-100 itself.

3.2.3 Horseradish Peroxidase Calibration

Before starting the nebulisation experiment, a calibration curve was generated in order to determine the appropriate concentration of HRP to be encapsulated within the liposomes. On a 96 well-plate, 100 µl aliquots of HRP at different concentrations were prepared: 0.002, 0.4, 0.8, 2, 5, 10, 15, 20 and 30 nM were used (Fig. 3.6 (a)), with three different incubation times of 90 s (black line), 60 s (red) and 30 s (blue) . The following concentrations were also tested: 5, 7.5, 10. 12.5, 15, 17.5 and 20 nM, at the same incubation time (Fig. 3.6

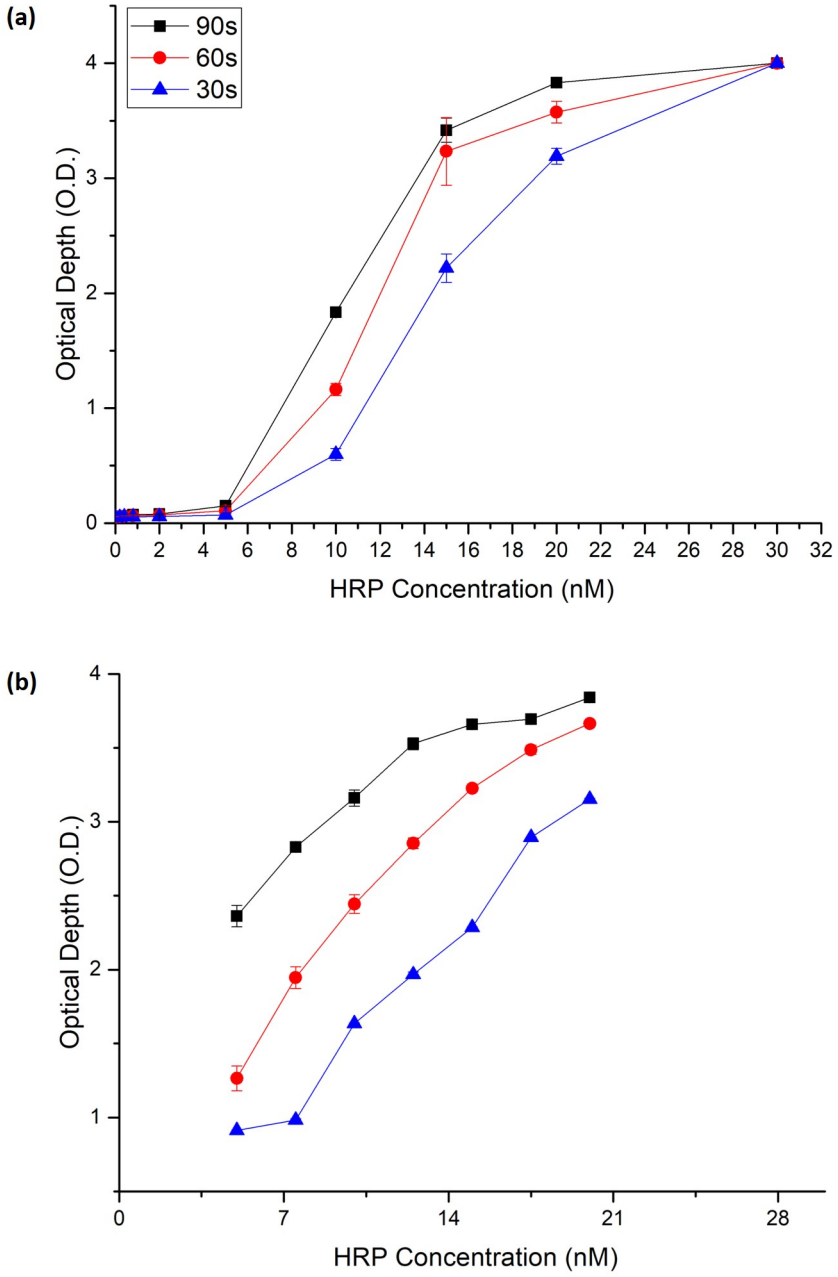

Figure 3.6: A HRP-TMB reaction calibration curve was obtained in a 96-well plate. 100 µl volumes of HRP at different concentrations were prepared (n=5). (a) Concentrations of 0.002, 0.4, 0.8, 2, 5, 10, 15, 20 and 30 nM were used, as were three different incubation times of 90 s (black), 60 s (red) and 30 s (blue). (b) The following concentrations were also tested: 5, 7.5, 10. 12.5, 15, 17.5 and 20 nM, at the same incubation time. PBS was used as a negative control.

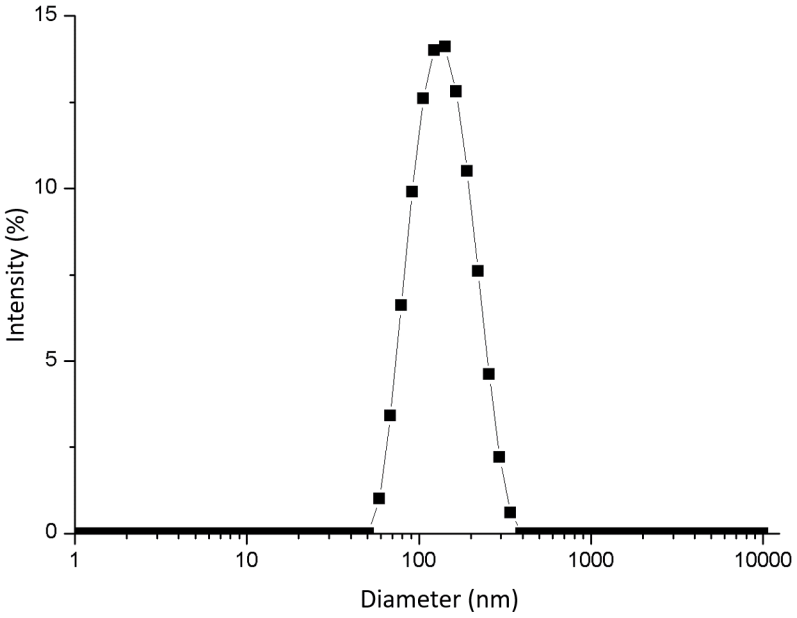

Figure 3.7: Size distribution of liposomes after extrusion through polycarbonate pores of 200 nm diameter. The peak width indicates a narrow, monodisperse distribution.

(b)).

100 µl of TMB was added to the HRP solution in each well. Then 100 µl of 1 M sulfuric acid solution was added in each well at 30, 60 or 90 s to stop the reactions. PBS was used as a negative control. Considering the obtained calibration curve, an HRP concentration of 20 nM was chosen for encapsulation in the liposomes, which would result in O.D. values detectable by the plate reader. HRP-encapsulated liposomes were made following the procedure described in Section 2.4.1.

3.2.4 Particle Size

Comparison of Vesicle Size During Dialysis and SAW Nebulisation

The dynamic light scattering method (see Section 2.5.1) was used to measure the size of the extruded liposomes and to determine changes in size after dialysis and SAW nebulisation. Fig. 3.7 shows the size distribution after extrusion of lipid solution through a membrane with 200 nm pores; the sharpness of the Gaussian distribution indicates low polydispersity of the sample with $PDI = 0.1$. A sharp Gaussian distribution represents a monodisperse sample, whose PDI lies within 0.01-0.4. According to the one size distribution peak hypothesis, the PDI is the square of the standard deviation divided by the square of the mean [227].

Size measurements were also carried out after dialysis and after SAW nebulisation in

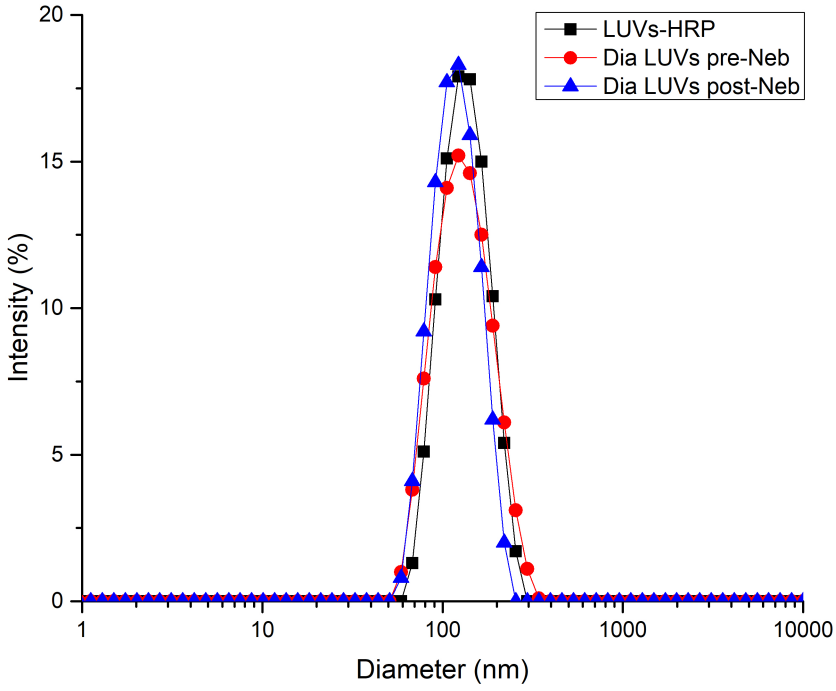

Figure 3.8: Size distribution of extruded liposomes containing HRP (in black). The same sample was then dialysed (results in red) and finally, the blue graph shows the size distribution after SAW nebulisation. The results show that SAW nebulisation is a suitable method for delivering liposomes that are 200 nm in diameter.

order to see if the size of the liposomes was maintained during these procedures. Fig. 3.8 shows that liposome structure was stable during dialysis and SAW nebulisation, or that most of the liposome population was the same size (200 nm in diameter). The same size distribution was obtained for samples collected after extrusion, after membrane dialysis and after SAW nebulisation. These results confirmed the suitability of SAW for nebulising liposomes that are $d = 100 - 200$ nm in diameter, without fragmenting the phospholipid bilayer.

3.2.5 Rhodamine B Calibration Curve and Capture Efficiency

In order to evaluate the particle loss during collection after SAW nebulisation, a solution of Rhodamine B (RhB) at a concentration of 100µm was nebulised using SAW. A calibration curve was made using different concentrations: 1, 2.5, 5, 10,15, 20, 25, 50 µM (Fig. 3.9, (a)). The calibration curve was fitted with an exponential curve and the following equation was obtained:

$$y = 8208 - 8440e^{-0.08x} \tag{3.1}$$

with a coefficient of determination R^2=0.99. 100 µl of 100 µM RhB solution was nebulised and collected in 25 µl of DI water, and 75 µl of DI water was added after collection to obtain a total volume of 100 µl, which was then subjected to fluorescence intensity measurements. The fluorescence intensity of the nebulised sample was compared with that of an equal volume of non-nebulised 100µM RhB solution (Fig. 3.9, (b)). Using the calibration curve, it was apparent that a concentration of 12.3 µM±0.9 was obtained following nebulisation. However, the solution had been diluted by a factor of 4 by the addition of DI water. Considering the dilution factor and that the 12.3 µM±0.9 was in the linear region, the effective post-nebulisation concentration was calculated to be 49.1 µM±3.6. This result indicates that around 51% of the solution was lost during nebulisation.

3.2.6 Nebulisation of Liposomes Loaded with HRP

Further experiments were carried out to test the feasibility of using SAW nebulisation to deliver a compound such as HRP without inducing enzymatic degradation, the setup was described in Section 2.7.1. HRP was encapsulated in the liposome and the remaining in the outer solution was removed by dialysis. The stability of liposomes during dialysis was tested collecting the nebulised solution as previously mentioned in Section 2.7.1. Moreover, TMB was added in the dialysed solution and measuring the O.D. resulting from the colourimetric reaction between HRP and TMB (Section 2.8.1). From the results, shown in Fig. 3.10, the optical depth signal before dialysis is high, due to the fact that not all of

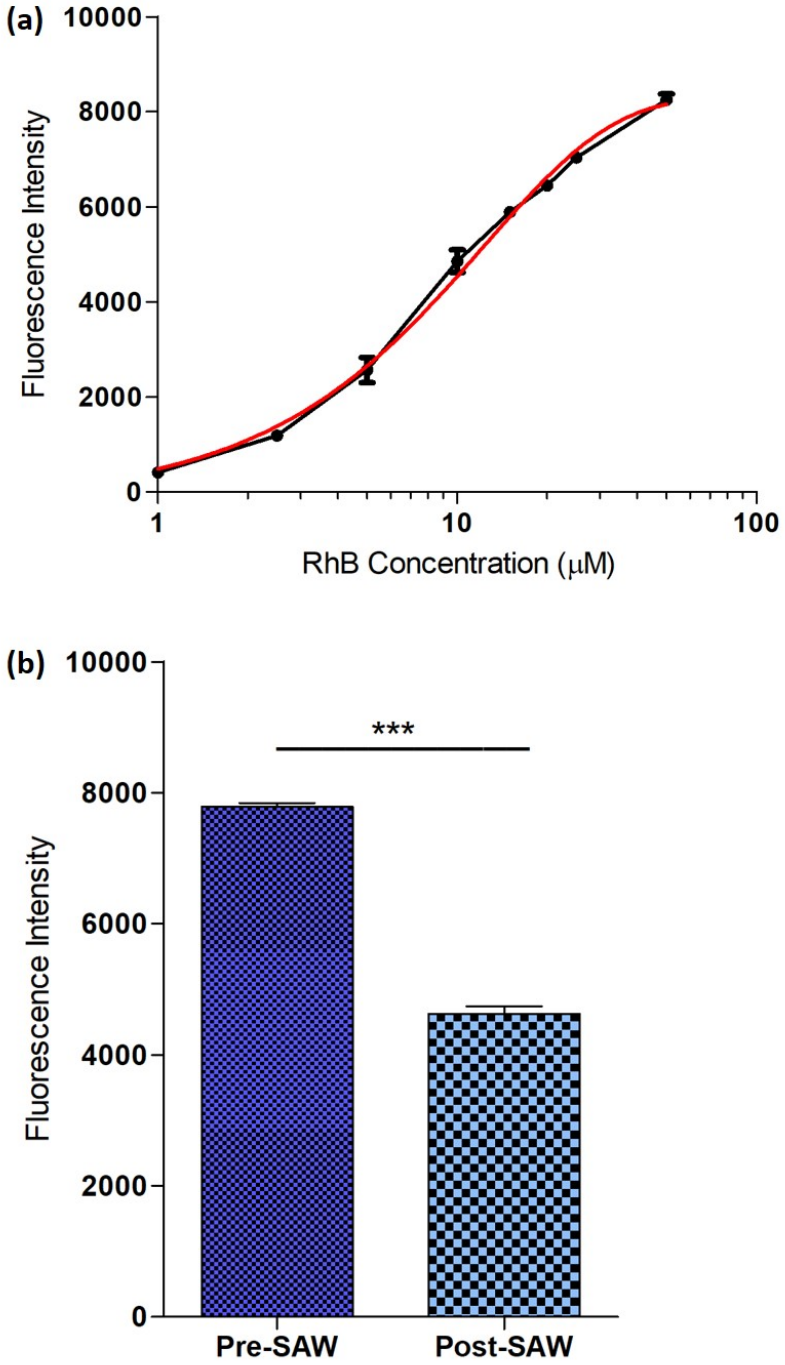

Figure 3.9: (a) A calibration curve was made using different concentrations: 1, 2.5, 5, 10, 15, 20, 25, 50 µM of RhB. (b) Comparison between Pre-SAW, which is made of 100 µM of RhB without nebulisation, and Post-SAW, which represent the same solution after SAW nebulisation. The reduction in signal indicates loss during nebulisation, which was calculated to be around 51%. The graphs show the mean of three measurements and the error bars represent the SD. ***$p<0.001$

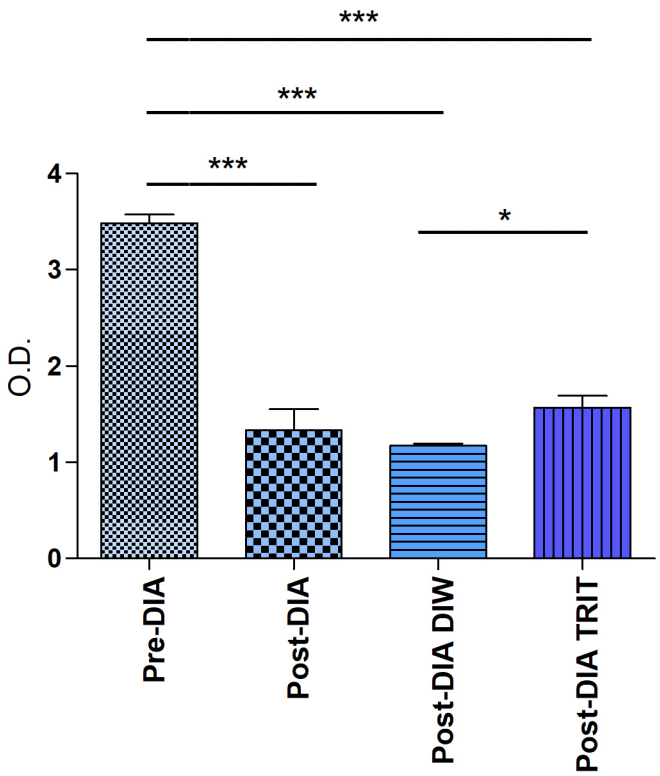

Figure 3.10: Optical depth measurements of HRP and TMB reaction products pre-dialysis, post-dialysis, post-dialysis with the addition of DI water and post-dialysis with the addition of Triton X-100 in the solution. The mean of three measurements is represented and error bars show standard deviation. For comparison between different groups, an ANOVA followed by a Tukey test was carried out with *$p<0.05$, **$p<0.01$, ***$p<0.001$.

the HRP was encapsulated in the liposomes. The signal after dialysis, decreased because the remaining HRP outside of the liposomes was cleared out, and the total quantity of liposomes is lower due to loss during dialysis. Finally, the OD after adding Triton X-100 in the solution is higher, showing that the HRP-containing liposomes were solubilised by the detergent and the encapsulated HRP release in the outer solution.

As shown in Fig. 3.10, dialysis was able to remove HRP from the outer solution and decrease the O.D. by more than 50%. Once dialysis had been tested, SAW nebulisation was commenced and the nebulised solution was collected in TMB buffer (results shown in Fig. 3.13). After collection, Triton X-100 was added to release the encapsulated HRP.

An increase in O.D. was noticed between pre- and post-nebulisation samples after the addition of the Triton X-100, indicating the release of encapsulated HRP. From the data shown in Fig. 3.11 and 3.13, statistically significant differences between the pre- and post-SAW nebulised groups are not always observed.

In Fig. 3.11, the particle loss during the nebulisation process is considered (Fig. 3.9. The O.D of the sample post-nebulisation after the addition of Triton X-100 was multiplied

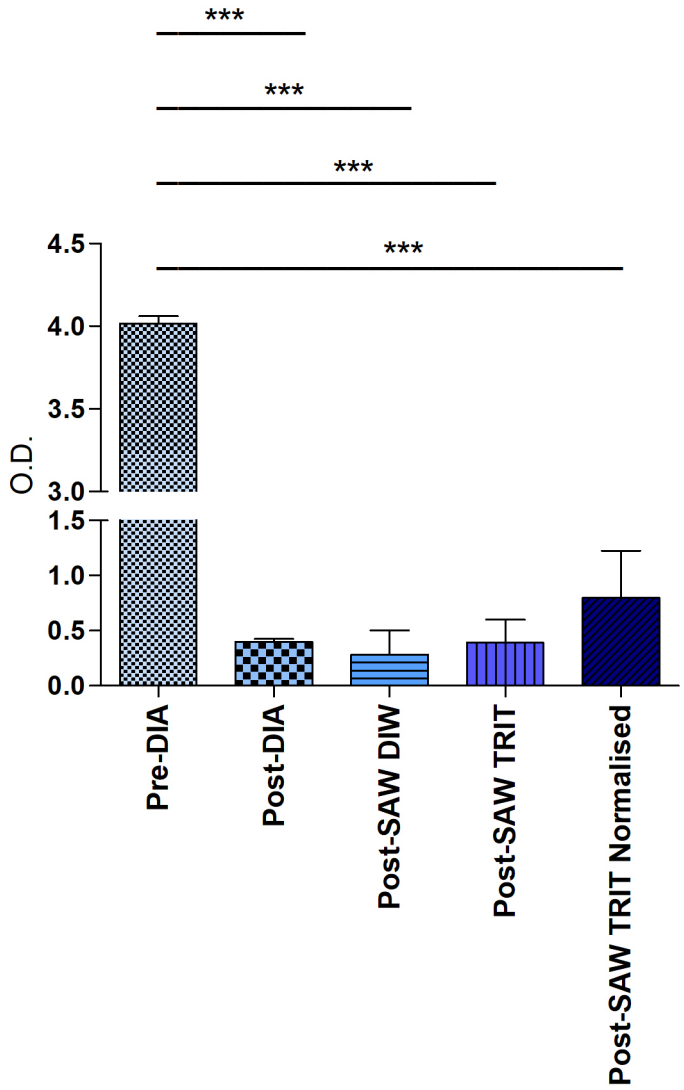

Figure 3.11: Optical depth measurements of HRP and TMB reaction pre-dialysis, post-dialysis, post-SAW nebulisation with the addition of DI water, post-SAW nebulisation with the addition of Triton X-100 in the solution and the Post-SAW with the addition of Triton X-100 normalised, taking into account the 51% loss of the original solution during nebulisation. The mean of three measurements is represented and error bars show standard deviation. For comparison between different groups, an ANOVA followed by a Tukey test was carried out with ***$p<0.001$. A higher signal was obtained for the nebulised sample following the addition of the detergent, showing the release of HRP from the liposome cores. In the drawing showing the level of OD, the blue circle represents an LUVs, the H is for HRP and the red cross indicates the action of the Triton X-100 during the bilayer solubilisation to release the encapsulated HRP.

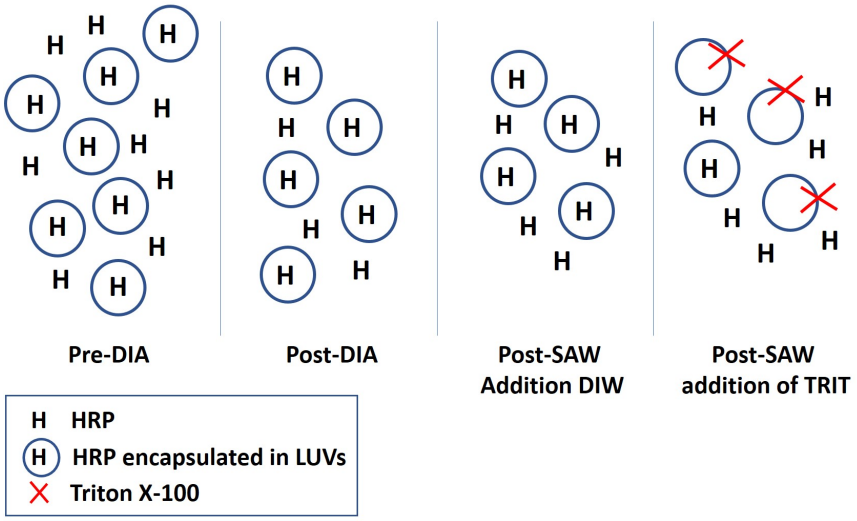

Figure 3.12: Schematic of Fig. 3.11. In the pre-dialysis sample, the HRP is both inside and outside the liposomes, after dialysis the concentration of the HRP in the outer solution decreased, but also the number of liposomes, due to the loss during pipetting and dialysis. After the SAW nebulisation, the number of liposomes decreased more due to the sub-optimal collection of the nebulised sample, the last sample shows the addition of Triton X-100 to the solution which causes the solubilisation of the liposomes and an increase of optical depth.

by the loss factor, but the difference in O.D value was still not statistically significant. In Fig. 3.13, the difference in O.D between the pre- and post-nebulisation samples were considered statistically significant based on an unpaired t-test. This variability in the measurements pre- and post-nebulisation is explicable by the suboptimal collection equipment and the variation of the loss occurring during SAW nebulisation. Optimising the design of the collection equipment should reduce the variability of the obtained measurements. Overall, the increase in O.D before and after SAW nebulisation (Fig. 3.15) provides preliminary evidence of the feasibility of SAW nebulisation to deliver an enzyme encapsulated in liposomes, without breaking the phospholipid bilayer. Further studies will be detailed in the following chapters, with the objective of proving the efficiency of the SAW nebulisation platform.

3.2.7 Enzyme Activity During SAW Nebulisation

As described in Section 2.7.1, a temperature test was carried out to check the suitability of SAW nebulisation in terms of not destroying the activity of the delivered HRP enzyme (Fig. 3.14). The solution was dispensed using a syringe pump and the Peltier was heated to 20°C, 65°C or 95°C. According to the results, enzyme activity was retained at each of the different temperatures used. Different powers were also employed to test their effects on the activity of HRP. Upon increasing the temperature, enzyme activity did not decrease. The fact that the optical depth was the same for the HRP nebulised at

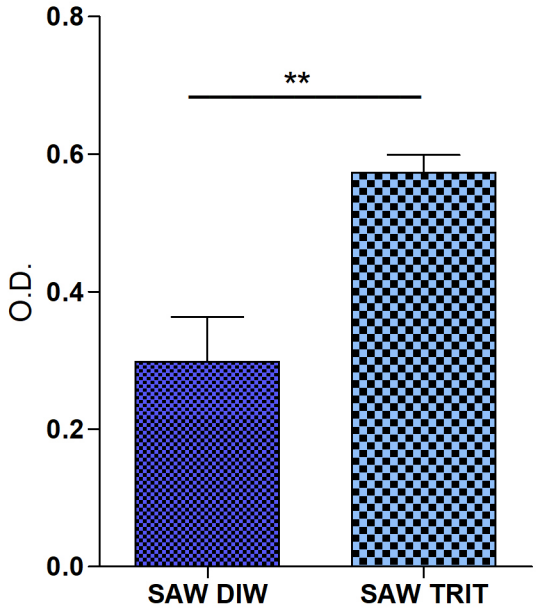

Figure 3.13: Optical depth measurements of HRP and TMB reaction, after SAW nebulisation with the addition of DI water and after SAW nebulisation with the addition of Triton X-100 in the solution. The mean of three measurements is represented and error bars show standard deviation. T-tests have been performed with **p<0.01 The higher optical depth after adding Triton X-100 shows the release of HRP encapsulated in the liposomes and the suitability of SAW to nebulise active compounds encapsulated in the liposomes without breaking them. An unpaired t-test was run, showing a statistically significant difference between the two samples with $p \leq 0.05$

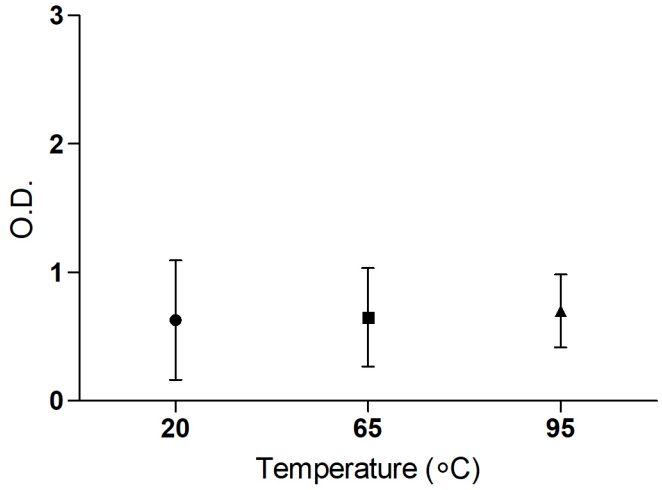

Figure 3.14: Optical depth measurements of HRP and TMB reactions after heating the nebulisation platform (IDT) at 20°C, 65°C and 95°C. The same OD value was observed following exposure to higher temperatures, showing that enzyme activity was not destroyed.

95°C (Fig. 3.14) demonstrates the feasibility of using SAW to nebulise active compounds without denaturing their structure. The configuration of the SAW nebulisation platform, using the syringe pump to gradually dispense the solution, minimised exposure of the enzyme to the high temperatures reached, helping to spare its activity.

3.2.8 Discussion and Conclusion

In this Chapter, the integrity of liposomes has been monitored in terms of the size distribution i.e. comparison of size distribution before and after nebulisation was performed. In previous studies, a decrease in the size indicated liposome damage during nebulisation [68]. Here, the integrity of liposomes after SAW nebulisation is measured, using different methods. Size stability was first tested using dynamic light scattering. Results showed that liposome size was unmodified by dialysis or by SAW nebulisation, as suggested by the maintenance of the same intensity peak (100-200 nm). After dialysis, the same liposome size was observed as before dialysis. That confirmed that dialysis left the majority of the vesicles intact. The size of liposomes after SAW nebulisation was checked, to determine if liposomes can be used as a carrier for drugs to be delivered by nebulisation. The results showed that the size of the liposomes was retained, indicating that SAW nebulisation did not fragment the liposome bilayers of 100 nm size. It represents the first step to test the feasibility of SAW to nebulised 100 nm of diameter vesicles to use as a drug carrier.

A shift in the intensity peak from 100-200 nm to 10-20 nm - the size of micelles - upon the addition of Triton X-100 to solubilise the liposome bilayer confirmed the presence of

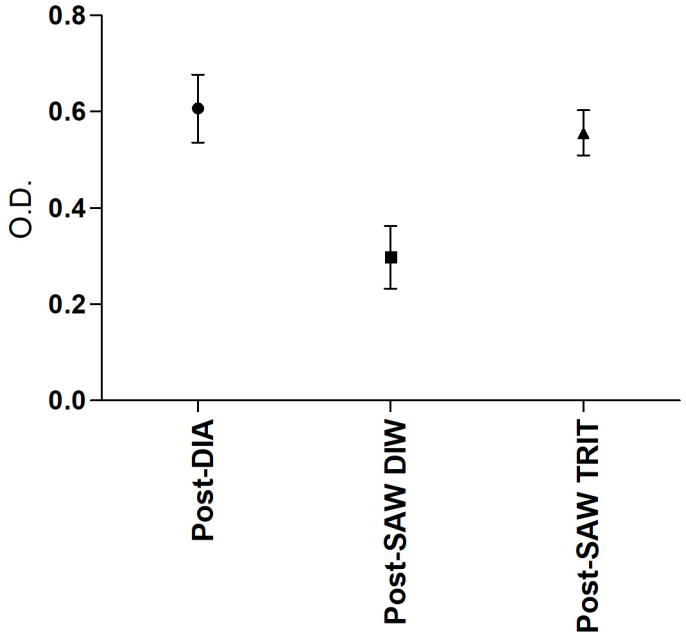

Figure 3.15: Optical depth measurements of HRP and TMB reaction, post-dialysis, post-SAW nebulisation with the addition of water and post-SAW nebulisation with the addition of Triton X-100. The graph shows that during the nebulisation process around 49% of the solution is lost. Then, after the addition of Triton X-100, the O.D increased again by 50%. Each point represents the mean values of three measurements. Error bars represent the standard deviation of three measurements.

the vesicles [228].

In order to prove that SAW nebulisation is suitable for delivering temperature-sensitive enzymes [225], an indirect method was used to test the integrity of liposomes after SAW nebulisation, using the HRP assay. The HRP was encapsulated in the liposomes through the thin film hydration method and then nebulised using SAWs. After the collection of the nebulised particles and the addition of Triton X-100 to release the HRP from the vesicles, TMB was added into the solution. According to the data shown in Fig. 3.15, the increase in signal from the HRP-TMB reaction showed that SAW nebulisation did not destroy the enzyme activity or the liposome structure. Comparison of the O.D. before and after nebulisation and the addition of Triton X-100 showed an increase (Fig. 3.13) of the signal, but the difference between the two measurements was not always statistically significant (Fig. 3.11). This is mainly due to particles loss during SAW nebulisation and the suboptimal collection equipment, so the total amount of vesicles in the solution is lower after nebulisation (Fig. 3.15). Improvements to the equipment configuration were made as detailed later on in this work, in order to reduce particle loss. A nebulisation box was designed (See Chapter 6) to confine the nebulised flow.

Elevated temperatures within the reservoirs of ultrasonic nebulisers can damage the active molecules being delivered, reducing their functionality [203]. A temperature test was

performed during SAW nebulisation, to see if the active compound (HRP) was denatured at high temperatures. The measured O.D. did not change as the temperature was increased (Fig. 3.14). The experimental equipment used the syringe pump to dispense the right amount of liquid and allow it to be nebulised instantly. This dispensing method minimised the exposure of the enzyme (HRP) to high temperatures, thus helping to protect its activity.

In conclusion, it was proven that SAW nebulisation is a suitable method for the delivery of temperature-sensitive proteins and enzymes and to nebulise pre-formed liposomes of 100 nm diameter, which can be used as drug carriers to encapsulate compound and deliver them via inhalation. The work carried out in this Chapter represents a preliminary test to show that SAW is a suitable method to nebulise and deliver liposomes. once the feasibility of using SAW to nebulise liposomes was tested, the next step was to try to combine the formation of liposomes and aerosols in one single step, without the requirement of pre-formulation.

Chapter 4

Liposome Formation *In-Situ* on a SAW Nebulisation Platform

4.1 Context and Aim of Result Chapter

A major problem with current drug delivery system is their inefficiency at delivering expensive drugs to their targets, leading to high overall treatment costs. In order to protect and deliver the high-value compound and control the release of the drug inside the cell, drugs are often encapsulated into protective liposomes [36]. However, a multistep process is required for their formation, often performed during the formulation step, therefore, limiting indirectly (e.g. freeze-drying step, or addiction of cryo-protectants) the range of drugs available or their shelf-life [229], [40], [230]. For instance, the preparation of liposomal Ciprofloxacin requires several different steps [231]: preparation of an MLV dispersion, extrusion of the unilamellar vesicles, which is time consuming (see Section 2.4.3), active loading of the drug and finally the nebulisation process. The work carried out in this Chapter hopes to address the issue of liposomes stability during the nebulisation, avoiding the need of liposomes prior-formulation and prolonging their shelf-life. Studies about the formation of liposomes using SAWs and to use cavities to confine the nebulised volume and thus, eliminating the production of large aerosols and indirectly of the large liposomes, were not made previously.

A new method based on Surface Acoustic Waves (SAWs), coupled with a microfabricated silicon chip, to produce aerosols within the desired range and together form liposomes *in-situ* within the delivery device, is presented. The size of produced aerosols and the formation of drug carriers for a successful delivery of pulmonary drug were evaluated and analysed.

The objective of this part of the work is to create liposome drug carriers within a SAW nebulisation platform and to control the aerosol's size within the respirable range. Unilamellar liposomes of 100 nm diameter were formed and encapsulated in aerosols of 1

to 5 µm. The results obtained are proving the potential of the SAW nebulisation platform as an efficient pulmonary drug delivery system.

4.2 Results

4.2.1 Aerosol Size Control with SAW Nebulisation in a Confined Space

As introduced in Chapter 1, one of the key parameters for an efficient pulmonary drug delivery system is the control of the aerosolised droplet size [232]. The complex nature of the SAW nebulisation process makes it hard to understand and despite various studies on the topic, the effect of specific parameters on the aerosol droplet size is not explicitly clear [117], [233], [137]. As discussed earlier, the high shear stresses of nebulisation techniques damage biological compound and fail to deliver them. However, SAW nebulisation is proved to be a promising method for delivering cells, polymers, nanoparticles, proteins and DNA [11], [234], [137], showing the presence of the undamaged compound after the SAW nebulisation.

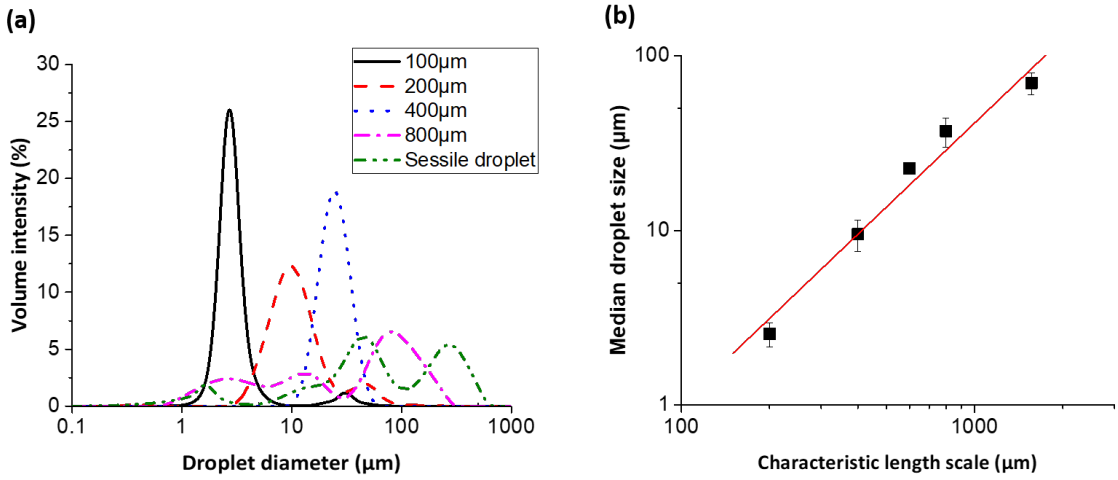

Figure 4.1: SAW Confined Nebulisation. (a) The graph shows volume intensity plotted against aerosol size distribution. From laser diffraction measurements a size distribution in the optimal size range for pulmonary drug delivery (1 µm < d < 5 µm)was obtained using a silicon chip with pore size of 100 µm. (b) The relationship between the characteristic length scale of the pores and the aerosol median droplet size. The graph shows that with the decrease of the pore sizes, from which the SAW nebulisation occurs, a decrease of the aerosol droplet size was obtained [235]. The mean of three measurements is represented and error bars show the standard deviation.

A specific study regarding the size of SAW-nebulised particles was made [235] with a completely new approach using a physical confinement made from a silicon wafer, as described in Section 2.3, to decrease indirectly the size of the nebulised droplets, by reducing

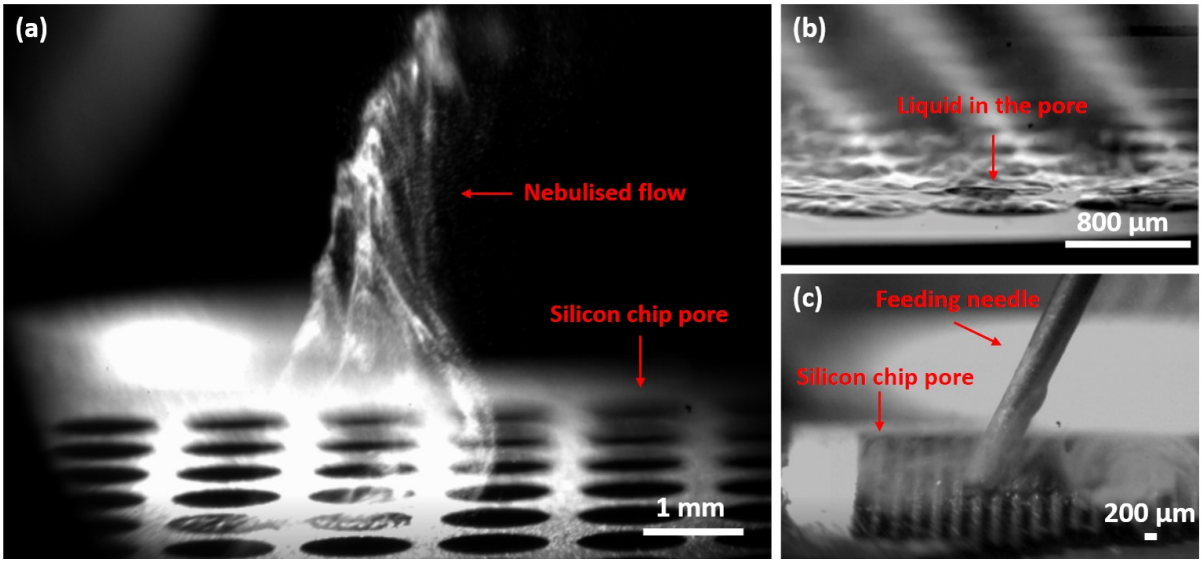

Figure 4.2: SAW nebulisation from silicon chip. (a) Nebulisation from 800 µm cavities in diameter. (b) Close-up of the SAW nebulisation within 800 µm cavities. (c) SAW nebulisation from 200 µm cavities.

the surface wave wavelength. Experimental evidence highlighted the relation between liquid length scale and capillary wavelength; the capillary wavelength decreases as the liquid length scale reduces [235]. The physical confinement can be consider as a low-pass filter, which filters out capillary wave's wavelength that results in the formation of large droplets. This theory is implemented by using a silicon chip with an array of wells (cavities), coupled with the IDT, as previously described in Section 2.7.2.

Using cavities of increasing diameters, the median droplet size of the aerosol produced increases. Cavities of diameter: 100, 200, 400, 600, 800 and 1200 µm were employed. For 100-200 µm cavity, a median droplet size distribution within 1 µm and 5 µm was acquired. Increasing the cavity size to 400, 600 and 800 µm, a size distribution of 20 µm and a multimodal size distribution with peaks around 80 µm and over 100 µm was obtained (Fig 4.1). The smaller the cavity from which the nebulisation occurs, the smaller the aerosol size, this is due to the physical restriction of the liquid, which decreases the wavelength of the SAW responsible for the production of the aerosol (Fig. 4.2). The aerosol's size was determined using the Spraytec, which is based on the laser diffraction principle, described in Section 2.6.1.

4.2.2 Size of SAW-Formed Liposomes

In order to form LUVs on SAW platform, two different methods were tested: (1) SAW nebulisation of MLV solution, previously made through a silicon chip made of cylindrical cavities and (2) spinning phospholipids on IDT, application of the silicon chip, incubation with DI water (consequent swelling of phospholipid, with the production of MLVs) and the

SAW nebulisation. The two methods were described in Section 2.7.2. After measuring the vesicle output from the two approaches and determining that the two methods produced the same size of vesicles (Fig. 4.4), the first method was chosen, because easier and faster to carry out.

Nebulisation of Lipid Solution

An MLV solution was prepared and nebulised with and without the silicon chip, coupled on the IDT, as described in Section 2.7.2. Size measurements of liposomes using dynamic light scattering have shown significant differences in size (Fig. 4.3) between: (1) the MLVs mixture, which presents a high-intensity peak at 4 µm diameter, (2) the MLVs subjected to SAW nebulisation without silicon structure, resulting in liposomes around 200 nm and 2 µm of diameter, and (3) SAW nebulisation with the silicon structure, exhibiting a pronounced peak around 200 nm. The nebulisation occurred for an input power of -4 dBm (Fig. 4.3, (a)). Same measurements were done for an input power of -2 dBm, and comparison between liposome populations produced using the two power settings are displayed in Fig.4.3, (b)). The results present a decrease in liposome size after nebulisation and a further decrease after the use of the silicon chip. The hypothesis is that SAWs are supplying the energy necessary to break down the multilamellar vesicles in smaller liposomes. Moreover, even smaller particle size distribution was measured when the SAW nebulisation occurred through the silicon chip, obtaining a monomodal-like size distribution around 200 nm. Higher input power (-2 dBm, 7.5 W) does not seem to decrease the size of the vesicles, but in the next few Sections, further measurements will be carried out in order to evaluate the effect of different parameters such as the cavities size, the lipid concentration and the input power on the size of the liposomes produced by SAW.

Compared to SAW nebulisation of the free sessile droplet, using a physical confinement to contain the liquid resulted in a smaller size distribution of nebulised particles. Further experiments were carried out, in order to test if the physical confinement could be also responsible for the liposomes formation as well as the aerosol production in the optimal size range (Fig. 4.1). For a better understading of the liposomes generation process, the formation during nebulisation was monitored. A sample of the nebulised solution was collected at different stages and checked using the confocal microscopy, as shown in Section 4.2.6. Observations confirmed that MLVs were initially broken down, due to the energy of SAWs, forming BPFs, which were then closing up due to the hydrophobic effect of the phospholipid's tail. Liposomes of sizes in the range of 100-200 nm were formed. Once the size was measured, Cryo-TEM was used to check the structure of the liposomes, particular the lamellarity (Section 4.2.7). SAW nebulisation is a fast process and although a fast speed camera was also employed, a real understanding of the process was difficult.

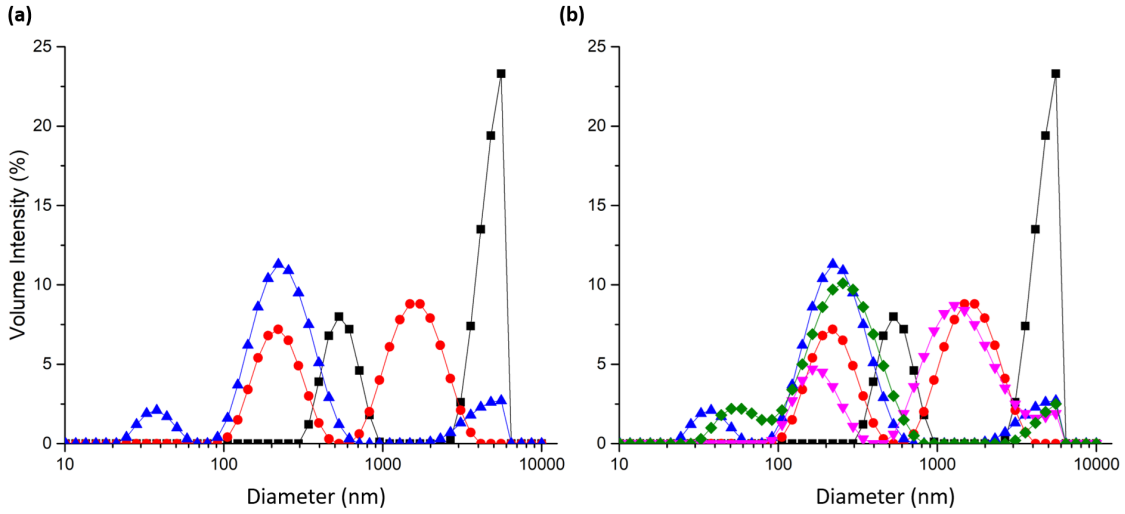

Figure 4.3: Size distribution from DLS of MLV mixture. (a) Measurements at an input power of -4 dBm. The black line shows the size distribution of MLV mixture, the red line represents the size of vesicles after SAW nebulisation without silicon structure and the blue line represents vesicle size after SAW nebulisation with silicon structure of 300 µm pores. A reduction in vesicle size occurred when the nebulisation was carried out through the silicon chip. (b) Measurements were repeated at -2 dBm input power. The black line shows the size distribution of MLV mixture, red (-4 dBm) and pink (-2 dBm) lines represent the size of liposomes after SAW nebulisation without silicon structure. Blue (-4 dBm) and green (-2 dBm) lines represent liposomes size after SAW nebulisation with silicon structure of 300 µm pores. When the nebulisation occurs through the chip, the power increase does not seem to change the size of the liposomes.

The presented results suggest that a combined effect of the SAW and the use of the silicon chip can be considered responsible for the production of liposomes around 100-200 nm in diameter. The silicon chip influenced indirectly the size of the vesicles, Fig. 4.3. By controlling the liquid length scale, a manipulation of the SAW's wavelength was obtained, which consequently modified the size of the nebulised droplets. This indirectly affected the size of the liposomes contained in the aerosols. The size of the aerosols is reduced, by the use of the silicon chip, and not enough liquid can surround the larger liposomes. Unsupported bilayers cannot exist outside of an aqueous environment, causing the collapse of the larger liposome structure as described in Table 4.1.

Spinning Lipids on IDT

From the phospholipid spinning approach, liposomes in the same size range obtained for the first method (described in Section 2.7.2) were formed. The same silicon chip with a

pore size of 300 µm and the same power were used, as described in Section 2.7.2.

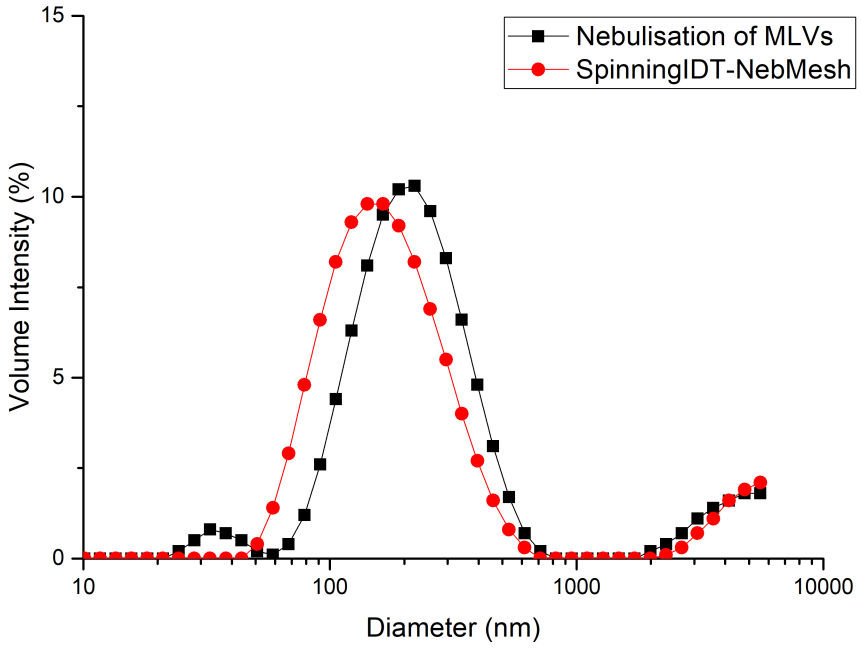

Figure 4.4: SAW-formed liposome size distribution from DLS. In red, spinning lipid approach, in black nebulisation of MLV solution, a small bump is present around 30-40 nm, which indicates that probably during the nebulisation some of the lipids collapsed into aggregates. Sample preparation: spin uniform layer on IDT, add silicon chip, incubate with DI water, application of SAWs.

Figure 4.4 shows the result from the second approach (red line) compared to the first approach (black line). MLVs and giant unilamellar vesicles (GUV) started to form from the chip pores, during the lipid hydration. Once SAWs were applied, the energy released was breaking down MLVs into BPFs as in the first approach. The size distributions from the two approaches are showing the same trend (Fig. 4.4), but the spinning method was not used, due to the time consuming procedure to spin down the lipids on the chip.

4.2.3 SAW Nebulisation Through Cylindrical Cavities of Different Pore Size

The combination of SAW nebulisation and the use of the silicon structure was considered responsible for the size decrease in the liposome population. In order to test the influence of the pore size of the silicon chip on the size of the liposomes formed after nebulisation, different measurements were made, nebulising the same concentration of MLV mixture through different cavity size: 800, 600, 400, 300 and 100 µm.

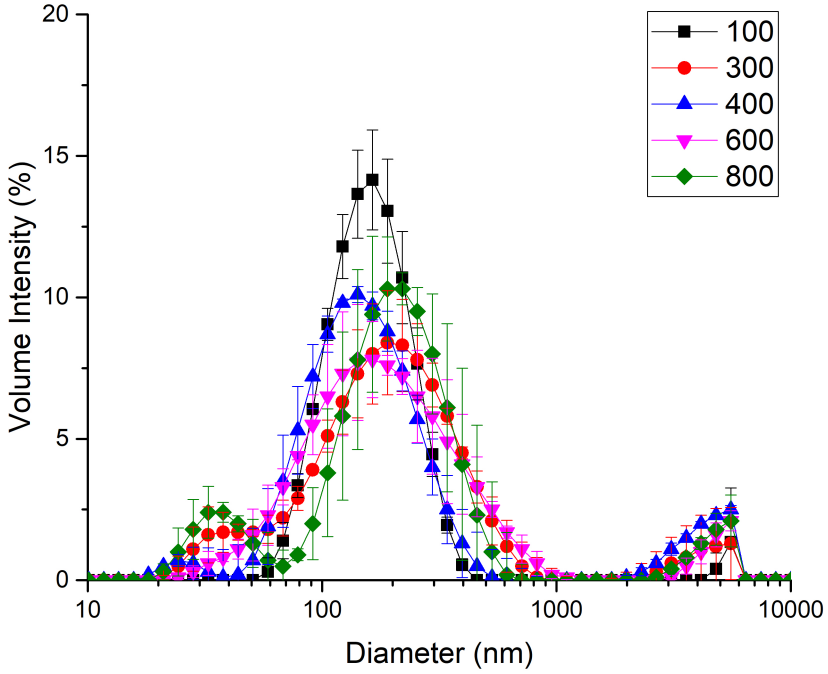

Figure 4.5: Size distribution of the liposomes obtained by SAW nebulising an MLV mixture through cavities of different size (100, 300, 400, 600 and 800 µm), as measured by DLS. The solution was made of 2.00 mg/ml DOPC in DI water. Three replicas were made for each cavity size. IDT parameters: 9.552 MHz with an input power of -4 dBm.

Liposomes Size

The results show that SAW nebulisation through dry etched cylindrical cavities breaks down MLVs into smaller vesicles (Fig. 4.5). However, changing the diameter of the cylindrical cavities did not lead to a significative change in the liposomes size.

The two students T-test was run to demonstrate that the difference between the set of measurements were not statistically significant. Thus, modifying the cavity size did not change the size of the SAW-formed liposomes.

The fact that the cavity length scale was 2 orders of magnitude larger than the size of the MLVs and 3 orders of magnitude larger than the liposome's size could be the reason for not having a specific relationship between the silicon chip pore size and liposome size. Evidence of the silicon structure effect, on the size of the aerosol and of the vesicles, was reported (Fig. 4.3). The use of physical confinement compared to the SAW nebulisation of the free sessile droplet is changing the size of the aerosol produced depending on the cavities size. Regarding the size of the liposomes encapsulated in the aerosols, a difference in size was occurred between the presence or not of the silicon chip (Fig. 4.3, (a)), but a specific relationship with the cavity size was not found (Fig. 4.6).

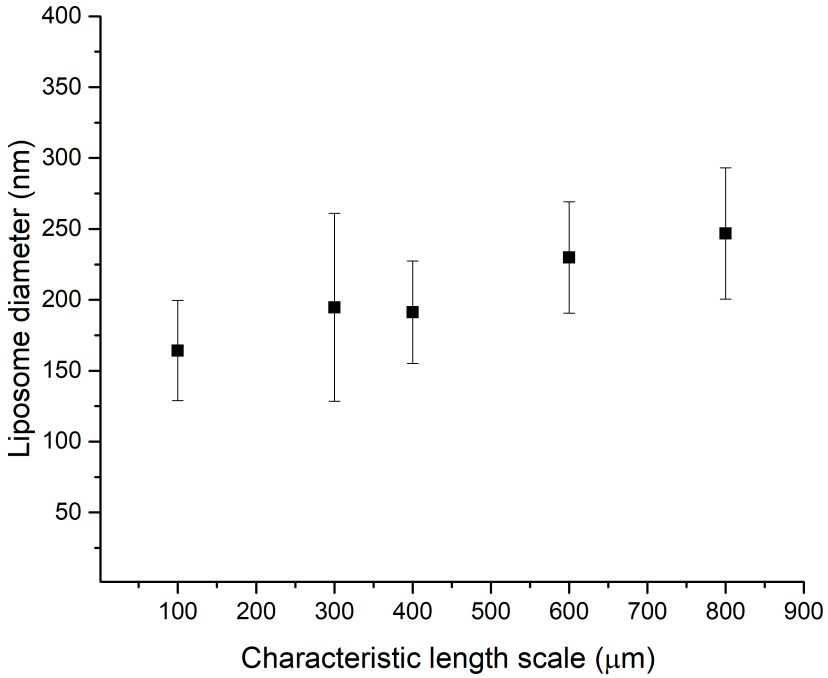

Figure 4.6: Two students T-test of liposome's size against cavity size. SAW nebulisation of a solution of 2.00 mg/ml DOPC in DI water was evaluated for cavity sizes of 100, 300, 400, 600 and 800 µm. This graph is showing that a clear relationship between the cavity size and the size of the liposomes produced cannot be made.

The use of the silicon structure with cavities in the range of 100 µm to 800 µm lead to a size distribution of vesicles around 100-200 nm, optimal for pulmonary drug delivery, as shown in Table 4.1. Due to the fact that a layer of water surrounding the liposomes is needed to avoid their rupture, a hypothesis regarding the unchanged size of vesicles against the cavity size was made. The use of cavity sizes below 800 µm resulted in the formation of smaller aerosols (between 1-20 µm) and liposomes with 100-200 nm diameter. The use of a silicon chip with cavity sizes above 800 µm or also in the case of the nebulisation of a sessile droplet, generated a bimodal size distribution of aerosol droplets (with the two peaks at 1-20 µm and around 100 µm) and two populations of liposomes, with sizes of 100-200 nm and 1-2 µm. The results are presented in Fig. 4.3. A minimum amount of water required to encapsulate the liposomes was considered as a factor in determining the size of the liposomes, and in the indirect elimination of larger liposomes.

Aerosol Size

Laser diffraction measurements were made using Spraytec (Malvern) to evaluate the size distribution of nebulised droplets (Fig. 4.7, (a)). Spraytec is a volume-sensitive technique as describe in Section 2.6.1. It is unable to differentiate between particle types. Thus, the

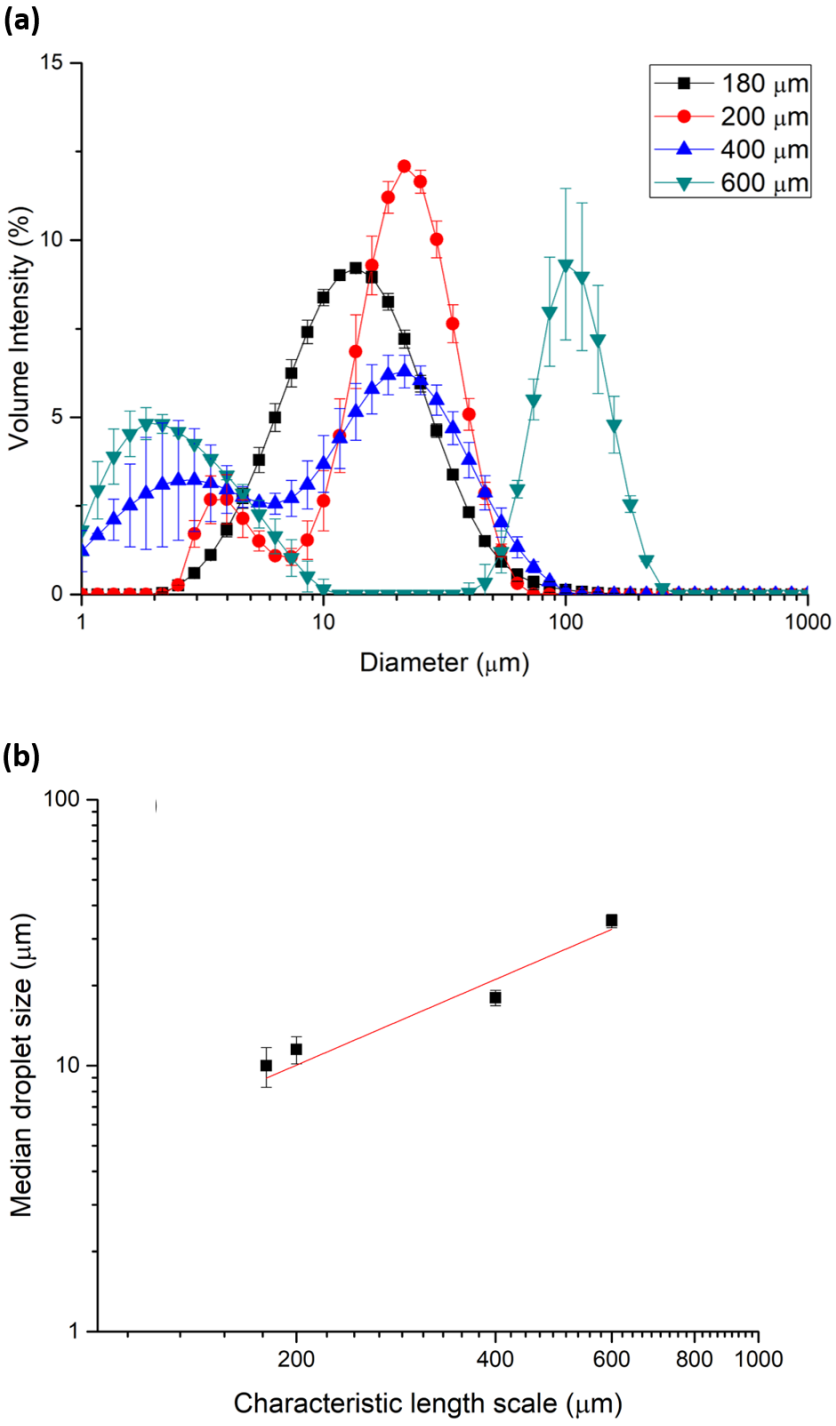

Figure 4.7: (a) Size distribution of nebulised droplets by laser diffraction. SAW nebulisation of DI water through cavities of black line 180 µm, red line 200 µm, blue line 400 µm and green line 600 µm. IDT parameters: 9.675 MHz with an amplitude of -6 dBm. (b) Vesicles size against cavity size, measured by laser diffraction. SAW nebulisation of a solution of 2.00 mg/ml DOPC in DI water was evaluated through cavities of 180 µm, 200 µm, 400 µm, and 600 µm. The graph shows a positive correlation between the cavities size and the size of the aerolised droplets. The mean value of three measurements is reported. Error bars show the standard deviation of three measurements.

Cavity diameter (D)	Aerosol size peak (µm)	Vesicle size peak (µm)
D >800 µm	100; 1-20	2.5; 0.1-0.2
D <800 µm	1-20	0.1-0.2

Table 4.1: Peak values of size distribution of aerosol droplets and vesicles generated by SAW. For cavities with D>800 µm, the SAW nebulisation generated two peaks of aerosol size distribution: (1) at 100 µm and (2) at 1-20 µm and two peaks of vesicle size distribution: (1) at 2.5 µm and (2) at 100-200 nm. For cavities with D<800 µm, the SAW nebulisation generated one peak of aerosol size distribution at 1-20 µm and a peak of vesicle size distribution at 100-200 nm.

size distribution obtained is representative of both aerosols and aerosols containing the SAW-formed liposomes. From the measurements, the size of the aerosols produce by SAW depends on the pore size of the silicon chip (Fig. 4.7, (b)), but not the size of the SAW-formed liposomes (Fig. 4.1 and 4.5). This was confirmed by nebulising both DI water and MLV dispersion, with the same pore size chip. The size distribution obtained was 5-10 µm larger when nebulising the MLV dispersion compared to DI water, which could be dependent on the viscosity of the nebulised sample. For cavities with the diameter of 180 µm and 200 µm, a size distribution between 1 µm and 10 µm was obtained. For 400 µm and for 600 µm cavities, aerosol droplets around 20 µm and 40 µm were produced.

4.2.4 SAW Nebulisation of Different Concentrations of MLVs Solution

The concentration of the phospholipid solution to be nebulised was analysed as a parameter that could possibly modify the size of the SAW-formed liposomes. MLV mixtures of 1.00 mg/ml, 5.00 mg/ml and 10.00 mg/ml were nebulised. Increasing the number of phospholipids in the solution was expected to lead to an increase in vesicles size.

Results did not show appreciable changes in the liposome size distributions from DLS measurements between the three concentrations (Fig. 4.8). Laser diffraction's measurements were also carried out, showing a small change in size from 1.00 mg/ml concentration to 5.00 mg/ml and a lower volume intensity of almost 10% less for the lowest concentration (1.00 mg/ml).

By increasing the concentration, we are increasing the number of vesicles produced, but not changing the size range of the vesicle population, which depends on the size of the aerosol encapsulating the vesicle.

4.2.5 SAW Nebulisation with Different Input Power

The power applied through SAW was tested, using the setup described in Section 2.7.2. For different input powers applied, the liposome size was measured using dynamic light

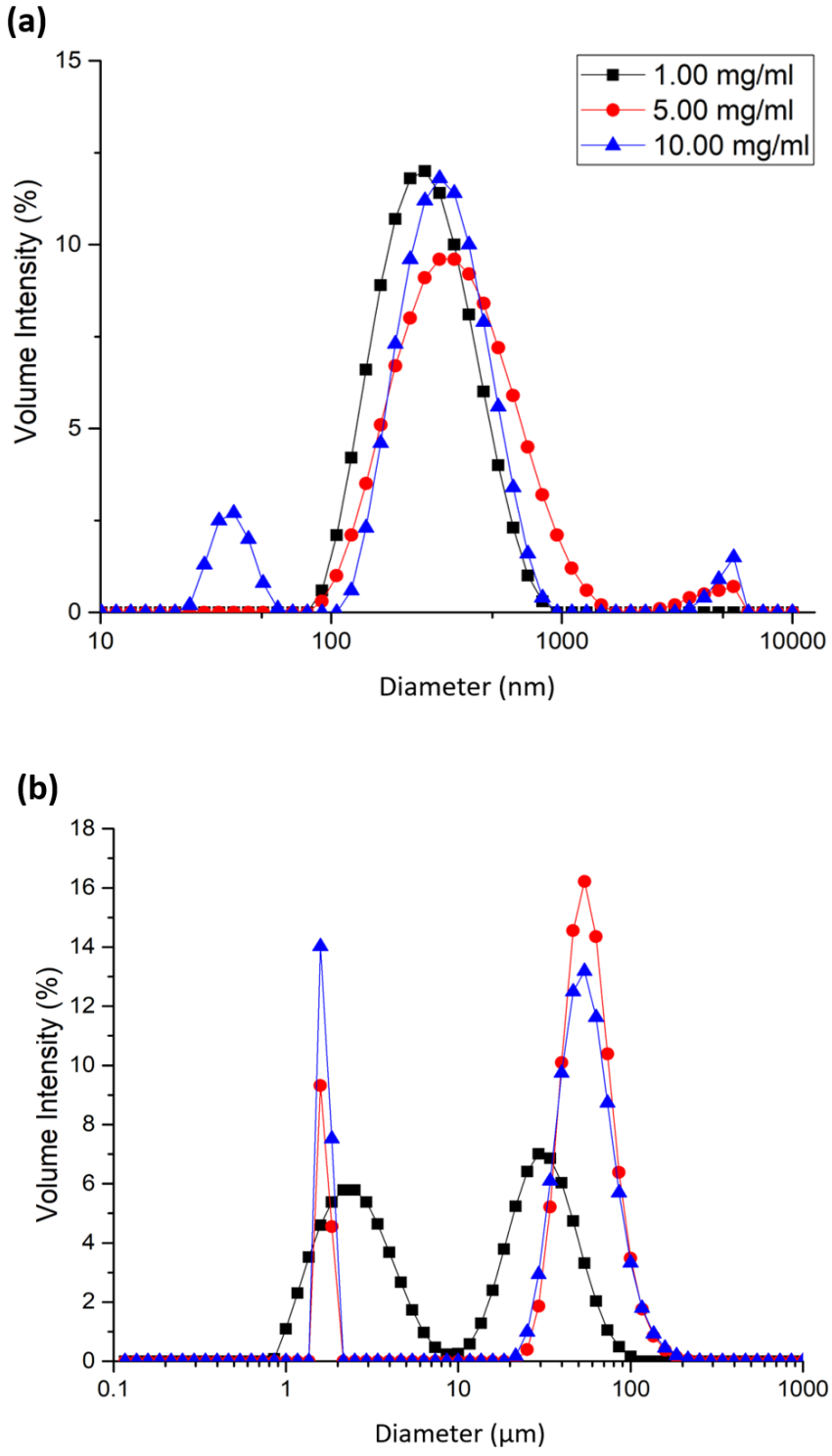

Figure 4.8: SAW nebulisation of different concentrations of MLV mixtures. Size distribution from (a) DLS and (b) laser diffraction of different concentrations of phospholipid dispersions, nebulised through 300 µm cavities. Black line is the size distribution of SAW nebulisation of a solution of 1.00 mg/ml DOPC in DI water, red line is the one of a solution of 5.00 mg/ml and blue line of a solution of 10.00 mg/ml.

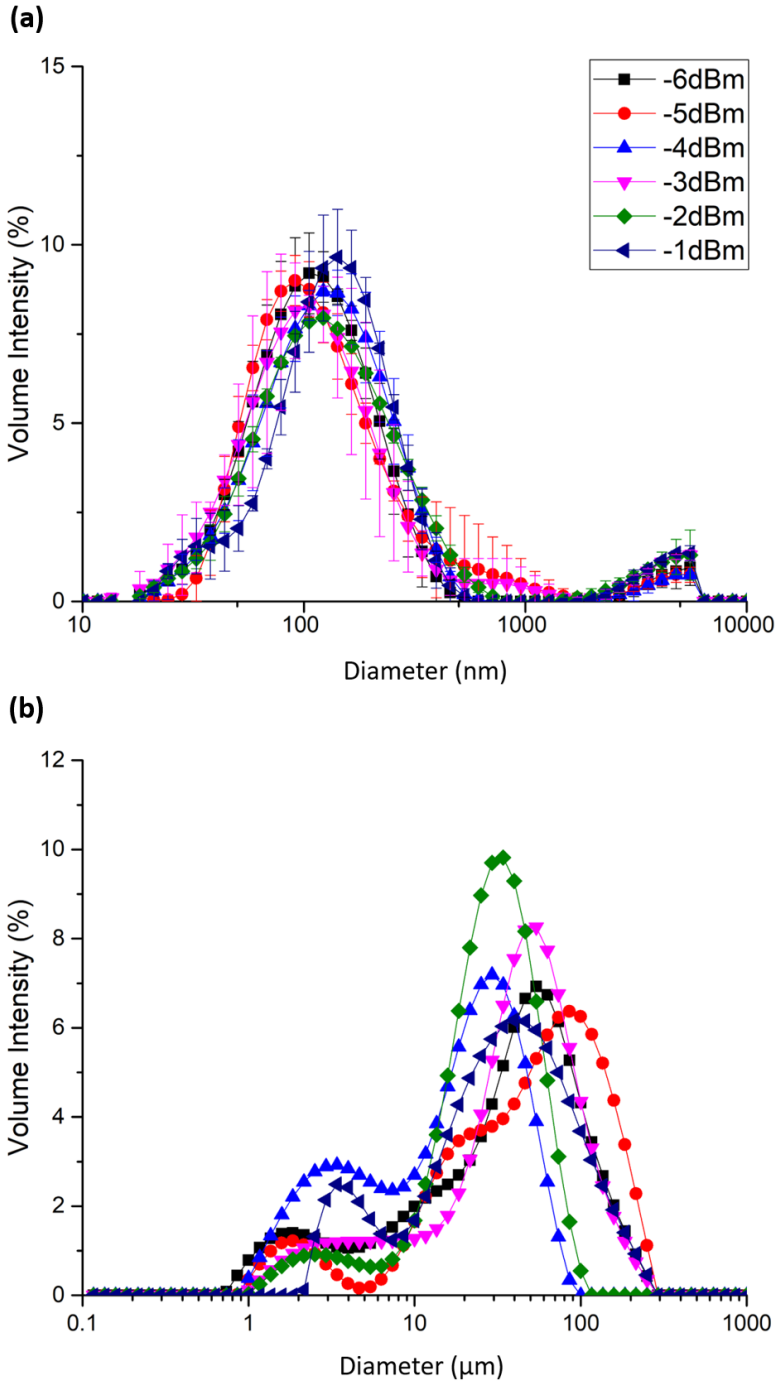

Figure 4.9: Size distribution of (a) SAW-formed vesicles and (b) Aerosol droplets at different input power. (a) Size distribution from DLS of different input power applied through SAW. Using input power range from -6 dBm to -1 dBm and amplified by 40 dB, the total power used is changing from 1 W to 5 W, not showing a significant change in size. The same result was obtained by laser diffraction measurements (b), a bi-modal distribution was established for the nebulisation using power from -6 dBm to -1 dBm.

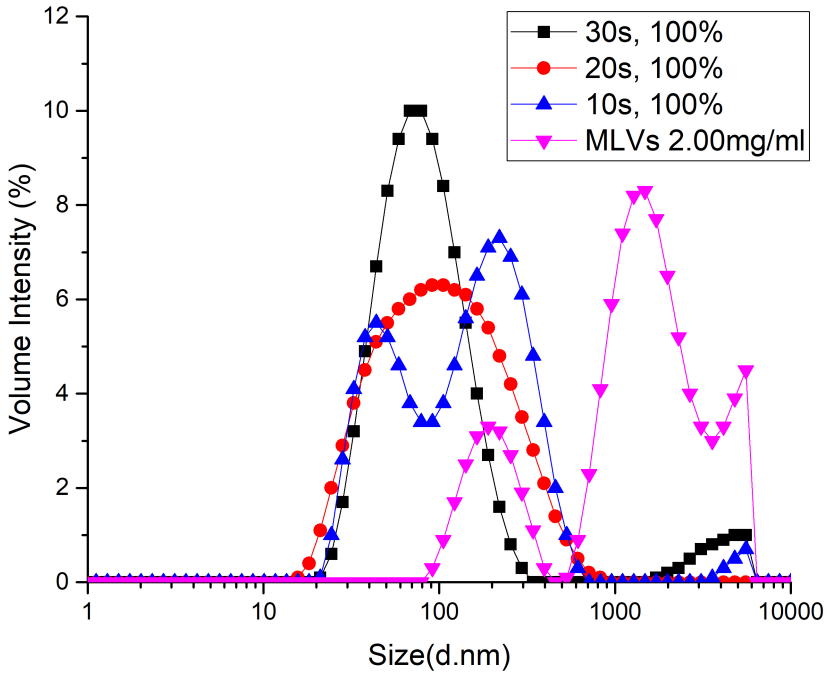

Figure 4.10: Probe sonication of MLV mixture. Sonication with 200 W power was conducted in 1 ml of MLV mixture (represented by pink line), for 10 s (blue line), 20 s (red line) and 30 s (black line). From the result, 30 s of sonication are necessary to be able to obtain a monomodal-like size distribution.

scattering, while aerosol size distribution was evaluated using laser diffraction (Fig. 4.9).

Three measurements for each sample were made and the mean values of the three measurements were shown. The SAW nebulisation was carried out with the silicon chip coupled with the IDT and for each measurement with DLS, the same amount of volume was collected, as described in Section 2.7.2. For laser diffraction 5 µl of volume were nebulised. Power from -6 dBm to -1 dBm was used. The power supplied to the system was limited, due to the high temperature reached during the nebulisation. For each measurement, the power was increased by 1 dBm (0.1 mW amplified with a gain of 40 dB, equal to an increase of 1 W for each measurement, Fig. 4.9). Based on the formula introduced in Chapter 1, Section 1.10.2 from [134], the energy required to disperse a volume of liquid into smaller droplets is approximately calculated to be around 3 mW, but a higher energy is used due to power losses during the nebulisation process. A comparison with the probe sonication method was made, as described in Section 2.4.4, as shown in Fig. 4.10. With the increase of the sonication time, the size of the liposomes decreased. After 30 s, a mono-modal size distribution was obtained, but the temperature, which was checked using an IR camera, reached over 80°C. The power used in probe sonication method was 100 times higher than the power employed with SAW nebulisation, which also produced LUVs in a faster and

more convenient way.

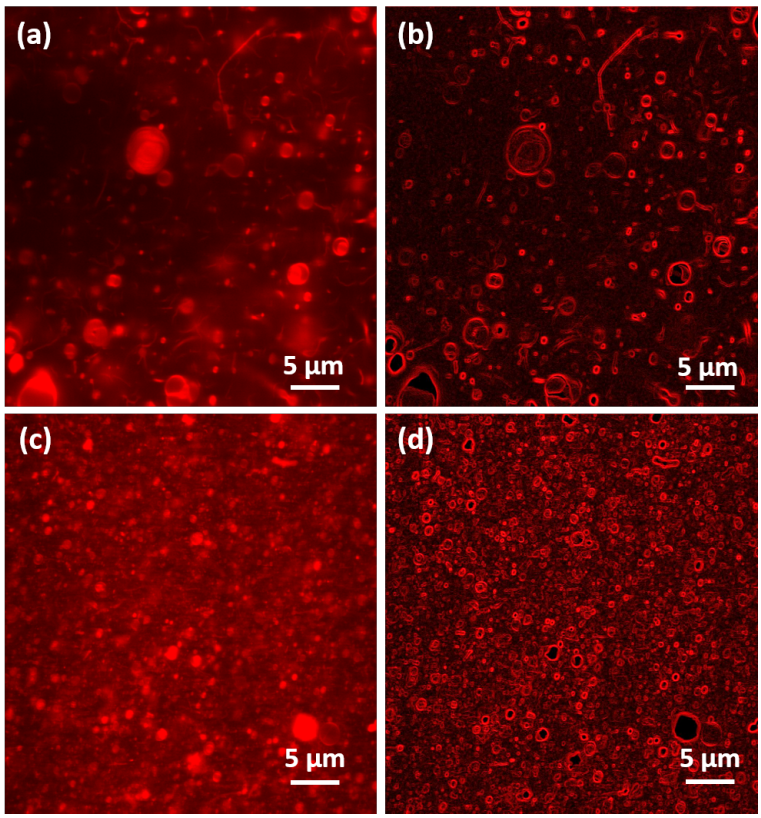

Figure 4.11: Confocal microscope image, 100x. (a) Picture of the MLV dispersion before the SAW nebulisation. (c) Sample during the SAW nebulisation, which was stopped to be able to retrieve the sample. The picture shows a decrease in vesicle size and higher monodispersity compared to picture (a). (b), (d) represent pictures (a) and (c) with enhanced edges to help to visualise the vesicle population.

4.2.6 Confocal Microscopy

Comparison between extruded and SAW-formed vesicles

Confocal microscopy was used to check the vesicle population at different times during SAW nebulisation. Samples were taken before nebulisation, during nebulisation (stopping the SAW) and after nebulisation. Due to the low resolution of the microscope, only an estimation of the vesicle population can be done. Fig. 4.11 shows that vesicle population before nebulisation is highly polydisperse with larger vesicles, while after stopping the SAW nebulisation, a clear decrease in vesicle population can be noticed with a lower degree of polydispersity. After showing the vesicles size changes during the SAW nebulisation, a comparison between SAW-formed vesicles and those obtained through extrusion showed a more uniform vesicles size from the latter method (Fig. 4.13). This is mainly due to the limited resolution of the microscope, which cannot determine further information regarding size, lamellarity and structure of the vesicles. Thus, samples were checked with

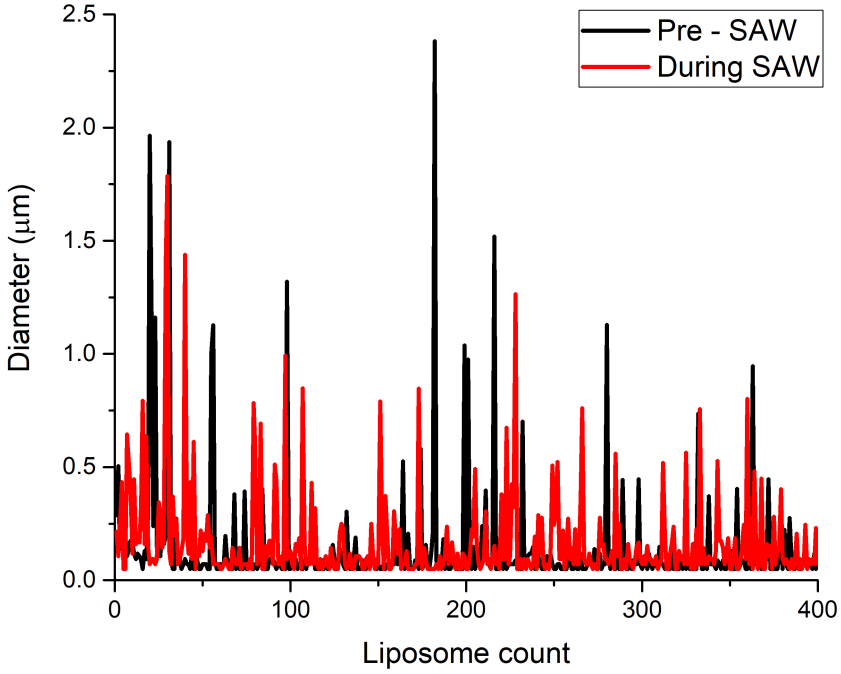

Figure 4.12: Size distribution of liposomes during SAW nebulisation of confocal images in Fig. 4.11. The black line is the size distribution of Fig. (4.11,(b)), which represents the pre-nebulisation sample. The red line is the size distribution of Fig. (4.11,(d)), which represents the size distribution after interrupting the nebulisation. A decrease in liposome's population size is showed.

cryo-TEM to establish the lamellarity of SAW formed liposomes. Additionally, the size of vesicles formed through the SAW and the extrusion method were compared using DLS measurements (Fig. 4.13). Results show a similar size distribution for both methods, indicating the suitability of SAW nebulisation for the *in-situ* formation of vesicles.

4.2.7 TEM Negative Staining and Cryo-TEM

TEM negative staining was used to test if sample concentrations were sufficient to be detectable using TEM and, to cross-examine the size distribution from DLS results. Comparing the images of SAW-formed liposomes and the extruded liposomes (control sample), shown in Fig. 4.14, some similarities were noticed. The concentration of SAW-formed liposomes was lower, but the structure appeared similar, (Fig. 4.14) shows a peculiar structure of the vesicles indicating that the liposomes collapsed (see Appendix D, Fig. D1). There are many potential factors that could be responsible. First of all, during sample preparation, the sample was blotted dry, thus the solution could have been evaporated. It could also be due to the differences in osmotic pressure between the external and internal core of the liposomes. In order to examine the vesicle lamellarity, further

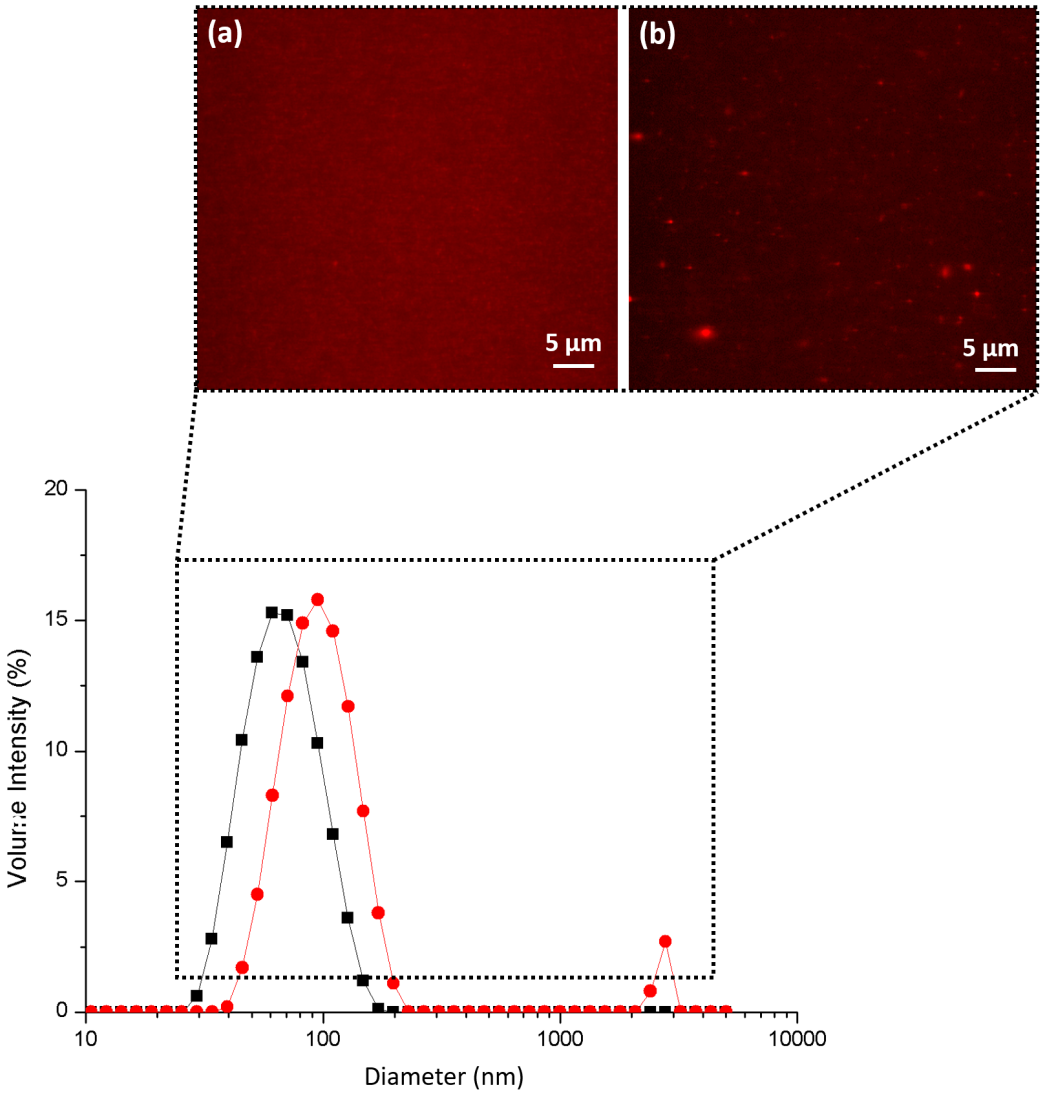

Figure 4.13: (a), (b) Confocal microscope image, 100x. (a) Vesicles extruded through 100 nm membrane (b) Liposomes formed using SAW and 300 µm cavities. In both cases, the vesicles were produced from a solution of 2.00 mg/ml DOPC in DI water. The graphs are showing the DLS size distribution of extruded liposomes through 100 nm membrane (black) and SAW-formed liposomes, nebulisation of MLVs through 300 µm cavities size (red). The results from the two methods are comparable in terms of size and volume intensity. Presence of a small peak around 3 µm indicates the presence of impurities or bigger vesicles.

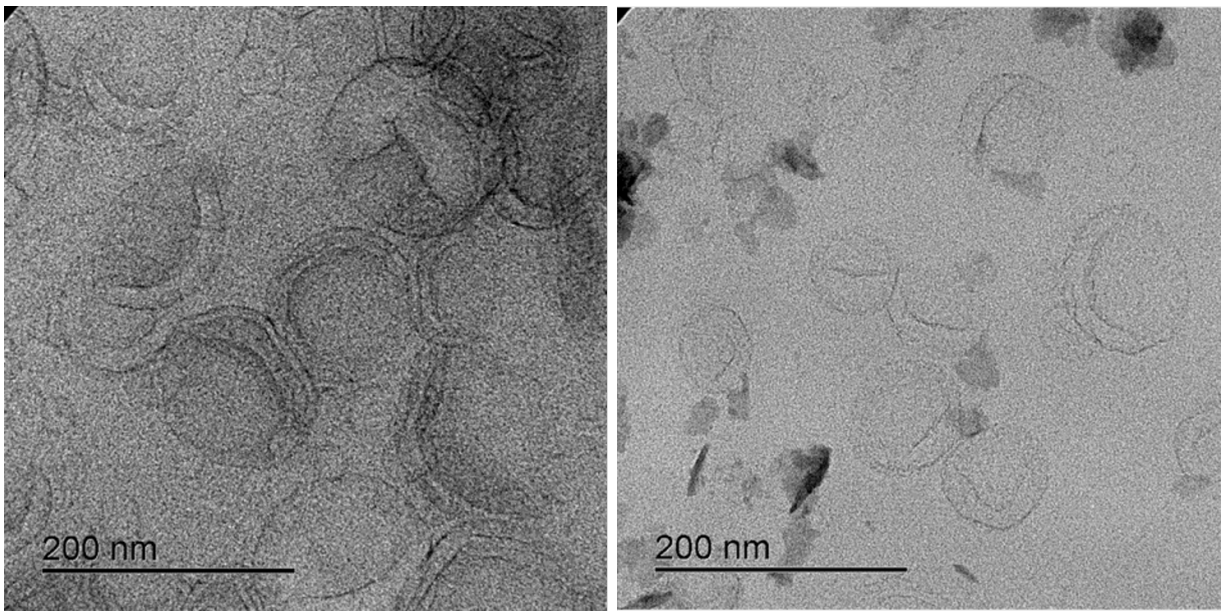

Figure 4.14: TEM negative staining. Liposomes made by extrusion through a membrane of 100 nm (left), and SAW-formed liposomes from the nebulisation of MLVs through 300 µm cavities.

measurements with Cryo-TEM were needed. As shown in Fig. 4.15 and 4.16, the number of vesicles was higher in the control sample, but the monodispersity was higher in SAW-formed liposomes sample. In the control sample, multiple vesicle populations of different size (50-250 nm) and various lamellarity could be seen, as highlighted in Fig. 4.15 by the red arrows. SAW-formed liposomes were in a smaller size range, namely 50 nm-100 nm and more monodisperse, but lower in terms of the number of vesicles. The vesicles from SAW nebulisation have optimal liposome characteristics of a monodisperse sample with a single lamellarity (see red arrows), even though the number of vesicles is lower (see Appendix, Fig. D2). The single lamellarity of the SAW-formed liposomes is key for a drug carrier, in terms of higher stability and control of the release compared to multilamellar ones.

4.2.8 Discussion

Liposomes have been an established drug delivery carriers since Bangham first described them in 1961 [38]. Multiple ways to produce them were introduced in the last decade [229], [36], but none of those methods was integrated into a platform to create an efficient drug delivery system. This chapter highlights the advantage of a new method capable of producing liposomes and delivering them directly into the lungs. The SAW platform has the combined advantage of producing aerosol within the optimal size range for deep lung absorption between 1 µm and 5 µm [4] and forming liposomes of a specific size (100 nm) during the nebulisation process. Other groups have previously reported the advantage of

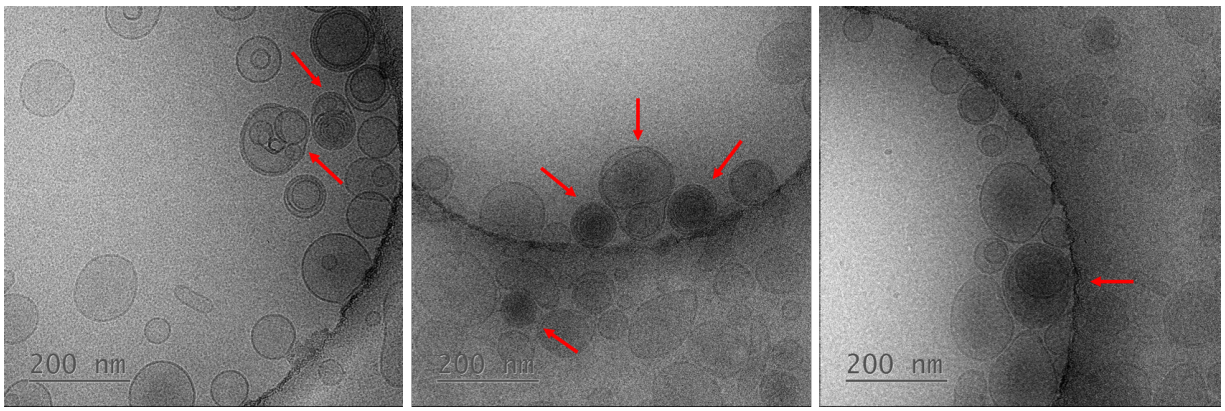

Figure 4.15: Cryo-TEM. Liposomes extruded through 100 nm membrane. Images are showing different size of vesicles with a range from 50 nm to 250 nm. Most of the vesicles have more than one bilayer, highlighted by the red arrows.

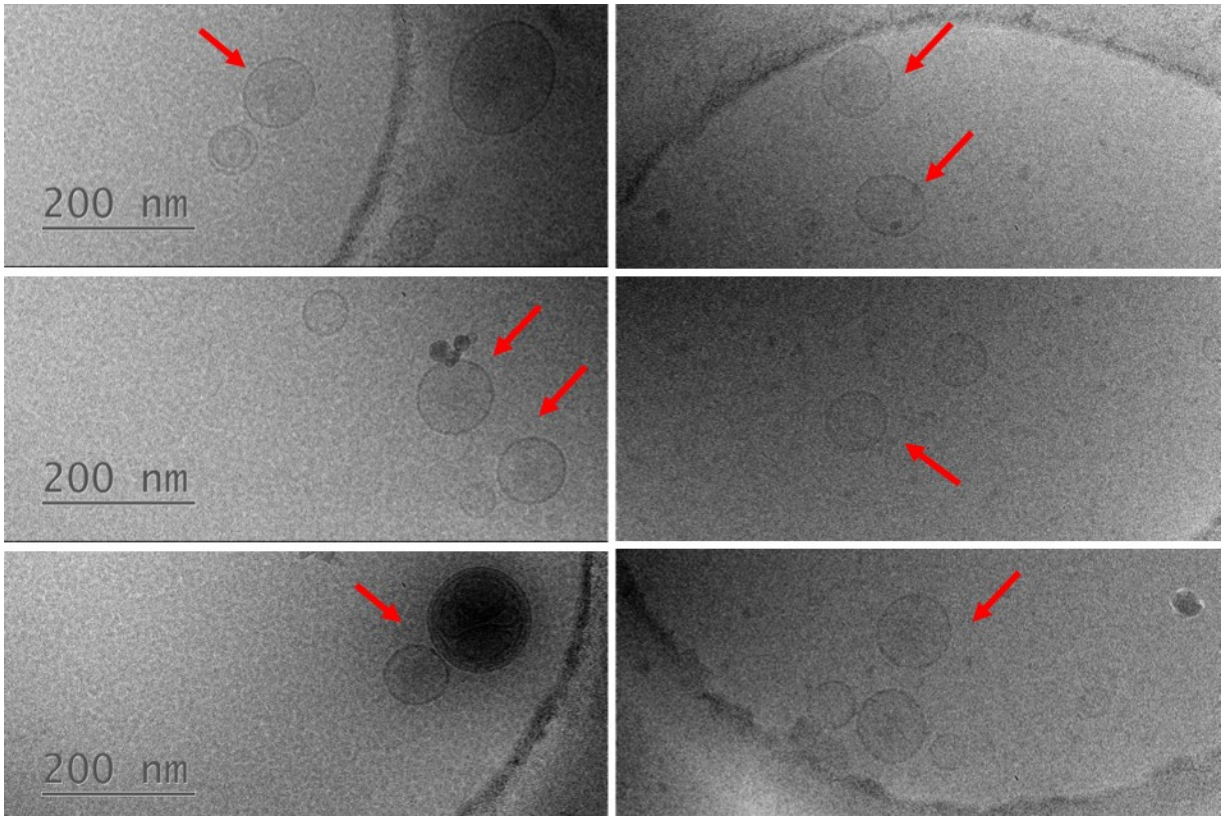

Figure 4.16: SAW-formed liposomes, produced via nebulisation of MLV mixture through cavities of 300 µm pore size. The size distribution is lower, with a lower concentration of vesicles. The sample is highly monodisperse ($PDI < 0.1$). As indicated by the red arrows, the vesicles produced are mainly unilamellar.

the SAW nebuliser [19], [117], [236] for the production of aerosols within the optimal range, but none of them showed a specific method of controlling the size of the aerosols. Fig. 4.1 showed a clear relationship between the cavity size, from where the nebulisation occurred, and the size of the aerosol droplets produced. The SAW nebulisation through a silicon chip with 100-200 µm cavities produced vesicles in the optimal lung absorption range.

Once the size of the aerosol droplets were tested, a phospholipid suspension was nebulised by SAW, in order to test if SAW was transferring enough energy to the suspension to break the MLVs into SUVs or LUVs. To explain the formation of unilamellar vesicles from a mixture of multilamellar vesicles, two different hypotheses were proposed. The first one is the 'filtering hypothesis ', which postulates that small unilamellar vesicles were already contained in the MLV mixture and subsequently, during the SAW nebulisation, larger vesicles are filtered out. This hypothesis was abandoned based on the DLS measurements presented in Fig. 4.3, the smallest peak corresponding to the size distribution of the MLVs in the mixture before the nebulisation, does not match with the size of the vesicles after the SAW nebulisation. A second hypothesis was formulated, which had been previously proposed by Lasic [47] in his studies. It is based on the formation of BPFs, as described in Chapter 1 (Fig. 1.7), where the energy given by SAW was breaking up the MLVs into lipids fragments. The BPFs, due to the hydrophobic nature of the phospholipid hydrocarbon chains, were closing themselves in unilamellar vesicles [54]. Fig. 4.3 showed the effect of the SAW only and the combined effect of the SAW and the use of the silicon chip. The use of the physical confinement not only decreased the size of the produced aerosols, by constraining the surface wave's wavelength, but also allowed the formation of small liposomes, creating a highly monodisperse sample. Different cavity sizes were employed to track changes in the produced liposomes. The changes in the size of the aerosols, obtained using different cavity sizes, were not noticed for the SAW-formed liposomes, a relationship between them was not found. Different concentrations and different values of input power were also tested to check whether those parameters were affecting the size of the liposomes produced within the SAW platform. The only notable change in the liposome size distribution was observed between the SAW nebulisation of the free sessile droplet and the SAW nebulisation coupled with a silicon chip with cavities between 100 µm and 800 µm. This was also confirmed by confocal microscopy, which showed changes in the vesicle population before, during and after the SAW nebulisation. A high degree of monodispersity and unilamellarity of the SAW-formed liposomes was obtained, as confirmed by TEM negative staining and Cryo-TEM. Size of the SAW-formed liposomes was confirmed by DLS. The formation of liposomes with the desired characteristics can be attributed, in terms of size and lamellarity, to both the use of silicon chip and high power. Using the SAW nebulisation with input power around 5 W (free sessile droplet without silicon chip) resulted in multimodal size distribution with a population of mainly larger vesicles. The employment of the silicon chip reduced the size of aerosols, but also indirectly eliminated larger vesicles from the collected sample. Larger vesicles did not survive the nebulisation without the existence of large enough aerosols to contain them. Therefore, larger vesicles collapsed in contact with air, creating an aggregate of phospholipids around 40 nm, as shown in Fig. 4.3. The formation of liposomes using the SAW and the silicon

chip is the result of a combined effect of different parameters, such as the amphipathic properties of the phospholipids, the energy transferred with the SAW and the use of the physical confinement to reduce the size of the aerosols, which contain the liposomes.

4.2.9 Conclusion

A new method to form liposomes was presented within the same SAW nebulisation platform, which will allow the delivery of different compounds using a single unique platform. The main advantage of this technique is the combination of two effects: the production of aerosol within the lung absorption optimal range and the production of the drug carrier, e.g., liposomes, to transport the compound into the cells. Different parameters were analysed in order to propose a theory behind the formation of liposomes during the SAW nebulisation. The effect of three parameters, such as the cavity size of the silicon chip, the concentration of the MLV's suspension and the power employed, on the size of both the aerosols and the liposomes was closely examined. The cavity size of the silicon chip was demonstrated to influence the size of the produced aerosols but did not directly affect the size of the liposomes. The liposomes' size changed only as a consequence of the reduction in the size of aerosols (Fig.4.3 and 4.7). Both the phospholipid concentration and the power supplied by the amplifier had no significant influence on the size of the vesicles. Once the platform was made, in Chapter 5 the size distribution of the aerosols produced by SAW will be measured using a standard device (cascade impactor) recommended in both the US and European Pharmacopeia and in Chapter 6 the platform will be tested *in-vitro* in lung cancer cells.

Chapter 5

Analytical Characterisation of Droplet Size From SAW Nebulisation

5.1 Context and Aim of Result Chapter

One of the most important parameters for aerosol characterisation is the particle size distribution, since the clinically validated size range is between 1-5 µm [102]. Particle size distribution can be determined using a direct method, such as microscopy or indirect ones such as inertial, diffusional and optical methods. In this Chapter, a cascade impactor, which is the standard recommended by both the US and European Pharmacopeia in determining aerosols' size, was employed to measure the size distribution of the SAW generated aerosols [237].

It is a method based on the inertial impaction and the aerodynamic diameter is evaluated, as described in Section 2.6.2.

The aim of the work carried out in this Chapter is to show the ability of the SAW nebuliser to generate aerosols in the optimal range and compare the newly developed nebuliser with a commercially available one, such as OMRON NE-U22. The size distribution of the aerosols generated from the SAW nebuliser with/without the use of the silicon cavity chip, previously described in Section 2.3, was measured and compared with OMRON NE-U22 nebuliser. The Andersen Cascade Impactor (ACI) was used to measure the particles deposition collected in each stage of the cascade and reconstruct the particle size distribution. Moreover, the stability of liposomes was tested in each stage of the cascade. Liposomes were delivered into the last stages of the impactor, indicating that the SAW nebuliser is able to efficiently nebulise drugs encapsulated in liposomes.

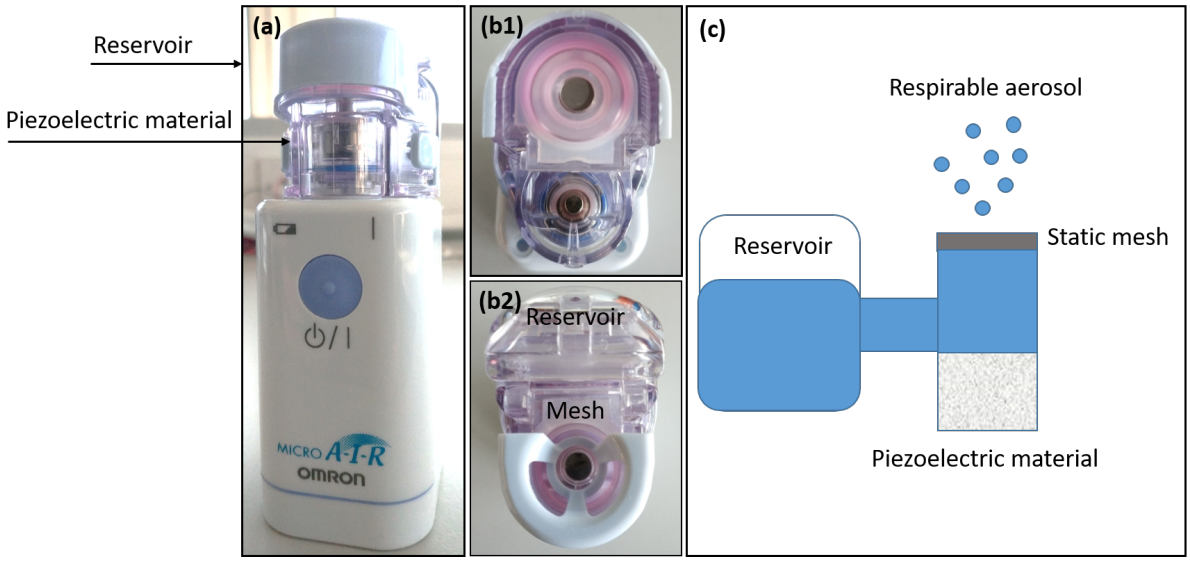

Figure 5.1: OMRON NE-U22 nebuliser. (a) Front view, (b1) Top view with the cap containing the mesh opened and the view of the piezoelectric material. (b2) Top view with the cap closed, the top view of the mesh and the reservoir at the back. (c) Drawing of the mesh nebuliser: the solution in the reservoir goes on top of the piezoelectric material, which pushes the solution through the mesh and creates the aerosol. Viscous solutions can clog the mesh pores.

5.1.1 OMRON NE-U22 Mesh Nebuliser

The OMRON NE-U22 Mesh Nebuliser (OMRON, Japan) was used as a control to test the efficiency of the SAW nebuliser. The commercially available nebuliser uses a piezoelectric crystal which vibrates at 180 KHz and pushes the liquid through the mesh (Fig. 5.1). Main disadvantages of the mesh nebuliser are the high cost (around GBP 100), the difficulty in nebulising viscous solutions and in cleaning the device. Furthermore, the employment of lower frequency compared to the SAW nebuliser (range of MHz) produces high shear stress that can damage the molecule, as described in Section 1.10.

5.2 Results

5.2.1 Calibration Curve of Rhodamine B and Fluorescence Measurements

The optimal concentration of Rhodamine B (RhB) to be nebulised in order to give a readable fluorescence intensity on the plate reader was obtained by constructing a calibration curve. Different concentrations were used: 1, 5, 10, 20, 37.5, 40, 50, 75, 100 µM (Fig. 5.2, (a)). A plateau value was reached at a concentration of 100 µM, which represented a higher limit. 1 mL of 100 µM solution of RhB was nebulised using three different nebulisers: (1) SAW nebuliser without the cavities, (2) SAW nebuliser with the cavities and

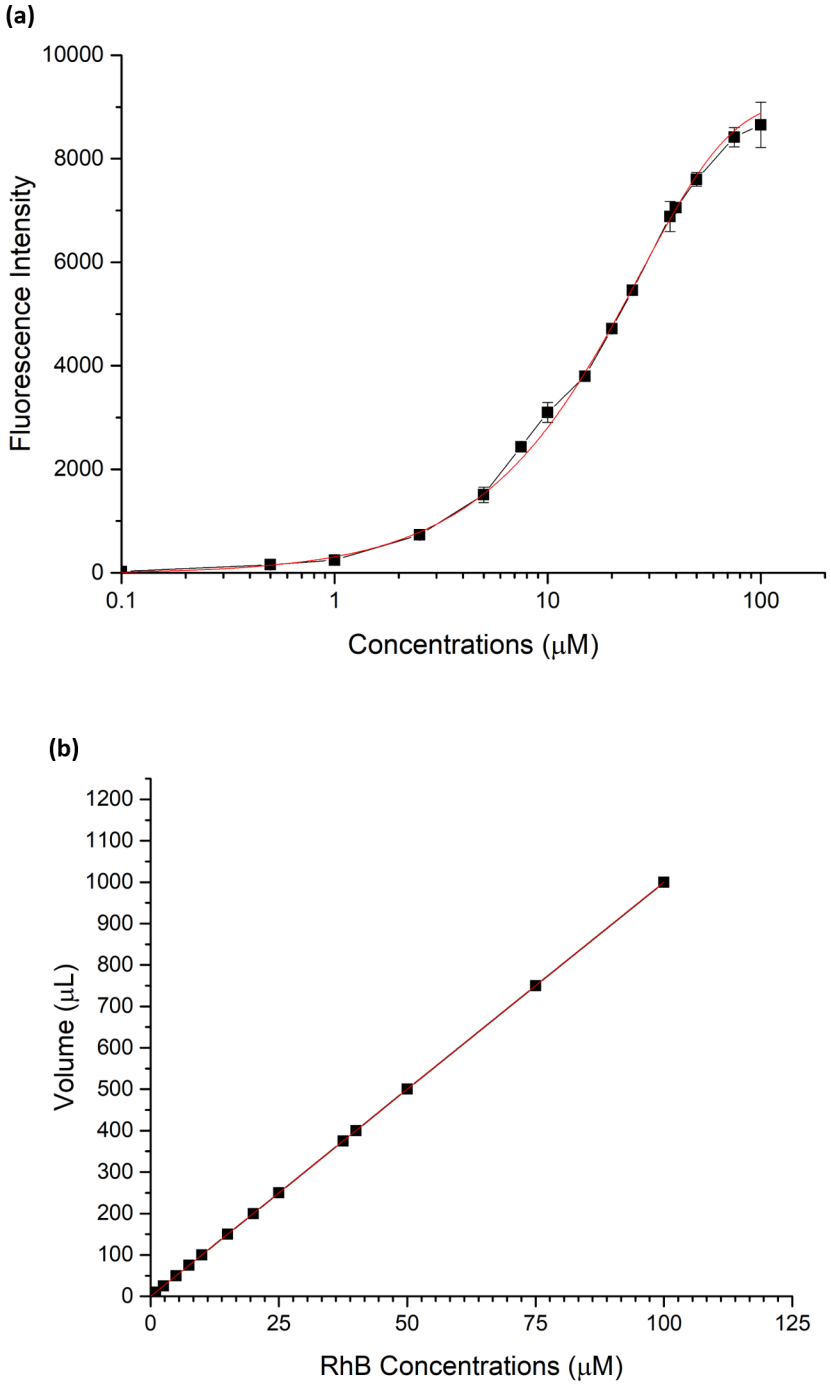

Figure 5.2: (a) Rhodamine B calibration curve was made, using the fluorescence intensity, measured at wavelength $\lambda = 590$ nm, of different concentrations of RhB: 1, 5, 10, 20, 37.5, 40, 50, 75, 100 µM. The curve shows a plateau value at 100 µM. (b) Starting from a solution of 100 µM different concentrations were obtained using a different fraction of volume of the starting solution. A volume/concentration curve was obtained, from which the particle size distribution was evaluated. Error bars are smaller than the size of the point and measurements were done in triplicate.

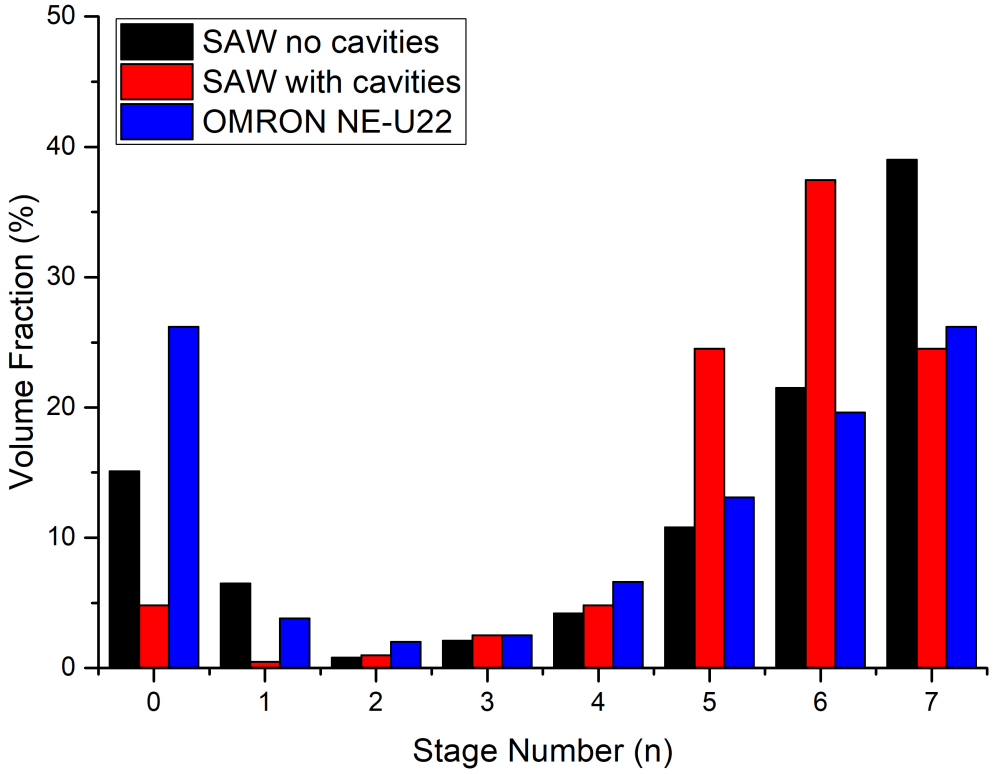

Figure 5.3: Aerosols deposition from the nebulisation of a 100 µM solution of rhodamine B. From the fluorescence measurements after SAW nebulisation without cavities (blue), with cavities (red) and OMRON NE-U22 (black), higher deposition in the optimum size range (stages 3-7) was observed for the SAW nebuliser with cavities.

(3) OMRON NE-U22. To retrieve the volume fractions for each stage of the cascade, each collection plate was washed using 1 mL of DI water, the solution was then collected and analysed. The fluorescence intensity was then measured at $\lambda = 590$ nm. The calibration curve (Fig.5.2, (a)) was fitted using an exponential curve and the following equation was obtained:

$$y = 9101 - 9124e^{-0.04x} \tag{5.1}$$

with a coefficient of determination R^2=0.99 To retrieve the particle size distribution for each stage, after building a calibration curve, a volume/concentration curve (Fig. 5.2, (b)) was made.

5.2.2 Fluorescence Measurements - Particle Deposition

A 100 µM Rhodamine B solution was nebulised using the SAW nebuliser with and without cavities, and using OMRON NE-U22. After the nebulisation of 1 mL of the initial solu-

Stage Number	SAW no cavities (%)	SAW with cavities (%)	OMRON NE-U22 (%)	Diameters (µm)
0	15.1	4.8	26.2	9.0+
1	6.5	0.48	3.8	5.8-9.0
2	0.8	0.98	2	4.7-5.8
3	2.1	2.5	2.5	3.3-4.7
4	4.2	4.8	6.6	2.1-3.3
5	10.8	24.5	13.1	1.1-2.1
6	21.5	37.44	19.6	0.7-1.1
7	39	24.5	26.2	0.4-0.7

Table 5.1: Percentage of the delivered volume by three different nebulisers, data from Fig. 5.3 showed that higher volume fraction in the clinical validated range were produced by the SAW nebuliser with cavities.

tion, each stage was washed with 1 mL of DI water. Fluorescence measurements for the SAW nebulisation with cavities indicate a higher intensity of the signal and thus, a higher volume fraction, in stages number 5 and 6, which represent the optimum range for lungs absorption. The SAW nebuliser with cavities produced a higher percentage of aerosols in the useful range compared to the commercial nebuliser OMRON NE-U22 (Fig. 5.3). Regarding upper stages (Fig. 5.3), such as stage 0 and 1 (larger cut-off diameter), the SAW nebuliser without cavities (in black) and OMRON NE-U22 (in blue) have the highest volume fraction, producing 3 and 5 times more the volume fraction from the SAW nebuliser with cavities (Fig. 5.1). The SAW nebuliser without cavities, as measured also with the laser diffraction method in Chapter 4, has a bi-modal particles size distribution, with the highest volume fraction for aerosols larger than 9 µm. OMRON NE-U22 is composed by a static mesh with pores around 5 µm and the size distribution from the Omron specifications of the nebuliser [238] indicates a mass median aerodynamic diameter (MMAD) approximately of 5 µm, which is the upper limit of the respirable range. Particles with a similar diameter to the size of the mesh aperture diameter were expected [113], but from the impactor measurements, a bi-modal size distribution was obtained with higher volume fractions for stages 6, 7 and stage 0. Therefore, particles with a diameter below 1 µm and above 9 µm were produced from the mesh nebuliser. Fluorescence measurements were substituted by conductivity measurements due to the photobleaching process, which could cause inaccurate size measurements of the aerosols and the toxicity of Rhodamine B, which forced the entire equipment to be enclosed in a fume hood.

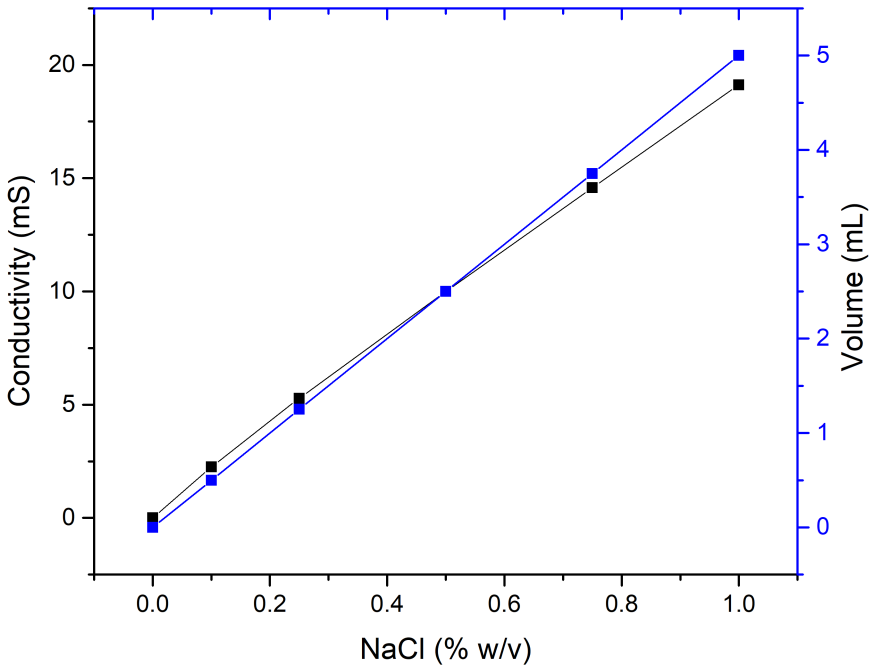

Figure 5.4: A sodium chloride calibration curve was made in order to check particles size distribution from the SAW nebulisation of a 1% w/v solution. Calibration was made with concentrations of 1%, 0.75%, 0.5%, 0.25%, 0.1% and 0.0% w/v of sodium chloride (black line). A volume/concentration curve of NaCl was also made in order to retrieve the particles size distribution after the SAW nebulisation with the silicon chip (blue line). Error bars are smaller than the size of the point and measurements were done in triplicate.

5.2.3 Calibration Curve of Sodium Chloride and Conductivity Measurements

Electrical conductivity represents the ability of a solution to transfer (conduct) electrical current. It is used to measure the concentration of dissolved salts, which have been ionised in a polar solvent such as water. Conductivity measurements of a sodium chloride solution at concentrations of 1%, 0.75%, 0.5%, 0.25% and 0.1% w/v were carried out.

A volume of 1 mL of 1% w/v solution of NaCl was nebulised using SAW nebuliser with cavities chip. An IDT with a resonance frequency of 9.68 MHz was used, with an input power of -2/-3 dBm and the cavities on the silicon chip were ranging from 100 to 200 µm. To retrieve the volume fractions from the different stages of the cascade, each collection plate was washed using 1 mL of DI water and then the solutions were analysed. The conductivity of the collected solution was normalised subtracting the value of DI water. All the measurements were taken using a conductivity meter (Jenway, Cole-Parmer, UK), which was first calibrated. The calibration curve was fitted linearly using the following

equation:

$$y = 19x \tag{5.2}$$

with a coefficient of determination R^2=1. After measuring the conductivity of each stage of the impactor, the calibration curve (Fig. 5.4, black line) equation was reversed and the NaCl (% w/v) associated to each stage was evaluated by means of a volume/concentration curve (Fig. 5.4, blue line). The total volume delivered by the SAW nebuliser was 74% of the total volume.

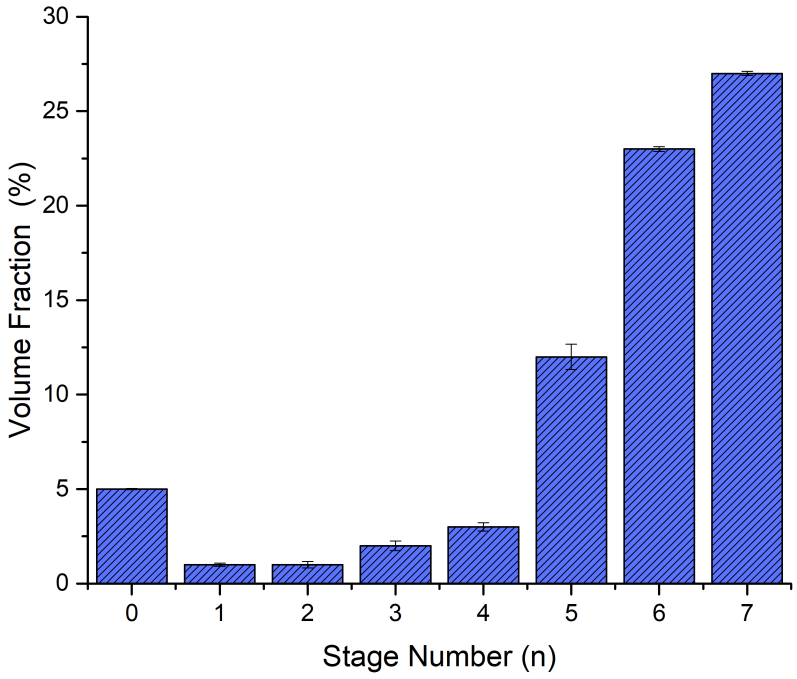

Figure 5.5: Aerosols deposition of a 1% w/v solution of NaCl from the SAW nebulisation with cavities (100-200 µm). Each collection plate of the cascade was washed with 1 mL and the conductivity associated with each plate was measured.

5.2.4 Conductivity Measurements - Particle Deposition

Conductivity measurements of the SAW nebulisation with cavities of 1 ml of NaCl, 1% w/v solution were carried out. From the conductivity/volume curve a percentage of the volume deposited on each stage was evaluated with: 3% of the particles being larger than 9 µm, 1% between 2.1-3.3 µm, 10% between 1.1-2.1 µm, 21% between 0.7-1.1 µm and 26% between 0.4-0.7 µm (Fig. 5.5). The measurement taken after the SAW nebulisation with cavities showed a particle size distribution with a prevalence of particles between 0.5-2.1

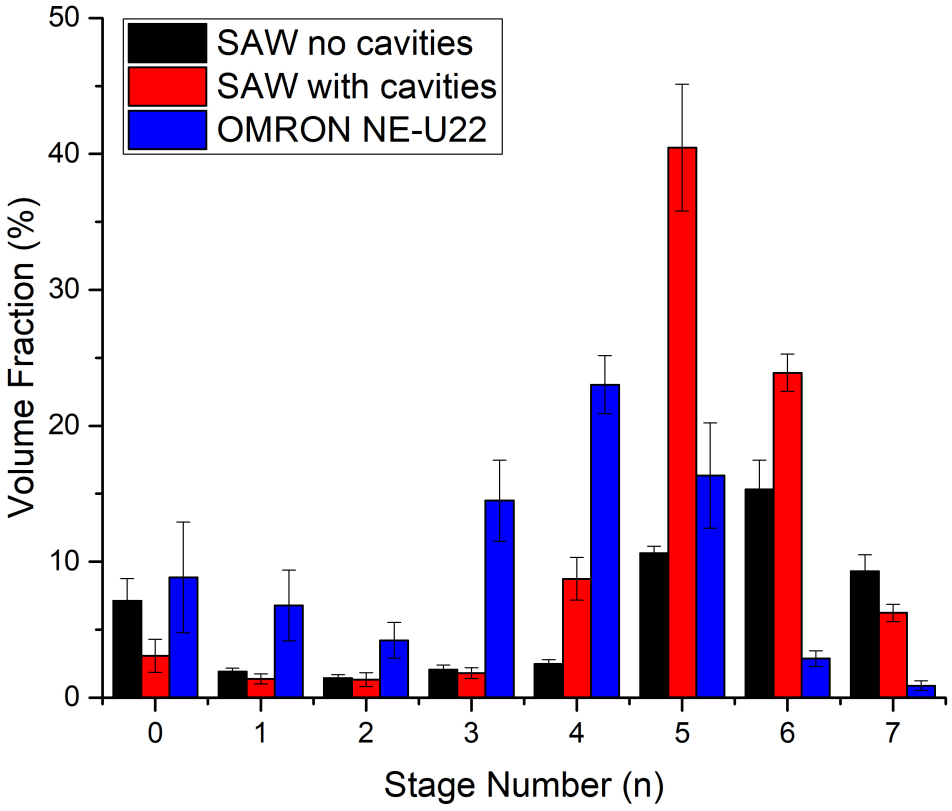

Figure 5.6: Percentage of the delivered volume by three different nebulisers, the data showed that higher volume fraction in the clinical validated range (stage 5) were produced by the SAW nebuliser with cavities.

µm, which means that the higher volume fraction of the produced aerosols were within the optimum respirable range of aerosols [239].

A comparison of aerosols' size produced by the three nebulisers: (1) SAW nebuliser without silicon chip, (2) SAW nebuliser with the silicon chip and (3) OMRON NE-U22 was also made. The silicon chip used was with 400 µm cavities. A shift towards larger droplet is represented compare to Fig. 5.5, for which the nebulisation occurred through a 100-200 µm cavities. Regarding the comparison between the three nebulisers, as shown in Table 5.2, the higher particles fraction, correspondent to stage 3 to 7, was obtained by the SAW nebulisation with cavities, with a percentage of 81.16%. For SAW with no cavities the volume fraction in the optimal range was of 39.78% with the majority of aerosols larger than 9 µm and for the OMRON NE-U22 the volume fraction in the useful range was of 57.59%. The SAW nebuliser with cavities demonstrated to produce 89.16% of the total volume in the form of aerosols with a diameter between 1 µm and 5 µm.

Stage Number	SAW no cavities (%)	SAW with cavities (%)	OMRON NE-U22 (%)	Diameters (µm)
0	7.11	3.08	8.84	9.0+
1	1.91	1.38	6.78	5.8-9.0
2	1.43	1.33	4.22	4.7-5.8
3	2.06	1.80	14.49	3.3-4.7
4	2.48	8.75	23.02	2.1-3.3
5	10.62	40.47	16.34	1.1-2.1
6	15.32	23.90	2.86	0.7-1.1
7	9.30	6.24	0.88	0.4-0.7

Table 5.2: Percentage of the delivered volume by three different nebulisers, data from Fig. 5.6 showed that higher volume fraction in the clinical validated range were produced by the SAW nebuliser with cavities.

5.2.5 Liposome Size

Pre-formed liposomes were made through extrusion and nebulised using SAW. Dynamic light scattering was utilised to measure the size of the liposomes before and after the nebulisation. Size stability of extruded liposomes was also measured on each stage of the cascade impactor. A sample of 100 µl was collected from each stage. Same size liposomes of the pre-nebulised sample were found in each stage. The result represented a proof of concept that the SAW nebuliser was able to deliver intact liposomes in the lower stages of the cascade and that the aerosol size was in the respirable range. Figure 5.7 shows the presence of liposomes in each stage of the cascade, maintaining the same size 100-200 nm in diameter of the initially extruded liposomes.

5.3 Discussion and Conclusion

The work carried out in this Chapter was aimed to measure the particle size distribution and compare the output from the SAW nebuliser with and without cavities to the commercial nebuliser OMRON NE-U22, but also to have a proof of concept of the SAW nebuliser's capability to deliver liposomes to different stages of the impactor.

The cascade impactor represents one of the standard characterisation methods that is widely accepted by regulatory bodies to measure the size of the aerosol distribution [240], but there are three major drawbacks about this method, such as it is time-consuming, the particles can bounce and end up in a stage that does not depends on the aerodynamic diameter and finally particles can be subjected to evaporation. Therefore, the size distributions can be skewed towards smaller sizes [197]. An improvement could be obtained increasing the humidity of the environment, and in order to reduce the losses of

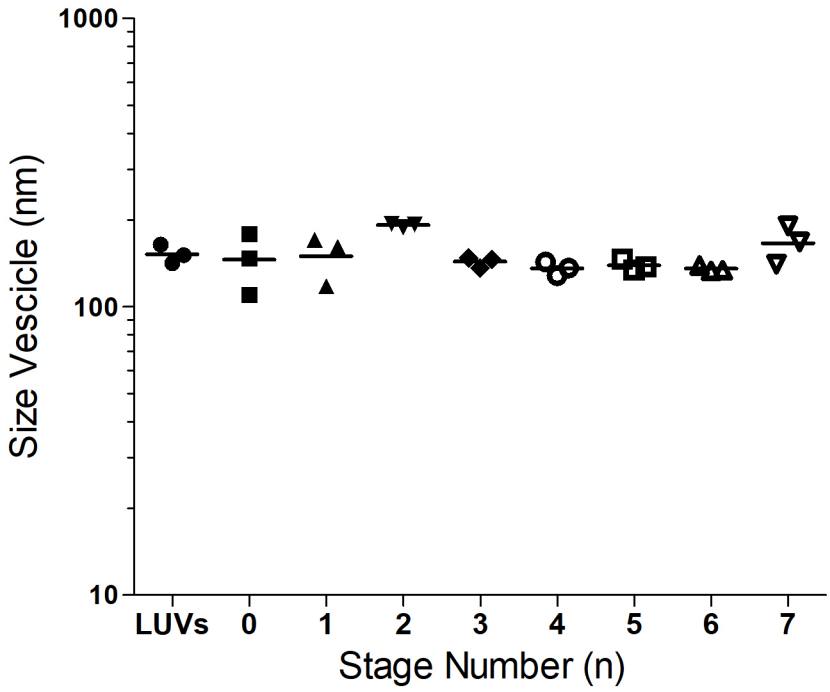

Figure 5.7: Dynamic light scattering measurements of the extruded liposomes after collection with the cascade impactor. The graph shows the SAW nebuliser ability to deliver 100-200 nm in different stages of the impactor, displaying the same liposomes size distribution over all stages.

the aerosols and increase the delivered volumes a box around the mouthpiece on top of the cascade and the SAW device can be made. This could avoid the flow from the fume hood to interfere. Also, more suitable mouthpiece can be designed. Generally, the data collected from cascade impactors are used to validate the performance of pharmaceutical inhalation products. Different groups [194], [136] employed cascade impactors to test the droplet size produced by SAW nebulisation or jet and ultrasonic nebulisers [241]. Regarding the SAW nebulisation, the delivery of peptides and antibodies was carried out, using afterwards high-performance liquid chromatography (HPLC) to test the concentration of the peptides in each stage and using Bradford assay for antibodies'concentration [139]. Previously in Chapter 4, the particle size distribution of the SAW nebuliser with cavities was measured by a laser diffraction method. In this Chapter, the *in-vitro* performance of the SAW nebuliser with cavities was compared to the OMRON NE-U22 and alternative assays to HPLC were found to retrieve the volume fraction of the nebulised particles in each stage. Conductivity measurements were carried out to obtain the particle size distribution of the aerosols produced by the SAW. For the conductivity measurements, the SAW nebuliser with cavities of 100-200 µm pores was employed and a particle size distribution with the majority of the aerosols produced (more than 90%) in the respirable range. A shift towards larger particles was found when a silicon chip with cavities of 400 µm was

used, with 81.16% of aerosols produced in the respirable range. Fluorescence measurements were also made to test the efficiency in producing aerosols in the optimum range of three different nebulisers: SAW nebuliser with and without cavities and the commercial nebuliser OMRON NE-U22. The SAW nebuliser with cavities presented higher deposition in stages 3, 4, 5 and 6 with the larger number of aerosols within the optimum aerosols range 0.5-5 µm. The particle size distribution was obtained through a calibration curve and a volume/concentration curve, which was then converted to the percentage of the volume in each stage. The fluorescence measurements were replaced by the conductivity measurements due to the photobleaching process which was affecting the recovery of the particles size distribution. The use of conductivity has not been previously used to assess the particle size distribution from the Andersen cascade impactor. It resulted in a fast way to obtain the volume fraction of each stage after the nebulisation.

The results from the SAW nebulisation with cavities showed in Tables 4.1 and 5.2, confirmed the same particle size distribution obtained previously (Chapter 4) using the laser diffraction method. Using the impactor, cavities of 100 µm) and 400 µm were tested, which have been proven to produce a monodisperse particle size distribution [132].

Extruded liposomes were nebulised through SAW nebuliser with cavities and their presence was found in each stage, as shown in Fig. 5.7. DLS measurements showed the presence of vesicles of 100 nm in diameter after washing the stages with the buffer. Negative control was run, nebulising the buffer without extruded liposomes in the solution, and from the DLS measurement, the analysed sample was indicated as blank. Liposomes were efficiently delivered on different stages of the cascade. The *in-vitro* analytical characterisation of droplet size from SAW nebulisation was performed, indicating a high potential of the SAW platform to deliver successfully liposomes and produced aerosols in the clinically validated range.

Chapter 6

SAW Nebulisation of siRNA and DNA for Gene Therapy

6.1 Context and Aim of Result Chapter

The increasing interest in gene therapy and the difficulties to deliver naked nucleic acids into cells, mainly due to the negative charge of their phosphate component, is the main motivation of the work carried out in this Chapter. Therefore, the work accomplished in this Chapter hopes to address this issue with the following aims:

- show that the SAW nebulisation did not alter the nucleic acid's structure
- demonstrate the feasibility of using a SAW-based device for cell transfection, through the delivery of a DNA luciferase plasmid and GAPDH siRNA to A549 epithelial lung cancer cells
- test the formation of liposomes during the nebulisation process
- compare the effect of extruded liposomes and SAW-formed liposomes in delivering nucleic acids.

A gel retardation assay was employed to assess if the SAW nebulisation was suitable to nebulise nucleic acid without modifying their structure, as described in Section 2.8.4. Then the platform was used to test the efficiency in delivering DNA plasmid and GAPDH siRNA, with the production *in-situ* of the lipid/nucleic acid complex during the nebulisation process, as reported in Section 1.11.1.

The use of a SAW device allows the integration of the manufacture of nucleic acid-liposome complexes with the delivery of the nebulised particles to target cells.

6.2 Results

6.2.1 Gel Retardation Assay

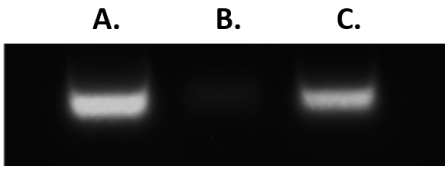

Figure 6.1: Gel retardation assay of HS-DNA before and after SAW nebulisation. The similar intensities of the two bands (A. HS-DNA solution before SAW and B. Solution with DI water and C. same solution of A. but after SAW nebulisation) indicate the suitability of SAW for the nebulisation of nucleic acids.

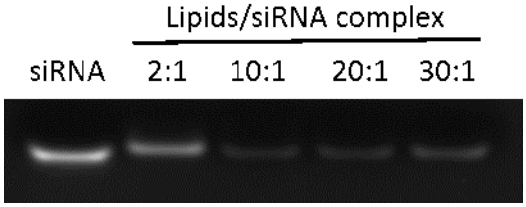

Figure 6.2: Gel retardation assay of DOTAP:cholesterol (4:1) and lipid-siRNA complexes prepared at 2:1, 10:1, 20:1 and 30:1 ratios (w/w). Lipid vesicle and siRNA complexes were incubated for 30 min.

Results from a gel retardation assay were analysed, for which samples were collected before and after nebulisation, the assay was performed as described in Section 2.8.4. ImageJ was used to compare the intensities of the bands (Fig. 6.1). Band A., which was a sample containing HS-DNA and not subjected to SAW, was used as a control. Band B. was a sample containing DI water, and used as a negative control, and Band C. represented the same sample as band A. but after SAW nebulisation. The results show that SAW nebulisation did not harm the structural integrity of the nucleic acids. Thus, it is a suitable means of nebulisation for the delivery of nucleic acids. A gel retardation assay was then performed to test the binding affinity of lipids and siRNA complexes. Cationic liposomes were formed by the extrusion method, described in Section 2.4.3 following the method described in Section 2.4.1. Results from the gel show a decrease in the band intensity as the lipid to siRNA ratio was increased, up to 20:1, past which the intensity increased again up to 30:1. Naked siRNA was saturated by lipid vesicles before the 30:1 ratio. The complete disappearance of the band when the ratio was 10:1 indicated full binding of the nucleic acids to the lipid vesicles. The optimal lipid to siRNA ratio was found to be between 2:1 and 10:1 (Fig. 6.2). Further measurements determined the best ratios for DOTAP:Chol and lipid:siRNA to be 4:1 and 6:1 respectively.

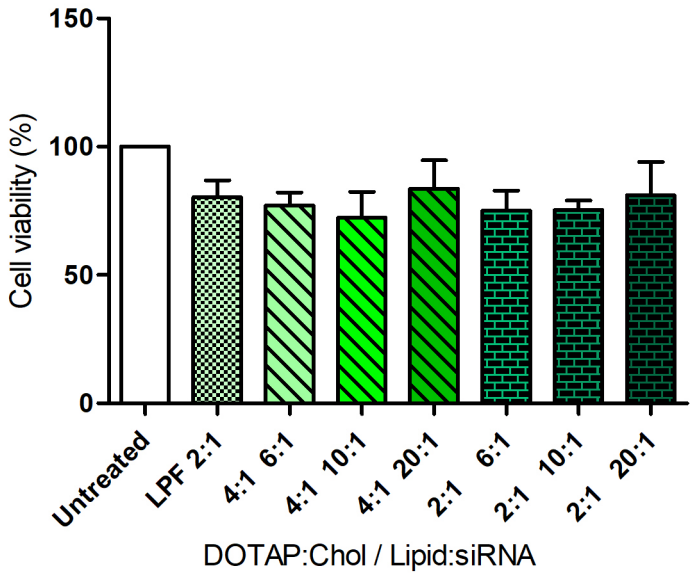

Figure 6.3: A549 cells were seeded in a 96-well plate. 24 h post-transfection, lipid vesicles complex bound with GAPDH siRNA were added to cells in order to test their toxicity. After 4 h, MTT solution (0.8 mg/ml) was added to the cells. After 2 h, the formazan precipitate was dissolved in 100 µl isopropanol and the absorbance was measured at $\lambda = 595$ nm. The graph shows the mean of three measurements and the error bars represent the SD.

6.2.2 MTT Cytotoxicity Assay

In order to test the cytotoxicity of the complexes towards A549 cells, the MTT assay was performed at 24 h post-transfection, as described in Section 2.8.6. As a control, samples that were subjected to the same changing of the medium as other samples, but not actually transfected, were included, so as to account for cells being removed or damaged during the changes of medium. For all the complexes prepared with lipid to siRNA ratios of up to 20:1, cell viability was over 80%. The lipid concentration was kept below 20 µg/mL. As shown in Fig. 6.3, the MTT assay showed that there were no significant differences in cell viability between the samples with the siRNA-lipid complexes and the control with Lipofectamine 2000. Compared to the untreated sample, the sample with phospholipids showed a decrease in cell viability of around 30%. An MTT assay of the sole lipid vesicles was also carried out. The result shows higher viability of the cells in the case of the delivery of the sole liposomes compare to the lipid:siRNA complexes (see Appendix E, Fig. E2), which was expected to due to the fact that the lipid:siRNA complex entered into the cells.

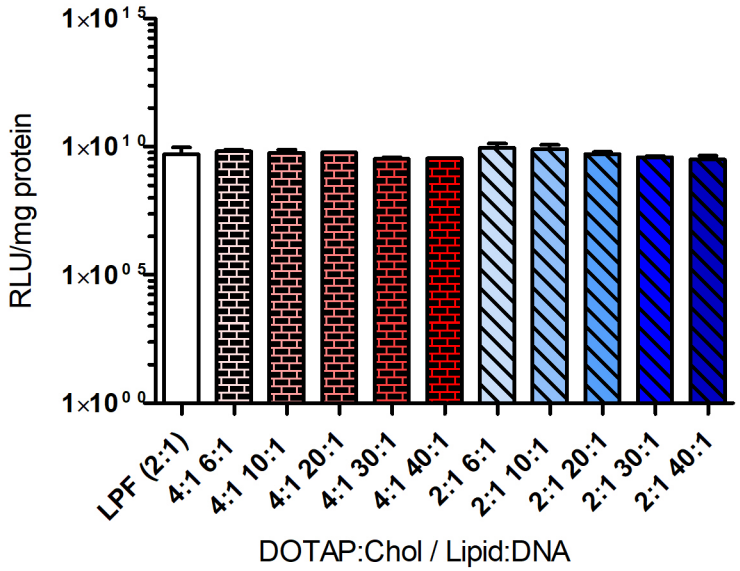

Figure 6.4: DNA luciferase luminescence measurements. Naked DNA and DNA bound with Lipofectamine 2000 were used as controls. Two different DOTAP:cholesterol lipid ratios - 4:1 and 2:1 - were tested. For each of them, different ratios of lipid to DNA were made in order to check the efficiency of the carrier. The graph shows the mean of three measurements and the error bars represent the SD.

6.2.3 DNA Transfection - Luciferase Assay

DNA transfection efficiency was tested using the Luciferase assay (see Section 2.8.2). The DNA luciferase plasmid was tested in different ratios in order to determine the best lipid carrier. Lipofectamine 2000 was used as a carrier control. For all of the samples, the luciferase signal was at least as high as for Lipofectamine (Fig. 6.4). The results are reported in terms of relative unit lights (RLU)/mg of protein. After obtaining RLU values from the luminometer, the Bradford assay, described in Section 2.8.3, was performed to evaluate the protein concentration in each sample. The results showed that lipid carriers made of DOTAP and cholesterol successfully delivered the DNA plasmid into cell nuclei, slightly better so at lower lipid to siRNA ratios. DOTAP:cholesterol vesicles are therefore a suitable carrier for DNA luciferase plasmid transfection.

6.2.4 Luciferase Assay Calibration - DNA quantification

In order to evaluate and compare the effectiveness with which different concentrations of DNA were delivered by the SAW platform, with that delivered by standard transfection, a calibration curve for standard transfection was generated. Different concentrations of DNA were delivered: 0, 0.25, 0.5, 0.75, 1.00, 1.50, 2.00, 2.50 µg/mL, in triplicate.

The curve was fitted with a third-degree polynomial equation, although between 0.75 µg/mL and 1.5 µg/mL the RLU signal increases linearly (Fig. 6.5).

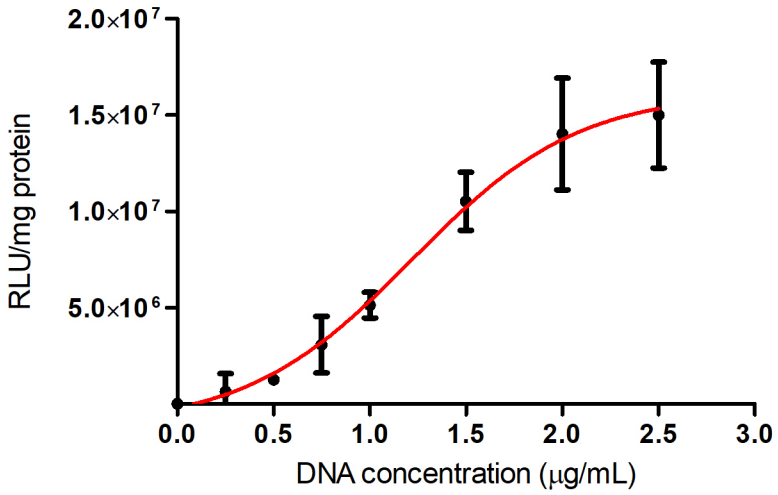

Figure 6.5: Luminescence measurements were made following the standard transfection of different concentrations of DNA luciferase plasmid. 0, 0.25, 0.5, 0.75, 1.00, 1.50, 2.00, 2.50 µg/mL of DNA were delivered in triplicate. A dose-response curve was obtained.

6.2.5 SiRNA Transfection: GAPDH siRNA

The efficiency with which GAPDH siRNA was transfected was tested in A549 cells using DOTAP-cholesterol vesicles as the siRNA carrier and verifying the gene knock-down through western blot, described in Section 2.8.5. Lipofectamine 2000 was used as a carrier control. The various ratios of lipid carriers used to deliver GAPDH siRNA all resulted in the knock-down of GAPDH expression. Over 50% knockdown resulted after using DOTAP -cholesterol at a 4:1 ratio and a lipid - siRNA ratio of 6:1; there was no significant difference between these results and those obtained from the use of Lipofectamine 2000.

Two samples with the same ratio of lipid-nucleic acid in complexes were transfected into A549 cells, with a positive control GAPDH siRNA and a negative control GAPDH siRNA. From the western blot (Fig. 6.6), samples transfected with the positive control GAPDH siRNA show a lower intensity of the GAPDH band compared to the same samples transfected with the negative control siRNA. This confirms that the GADPH siRNA entered the cytoplasm and blocked the expression of the protein. β-actin was used as an internal control, and showed a similar intensity of band across all the samples. The densities of the GADPH bands were normalised to those of β-actin.

6.2.6 SAW DNA Transfection

After testing the transfection efficiency of DOTAP-cholesterol extruded vesicles using standard cell culture transfection, SAW nebulisation-based transfection was tested for the delivery of the nucleic acid directly into cells, the equipment used is described in Section 2.9.2 and 2.9.2. In both methods, extruded cationic liposomes ($d = 200$ nm) and multilamellar

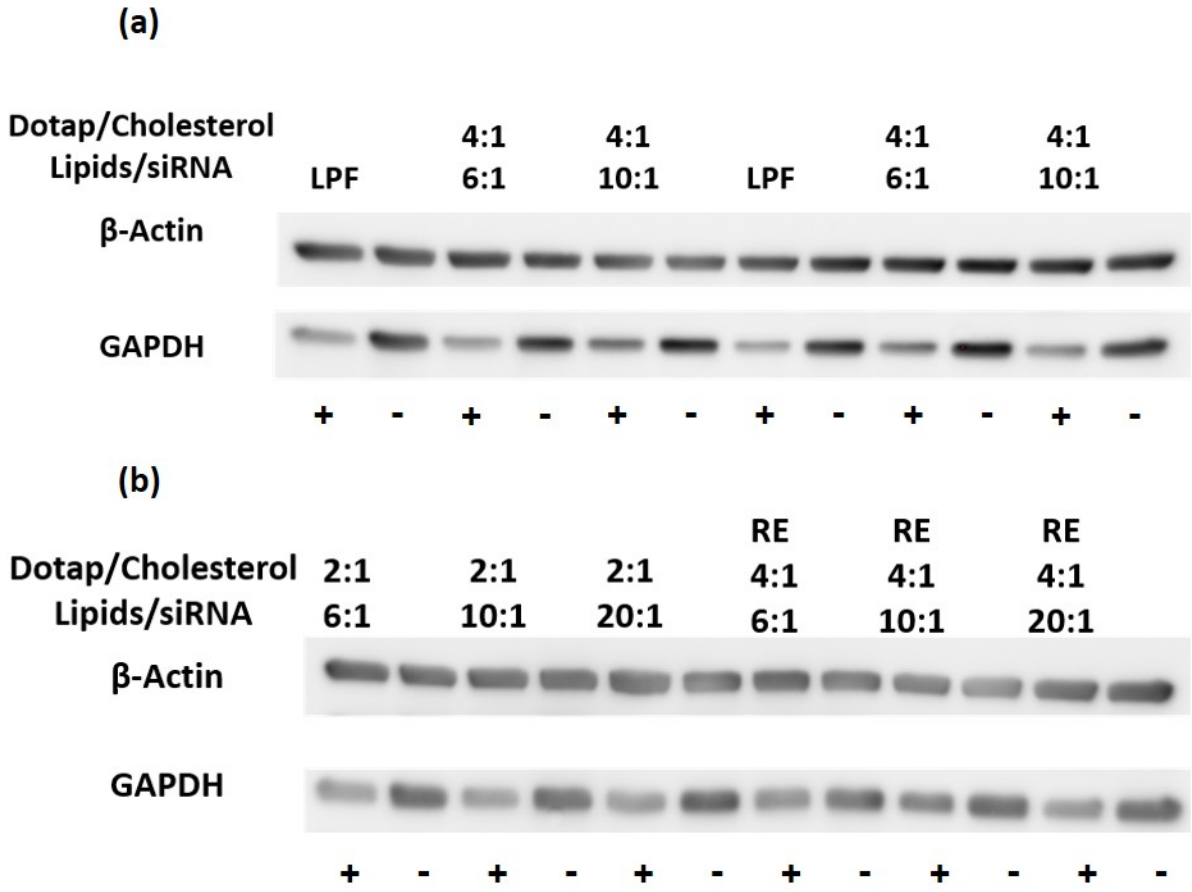

Figure 6.6: Western blot of lipid - siRNA complexes prepared with: A. DOTAP-Cholesterol ratio of 4:1, 2.4 mg/mL and a lipid-siRNA ratio of 6:1 or 10:1. B. DOTAP-Cholesterol ratio of 2:1, 2.4 mg/mL and ratio of lipid-siRNA of 6:1, 10:1, or 20:1. RE samples were prepared by the hydration of the lipids. (+) indicates transfection with the positive GAPDH siRNA, and (-) with negative control siRNA. In each sample, the density of the band for (+) samples is lower than in those transfected with negative control siRNA (-). This demonstrates the successful knockdown of GAPDH expression in A549 cells.

vesicle mixture (MLVs 2.4 mg/mL, 4:1 DOTAP:chol), and a lipid:DNA ratio of 6:1 were used for transfection (see Section 2.4.1).

The amount of DNA delivered by upright SAW nebulisation-based transfection was lower than that delivered by standard transfection (Fig. 6.7). This could be due to loss of DNA during nebulisation. The experiments were carried out in a cell culture fume hood, the air flow inside which could have reduced the capture efficiency. Using the upside-down nebulisation setup, comparable results were obtained from the standard and SAW-based transfection methods for MLV dispersion (Fig. 6.8), indicating that the upside-down setup reduced the loss induced by the nebulisation process. LUV STD is the sample made of extruded liposomes bound with DNA, and MLV STD is made of multilamellar vesicles bound with DNA. Both solutions were also delivered using the standard transfection method. To

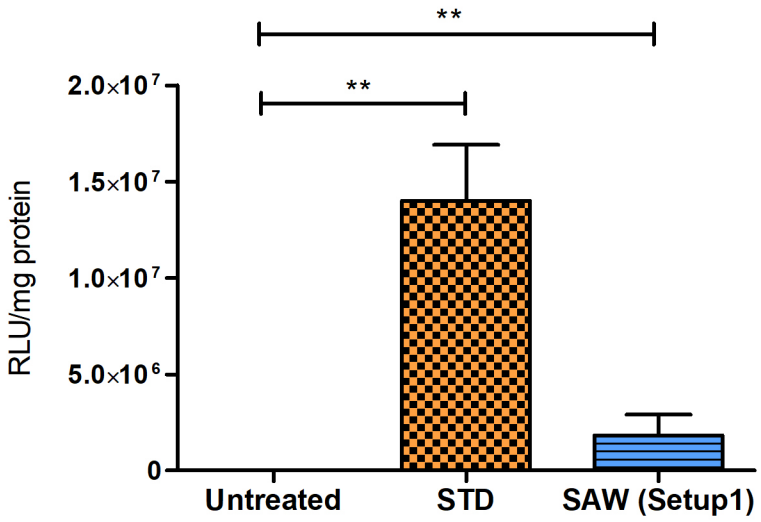

Figure 6.7: Comparison between the untreated sample, standard transfection of extruded liposomes and SAW transfection with the upright nebulisation setup (Section 2.9.2 of MLV mixture. The luminescence value of the SAW-transfected sample is very low compared to that of the standard transfected one, although higher than that of the untreated sample. The main reason for this is loss during SAW nebulisation. The graph shows the mean of three measurements and the error bars represent the SD. **p<0.01

test the efficacy of the lipid carriers formed during SAW nebulisation, an MLV mixture (the same solution that was used for transfection by the standard method) was transfected using SAW. The unilamellar vesicles formed during SAW nebulisation were similar to those produced by extrusion and transfected by the standard method (Fig. 6.8). Therefore, it is proved that: (1) SAW nebulisation of MLVs mixture obtained the same transfection efficiency than the standard transfection with pre-formed liposomes; as a consequence, during the SAW nebulisation, unilamellar vesicles are formed, (2) MLV mixtures were delivered both using the standard and SAW nebulisation, showing a higher transfection efficiency with SAW.

This demonstrates that the SAW nebuliser is an optimal platform for pulmonary drug delivery that eliminates the lipoplex production step and delivers DNA to cell nuclei quickly and efficiently.

Multilamellar vesicles with DNA at concentrations of 3.33 µg/mL and 6.66 µg/mL (Fig. 6.9), were transfected using both standard method and SAW nebulisation. During the nebulisation, the formation of LUVs showed an improved transfection of DNA into the cell. The standard transfection of MLVs resulted in a lower signal of the luciferase, due to the fact that the MLV mixture is made of a heterogeneous population of the vesicle. It is also demonstrated that increasing the DNA concentration and amount of lipids (so that the lipid:DNA ratio of 6:1 is maintained), the amount of DNA delivered increases. This study demonstrates the suitability of using a SAW-based nebuliser to deliver a DNA

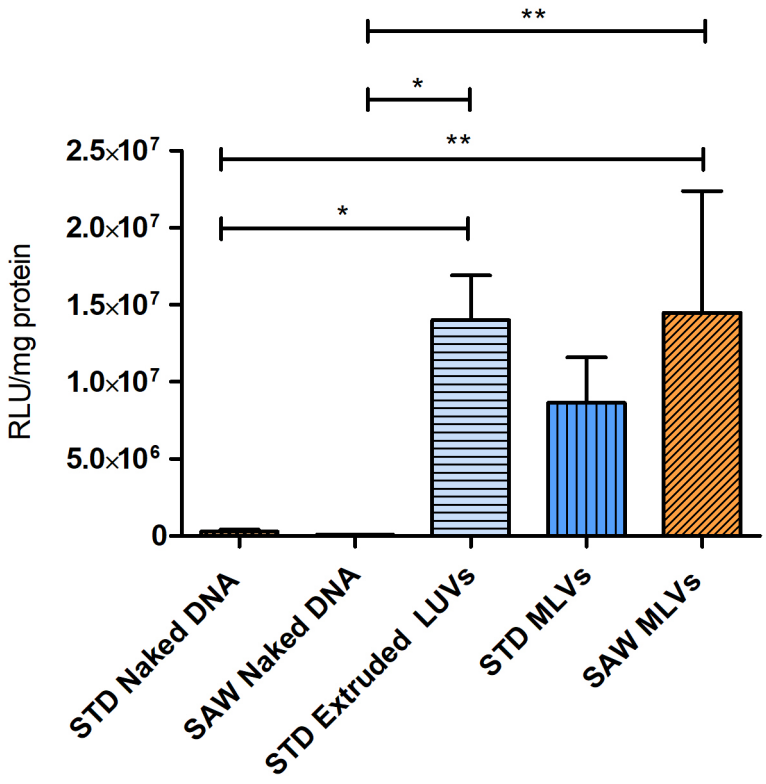

Figure 6.8: DNA luciferase transfection was carried out using both STD, the standard transfection method, and the SAW nebulisation-based method with the optimised upside-down setup. Both extruded cationic liposomes and multilamellar lipid solution were used as carriers. SAW-based and standard transfection were compared in order to test the feasibility of using the SAW platform to nebulise nucleic acids for drug delivery in the lungs. For the standard transfection of naked DNA and the SAW transfection of naked DNA, the delivered DNA resulted almost null. The standard transfection of extruded liposomes and the SAW transfection of MLV mixture obtained comparable signals, indicating the formation during the SAW nebulisation of the nucleic acid carriers. When using the same lipid solution MLVs but through the standard transfection method, a lower transfection efficiency, 30% reduction of the signal, was reported, which can be explained by the fact that unilamellar vesicles were forming during the SAW nebulisation. The graph shows the mean of three measurements and the error bars represent the SD. *$p<0.05$, **$p<0.01$

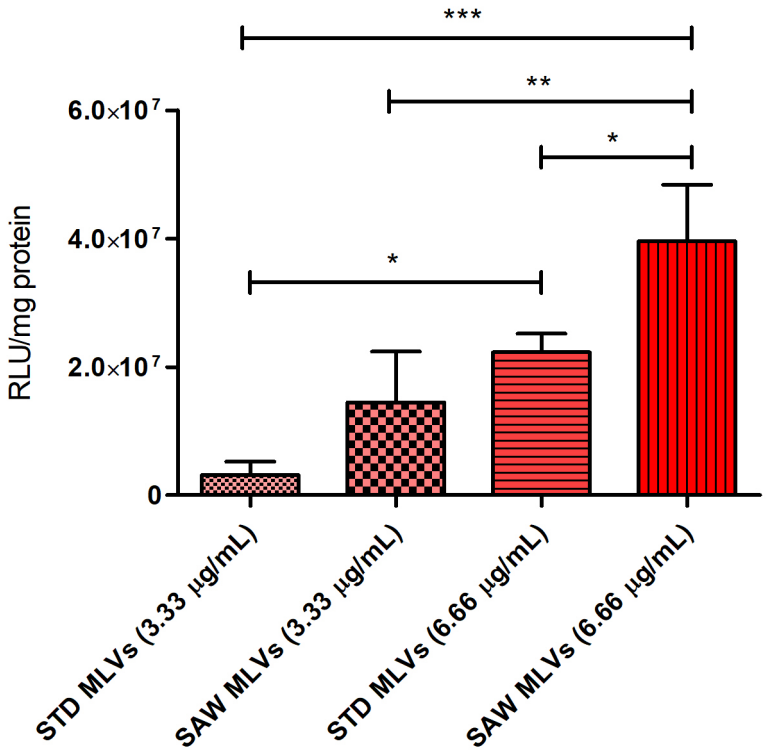

Figure 6.9: SAW transfection was employed to transfect the same MLV mixtures, bound with DNA at a concentration of 3.33 µg/mL and 6.66 µg/mL, but using standard transfection method and SAW nebulisation. SAW transfection of MLVs resulted in 50% higher signal compared to the standard transfection method of MLVs. It is shown that: (1) increasing the DNA concentration and amount of lipids (so as to maintain the 6:1 lipid:DNA ratio), increased the amount of DNA delivered, (2) during SAW nebulisation compared to standard transfection the formation of LUVs occurred, which increased the quantity of DNA that entered into the cell. *$p<0.05$, **$p<0.01$, ***$p<0.001$

plasmid, whilst simultaneously forming the nucleic acid carriers that assist its entry into the cell nuclei.

6.2.7 SAW GAPDH siRNA Transfection

The efficiency of transfecting GAPDH or negative control siRNA by SAW nebulisation was tested, with DOTAP-cholesterol vesicles as the siRNA carrier. Nebulisation was performed for 2 min inside the well containing the A549 cells, as described in Section 2.9.2. The standard cell culture transfection method was also used for comparison. With both methods, decreases in GADPH expression compared to the untreated sample (UT) were observed, confirming the cellular uptake of the GAPDH siRNA. No significant differences in remaining GAPDH expression were noticed following transfection by the two different methods, demonstrating that the SAW nebuliser is a similarly efficient method of delivering siRNA into the cells. GADPH was knocked down by over 50% when the DOTAP:cholesterol ratio

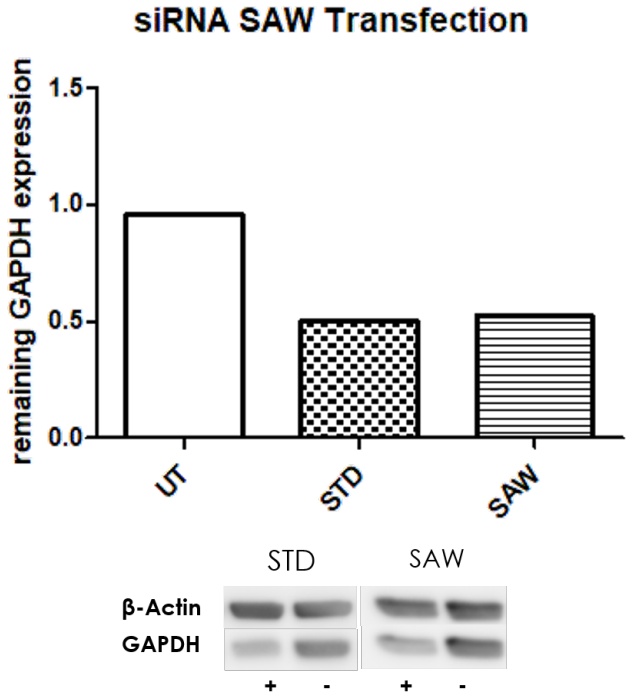

Figure 6.10: siRNA GAPDH transfection was carried out using extruded cationic liposomes as a carrier. SAW-based and standard transfection methods were compared. (A) Untreated sample, (B) Standard transfection of extruded LUVs and (C) SAW transfection of MLVs. Results show the comparable performance of the SAW-based and standard transfection methods.

was 4:1 and the lipid:siRNA ratio was 6:1. Similar samples (containing $1.6 \times (10)^5$ cells) were transfected with DNA at 2.00 µg/mL for standard transfection, and 3.33 µg/mL for SAW transfection, along with a (-) negative control siRNA and a (+) GAPDH siRNA. From the western blot (Fig. 6.10), it is clear that the density of the band for the GAPDH siRNA sample is lower than that for the negative control siRNA sample, indicating knockdown of GAPDH expression, and thus the successful entry of the siRNA into the cytoplasm. In order to quantify the knockdown, the densities of the bands were normalised to those of β-actin.

6.2.8 Confocal Microscopy

Live confocal imaging was used to check the efficiency of transfection by the SAW nebulisation platform compared to that of the standard cell culture transfection method, as reported in Section 2.9.3. A solution of DOTAP-cholesterol (4:1) at 2.4 mg/mL was prepared - without pre-forming - liposomes, in order to check if the SAW nebulisation process was able to form the siRNA carriers and then deliver the complexes into the cells. MISSION siRNA Fluorescent Universal Negative Control conjugated to 6FAM was added in the solution, and incubated with the cells for 30 min. Cell nuclei were stained using

Hoechst (blue stain). As showed in Fig. 6.11, standard transfection was not successful in delivering siRNA into the cell cytoplasm, because unilamellar lipid vesicles were not forming that would facilitate cell entry. As shown in Fig. 6.12, SAW transfection resulted in the efficient delivery of siRNA due to the formation of liposomes during the nebulisation process, creating small lipid carriers that facilitated entry of the siRNA into the cells (see Appendix B Fig. E4). In order to be sure that siRNA entered the cells, and to remove any unbound siRNA, the wells containing the cells were rinsed 10 times in PBS and then visualised under a confocal microscope. The concentration of siRNA around the nuclei is clear in the SAW-transfected samples compared with those subject to standard transfection of the MLV solution.

6.2.9 Discussion and Conclusion

The work carried out in this Chapter demonstrates the feasibility of using a SAW nebuliser as a method of transfecting nucleic acids into cells. It represents a step towards the *in-vivo* testing of the platform. The SAW nebuliser successfully delivered nucleic acids such as DNA luciferase plasmid and GAPDH siRNA to A549 lung epithelial carcinoma cells, showing that the SAW nebuliser constitutes a versatile new tool for gene therapy. A gel retardation assay showed that SAW did not destroy the functionality of either the DNA luciferase plasmid or the GAPDH siRNA.

Different compounds can be carried in different parts of the lipid carrier for delivery via the SAW platform; a polar compound can be encapsulated in the inner hydrophilic core or bound with the polar headgroups in the outer layer, while hydrophobic material can be carried within the membrane.

The *in-vitro* experiments confirmed that once the nucleic acids reached the deep lung, by means of SAW nebulisation coupled with a mesh structure, the DNA or siRNA can be absorbed effectively by the cells. Only the SAW nebulisation platform has the capabilities of delivering an aerosol within a specific size range, whilst simultaneously forming the vectors for the delivery of nucleic acids in gene therapy. It also overcomes stability issues with respect to the drugs or other compounds bound to the liposomes. The platform could have different compartments, separately containing the active compound and the lipid solution, preventing them from being mixed until patient treatment is to be commenced. One of the main innovative aspects of the SAW platform is the formation of the carriers for the nucleic acids or drugs during the nebulisation process itself. It achieves greater delivery efficiency compared methods proposed by other groups work [137]; the SAW platform transfected DNA of concentration 100 times lower with even greater efficiency. Advantages of forming the lipoplexes dynamically during the aerosol formation process are not only that it assists the entry of the nucleic acids into the cells, but that it is also less time-consuming compared to the production of liposomes by the standard method (extrusion).

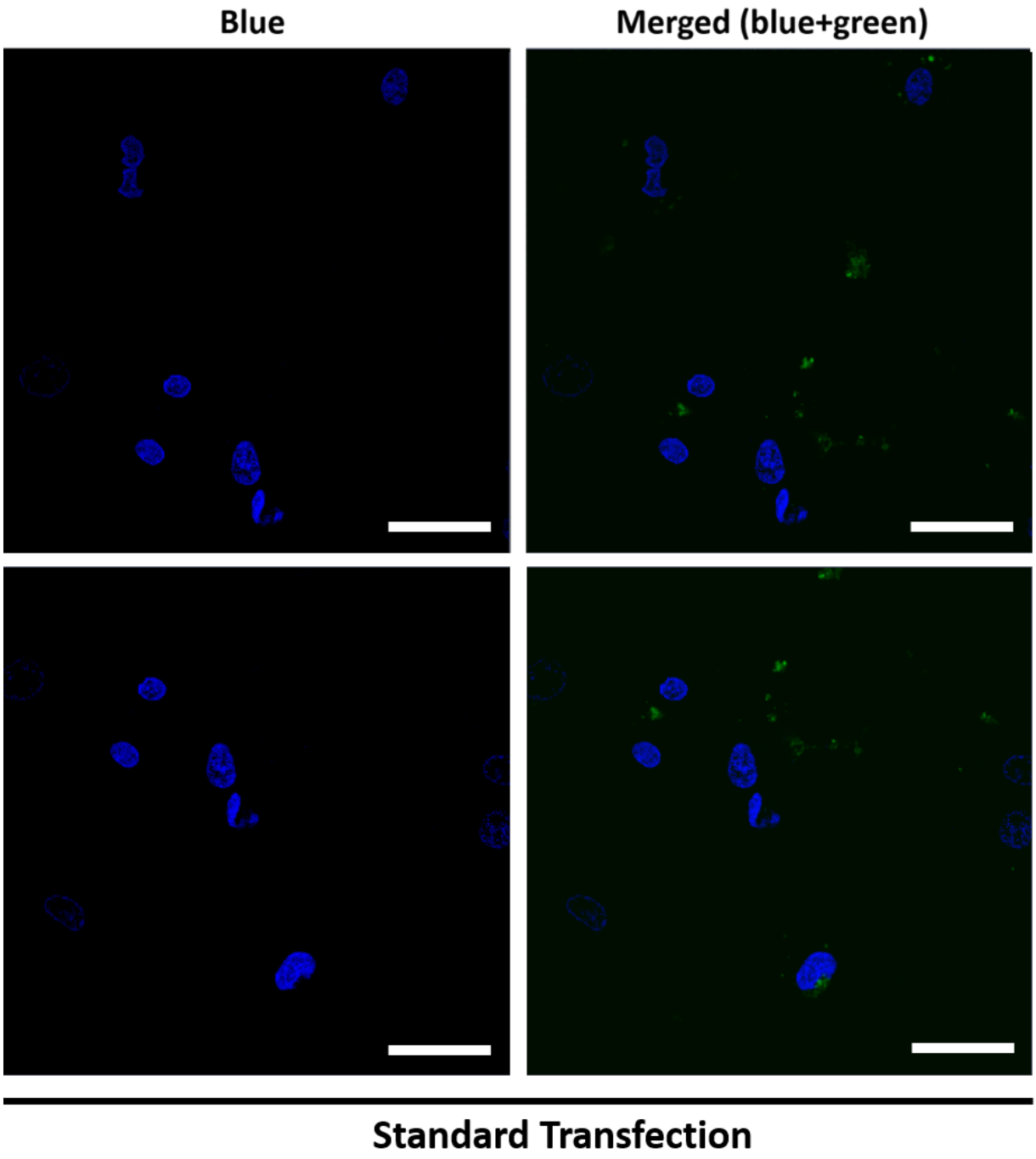

Figure 6.11: Confocal Images of A549 cells at 4 h post-transfection. The cell was transfected by standard transfection. A lipid-siRNA mixture was used, made of DOTAP-cholesterol (4:1) in 5% glucose, with a lipid-siRNA ratio of 6:1. Cell nuclei (blue) were stained with Hoechst. No cellular uptake resulted from the standard transfection of the lipid-siRNA mixture. The wells containing the cells were rinsed 10 times using PBS and then visualised under the confocal microscope. Scale bar 40 µm.

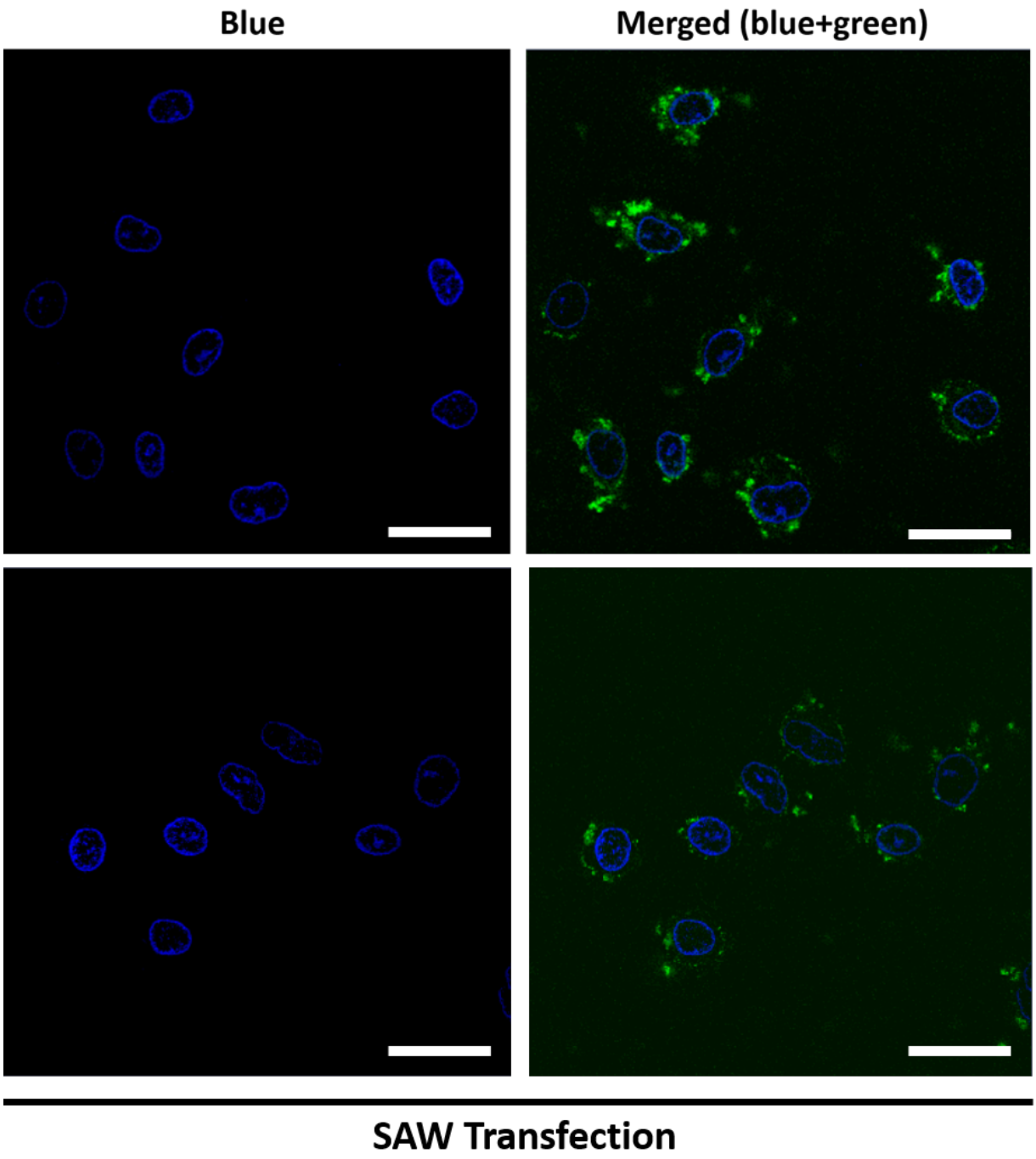

Figure 6.12: Confocal Images of A549 cells at 4 h post-transfection. Cell were transfected by SAW transfection. A lipid-siRNA mixture identical to that used for standard transfection was used, made of DOTAP-cholesterol (4:1) in 5% glucose, with a lipid-siRNA ratio of 6:1. Regarding SAW transfection, a total volume of 200 µl solution was nebulised for 2 min. siRNA (green) was labelled; the nuclei (blue) were stained with Hoechst. High cellular uptake resulted from SAW transfection, showing that lipid vesicles were formed during SAW nebulisation that were able to act as siRNA carriers. Scale bar 40 µm.

Using the SAW platform, three different steps can be integrated into one, increasing the efficiency of delivery, reducing the operation time, and improving the stability of the active compound. Despite the numerous advantages of the SAW nebuliser platform thus far demonstrated, there are still some improvements to be made, such as optimising the setup to even further minimise DNA loss. The last Chapter will describe future work to be done in order to test the SAW platform *in-vivo* in a small animal model and will illustrate the designs of both an integrated platform and a mouse inhalation chamber.

Chapter 7

Conclusion and Future Works

7.1 Summary of Findings and Conclusion

Lungs diseases affect millions of people lives. Engineering and biology tools could help in solving this problem, creating an efficient pulmonary drug delivery system. The respiratory tract is one of the oldest routes employed to deliver drugs. Although the term 'aerosol 'was coined only around 1920, the inhalation therapy for asthma was born at least 4,000 years ago in India with cigarettes made of herbal mixture. Since then, a lot of improvements were made in the aerosol therapy field, but there is still a lack of control in current nebulisers on the market. As mentioned in the introduction (see Chapter 1), an effective nebuliser delivers the drug in a targeted way with minimum wastage and at a low-cost [6]. That means tight control over the produced droplet size and the formation of a drug carrier to help the entry of compounds across cell membranes. Plus, to reduce the cost of the nebuliser production, the employment of disposable superstrates on top of the nebuliser and the versatility of the platform to be used with a different type of compounds can be of help. It is the first SAW nebuliser which is able to have precise control over the size of the droplets and that is capable to produce liposomes/nucleic acid complexes during the nebulisation.

The aim of this thesis was to develop a pulmonary drug delivery platform, which has all the features previously mentioned and that can deliver complex compounds, such as nucleic acids into lung cancer cells. The main findings in this study will be divided per chapter.

In Chapter 3, differently from the ultrasonic nebuliser, which caused damage to liposomes during the nebulisation process, SAW nebulisation was proven to be suitable to nebulise pre-formed liposomes of 100 nm in diameter. The stability of the liposomes was measured using DLS to check the size before and after nebulisation and also using an indirect method as the HRP assay. The liposomes encapsulating HRP were voluntarily solubilised in order for the HRP to react with the substrate, showing an increased in op-

tical depth, after the nebulisation. In Chapter 4, a study about the control of the size of the aerosols was made. Previous reports have shown a correlation between wavelength on the surface of liquid and median droplet size of the resulting aerosol. By manipulating the liquid length scale, using a microfabricated silicon chip, the waves on the surface of a vibrating liquid were controlled and consequently the size of the nebulised droplets. Changing the liquid length scale and confining the volume in small wells of 100 µm in diameter, the shorter wavelength of the surface waves (capillary wavelengths) were created and thus, smaller aerosols. Another finding in this chapter is regarding the formation of unilamellar vesicles *in-situ* in the SAW platform. The SAW nebulisation with power around 5 W, gives the energy to break down multilamellar vesicles in phospholipid fragments, which in contact with water closed immediately themselves, due to the hydrophobic effect of the hydrocarbon chains. It has to be mentioned that a relationship between the cavities size and the size of the vesicles encapsulated in the aerosol, was not found. For cavities size below 800 µm, in diameter, vesicles of 100 nm encapsulated in aerosols of around 2 µm were found. For cavities size above 800 µm, same size of vesicles (100 nm in 2 µm aerosols) were found and also vesicles of 2.5 µm in diameter encapsulated in 100 µm aerosols. The polar heads of the phospholipids are exposed to the inner core and the outer solution, forcing the liposomes to have a layer of water, which are surrounding them. There is a minimum amount of water that has to be around the liposomes. Changing the cavities size and consequently the size of the aerosols, we are indirectly filtering different size of liposomes. The big advantage of this new method to form liposomes is that in one single step, we produced the drug carrier encapsulated in aerosols of the optimum size range for lungs absorption.

In Chapter 5, the Andersen cascade impactor, a standard characterisation method to evaluate the aerosol size, was employed to measure the particle size distribution from the SAW nebulisation. Two methods (conductivity and fluorescence measurements) were used to test the collected aerosols in each stage of the impactor and the results confirmed the same size distributions obtained previously (see Chapter 4) with laser diffraction measurements. Also, a comparison with the mesh nebuliser OMRON NE U-22 was made, showing a larger production of particles in the optimum range from the SAW nebuliser.

Finally, in Chapter 6, an *in-vitro* study of the platform was made. We demonstrated that the SAW nebuliser is capable of delivering nucleic acids of different size (in base pairs), such as DNA luciferase plasmid and GAPDH siRNA. Firstly, it was showed that the SAW nebulisation did not alter the structure of DNA and siRNA. Then, the production of a carrier, during the nebulisation was confirmed, comparing the nebulisation of naked nucleic acid with the MLVs dispersion with nucleic acids. The results highlighted the role of the positively charged phospholipids in helping the nucleic acid to cross the cell membrane and enter the nucleus or cytoplasm, in siRNA case.

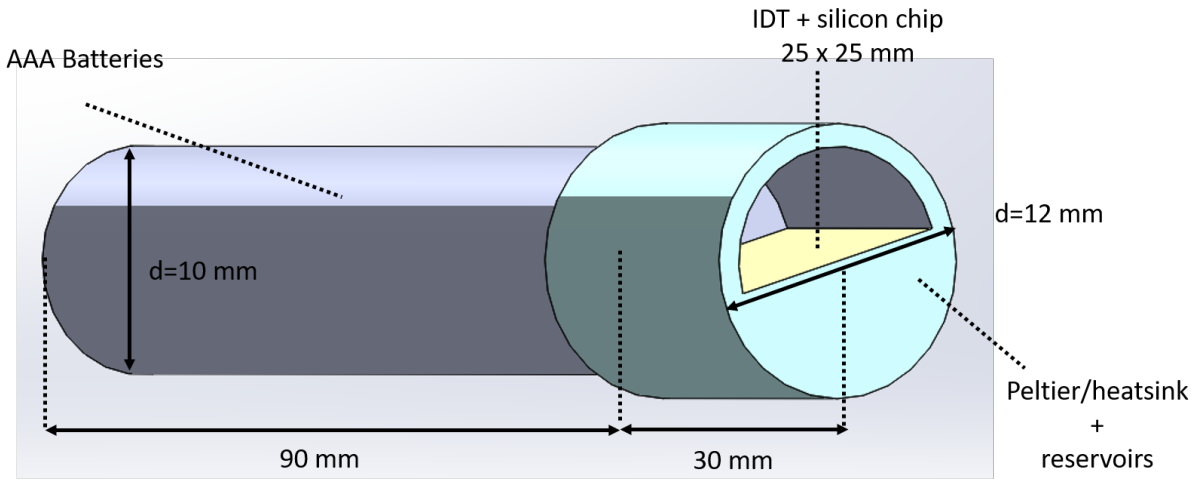

Figure 7.1: Prototype of the SAW nebuliser. The back side will contain AAA type batteries, while the front part will be composed by the Peltier and heat sink, with 2 reservoirs, one for the MLVs mixture and the other for the compound to deliver. On top of it, there will be the IDT and the silicon chip.

In conclusion, the work carried out in this thesis showed a new device for pulmonary drug delivery, which is capable of delivering biologics, thanks to the formation *in-situ* of liposomes that can guide the nucleic acids into the cells. It is also shown the control of the aerosols' size during the nebulisation, through the use of silicon chip, which is one of the main critical parameter for a targeted delivery of the compound into the lungs.

7.2 Future Works

As future works, *in-vivo* testing of the SAW nebulisation platform will be carried out. The aim is to prove that using the platform we can deliver different compounds in deep lungs in small animal models.

In order to have less variability in the measurements, an optimised design is needed. Fixed position of the IDT, silicon chip and a feeding tube can increase the reproducibility of the experiments and the portability of the setup. A prototype of the nebuliser will be built. As shown in Fig. 7.1, the SAW neb platform will have two chambers, one for the power supply and the first part will be dedicated to the nebuliser. The first chamber will contain two reservoirs one for the drug carrier mixture and the other for the compound to deliver. The IDT and the silicon chip will be placed on top of it. Both laser cutting and 3D printing will be employed to build the prototype. Moreover, a mice inhalation chamber will be designed. Figure 7.2 shows a nose-only exposure chamber (CH technologies, USA) used by Mainelis et al, [82]. The containment tubes are connected to the distribution chamber, the nebuliser was placed outside and connected to the distribution chamber. The SAW nebuliser could be placed inside the distribution chamber to reduce the loss during the

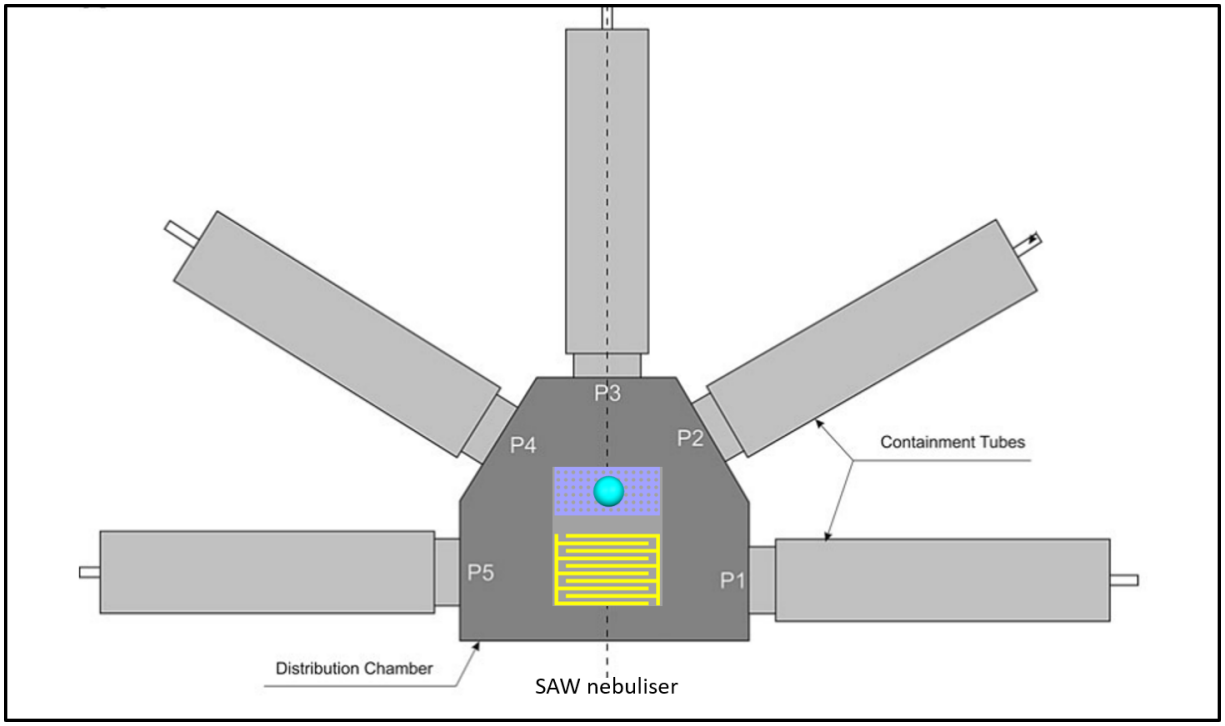

Figure 7.2: A 5 port nose-only inhalation exposure chamber from CH Technologies. A distribution chamber is represented with 5 mice containers. Figure adapted from [82], where the SAW nebuliser was placed in the center of the distribution chamber.

nebulisation, as shown in Fig. 7.2, [82]. The advantage of using a nose-only inhalation exposure system is the elimination of alternative exposure routes, like dermal absorption. A drawback of the system is the animal discomfort, created by the limited space, which raises ethical concerns, causing also animal's hyperventilation (Fig. 7.4, (B)). Da Silva et al. [242], adapted an Erlenmeyer flask as a nose-only inhalation chamber. Other methods to deliver compounds *in-vivo* are the intratracheal delivery (Fig. 7.4, (C)) or using a whole body inhalation exposure chamber (Fig. 7.4, (A)), which will reduce the animal stress but will increase the wastage and includes other delivery routes.

7.2.1 In Vivo Experimentation

In animal studies and clinical trials, one of the most important components of the design of an experiment is the calculation of sample size, which is needed to answer a research question [243]. If a lower number of animals is selected, the study could be not representative of the population and the real effect in the experiments can be missed. On the other side, if the sample is too large, it leads to a wastage of resources and ethical issues. To calculate the sample size, two different calculations can be made, one is the power analysis and the second is called the resource equation We want to prove the SAW Nebulisation platform efficiency in delivering compounds in lungs. Thus, in the power analysis, two hypotheses are considered [244]:

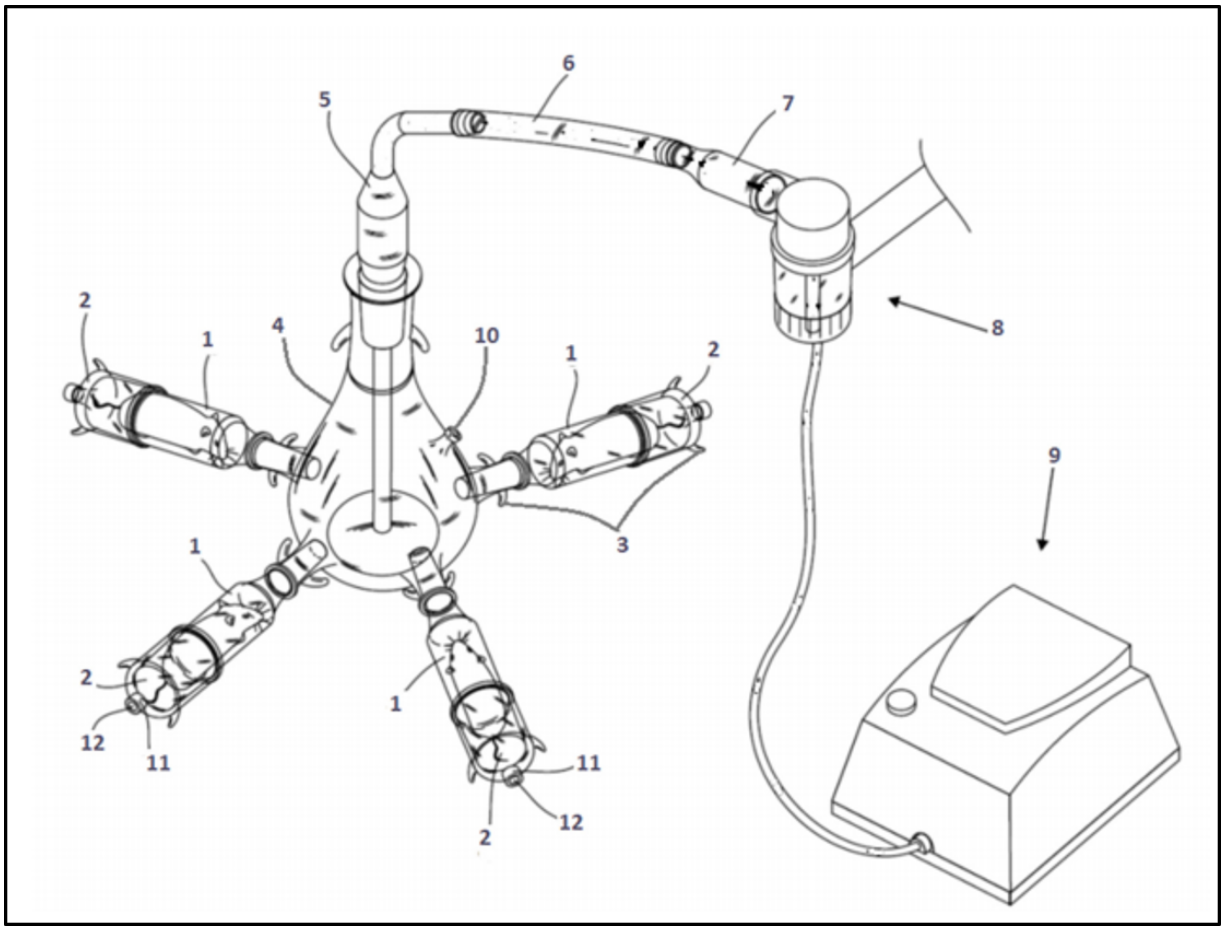

Figure 7.3: A 4 port nose-only inhalation exposure chamber from Silva et al., [242], where an Erlenmeyer flask was adapted and used as a distribution chamber. Inhalation chamber coupled with nebuliser. From [242], (1) animal holder; (2) lid; (3) later hooks; (4) central part; (5) head; (6)silicon hose; (7) glass joint; (8) nebuliser cup; (9) nebuliser; (10) sampling port; (11) plastic screw cap; (12) air output.

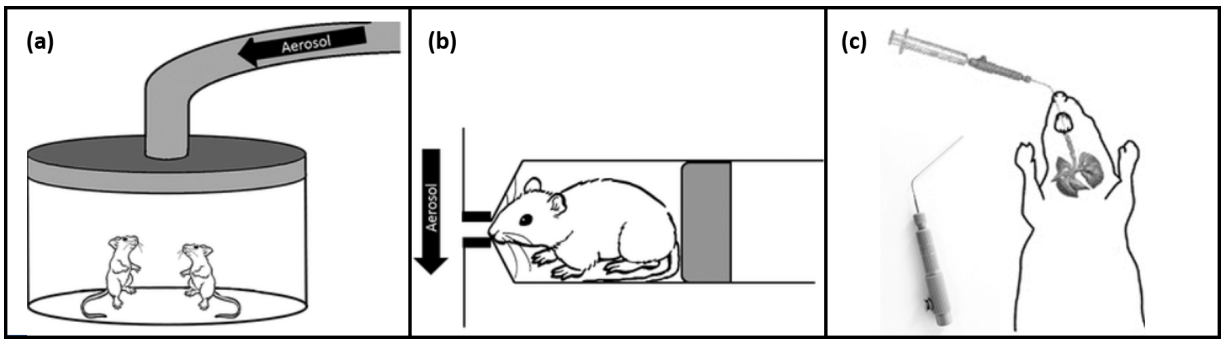

Figure 7.4: Different *in-vivo* delivery method. (A) Total body exposure chamber. (B) Nose-only inhalation exposure chamber. (C) Intratracheal instillation. Fig. adapted from [245]

- the null hypothesis implies no difference or effect of the study
- the alternative hypothesis states a statistical significance between two measured phenomena

In this future study, a proof of concept that shows the efficiency of SAW nebuliser to deliver nucleic acids in mice lungs will be carried out.

Power analysis will be employed later in this study, but here, an estimation of the sample size using the resource equation will be shown. This method is used in exploratory studies, where the testing of the hypothesis is not the primary objective, but only the understanding of differences between the groups [244]. A value 'E' is measured as followed:

$$E = TotalNumberOfAnimals - TotalNumberOfGroups \tag{7.1}$$

where experiments with $10 < E < 20$ are considered appropriate. If E is less than 10, more animals should be added to the study to increase the significance of the result. If E is more than 20, adding more animals will not increase the significance. In our study, three groups will be tested: (1) positive control group (intratracheal delivery), (2) negative control group (healthy mice) and (3) SAW group. If we consider 5 mice per each group (3 in total), $E = 12$ is within the range of the adequate experiments.

Bibliography

[1] "WHO | Chronic respiratory diseases (CRDs)". In: *WHO* (2018). URL: https://www.who.int/respiratory/en/.

[2] William Berger. "Aerosol Devices and Asthma Therapy". In: *Current Drug Delivery* 6.1 (Jan. 2009), pp. 38–49. ISSN: 15672018. DOI: 10.2174/156720109787048203. URL: http://www.eurekaselect.com/openurl/content.php?genre=article%7B%5C&%7Dissn=1567-2018%7B%5C&%7Dvolume=6%7B%5C&%7Dissue=1%7B%5C&%7Dspage=38.

[3] Byron P R Patton J S. "Inhaling medicines:delivering drugs to the body through the lungs". In: (2007). DOI: 10.1038/nrd2153. URL: https://www.nature.com/articles/nrd2153.pdf.

[4] Mariam Ibrahim, Rahul Verma, and Lucila Garcia-Contreras. "Inhalation drug delivery devices: technology update." In: *Medical devices (Auckland, N.Z.)* 8 (2015), pp. 131–9. ISSN: 1179-1470. DOI: 10.2147/MDER.S48888. URL: http://www.ncbi.nlm.nih.gov/pubmed/25709510%20http://www.pubmedcentral.nih.gov/articlerender.fcgi?artid=PMC4334339.

[5] Arzu Ari. "Jet, Ultrasonic, and Mesh Nebulizers: An Evaluation of Nebulizers for Better Clinical Outcomes". In: *Eurasian J Pulmonol* 16.1 (2014), p. 7. ISSN: 21483620. DOI: 10.5152/ejp.2014.00087.

[6] C O'Callaghan and P W Barry. "The science of nebulised drug delivery." In: *Thorax* 52 Suppl 2.Suppl 2 (1997), S31–S44. ISSN: 0040-6376. DOI: 10.1136/thx.52.2008.S31.

[7] S P Newman and M T Newhouse. "Effect of add-on devices for aerosol drug delivery: deposition studies and clinical aspects." In: *Journal of aerosol medicine : the official journal of the International Society for Aerosols in Medicine* 9.1 (1996), pp. 55–70. ISSN: 0894-2684. DOI: 10.1089/jam.1996.9.55.

[8] N. R. Labiris and M. B. Dolovich. "Pulmonary drug delivery. Part I: Physiological factors affecting therapeutic effectiveness of aerosolized medications". In: *British Journal of Clinical Pharmacology* 56.6 (2003), pp. 588–599. ISSN: 03065251. DOI: 10.1046/j.1365-2125.2003.01892.x.

[9] John N Pritchard, Ross Hm Hatley, John Denyer, and Dirk Von Hollen. "Mesh nebulizers have become the first choice for new nebulized pharmaceutical drug developments". In: (). DOI: 10.4155/tde-2017-0102. URL: https://clinicaltrials.gov.

[10] Julien Reboud, Rab Wilson, Yi Zhang, Mohd H Ismail, Yannyk Bourquin, and Jonathan M Cooper. "Nebulisation on a disposable array structured with phononic lattices." In: *Lab on a chip* 12.7 (2012), pp. 1268–73. ISSN: 1473-0189. DOI: 10.1039/c2lc20705b. URL: http://www.ncbi.nlm.nih.gov/pubmed/22327572.

[11] Leslie Y Yeo, James R Friend, Michelle P McIntosh, Els N T Meeusen, and David a V Morton. "Ultrasonic nebulization platforms for pulmonary drug delivery." In: *Expert opinion on drug delivery* 7.6 (2010), pp. 663–679. ISSN: 1742-5247. DOI: 10.1517/17425247.2010.485608.

[12] Yue Huang, Sung Hwan Yoon, Scott R. Heron, Christophe D. Masselon, J. Scott Edgar, Frantisek Turecek, and David R. Goodlett. "Surface acoustic wave nebulization produces ions with lower internal energy than electrospray ionization". In: *Journal of the American Society for Mass Spectrometry* 23.6 (2012), pp. 1062–1070. ISSN: 10440305. DOI: 10.1007/s13361-012-0352-8.

[13] Liqiang Ren, Yuchao Chen, Peng Li, Zhangming Mao, Po-Hsun Huang, Joseph Rufo, Feng Guo, Lin Wang, J Philip Mccoy, Stewart J Levine, and Tony Jun Huang. "A high-throughput standing surface acoustic wave (SSAW)-based cell sorter". In: (). DOI: 10.1039/c5lc00706b. URL: https://www.ncbi.nlm.nih.gov/pmc/articles/PMC4641751/pdf/nihms-717385.pdf.

[14] J. Reboud, Y. Bourquin, R. Wilson, G. S. Pall, M. Jiwaji, A. R. Pitt, A. Graham, A. P. Waters, and J. M. Cooper. "Shaping acoustic fields as a toolset for microfluidic manipulations in diagnostic technologies". In: *Proceedings of the National Academy of Sciences* 109.38 (2012), pp. 15162–15167. ISSN: 0027-8424. DOI: 10.1073/pnas.1206055109. URL: http://www.pnas.org/cgi/doi/10.1073/pnas.1206055109.

[15] Tao Wang, Ryan Green, Rajesh Ramakrishnan Nair, Mark Howell, Subhra Mohapatra, Rasim Guldiken, Shyam Sundar Mohapatra, Zhiping Wang, and Charles Chun Yang. "Surface Acoustic Waves (SAW)-Based Biosensing for Quantification of Cell Growth in 2D and 3D Cultures". In: *Sensors* 15 (2015), pp. 32045–32055. DOI: 10.3390/s151229909. URL: www.mdpi.com/journal/sensors.

[16] Minoru Kurosawa, Takayuki Watanabe, Akira Futami, and Toshiro Higuchi. *Surface acoustic wave atomizer*. 1995. DOI: 10.1016/0924-4247(96)80086-0. URL: http://linkinghub.elsevier.com/retrieve/pii/0924424796800860.

[17] Leslie Y Yeo, James R Friend, Michelle P McIntosh, Els NT Meeusen, and David AV Morton. "Ultrasonic nebulization platforms for pulmonary drug delivery". In: (1742). DOI: 10.1517/17425247.2010.485608. URL: https://pdfs.semanticscholar.org/6d7f/9377c5d016c89fa90a903b6d0a47a59ffa8e.pdf.

[18] James R Friend, Leslie Y Yeo, Dian R Arifin, and Adam Mechler. "Evaporative self-assembly assisted synthesis of polymeric nanoparticles by surface acoustic wave atomization Recent citations This content was downloaded from IP address Evaporative self-assembly assisted synthesis of polymeric nanoparticles by surface ac". In: *NANOTECHNOLOGY* 19 (2008), p. 6. DOI: 10.1088/0957-4484/19/14/145301. URL: http://iopscience.iop.org/article/10.1088/0957-4484/19/14/145301/pdf.

[19] Leslie Y. Yeo and James R. Friend. "Surface Acoustic Wave Microfluidics". In: *Annual Review of Fluid Mechanics* 46.1 (2014), pp. 379–406. ISSN: 0066-4189. DOI: 10.1146/annurev-fluid-010313-141418. URL: http://www.annualreviews.org/doi/abs/10.1146/annurev-fluid-010313-141418.

[20] Katsumi Chono, Norifumi Shimizu, Yoshikazu Matsui, Jun Kondoh, and Showko Shiokawa. "Development of novel atomization system based on SAW streaming". In: *Japanese Journal of Applied Physics, Part 1: Regular Papers and Short Notes and Review Papers* 43.5 B (2004), pp. 2987–2991. ISSN: 00214922. DOI: 10.1109/ULTSYM.2003.1293259.

[21] Yannyk Bourquin, Julien Reboud, Rab Wilson, and Jonathan M. Cooper. "Tuneable surface acoustic waves for fluid and particle manipulations on disposable chips". In: *Lab on a Chip* 10.15 (2010), p. 1898. ISSN: 1473-0197. DOI: 10.1039/c004506c. URL: http://xlink.rsc.org/?DOI=c004506c.

[22] Rab Wilson, Julien Reboud, Yannyk Bourquin, Steven L. Neale, Yi Zhang, and Jonathan M. Cooper. "Phononic crystal structures for acoustically driven microfluidic manipulations". In: *Lab Chip* 11.2 (2011), pp. 323–328. ISSN: 1473-0197. DOI: 10.1039/C0LC00234H. URL: http://xlink.rsc.org/?DOI=C0LC00234H.

[23] H. Rasool and a. Bassam. "Overview on Drug Delivery System". In: *Pharmaceutica Analytica Acta* 03.10 (2012), p. 4172. ISSN: 21532435. DOI: 10.4172/2153-2435.1000e137. URL: http://www.omicsonline.org/overview-on-drug-delivery-system-2153-2435.1000e137.php?aid=10652.

[24] *Drug Delivery Systems: Getting Drugs to Their Targets in a Controlled Manner | National Institute of Biomedical Imaging and Bioengineering*. URL: https://www.nibib.nih.gov/science-education/science-topics/drug-delivery-systems-getting-drugs-their-targets-controlled-manner (visited on 10/15/2018).

[25] *Routes of administration - an overview | ScienceDirect Topics*. URL: https://www.sciencedirect.com/topics/pharmacology-toxicology-and-pharmaceutical-science/routes-of-administration (visited on 10/15/2018).

[26] Shuguang Hou, Jiangyue Wu, Xu Li, and Hong Shu. "Practical, regulatory and clinical considerations for development of inhalation drug products". In: *Asian Journal of Pharmaceutical Sciences* 10.6 (Dec. 2015), pp. 490–500. ISSN: 1818-0876. DOI: 10.1016/J.AJPS.2015.08.008. URL: https://www.sciencedirect.com/science/article/pii/S1818087615000690.

[27] C. Darquenne. "Particle deposition in the lung". In: *Encyclopedia of Respiratory Medicine* (2006), pp. 300–304.

[28] Chen Hou, Stefan Gheorghiu, Virginia H. Huxley, and Peter Pfeifer. "Reverse engineering of oxygen transport in the lung: Adaptation to changing demands and resources through space-filling networks". In: *PLoS Computational Biology* 6.8 (2010). ISSN: 1553734X. DOI: 10.1371/journal.pcbi.1000902.

[29] J S Patil and S Sarasija. "Pulmonary drug delivery strategies: A concise, systematic review." In: *Lung India : official organ of Indian Chest Society* 29.1 (Jan. 2012), pp. 44–9. ISSN: 0974-598X. DOI: 10.4103/0970-2113.92361. URL: http://www.ncbi.nlm.nih.gov/pubmed/22345913%20http://www.pubmedcentral.nih.gov/articlerender.fcgi?artid=PMC3276033.

[30] Rajesh Singh, Shailesh Singh, and James W Lillard. "Past, present, and future technologies for oral delivery of therapeutic proteins." In: *Journal of pharmaceutical sciences* 97.7 (July 2008), pp. 2497–523. ISSN: 1520-6017. DOI: 10.1002/jps.21183. URL: http://www.ncbi.nlm.nih.gov/pubmed/17918721%20http://www.pubmedcentral.nih.gov/articlerender.fcgi?artid=PMC4627499.

[31] T V Thulasiramaraju, B Tejeswar Kumar, and M Nikilesh Babu. *PULMONARY DRUG DELIVERY SYSTEM: AN OVERVIEW*. Tech. rep. 1. 2013, pp. 16–34. URL: www.uptodateresearchpublication.com.

[32] A H Kendrick and C Newall. "Chapter 2 - Anatomy & Physiology of the Respiratory System". In: *ARTP Ebooks Pdf and Magazines Free Download Manuals* (). URL: http://www.freebookspdf.org/free/pdf/b-anatomy-and-physiology-of-the-respiratory-system-artp.html.

[33] N. R. Labiris and M. B. Dolovich. "Pulmonary drug delivery. Part II: The role of inhalant delivery devices and drug formulations in therapeutic effectiveness of aerosolized medications". In: *British Journal of Clinical Pharmacology* 56.6 (Aug. 2003), pp. 600–612. ISSN: 03065251. DOI: 10.1046/j.1365-2125.2003.01893.x. URL: http://doi.wiley.com/10.1046/j.1365-2125.2003.01893.x.

[34] David J Paterson, Manlio Tassieri, Julien Reboud, Rab Wilson, and Jonathan M Cooper. "Lipid topology and electrostatic interactions underpin lytic activity of linear cationic antimicrobial peptides in membranes". In: (). DOI: 10.1073/pnas.1704489114. URL: http://www.pnas.org/content/pnas/114/40/E8324.full.pdf.

[35] Abolfazl Akbarzadeh, Rogaie Rezaei-Sadabady, Soodabeh Davaran, Sang Woo Joo, Nosratollah Zarghami, Younes Hanifehpour, Mohammad Samiei, Mohammad Kouhi, and Kazem Nejati-Koshki. "Liposome: classification, preparation, and applications." en. In: *Nanoscale research letters* 8.1 (Jan. 2013), p. 102. ISSN: 1931-7573. DOI: 10.1186/1556-276X-8-102. URL: http://www.nanoscalereslett.com/content/8/1/102.

[36] Dr. a. K. Bhandari J.S. Dua, Prof. A. C. Rana. "Review Article LIPOSOME : METHODS OF PREPARATION AND APPLICATIONS". In: *International Journal of Pharmaceutical Studies and Research* III.II (2012), p. 7.

[37] A D Bangham, M M Standish, and J C Watkins. *Diffusion of Univalent Ions across the Lamellae of Swollen Phospholipids*. Tech. rep. 1965, 238–252, IN26–IN27. DOI: 10.1016/S0022-2836(65)80093-6. URL: https://ac.els-cdn.com/S0022283665800936/1-s2.0-S0022283665800936-main.pdf?%7B%5C_%7Dtid=1436ab04-dbf9-46e2-b8cc-c13be53c8ccc%7B%5C&%7Dacdnat=1533821535%7B%5C_%7D40bba01982580fb6809ef829e06c4aad.

[38] A. D. Bangham. "Liposomes: the Babraham connection". In: *Chemistry and Physics of Lipids* 64.1-3 (1993), pp. 275–285. ISSN: 00093084. DOI: 10.1016/0009-3084(93)90071-A.

[39] Aus Der Wissenschaft. "The Discovery of Liposomes". In: (1994), pp. 1064–1067.

[40] F Szoka and D Papahadjopoulos. "Comparative properties and methods of preparation of lipid vesicles (liposomes)." In: *Annual review of biophysics and bioengineering* 9 (1980), pp. 467–508. ISSN: 0084-6589. DOI: 10.1146/annurev.bb.09.060180.002343.

[41] F Szoka, D Papahadjopoulos, and D Papahadjopoulos. "Procedure for preparation of liposomes with large internal aqueous space and high capture by reverse-phase evaporation." In: *Proceedings of the National Academy of Sciences of the United States of America* 75.9 (Sept. 1978), pp. 4194–8. ISSN: 0027-8424. URL: http://www.ncbi.nlm.nih.gov/pubmed/279908%20http://www.pubmedcentral.nih.gov/articlerender.fcgi?artid=PMC336078.

[42] S. Vemuri and C. T. Rhodes. "Preparation and characterization of liposomes as therapeutic delivery systems: A review". In: *Pharmaceutica Acta Helvetiae* 70.2 (1995), pp. 95–111. ISSN: 00316865. DOI: 10.1016/0031-6865(95)00010-7.

[43] *What Is The Transition Temperature Of The Lipid? | Avanti Polar Lipids*. URL: https://avantilipids.com/tech-support/faqs/transition-temperature/ (visited on 07/18/2018).

[44] W. W. Sułkowski, D. Pentak, K. Nowak, and a. Sułkowska. "The influence of temperature, cholesterol content and pH on liposome stability". In: *Journal of Molecular Structure* 744-747.SPEC. ISS. (2005), pp. 737–747. ISSN: 00222860. DOI: 10.1016/j.molstruc.2004.11.075.

[45] "Spherical Ellipsoid Cylindrical". In: (). URL: https://onlinelibrary.wiley.com/doi/pdf/10.1016/0307-4412(91)90103-F.

[46] J Du Plessis, C Ramachandran, N Weiner, and D G Moiler. "The influence of lipid composition and lamellarity of liposomes on the physical stability of liposomes upon storage". In: *International Journal of Pharmaceutics* 127 (1996), pp. 273–278. URL: https://ac.els-cdn.com/0378517395042814/1-s2.0-0378517395042814-main.pdf?%7B%5C_%7Dtid=608b94f3-5d8d-4855-b5e4-d54a9bc6d15d%7B%5C&%7Dacdnat=1522321741%7B%5C_%7D0d2182f6cbd4c0f811c420010bc6c138.

[47] D. D. Lasic and F. J. Martin. "On the mechanism of vesicle formation". In: *Journal of Membrane Science* 50.2 (1990), pp. 215–222. ISSN: 03767388. DOI: 10.1016/S0376-7388(00)80317-8.

[48] R L Juliano. "Factors affecting the clearance kinetics and tissue distribution of liposomes, microspheres and emulsions". In: *Advanced Drug Delivery Reviews* 2 (1988), pp. 31–54. URL: https://ac.els-cdn.com/0169409X8890004X/1-s2.0-0169409X8890004X-main.pdf?%7B%5C_%7Dtid=8cfefdb0-7636-40b9-ae55-3332dfbf083d%7B%5C&%7Dacdnat=1526896053%7B%5C_%7D87e5ad3fe786ee055f0b20ea268

[49] D. D. Lasic and F. J. Martin. "On the mechanism of vesicle formation". In: *Journal of Membrane Science* 50.2 (1990), pp. 215–222. ISSN: 03767388. DOI: 10.1016/S0376-7388(00)80317-8.

[50] Jacob N Israelachvil1, D John Mitchell, and Barry W Ninham. "Theory of Self-Assembly of Hydrocarbon Amphiphiles into Micelles and Bilayers FORMULATION OF A MODEL FOR THE FREE ENERGIES". In: (). URL: http://pubs.rsc.org/en/content/articlepdf/1976/f2/f29767201525.

[51] Taras Sych, Yves Mély, and Winfried Römer. "Lipid self-assembly and lectin-induced reorganization of the plasma membrane". In: (). DOI: 10.1098/rstb.2017.0117. URL: http://dx.doi.org/10.1098/rstb.2017.0117.

[52] V V Kumar. "Complementary molecular shapes and additivity of the packing parameter of lipids." In: *Proceedings of the National Academy of Sciences of the United States of America* 88.2 (1991), pp. 444–448. ISSN: 0027-8424. DOI: 10.1073/pnas.88.2.444.

[53] Danilo D. Lasic. "A General Model of Vesicle Formation". In: *Journal of Theoretical Biology* 124.June 1985 (1987), pp. 35–41. DOI: 10.1016/S0022-5193(87)80250-3.

[54] DD Lasic, A Belic, and T Valentincic. "A new method for the instant preparation of large unilamellar vesicles". In: *Journal of the American ...* 9 (1988), pp. 970–971. ISSN: 00027863. URL: http://pubs.acs.org/doi/abs/10.1021/ja00211a049.

[55] Herre Talsma, Mies J. Van Steenbergen, Johan C.H. Borchert, and Daan J.A. Crommelin. "A Novel Technique for the One-Step Preparation of Liposomes and Nonionic Surfactant Vesicles without the Use of Organic Solvents. Liposome Formation in a Continuous Gas Stream: The 'Bubble' Method". In: *Journal of Pharmaceutical Sciences* 83.3 (Mar. 1994), pp. 276–280. ISSN: 0022-3549. DOI: 10.1002/JPS.2600830303. URL: https://www.sciencedirect.com/science/article/pii/S0022354915493803?via%7B%5C%%7D3Dihub.

[56] Jie Feng, Matthieu Roché, Daniele Vigolo, Luben N Arnaudov, Simeon D Stoyanov, Theodor D Gurkov, Gichka G Tsutsumanova, and Howard A Stone. "Nanoemulsions obtained via bubble-bursting at a compound interface". In: (2014). DOI: 10.1038/NPHYS3003. URL: https://www.nature.com/articles/nphys3003.pdf.

[57] "ORGANIC LABORATORY TECHNIQUES 8". In: (). URL: http://www.chem.ucalgary.ca/courses/351/laboratory/rotavap.pdf.

[58] Abolfazl Akbarzadeh, Rogaie Rezaei-Sadabady, Soodabeh Davaran, Sang Woo Joo, Nosratollah Zarghami, Younes Hanifehpour, Mohammad Samiei, Mohammad Kouhi, and Kazem Nejati-Koshki. "Liposome: classification, preparation, and applications." In: *Nanoscale research letters* 8.1 (Feb. 2013), p. 102. ISSN: 1931-7573. DOI: 10.1186/1556-276X-8-102. URL: http://www.ncbi.nlm.nih.gov/pubmed/23432972%20http://www.pubmedcentral.nih.gov/articlerender.fcgi?artid=PMC3599573.

[59] Hongwei Zhang. "Thin-Film Hydration Followed by Extrusion Method for Liposome Preparation". In: *Methods in molecular biology (Clifton, N.J.)* Vol. 1522. 2017, pp. 17–22. DOI: 10.1007/978-1-4939-6591-5_2. URL: http://www.ncbi.nlm.nih.gov/pubmed/27837527%20http://link.springer.com/10.1007/978-1-4939-6591-5%7B%5C_%7D2.

[60] Uri Pick. "Liposomes with a large trapping capacity prepared by freezing and thawing of sonicated phospholipid mixtures". In: *Archives of Biochemistry and Biophysics* 212.1 (Nov. 1981), pp. 186–194. ISSN: 0003-9861. DOI: 10.1016/0003-9861(81)90358-1. URL: https://www.sciencedirect.com/science/article/pii/0003986181903581.

[61] F Olson, C a Hunt, F C Szoka, W J Vail, and D Papahadjopoulos. "Preparation of liposomes of defined size distribution by extrusion through polycarbonate membranes." In: *Biochimica et biophysica acta* 557.1 (1979), pp. 9–23. ISSN: 00052736. DOI: 10.1016/0005-2736(79)90085-3.

[62] F Szoka and D Papahadjopoulos. "Comparative properties and methods of preparation of lipid vesicles (liposomes)." In: *Annual review of biophysics and bioengineering* 9 (1980), pp. 467–508. ISSN: 0084-6589. DOI: 10.1146/annurev.bb.09.060180.002343.

[63] Danieli Lasic Thomas Fisher. "Molecular Crystals and Liquid Crystals". In: (). DOI: 10.1080/01406568408072064. URL: http://www.tandfonline.com/action/journalInformation?journalCode=gmcl16.

[64] W Jiskoot, T Teerlink, E C Beuvery, and D J Crommelin. "Preparation of liposomes via detergent removal from mixed micelles by dilution. The effect of bilayer composition and process parameters on liposome characteristics." In: *Pharmaceutisch weekblad. Scientific edition* 8.5 (Oct. 1986), pp. 259–65. ISSN: 0167-6555. URL: http://www.ncbi.nlm.nih.gov/pubmed/3786108.

[65] F Olson, C a Hunt, F C Szoka, W J Vail, and D Papahadjopoulos. "Preparation of liposomes of defined size distribution by extrusion through polycarbonate membranes." In: *Biochimica et biophysica acta* 557.1 (1979), pp. 9–23. ISSN: 00052736. DOI: 10.1016/0005-2736(79)90085-3.

[66] A.M.A. Elhissi and K.M.G. Taylor. "Delivery of liposomes generated from proliposomes using air-jet, ultrasonic, and vibrating-mesh nebulisers". In: *Journal of Drug Delivery Science and Technology* 15.4 (Jan. 2005), pp. 261–265. ISSN: 1773-2247. DOI: 10.1016/S1773-2247(05)50047-9. URL: https://www.sciencedirect.com/science/article/pii/S1773224705500479.

[67] *Stability aspects of liposomes*. URL: https://www.slideshare.net/Harnishapatel1/stability-aspects-of-liposomes (visited on 07/16/2018).

[68] Paul a. Bridges and K. M G Taylor. "Nebulisers for the generation of liposomal aerosols". In: *International Journal of Pharmaceutics* 173.1-2 (1998), pp. 117–125. ISSN: 03785173. DOI: 10.1016/S0378-5173(98)00212-9.

[69] Paul A Bridges and Kevin M G Taylor. "An investigation of some of the factors influencing the jet nebulisation of liposomes". In: *International Journal of Pharmaceutics* 204 (2000), pp. 69–79. URL: www.elsevier.com/locate/ijpharm.

[70] K M G Taylor, G Taylor, I W Kellaway, and J Stevens. "The stability of liposomes to nebulisation". In: *International Journal of Pharmaceutics* 58 (1990), pp. 57–61. URL: https://ac.els-cdn.com/037851739090287E/1-s2.0-037851739090287E-main.pdf?%7B%5C_%7Dtid=8e3035ff-b5b2-416e-98fa-79c7ef538f59%7B%5C&%7Dacdnat=1531736690%7B%5C_%7D66888d795ef82ac26409a0247b3

[71] O. N M Mc Callion, K. M G Taylor, M. Thomas, and a. J. Taylor. "The influence of surface tension on aerosols produced by medical nebulisers". In: *International Journal of Pharmaceutics* 129.1-2 (1996), pp. 123–136. ISSN: 03785173. DOI: 10.1016/0378-5173(95)04279-2.

[72] K M Taylor and J M Newton. "Liposomes for controlled delivery of drugs to the lung." In: *Thorax* 47.4 (1992), pp. 257–259. ISSN: 0040-6376. DOI: 10.1136/thx.47.4.257.

[73] Brian Wowk. *HOW Cryoprotectants Work*. Tech. rep. URL: www.alcor.org.

[74] David Cipolla, Huiying Wu, Igor Gonda, and Hak-Kim Chan. "Aerosol Performance and Stability of Liposomes Containing Ciprofloxacin Nanocrystals". In: (). DOI: 10.1089/jamp.2015.1241. URL: https://www.ncbi.nlm.nih.gov/pmc/articles/PMC4685509/pdf/jamp.2015.1241.pdf.

[75] F Ross Hallett, Jackie Marsh, Bernie G Nickel, and Janet M Wood. *Mechanical properties of vesicles. II. A model for osmotic swelling and lysis*. Tech. rep. DOI: 10.1016/S0006-3495(93)81384-5. URL: https://ac.els-cdn.com/S0006349593813845/1-s2.0-S0006349593813845-main.pdf?%7B%5C_%7Dtid=60acab5d-e4c2-4d06-a2d2-ce8336f3d929%7B%5C&%7Dacdnat=1538386482%7B%5C_%7D72bd1fda1e17d8edb65d6fbdfac35dc8.

[76] Alexander Ewe and Achim Aigner. "Nebulization of liposome-polyethylenimine complexes (lipopolyplexes) for DNA or siRNA delivery: Physicochemical properties and biological activity". In: *European Journal of Lipid Science and Technology* 116.9 (Sept. 2014), pp. 1195–1204. ISSN: 14387697. DOI: 10.1002/ejlt.201300404. URL: http://doi.wiley.com/10.1002/ejlt.201300404.

[77] A E Canonico, J D Plitman, J T Conary, B O Meyrick, and K L Brigham. "No lung toxicity after repeated aerosol or intravenous delivery of plasmid-cationic liposome complexes." In: *Journal of applied physiology (Bethesda, Md. : 1985)* 77.1 (July 1994), pp. 415–9. ISSN: 8750-7587. DOI: 10.1152/jappl.1994.77.1.415. URL: http://www.ncbi.nlm.nih.gov/pubmed/7961263.

[78] C. F. Verschraegen, Brian E Gilbert, Evelyne Loyer, Armando Huaringa, Garrett Walsh, Robert A Newman, and Vernon Knight. "Clinical Evaluation of the Delivery and Safety of Aerosolized Liposomal 9-Nitro-20(S)-Camptothecin in Patients with Advanced Pulmonary Malignancies". In: *Clinical Cancer Research* 10.7 (Apr. 2004), pp. 2319–2326. ISSN: 1078-0432. DOI: 10.1158/1078-0432.CCR-0929-3. URL: http://www.ncbi.nlm.nih.gov/pubmed/15073107%20http://clincancerres.aacrjournals.org/cgi/doi/10.1158/1078-0432.CCR-0929-3.

[79] V Knight, E S Kleinerman, J C Waldrep, B C Giovanella, B E Gilbert, and N V Koshkina. "9-Nitrocamptothecin liposome aerosol treatment of human cancer subcutaneous xenografts and pulmonary cancer metastases in mice." In: *Annals of the New York Academy of Sciences* 922.July (2000), pp. 151–163. ISSN: 0077-8923.

[80] Mindaugas Rudokas, Mohammad Najlah, Mohamed Albed Alhnan, and Abdelbary Elhissi. "Liposome Delivery Systems for Inhalation: A Critical Review Highlighting Formulation Issues and Anticancer Applications". In: *Medical Principles and Practice* 25.2 (2016), pp. 60–72. ISSN: 14230151. DOI: 10.1159/000445116. URL: www.karger.com/OA-license.

[81] Mindaugas Rudokas, Mohammad Najlah, Mohamed Albed Alhnan, and Abdelbary Elhissi. "E-Mail Liposome Delivery Systems for Inhalation: A Critical Review Highlighting Formulation Issues and Anticancer Applications". In: (2016). DOI: 10.1159/000445116. URL: www.karger.com/OA-license.

[82] G Mainelis, S Seshadri, O B Garbuzenko, T Han, Z Wang, and T Minko. "Characterization and application of a nose-only exposure chamber for inhalation delivery of liposomal drugs and nucleic acids to mice." In: *Journal of aerosol medicine and pulmonary drug delivery* 26.6 (2013), pp. 345–54. ISSN: 1941-2703. DOI: 10.1089/jamp.2011-0966. URL: http://www.pubmedcentral.nih.gov/articlerender.fcgi?artid=3889495%7B%5C&%7Dtool=pmcentrez%7B%5C&%7Drendertype=abstract.

[83] G Mainelis, S Seshadri, O B Garbuzenko, T Han, Z Wang, and T Minko. "Characterization and application of a nose-only exposure chamber for inhalation delivery of liposomal drugs and nucleic acids to mice." In: *Journal of aerosol medicine and pulmonary drug delivery* 26.6 (2013), pp. 345–54. ISSN: 1941-2703. DOI: 10.1089/jamp.2011-0966. URL: http://www.pubmedcentral.nih.gov/articlerender.fcgi?artid=3889495%7B%5C&%7Dtool=pmcentrez%7B%5C&%7Drendertype=abstract.

[84] Paul B. Myrdal, Poonam Sheth, and Stephen W. Stein. "Advances in Metered Dose Inhaler Technology: Formulation Development". In: *AAPS PharmSciTech* 15.2 (Apr. 2014), p. 434. ISSN: 1530-9932. DOI: 10.1208/S12249-013-0063-X. URL: http://www.ncbi.nlm.nih.gov/pubmed/24452499%20http://www.pubmedcentral.nih.gov/articlerender.fcgi?artid=PMC3969484.

[85] Luca Lelli. "Aerosol and Clouds WS2014 - Scattering Regimes". In: November (2014), p. 47. URL: http://www.iup.uni-bremen.de/%7B~%7Dluca/?download=01%7B%5C_%7DLL%7B%5C_%7DVO.pdf.

[86] D. Arzenšek. "Dynamic light scattering and application to proteins in solutions". In: (2010), pp. 1–19.

[87] M Instruments and Malvern Instruments. "Dynamic Light Scattering: An Introduction in 30 Minutes". In: *Http://Www.Malvern.Com/En/Products/Technology/Dynamic-Light-Scattering/* (2000), pp. 1–8. URL: http://scholar.google.com/scholar?hl=en%7B%5C&%7DbtnG=Search%7B%5C&%7Dq=intitle:Dynamic+Light+Scattering+:+An+Introduction+in+30+Minutes%7B%5C#%7D3.

[88] W. I. Goldburg. "Dynamic light scattering". In: *American Journal of Physics* 67.12 (1999), p. 1152. ISSN: 00029505. DOI: 10.1119/1.19101. URL: http://link.aip.org/link/?AJP/67/1152/1%7B%5C&%7DAgg=doi.

[89] B. J. Berne and R. Pecora. "Dynamic light scattering. With applications to chemistry, biology, and physics." In: *Dynamic light scattering. With applications to chemistry, biology, and physics., by Berne, B. J.; Pecora, R.. New York, NY (USA): Wiley-Interscience, 8 + 376 p.* (1976). URL: http://adsabs.harvard.edu/abs/1976dlsw.book.....B.

[90] Malvern Instruments. "Inform White Paper Dynamic Light Scattering". In: *Malvern Guides* (2011), pp. 1–6.

[91] F. R. Hallett, J. Watton, and P. Krygsman. "Vesicle sizing: Number distributions by dynamic light scattering". In: *Biophysical Journal* 59.2 (1991), pp. 357–362. ISSN: 00063495. DOI: 10.1016/S0006-3495(91)82229-9.

[92] Denis Semwogerere and Eric R Weeks. "Confocal Microscopy". In: (). DOI: 10.1081/E-EBBE-120024153. URL: http://www.physics.emory.edu/faculty/weeks//lab/papers/ebbe05.pdf.

[93] Robert and Webb. "Confocal optical microscopy". In: *Rep. Prog. Phys* 59 (1996). URL: http://iopscience.iop.org/article/10.1088/0034-4885/59/3/003/pdf.

[94] T Dokland. "Back to the basics: The fundamentals of cryo-electron microscopy". In: *Microscopy and Microanalysis* 15.S2 (2009), p. 1538. ISSN: 1431-9276. DOI: 10.1017/S1431927609099280. URL: http://www.journals.cambridge.org/abstract%7B%5C_%7DS1431927609099280.

[95] The University of Utah. *Introduction to Electron Microscopy - Advanced Microscopy - Imaging Facilities - The University of Utah.* URL: http://advanced-microscopy.utah.edu/education/electron-micro/ (visited on 04/04/2018).

[96] Debora Ferreira Barreto-Vieira and Ortrud Monika Barth. "Negative and Positive Staining in Transmission Electron Microscopy for Virus Diagnosis". In: *Microbiology in Agriculture and Human Health*. InTech, July 2015. DOI: 10.5772/60511. URL: http://www.intechopen.com/books/microbiology-in-agriculture-and-human-health/negative-and-positive-staining-in-transmission-electron-microscopy-for-virus-diagnosis.

[97] Rebecca F. Thompson, Matt Walker, C. Alistair Siebert, Stephen P. Muench, and Neil A. Ranson. "An introduction to sample preparation and imaging by cryo-electron microscopy for structural biology". In: *Methods* 100 (2016), pp. 3–15. ISSN: 10959130. DOI: 10.1016/j.ymeth.2016.02.017. URL: http://dx.doi.org/10.1016/j.ymeth.2016.02.017.

[98] T Dokland. "Back to the basics: The fundamentals of cryo-electron microscopy". In: *Microscopy and Microanalysis* 15.S2 (2009), p. 1538. ISSN: 1431-9276. DOI: 10.1017/S1431927609099280. URL: http://www.journals.cambridge.org/abstract%7B%5C_%7DS1431927609099280.

[99] Mats Almgren, Katarina Edwards, and Göran Karlsson. "Cryo transmission electron microscopy of liposomes and related structures". In: *Colloids and Surfaces A: Physicochemical and Engineering Aspects* 174.1-2 (2000), pp. 3–21. ISSN: 09277757. DOI: 10.1016/S0927-7757(00)00516-1.

[100] Rajesh Singh and James W Lillard. "Nanoparticle-based targeted drug delivery". In: (). DOI: 10.1016/j.yexmp.2008.12.004. URL: https://www.ncbi.nlm.nih.gov/pmc/articles/PMC3249419/pdf/nihms87089.pdf.

[101] Khalil Hafiz Luqman. *Methods of particle size measrement*. URL: https://www.slideshare.net/maan%7B%5C_%7Dali/methods-of-particle-size-measrement-032 (visited on 08/27/2018).

[102] John S. Patton. "Mechanisms of macromolecule absorption by the lungs". In: *Advanced Drug Delivery Reviews* 19.1 (1996), pp. 3–36. ISSN: 0169409X. DOI: 10.1016/0169-409X(95)00113-L.

[103] *WHITEPAPER 2 A basic guide to particle characterization 2. Better understanding of products, ingredients and processes*. Tech. rep. URL: https://www.cif.iastate.edu/sites/default/files/uploads/Other%7B%5C_%7DInst/Particle%20Size/Particle%20Characterization%20Guide.pdf.

[104] Ju-Hyeong Park. *Impactors and Particle Size Distribution (1) Particle motion, particle size, and aerodynamic diameter*. Tech. rep. URL: http://www.industrialventilation.net/ClassDownloads/IHS%7B%5C_%7D725/L11%20Impactor%20Data%20Reduction/Impactor%7B%5C_%7DPark%20%7B%5C%%7D281%7B%5C%%7D29.pdf.

[105] *An Overview of the Different Particle Size Measurement Techniques - ATA Scientific*. URL: https://www.atascientific.com.au/overview-particle-size-measurement-techniques/ (visited on 08/15/2018).

[106] Mark Copley. "Understanding cascade impaction and its importance for inhaler testing". In: (2007), pp. 1–6.

[107] Jolyon P Mitchell, Mark W Nagel, Kimberly J Wiersema, and Cathy C Doyle. *Aerodynamic Particle Size Analysis of Aerosols from Pressurized Metered-Dose Inhalers: Comparison of Andersen 8-Stage Cascade Impactor, Next Generation Pharmaceutical Impactor, and Model 3321 Aerodynamic Par-ticle Sizer Aerosol Spectrometer*. Tech. rep. 4. 2003, p. 54. URL: http://www.aapspharmscitech.org.

[108] Malvern Instruments Ltd. "A basic guide to particle characterization". In: *Inform White Paper* (2012), pp. 1–26.

[109] *Fraunhofer Diffraction Theory and Mie Scattering Theory : SHIMADZU (Shimadzu Corporation)*. URL: https://www.shimadzu.com/an/powder/support/practice/p01/lesson13.html (visited on 10/08/2018).

[110] S. Pedersen. "Inhalers and nebulizers: Which to choose and why". In: *Respiratory Medicine* 90.2 (1996), pp. 69–77. ISSN: 09546111. DOI: 10.1016/S0954-6111(96)90201-2.

[111] Early Atomizers, Asthma Cigarettes, Hand-bulb Nebulizer, Early Electric, Compressor Nebulizers, Theoretical Models, and Particle Sizing Techniques. "History of Aerosol Therapy : Liquid Nebulization to MDIs to DPIs Ceramic Inhalers (19th Century)". In: *Respiratory care* 50.9 (2005), pp. 1139–1149.

[112] Myrna B. Dolovich and Rajiv Dhand. "Aerosol drug delivery: Developments in device design and clinical use". In: *The Lancet* 377.9770 (2011), pp. 1032–1045. ISSN: 01406736. DOI: 10.1016/S0140-6736(10)60926-9. URL: http://dx.doi.org/10.1016/S0140-6736(10)60926-9.

[113] *Nebulisers review*. Tech. rep. URL: https://www.ers-education.org/lrmedia/2006/pdf/40403.pdf.

[114] C J Harvey, M J O'doherty, C J Page, S H L Thomas, T O Nunan, and D F Treacher. "Comparison of jet and ultrasonic nebulizer pulmonary aerosol deposition during mechanical ventilation". In: *Eur Respir J* 10 (1997), pp. 905–909. DOI: 10.1183/09031936.97.10040905. URL: https://erj.ersjournals.com/content/erj/10/4/905.full.pdf.

[115] C O'Callaghan and P W Barry. "The science of nebulised drug delivery." In: *Thorax* 52 Suppl 2.Suppl 2 (1997), S31–S44. ISSN: 0040-6376. DOI: 10.1136/thx.52.2008.S31.

[116] Eugene R. Arulmuthu, David J. Williams, Helen Baldascini, Henk K. Versteeg, and Mike Hoare. "Studies on aerosol delivery of plasmid DNA using a mesh nebulizer". In: *Biotechnology and Bioengineering* 98.5 (Dec. 2007), pp. 939–955. ISSN: 00063592. DOI: 10.1002/bit.21493. URL: http://doi.wiley.com/10.1002/bit.21493.

[117] Aisha Qi, Leslie Y. Yeo, and James R. Friend. "Interfacial destabilization and atomization driven by surface acoustic waves". In: *Physics of Fluids* 20.7 (2008). ISSN: 10706631. DOI: 10.1063/1.2953537.

[118] Julien Reboud, Rab Wilson, Yi Zhang, Mohd H Ismail, Yannyk Bourquin, and Jonathan M Cooper. "Nebulisation on a disposable array structured with phononic lattices." In: *Lab on a chip* 12.7 (2012), pp. 1268–73. ISSN: 1473-0189. DOI: 10.1039/c2lc20705b. URL: http://www.ncbi.nlm.nih.gov/pubmed/22327572.

[119] Safa Kasap. *Principles of electronic materials and devices*, p. 978. ISBN: 0078028183. URL: http://materials.usask.ca/.

[120] Ahmad Safari and E.Koray Akdogan. *Piezoelectric and Acoustic Materials for Transducer Applications - Google Libri*. URL: https://books.google.co.uk/books?hl=it%7B%5C&%7Dlr=%7B%5C&%7Did=gvDjYzHTfYkC%7B%5C&%7Doi=fnd%7B%5C&%7Dpg=PR5%7B%5C&%7Ddq=piezoelectric+materials+structure+properties+and+applications%7B%5C&%7Dots=-aDYbIqt4V%7B%5C&%7Dsig=dvmNht4Z9A0gKbRu3pBqLu%7B%5C_%7D07A8%7B%5C#%7Dv=onepage%7B%5C&%7Dq=piezoelectric%7B%5C%%7D252520materials%7B%5C%%7D252520structure%7B%5C%%7D252520properties%7B%5C%%7D252.

[121] Farhin Rehnuma et al. *Piezoelectric Materials*. URL: https://www.slideshare.net/foysalmd/piezoelectric-materials (visited on 09/20/2018).

[122] *CRYSTAL SYMMETRY*. Tech. rep. URL: http://academic.uprm.edu/pcaceres/Courses/Smart/SMD-5A.pdf.

[123] *Earthquake Glossary*. URL: https://earthquake.usgs.gov/learn/glossary/?term=Rayleigh%20wave (visited on 10/24/2018).

[124] Kazuhiko Yamanouchi. "Propagation and Amplification of Rayleigh Waves and Piezoelectric Leaky Surface Waves in LiNbO3". In: *Journal of Applied Physics* 43.3 (1972), p. 856. ISSN: 00218979. DOI: 10.1063/1.1661294. URL: http://scitation.aip.org/content/aip/journal/jap/43/3/10.1063/1.1661294.

[125] Leslie Y Yeo and James R Friend. "Ultrafast microfluidics using surface acoustic waves." In: *Biomicrofluidics* 3.1 (Jan. 2009), p. 12002. ISSN: 1932-1058. DOI: 10.1063/1.3056040. URL: http://www.ncbi.nlm.nih.gov/pubmed/19693383%20http://www.pubmedcentral.nih.gov/articlerender.fcgi?artid=PMC2717600.

[126] Leslie Y Yeo and James R Friend. "Surface Acoustic Wave Microfluidics Review". In: *Annu. Rev. Fluid Mech* 46 (2014), pp. 379–406. DOI: 10.1146/annurev-fluid-010313-141418. URL: www.annualreviews.org.

[127] Ming K Tan, James R Friend, Omar K Matar, and Leslie Y Yeo. "Capillary wave motion excited by high frequency surface acoustic waves Frequency effect on streaming phenomenon induced by Rayleigh surface acoustic wave in microdroplets Capillary wave motion excited by high frequency surface acoustic waves". In: *Physics of Fluids Journal of Applied Physics Acoustical Society of America Applied Physics Letters Journal of Applied Physics* 221.10 (2010), pp. 112112–14910. DOI: 10.1063/1.1754276. URL: https://doi.org/10.1063/1.3505044%20http://aip.scitation.org/toc/phf/22/11.

[128] Robert J Lang and Robert J Lano. "Mechanisms of free-surface breakup in vibration-induced liquid atomization". In: *Ultrasonic Atomization Studies The Journal of the Acoustical Society of America* 34 (1962), p. 515. DOI: 10.1121/1.1909020. URL: http://asa.scitation.org/toc/jas/34/1.

[129] Rayleigh. "The theory of sound : Rayleigh, John William Strutt, Baron, 1842-1919 : Free Download, Borrow, and Streaming : Internet Archive". In: (1877). URL: https://archive.org/details/theorysound06raylgoog/page/n7.

[130] L. Gaete-Garretón, D. Briceño-Gutiérrez, Y. Vargas-Hernández, and C. I. Zanelli. "Ultrasonic atomization of distilled water". In: *The Journal of the Acoustical Society of America* 144.1 (2018), pp. 222–227. ISSN: 0001-4966. DOI: 10.1121/1.5045558. URL: http://asa.scitation.org/doi/10.1121/1.5045558.

[131] James Friend and Leslie Y. Yeo. "Microscale acoustofluidics: Microfluidics driven via acoustics and ultrasonics". In: *Reviews of Modern Physics* 83.2 (2011), pp. 647–704. ISSN: 00346861. DOI: 10.1103/RevModPhys.83.647.

[132] Elijah Nazarzadeh, Rab Wilson, Xi King, Julien Reboud, Manlio Tassieri, and Jonathan M. Coopera. "Confinement of surface waves at the air-water interface to control aerosol size and dispersity". In: *Physics of Fluids* 29.11 (2017). ISSN: 10897666. DOI: 10.1063/1.4993793.

[133] M. Kurosawa, a. Futami, and T. Higuchi. "Characteristics of liquids atomization using surface acoustic wave". In: *Proceedings of International Solid State Sensors and Actuators Conference (Transducers '97)* 2.November (1997), pp. 4–7. DOI: 10.1109/SENSOR.1997.635221.

[134] "New Piezoelectrical Droplets Generator". In: *Ultrasonics* 8 (1994), pp. 611–614.

[135] Aisha Qi, James R Friend, Leslie Y Yeo, David a V Morton, Michelle P McIntosh, and Leone Spiccia. "Miniature inhalation therapy platform using surface acoustic wave microfluidic atomization." In: *Lab on a chip* 9.15 (2009), pp. 2184–2193. ISSN: 1473-0197. DOI: 10.1039/b903575c.

[136] Christina Cortez-Jugo, Aisha Qi, Anushi Rajapaksa, James R. Friend, and Leslie Y. Yeo. "Pulmonary monoclonal antibody delivery via a portable microfluidic nebulization platform". In: *Biomicrofluidics* 9.5 (Sept. 2015), p. 052603. ISSN: 1932-1058. DOI: 10.1063/1.4917181. URL: http://www.ncbi.nlm.nih.gov/pubmed/25945147%20http://www.pubmedcentral.nih.gov/articlerender.fcgi?artid=PMC4393410%20http://aip.scitation.org/doi/10.1063/1.4917181.

[137] Anushi E Rajapaksa, Jenny J Ho, Aisha Qi, Rob Bischof, Tri-Hung Nguyen, Michelle Tate, David Piedrafita, Michelle P McIntosh, Leslie Y Yeo, Els Meeusen, Ross L Coppel, and James R Friend. "Effective pulmonary delivery of an aerosolized plasmid DNA vaccine via surface acoustic wave nebulization." In: *Respiratory research* 15 (2014), p. 60. ISSN: 1465-993X. DOI: 10.1186/1465-9921-15-60. URL: http://www.pubmedcentral.nih.gov/articlerender.fcgi?artid=4040411%7B%5C&%7Dtool=pmcentrez%7B%5C&%7Drendertype=abstract.

[138] Layla Alhasan, Aisha Qi, Amgad R Rezk, Leslie Y Yeo, and Peggy P Y Chan. "Integrative Biology Assessment of the potential of a high frequency acoustomicrofluidic nebulisation platform for inhaled stem cell therapy †". In: *This journal is Cite this: Integr. Biol* 8 (2016), p. 12. DOI: 10.1039/c5ib00206k. URL: www.rsc.org/ibiology.

[139] Christina Cortez-Jugo, Aisha Qi, Anushi Rajapaksa, James R Friend, and Leslie Y Yeo. "Pulmonary monoclonal antibody delivery via a portable microfluidic nebulization platform". In: (). DOI: 10.1063/1.4917181. URL: https://www.ncbi.nlm.nih.gov/pmc/articles/PMC4393410/pdf/BIOMGB-000009-052603%7B%5C_%7D1.pdf.

[140] *Nucleic acid - an overview | ScienceDirect Topics*. URL: https://www.sciencedirect.com/topics/neuroscience/nucleic-acid (visited on 05/16/2018).

[141] Joanna B. Opalinska and Alan M. Gewirtz. "Nucleic-acid therapeutics: basic principles and recent applications". In: *Nature Reviews Drug Discovery* 1.7 (2002), pp. 503–514. ISSN: 14741784. DOI: 10.1038/nrd837. URL: http://www.nature.com/doifinder/10.1038/nrd837.

[142] Enrico Mastrobattista, Wim E. Hennink, and Raymond M. Schiffelers. "Delivery of nucleic acids". In: *Pharmaceutical Research* 24.8 (2007), pp. 1561–1563. ISSN: 07248741. DOI: 10.1007/s11095-007-9349-6.

[143] U.S National Library of Medicine. *What is gene therapy? - Genetics Home Reference*. URL: https://ghr.nlm.nih.gov/primer/therapy/genetherapy (visited on 03/22/2018).

[144] Luigi Naldini. *Gene therapy returns to centre stage*. 2015. DOI: 10.1038/nature15818.

[145] Sanjukta Misra. *Human gene therapy: a brief overview of the genetic revolution.* 2013.

[146] Jack McCain. "The future of gene therapy." In: *Biotechnology healthcare* 2.3 (June 2005), pp. 52–60. ISSN: 1554-169X. URL: http://www.ncbi.nlm.nih.gov/pubmed/23393464%20http://www.pubmedcentral.nih.gov/articlerender.fcgi?artid=PMC3564347.

[147] Timothy P. O'Connor and Ronald G. Crystal. "Genetic medicines: treatment strategies for hereditary disorders". In: *Nature Reviews Genetics* 7.4 (Apr. 2006), pp. 261–276. ISSN: 1471-0056. DOI: 10.1038/nrg1829. URL: http://www.nature.com/doifinder/10.1038/nrg1829.

[148] Rosenberg et al. "Gene Transfer Into Humans". In: *The New England Journal of Medicine Downloaded from nejm.org at GLASGOW UNIVERSITY LIBRARY on March* 22 (2018). URL: http://www.nejm.org/doi/pdf/10.1056/NEJM199008303230904.

[149] Eve Hanna, Cécile Rémuzat, Pascal Auquier, and Mondher Toumi. "Gene therapies development: slow progress and promising prospect." In: *Journal of market access & health policy* 5.1 (2017), p. 1265293. ISSN: 2001-6689. DOI: 10.1080/20016689.2017.1265293. URL: http://www.ncbi.nlm.nih.gov/pubmed/28265348%20http://www.pubmedcentral.nih.gov/articlerender.fcgi?artid=PMC5328344.

[150] B Sibbald. "Death but one unintended consequence of gene-therapy trial." In: *CMAJ : Canadian Medical Association journal = journal de l'Association medicale canadienne* 164.11 (May 2001), p. 1612. ISSN: 0820-3946. URL: http://www.ncbi.nlm.nih.gov/pubmed/11402803%20http://www.pubmedcentral.nih.gov/articlerender.fcgi?artid=PMC81135.

[151] Jie Wang, Ze Lu, M Guillaume Wientjes, and Jessie L-S Au. "Delivery of siRNA therapeutics: barriers and carriers." In: *The AAPS journal* 12.4 (Dec. 2010), pp. 492–503. ISSN: 1550-7416. DOI: 10.1208/s12248-010-9210-4. URL: http://www.ncbi.nlm.nih.gov/pubmed/20544328%20http://www.pubmedcentral.nih.gov/articlerender.fcgi?artid=PMC2977003.

[152] Yingshan Qiu, Jenny K.W. Lam, Susan W.S. Leung, and Wanling Liang. "Delivery of RNAi Therapeutics to the Airways—From Bench to Bedside". In: *Molecules* 21.9 (2016), p. 1249. ISSN: 1420-3049. DOI: 10.3390/molecules21091249. URL: http://www.mdpi.com/1420-3049/21/9/1249.

[153] Volker A. Erdmann and Jan Barciszewski. "From nucleic acids sequences to molecular medicine". In: *From Nucleic Acids Sequences to Molecular Medicine* (2012), pp. 1–654. DOI: 10.1007/978-3-642-27426-8.

[154] Kelly M Martinovich, Nicole C Shaw, Anthony Kicic, André Schultz, Sue Fletcher, Steve D Wilton, and Stephen M Stick. "The potential of antisense oligonucleotide therapies for inherited childhood lung diseases." In: *Molecular and cellular pediatrics* 5.1 (Feb. 2018), p. 3. ISSN: 2194-7791. DOI: 10.1186/s40348-018-0081-6. URL: http://www.ncbi.nlm.nih.gov/pubmed/29411170%20http://www.pubmedcentral.nih.gov/articlerender.fcgi?artid=PMC5801198.

[155] Nathalie Dias and C a Stein. "Minireview Antisense Oligonucleotides : Basic Concepts and Mechanisms". In: *Molecular Cancer Therapeutics* 1.March (2002), pp. 347–355. ISSN: 15357163. DOI: 10.1016/s1357-4310(99)01638-x. URL: http://www.ncbi.nlm.nih.gov/pubmed/12489851.

[156] G B Mulamba, A Hu, R F Azad, K P Anderson, and D M Coen. "Human cytomegalovirus mutant with sequence-dependent resistance to the phosphorothioate oligonucleotide fomivirsen (ISIS 2922)." In: *Antimicrobial agents and chemotherapy* 42.4 (Apr. 1998), pp. 971–3. ISSN: 0066-4804. URL: http://www.ncbi.nlm.nih.gov/pubmed/9559825%20http://www.pubmedcentral.nih.gov/articlerender.fcgi?artid=PMC105584.

[157] Sven Kruspe and Paloma Giangrande. "Aptamer-siRNA Chimeras: Discovery, Progress, and Future Prospects". In: *Biomedicines* 5.3 (2017), p. 45. ISSN: 2227-9059. DOI: 10.3390/biomedicines5030045. URL: http://www.mdpi.com/2227-9059/5/3/45.

[158] Nill Bergstrand. *Liposomes for Drug Delivery from Physico-chemical Studies to Application*. 2003. ISBN: 9155455921.

[159] et al. Griffiths AJF, Miller JH, Suzuki DT. *An Introduction to Genetic Analysis - Transcription and RNA polymerase*. 2000. DOI: 10.1111/j.1365-2141.2011.08807.x. URL: http://doi.wiley.com/10.1111/j.1365-2141.2011.08807.x.

[160] et al. Alberts B, Johnson A, Lewis J. *Molecular Biology of the Cell - From DNA to RNA*. 2002. DOI: 10.1111/j.1365-2141.2011.08807.x. URL: http://doi.wiley.com/10.1111/j.1365-2141.2011.08807.x.

[161] Randy Schekman. "Merging cultures in the study of membrane traffic". In: *Nature Cell Biology* 6.6 (June 2004), pp. 483–486. ISSN: 1465-7392. DOI: 10.1038/ncb0604-483. URL: http://www.nature.com/articles/ncb0604-483.

[162] Jenny K W Lam, Michael Y T Chow, Yu Zhang, and Susan W S Leung. "siRNA Versus miRNA as Therapeutics for Gene Silencing." In: *Molecular therapy. Nucleic acids* 4.9 (Sept. 2015), e252. ISSN: 2162-2531. DOI: 10.1038/mtna.2015.23. URL: http://www.ncbi.nlm.nih.gov/pubmed/26372022%20http://www.pubmedcentral.nih.gov/articlerender.fcgi?artid=PMC4877448.

[163] Jenny K.W. Lam, Michael Y.T. Chow, Yu Zhang, and Susan W.S. Leung. "siRNA versus miRNA as therapeutics for gene silencing". In: *Molecular Therapy - Nucleic Acids* 4.9 (2015), pp. 1–20. ISSN: 21622531. DOI: 10.1038/mtna.2015.23.

[164] R C C Ryther, A S Flynt, J A Phillips, and J G Patton. "siRNA therapeutics: big potential from small RNAs". In: *Gene Therapy* 12.1 (2005), pp. 5–11. ISSN: 0969-7128. DOI: 10.1038/sj.gt.3302356. URL: http://www.nature.com/doifinder/10.1038/sj.gt.3302356.

[165] Michael Y.T. Chow, Yingshan Qiu, Fiona F.K. Lo, Hinson H.S. Lin, Hak Kim Chan, Philip C.L. Kwok, and Jenny K.W. Lam. "Inhaled powder formulation of naked siRNA using spray drying technology with L-leucine as dispersion enhancer". In: *International Journal of Pharmaceutics* 530.1-2 (2017), pp. 40–52. ISSN: 18733476. DOI: 10.1016/j.ijpharm.2017.07.013. URL: http://dx.doi.org/10.1016/j.ijpharm.2017.07.013.

[166] Neema Agrawal, P V N Dasaradhi, Asif Mohmmed, Pawan Malhotra, Raj K Bhatnagar, and Sunil K Mukherjee. "RNA interference: biology, mechanism, and applications." In: *Microbiology and molecular biology reviews : MMBR* 67.4 (Dec. 2003), pp. 657–85. ISSN: 1092-2172. DOI: 10.1128/MMBR.67.4.657-685.2003. URL: http://www.ncbi.nlm.nih.gov/pubmed/14665679%20http://www.pubmedcentral.nih.gov/articlerender.fcgi?artid=PMC309050.

[167] P. Gonzalez-Alegre. "RNA Interference". In: *Encyclopedia of Movement Disorders*. Elsevier, 2010, pp. 47–49. ISBN: 9780123741059. DOI: 10.1016/B978-0-12-374105-9.00192-1. URL: http://linkinghub.elsevier.com/retrieve/pii/B9780123741059001921.

[168] Jenny Ka-Wing Lam, Wanling Liang, and Hak-Kim Chan. "Pulmonary delivery of therapeutic siRNA". In: *Advanced Drug Delivery Reviews* 64.1 (2012), pp. 1–15. ISSN: 0169409X. DOI: 10.1016/j.addr.2011.02.006. URL: http://dx.doi.org/10.1016/j.addr.2011.02.006.

[169] Richard W Carthew and Erik J Sontheimer. "Origins and Mechanisms of miRNAs and siRNAs." In: *Cell* 136.4 (Feb. 2009), pp. 642–55. ISSN: 1097-4172. DOI: 10.1016/j.cell.2009.01.035. URL: http://www.ncbi.nlm.nih.gov/pubmed/19239886%20http://www.pubmedcentral.nih.gov/articlerender.fcgi?artid=PMC2675692.

[170] Chuan Huang, Min Li, Changyi Chen, and Qizhi Yao. "Small interfering RNA therapy in cancer: mechanism, potential targets, and clinical applications." In: *Expert opinion on therapeutic targets* 12.5 (2008), pp. 637–645. ISSN: 1472-8222. DOI: 10.1517/14728222.12.5.637.

[171] Olivia M Merkel, Israel Rubinstein, and Thomas Kissel. "siRNA delivery to the lung: what's new?" In: *Advanced drug delivery reviews* 75 (Aug. 2014), pp. 112–28. ISSN: 1872-8294. DOI: 10.1016/j.addr.2014.05.018. URL: http://www.ncbi.nlm.nih.gov/pubmed/24907426%20http://www.pubmedcentral.nih.gov/articlerender.fcgi?artid=PMC4160355.

[172] Bieong Kil Kim, Guen Bae Hwang, Young Bae Seu, Jong Soo Choi, Kyeong Sik Jin, and Kyung Oh Doh. "DOTAP/DOPE ratio and cell type determine transfection efficiency with DOTAP-liposomes". In: *Biochimica et Biophysica Acta - Biomembranes* 1848.10 (2015), pp. 1996–2001. ISSN: 18792642. DOI: 10.1016/j.bbamem.2015.06.020. URL: http://dx.doi.org/10.1016/j.bbamem.2015.06.020.

[173] Xiaoming Xu, Mansoor A. Khan, and Diane J. Burgess. "Predicting hydrophilic drug encapsulation inside unilamellar liposomes". In: *International Journal of Pharmaceutics* 423.2 (2012), pp. 410–418. ISSN: 03785173. DOI: 10.1016/j.ijpharm.2011.12.019. URL: http://dx.doi.org/10.1016/j.ijpharm.2011.12.019.

[174] Martin Kolb, Gail Martin, Maria Medina, Kjetil Ask, and Jack Gauldie. "Gene Therapy for Pulmonary Diseases". In: *Chest* 130.3 (Sept. 2006), pp. 879–884. ISSN: 0012-3692. DOI: 10.1378/CHEST.130.3.879. URL: https://www.sciencedirect.com/science/article/pii/S0012369215528055?via%7B%5C%%7D3Dihub.

[175] Roberto Sessa and Akiko Hata. "Role of microRNAs in lung development and pulmonary diseases." In: *Pulmonary circulation* 3.2 (Apr. 2013), pp. 315–28. ISSN: 2045-8932. DOI: 10.4103/2045-8932.114758. URL: http://www.ncbi.nlm.nih.gov/pubmed/24015331%20http://www.pubmedcentral.nih.gov/articlerender.fcgi?artid=PMC3757825.

[176] Amir K. Varkouhi, Marije Scholte, Gert Storm, and Hidde J. Haisma. "Endosomal escape pathways for delivery of biologicals". In: *Journal of Controlled Release* 151.3 (May 2011), pp. 220–228. ISSN: 0168-3659. DOI: 10.1016/J.JCONREL.2010.11.004. URL: https://www.sciencedirect.com/science/article/pii/S0168365910009053?via%7B%5C%%7D3Dihub.

[177] CrispinR. Dass. "Lipoplex-mediated delivery of nucleic acids: factors affecting in vivo transfection". In: *Journal of Molecular Medicine* 82.9 (Sept. 2004), pp. 579–591. ISSN: 0946-2716. DOI: 10.1007/s00109-004-0558-8. URL: http://link.springer.com/10.1007/s00109-004-0558-8.

[178] Xiao-Xiang Zhang, Thomas J McIntosh, and Mark W Grinstaff. "Functional lipids and lipoplexes for improved gene delivery." In: *Biochimie* 94.1 (Jan. 2012), pp. 42–58. ISSN: 1638-6183. DOI: 10.1016/j.biochi.2011.05.005. URL: http://www.ncbi.nlm.nih.gov/pubmed/21621581%20http://www.pubmedcentral.nih.gov/articlerender.fcgi?artid=PMC3771368.

[179] Peter Lönn, Apollo D. Kacsinta, Xian Shu Cui, Alexander S. Hamil, Manuel Kaulich, Khirud Gogoi, and Steven F. Dowdy. "Enhancing Endosomal Escape for Intracellular Delivery of Macromolecular Biologic Therapeutics". In: *Scientific Reports* 6.March (2016), pp. 1–9. ISSN: 20452322. DOI: 10.1038/srep32301. URL: http://dx.doi.org/10.1038/srep32301.

[180] Yoshihiro Sasaki, Sayaka Toita, and Kazunari Akiyoshi. "Cycloamylose-based nanocarriers as a nucleic acid delivery system". In: *Colloid and Interface Science in Pharmaceutical Research and Development*. Elsevier, 2014, pp. 369–388. ISBN: 9780444626141. DOI: 10.1016/B978-0-444-62614-1.00018-1. URL: http://linkinghub.elsevier.com/retrieve/pii/B9780444626141000181.

[181] Paul D. Robbins, Hideaki Tahara, and Steven C. Ghivizzani. "Viral vectors for gene therapy". In: *Trends in Biotechnology* 16.1 (Jan. 1998), pp. 35–40. ISSN: 01677799. DOI: 10.1016/S0167-7799(97)01137-2. URL: http://www.ncbi.nlm.nih.gov/pubmed/9470229%20http://linkinghub.elsevier.com/retrieve/pii/S0167779997011372.

[182] Murali Ramamoorth and Aparna Narvekar. "Non viral vectors in gene therapy- an overview." In: *Journal of clinical and diagnostic research : JCDR* 9.1 (Jan. 2015), GE01–6. ISSN: 2249-782X. DOI: 10.7860/JCDR/2015/10443.5394. URL: http://www.ncbi.nlm.nih.gov/pubmed/25738007%20http://www.pubmedcentral.nih.gov/articlerender.fcgi?artid=PMC4347098.

[183] Adam J Mellott, M Laird Forrest, and Michael S Detamore. "Physical non-viral gene delivery methods for tissue engineering." In: *Annals of biomedical engineering* 41.3 (Mar. 2013), pp. 446–68. ISSN: 1573-9686. DOI: 10.1007/s10439-012-0678-1. URL: http://www.ncbi.nlm.nih.gov/pubmed/23099792%20http://www.pubmedcentral.nih.gov/articlerender.fcgi?artid=PMC5102682.

[184] Lynn F Gottfried and David a Dean. "Extracellular and Intracellular Barriers to Non-Viral Gene Transfer". In: *Novel Gene Therapy Approaches* (2013), pp. 75–88. DOI: 10.5772/54699.

[185] Jonas Gustafsson, Gösta Arvidson, Göran Karlsson, and Mats Almgren. "Complexes between cationic liposomes and DNA visualized by cryo-TEM". In: *Biochimica et Biophysica Acta (BBA) - Biomembranes* 1235.2 (May 1995), pp. 305–312.

ISSN: 0005-2736. DOI: 10.1016/0005-2736(95)80018-B. URL: https://www.sciencedirect.com/science/article/pii/000527369580018B.

[186] Kai K. Ewert, Alexandra Zidovska, Ayesha Ahmad, Nathan F. Bouxsein, Heather M. Evans, Christopher S. McAllister, Charles E. Samuel, and Cyrus R. Safinya. "Cationic liposome-nucleic acid complexes for gene delivery and silencing: Pathways and mechanisms for plasmid DNA and siRNA". In: *Topics in Current Chemistry* 296.Cl (2010), pp. 191–226. ISSN: 03401022. DOI: 10.1007/128_2010_70.

[187] *Molecular Interactions (Noncovalent Interactions)*. URL: https://ww2.chemistry.gatech.edu/%7B~%7Dlw26/structure/molecular%7B%5C_%7Dinteractions/mol%7B%5C_%7Dint.html%7B%5C#%7DB (visited on 05/09/2018).

[188] A. Schroeder, C. G. Levins, C. Cortez, R. Langer, and D. G. Anderson. "Lipid-based nanotherapeutics for siRNA delivery". In: *Journal of Internal Medicine* 267.1 (Jan. 2010), pp. 9–21. ISSN: 09546820. DOI: 10.1111/j.1365-2796.2009.02189.x. URL: http://doi.wiley.com/10.1111/j.1365-2796.2009.02189.x.

[189] Magendira Mani. *Electrophoresis and factors affecting electrophoresis*. URL: https://www.slideshare.net/magendiramanivinayag/electrophoresis-and-factors-affecting-electrophoresis (visited on 05/17/2018).

[190] "Network Analyser Manual". In: ().

[191] *File:Vna3.png - Wikimedia Commons*. URL: https://commons.wikimedia.org/wiki/File:Vna3.png (visited on 10/05/2018).

[192] *Dry etching - an overview | ScienceDirect Topics*. URL: https://www.sciencedirect.com/topics/materials-science/dry-etching (visited on 06/01/2018).

[193] Tech Support. "Preparing Large, Unilamellar Vesicles by Extrusion (LUVET) | Avanti Polar Lipids". In: (2018), pp. 10–11. URL: https://avantilipids.com/tech-support/liposome-preparation/luvet.

[194] Anna Wang, Christopher Chan Miller, and Jack W Szostak. "Interpreting turbidity measurements for vesicle studies". In: (). DOI: 10.1101/348904. URL: http://dx.doi.org/10.1101/348904.

[195] Vanessa Cabra and Montserrat Samsó. "Do's and don'ts of cryo-electron microscopy: a primer on sample preparation and high quality data collection for macromolecular 3D reconstruction." In: *Journal of visualized experiments : JoVE* 95 (2015), p. 52311. ISSN: 1940-087X. DOI: 10.3791/52311. URL: http://www.jove.com/video/52311/do-s-don-ts-cryo-electron-microscopy-primer-on-sample-preparation.

[196] Cardinal Arithmetic. "Sampling and Characterization of Bioaerosols". In: *NIOSH Manual of Analytical Methods* March (1998), pp. 82–112. ISSN: 10980121. DOI: 10.1103/PhysRevB.71.165307.

[197] Joseph G. Vasiliou, Diana Sorensen, and Peter H. McMurry. "Sampling at controlled relative humidity with a cascade impactor". In: *Atmospheric Environment* 33.7 (Mar. 1999), pp. 1049–1056. ISSN: 1352-2310. DOI: 10.1016/S1352-2310(98)00323-9. URL: https://www.sciencedirect.com/science/article/pii/S1352231098003239.

[198] Sarah M. Andrew, Julie A. Titus, and Louis Zumstein. "Dialysis and Concentration of Protein Solutions". In: *Current Protocols in Toxicology*. Vol. Appendix 3. Hoboken, NJ, USA: John Wiley & Sons, Inc., Feb. 2002, A.3H.1–5. DOI: 10.1002/0471140856.txa03hs10. URL: http://www.ncbi.nlm.nih.gov/pubmed/20976673%20http://doi.wiley.com/10.1002/0471140856.txa03hs10.

[199] *Selection Guide: Separation Products for Centrifugal and Tangential Flow Filtration*. Tech. rep. URL: www.pall.com/contact.

[200] *Selection Guide: Separation Products for Centrifugal and Tangential Flow Filtration*. Tech. rep. URL: www.pall.com/contact.

[201] *Biotech Grade Dialysis Membranes Cellulose Ester (CE) Regenerated Cellulose (RC) Spectra/Por Biotech RC Membranes*. Tech. rep. URL: http://spectrumlabs.com/lit/420x10688x000.pdf.

[202] *Chemistry for Biologists: Enzymes*. URL: http://www.rsc.org/Education/Teachers/Resources/cfb/enzymes.htm (visited on 08/11/2018).

[203] R W Niven, A Y Ip, S Mittelman, S J Prestrelski, and T Arakawa. "Some factors associated with the ultrasonic nebulization of proteins." In: *Pharmaceutical research* 12.1 (Jan. 1995), pp. 53–9. ISSN: 0724-8741. URL: http://www.ncbi.nlm.nih.gov/pubmed/7724488.

[204] Maria-Angeles Urbaneja, Ftlix M Gori, and Alicia Alonso. *Structural changes induced by Triton X-100 on sonicated phosphatidylcholine liposomes*. Tech. rep. 1988, pp. 585–588. URL: https://febs.onlinelibrary.wiley.com/doi/pdf/10.1111/j.1432-1033.1988.tb14039.x.

[205] Dov Lichtenberg, Hasna Ahyayauch, Alicia Alonso, Fé Lix, and M Goñ. "Detergent solubilization of lipid bilayers: a balance of driving forces". In: *Trends in Biochemical Sciences* 38.2 (2013), pp. 85–93. DOI: 10.1016/j.tibs.2012.11.005. URL: http://dx.doi.org/10.1016/.

[206] Dipankar Koley and Allen J Bard. "Triton X-100 concentration effects on membrane permeability of a single HeLa cell by scanning electrochemical microscopy (SECM)". In: (). DOI: 10.1073/pnas.1011614107/-/DCSupplemental. URL: www.pnas.org/lookup/suppl/.

[207] A R I Helenius and K A I Simons. "BY DETERGENTS membrane structure and function it is usually necessary to dissociate the membrane into its components . The techniques for extraction and analysis of the membrane lipids are well worked out , and are mainly based on the use of organic solve". In: 415 (1975), pp. 29–79.

[208] Dov Lichtenberg, Hasna Ahyayauch, Fé Lix, and M Goñ. "The Mechanism of Detergent Solubilization of Lipid Bilayers". In: *Biophysj* 105 (2013), pp. 289–299. DOI: 10.1016/j.bpj.2013.06.007. URL: https://www.ncbi.nlm.nih.gov/pmc/articles/PMC3714928/pdf/main.pdf.

[209] Hasna Ahyayauch, Banafshe Larijani, Alicia Alonso, and Félix M Goñi. "Detergent solubilization of phosphatidylcholine bilayers in the fluid state: Influence of the acyl chain structure". In: (2006). DOI: 10.1016/j.bbamem.2006.01.016. URL: http://www.elsevier.com/locate/bba.

[210] "Luciferase Reporters". In: (). URL: https://www.thermofisher.com/us/en/home/life-science/protein-biology/protein-biology-learning-center/protein-biology-resource-library/pierce-protein-methods/luciferase-reporters.html.

[211] *The Luciferase Reporter Assay: How it works - Bitesize Bio*. URL: https://bitesizebio.com/10774/the-luciferase-reporter-assay-how-it-works/ (visited on 05/09/2018).

[212] *Why You Don't Need to Select a Wavelength for a Luciferase Assay |*. URL: https://www.promegaconnections.com/why-you-dont-need-to-select-a-wavelength-for-a-luciferase-assay/ (visited on 05/16/2018).

[213] "Overview of Protein Assays Methods". In: (). URL: https://www.thermofisher.com/us/en/home/life-science/protein-biology/protein-biology-learning-center/protein-biology-resource-library/pierce-protein-methods/overview-protein-assays.html.

[214] "Chemistry of Protein Assays". In: (). URL: https://www.thermofisher.com/us/en/home/life-science/protein-biology/protein-biology-learning-center/protein-biology-resource-library/pierce-protein-methods/chemistry-protein-assays.html.

[215] *Ethidium bromide - an overview | ScienceDirect Topics*. URL: https://www.sciencedirect.com/topics/neuroscience/ethidium-bromide (visited on 05/16/2018).

[216] *Ethidium Bromide | Environmental Health and Safety*. URL: https://ehs.research.uiowa.edu/ethidium-bromide (visited on 05/16/2018).

[217] Tahrin Mahmood and Ping-Chang Yang. "Western blot: technique, theory, and trouble shooting." In: *North American journal of medical sciences* 4.9 (Sept. 2012), pp. 429–34. ISSN: 1947-2714. DOI: 10.4103/1947-2714.100998. URL: http://www.ncbi.nlm.nih.gov/pubmed/23050259%20http://www.pubmedcentral.nih.gov/articlerender.fcgi?artid=PMC3456489.

[218] Yingshan Qiu, Michael Y. T. Chow, Wanling Liang, Winnie W. Y. Chung, Judith C. W. Mak, and Jenny K. W. Lam. "From Pulmonary Surfactant, Synthetic KL4 Peptide as Effective siRNA Delivery Vector for Pulmonary Delivery". In: *Molecular Pharmaceutics* 14.12 (Dec. 2017), pp. 4606–4617. ISSN: 1543-8384. DOI: 10.1021/acs.molpharmaceut.7b00725. URL: http://pubs.acs.org/doi/10.1021/acs.molpharmaceut.7b00725.

[219] Rufang Zhang, Deyu Yang, Chanjuan Zhou, Ke Cheng, Zhao Liu, Liang Chen, Liang Fang, and Peng Xie. "β-Actin as a loading control for plasma-based Western blot analysis of major depressive disorder patients". In: *Analytical Biochemistry* 427.2 (Aug. 2012), pp. 116–120. ISSN: 00032697. DOI: 10.1016/j.ab.2012.05.008. URL: http://www.ncbi.nlm.nih.gov/pubmed/22617797%20http://linkinghub.elsevier.com/retrieve/pii/S0003269712002692.

[220] *MTT assay - an overview | ScienceDirect Topics*. URL: https://www.sciencedirect.com/topics/neuroscience/mtt-assay (visited on 05/09/2018).

[221] Matthew Trendowski, Guowu Yu, Victoria Wong, Christopher Acquafondata, Timothy Christen, and Thomas P. Fondy. "The real deal: Using cytochalasin B in sonodynamic therapy to preferentially damage leukemia cells". In: *Anticancer Research* 34.5 (2014), pp. 2195–2202. ISSN: 02507005. DOI: 10.1016/S1387-2656(05)11004-7.

[222] *A549 ATCC*. URL: https://www.lgcstandards-atcc.org/Products/All/CCL-185?geo%7B%5C_%7Dcountry=gb%7B%5C#%7Dculturemethod (visited on 05/17/2018).

[223] "AM4605 Silencer GAPDH siRNA Control". In: (2007). URL: https://assets.thermofisher.com/TFS-Assets/LSG/manuals/sp%7B%5C_%7D4605.pdf.

[224] a. M a Elhissi, M. Faizi, W. F. Naji, H. S. Gill, and K. M G Taylor. "Physical stability and aerosol properties of liposomes delivered using an air-jet nebulizer and a novel micropump device with large mesh apertures". In: *International Journal of Pharmaceutics* 334.1-2 (2007), pp. 62–70. ISSN: 03785173. DOI: 10.1016/j.ijpharm.2006.10.022.

[225] Krishnananda Chattopadhyay and Shyamalava Mazumdar. "Structural and Conformational Stability of Horseradish Peroxidase: Effect of Temperature and pH". In: (2000). DOI: 10.1021/bi990729o. URL: https://pubs.acs.org/sharingguidelines.

[226] Arne Thomas. *Micelle Formation*. Tech. rep. URL: https://www.mpikg.mpg.de/886719/MicelleFormation.pdf.

[227] *Can one calculate a PDI value for an individual peak in DLS?* URL: https://www.materials-talks.com/blog/2015/03/31/pdi-from-an-individual-peak-in-dls/ (visited on 10/28/2018).

[228] *Structural Biochemistry/Lipids/Micelles - Wikibooks, open books for an open world*. URL: https://en.wikibooks.org/wiki/Structural%7B%5C_%7DBiochemistry/Lipids/Micelles (visited on 09/05/2018).

[229] Lisa Sercombe, Tejaswi Veerati, Fatemeh Moheimani, Sherry Y Wu, Anil K Sood, and Susan Hua. "Advances and Challenges of Liposome Assisted Drug Delivery." In: *Frontiers in pharmacology* 6 (2015), p. 286. ISSN: 1663-9812. DOI: 10.3389/fphar.2015.00286. URL: http://www.ncbi.nlm.nih.gov/pubmed/26648870%20http://www.pubmedcentral.nih.gov/articlerender.fcgi?artid=PMC4664963.

[230] K. Kuribayashi, G. Tresset, Ph Coquet, H. Fujita, and S. Takeuchi. "Electroformation of giant liposomes in microfluidic channels". In: *Digest of Technical Papers - International Conference on Solid State Sensors and Actuators and Microsystems, TRANSDUCERS '05* 2 (2005), pp. 1159–1162. ISSN: 0957-0233. DOI: 10.1109/SENSOR.2005.1497283.

[231] David Cipolla, Huiying Wu, Igor Gonda, and Hak-Kim Chan. "Aerosol Performance and Stability of Liposomes Containing Ciprofloxacin Nanocrystals". In: *Journal of Aerosol Medicine and Pulmonary Drug Delivery* 28.6 (2015), pp. 411–422. ISSN: 1941-2711. DOI: 10.1089/jamp.2015.1241. URL: http://online.liebertpub.com/doi/10.1089/jamp.2015.1241.

[232] Gerhard Scheuch, Martin J. Kohlhaeufl, Peter Brand, and Ruediger Siekmeier. "Clinical perspectives on pulmonary systemic and macromolecular delivery". In: *Advanced Drug Delivery Reviews* 58.9-10 (2006), pp. 996–1008. ISSN: 0169409X. DOI: 10.1016/j.addr.2006.07.009.

[233] Mar Alvarez, James Friend, and Leslie Y Yeo. "Rapid generation of protein aerosols and nanoparticles via surface acoustic wave atomization". In: *Nanotechnology* 19.45 (2008), p. 455103. ISSN: 0957-4484. DOI: 10.1088/0957-4484/19/45/455103. URL: http://stacks.iop.org/0957-4484/19/i=45/a=455103?key=crossref.12e4470f7cbfbaa87d97a2d9194e9f00.

[234] Leslie Y. Yeo, Hsueh Chia Chang, Peggy P Y Chan, and James R. Friend. "Microfluidic devices for bioapplications". In: *Small* 7.1 (2011), pp. 12–48. ISSN: 16136810. DOI: 10.1002/smll.201000946.

[235] Elijah Nazarzadeh, Rab Wilson, Xi King, Julien Reboud, Manlio Tassieri, and Jonathan M Cooper. "Confinement of surface waves at the air-water interface to control aerosol size and dispersity". In: *Citation: Physics of Fluids* 29 (2017). URL: https://doi.org/10.1063/1.4993793%20http://aip.scitation.org/toc/phf/29/11.

[236] Aisha Qi, Peggy Chan, Jenny Ho, Anushi Rajapaksa, James Friend, and Leslie Yeo. "Template-free synthesis and encapsulation technique for layer-by-layer polymer nanocarrier fabrication". In: *ACS Nano* 5.12 (2011), pp. 9583–9591. ISSN: 19360851. DOI: 10.1021/nn202833n.

[237] Based Nottingham. "Quality Solutions for Who are Copley". In: (2012).

[238] *Omron Manual Specifications*. Tech. rep. URL: https://omronhealthcare.com.au/pdf/omron-NE-U22-instructions.pdf.

[239] Ana Fernández Tena and Pere Casan Clarà. "Depósito pulmonar de partículas inhaladas". In: *Archivos de Bronconeumología* 48.7 (July 2012), pp. 240–246. ISSN: 03002896. DOI: 10.1016/j.arbres.2012.02.003. URL: http://www.ncbi.nlm.nih.gov/pubmed/22464044%20http://linkinghub.elsevier.com/retrieve/pii/S0300289612000646.

[240] W T Jenny Kwong, Sharon L Ho, and Allan L Coates. *Comparison of Nebulized Particle Size Distribution with Malvern Laser Diffraction Analyzer Versus Andersen Cascade Impactor and Low-Flow Marple Personal Cascade Impactor*. Tech. rep. 4. 2000, pp. 303–314. URL: www.liebertpub.com.

[241] A H Hashish. "Droplet Size and Charge Distribution Analysis of Aerosols Generated by Jet and Ultrasonic Nebulizers". In: *Rdd2012* May 2012 (2008), pp. 751–756. DOI: 10.13140/2.1.5034.5929.

[242] Eduardo R Da Silva, Humberto R Bizzo, Patrícia D Fernandes, Valdir F Da Veiga Junior, Suzana G Leitão, and Danilo R De Oliveira. "Development and evaluation of an inhalation chamber for in vivo tests". In: *An Acad Bras Cienc* 89.3 (2017), pp. 1643–1653. ISSN: 1678-2690. DOI: 10.1590/0001-3765201720160793. URL:

http://dx.doi.org/10.1590/0001-3765201720160793www.scielo.br/aabc%7B%5C%%7D7Cwww.fb.com/aabcjournal.

[243] S R Jones, S Carley, and M Harrison. "An introduction to power and sample size estimation". In: *Emerg Med J* 20 (2003), pp. 453–458. DOI: 10.1136/emj.20.5.453. URL: www.emjonline.com.

[244] Jaykaran Charan and N D Kantharia. "How to calculate sample size in animal studies?" In: *Journal of pharmacology & pharmacotherapeutics* 4.4 (Oct. 2013), pp. 303–6. ISSN: 0976-500X. DOI: 10.4103/0976-500X.119726. URL: http://www.ncbi.nlm.nih.gov/pubmed/24250214%20http://www.pubmedcentral.nih.gov/articlerender.fcgi?artid=PMC3826013.

[245] Dominique N Price, Nitesh K Kunda, and Pavan Muttil. "Challenges Associated with the Pulmonary Delivery of Therapeutic Dry Challenges Associated with the Pulmonary Delivery of Therapeutic Dry Powders for Preclinical Testing †". In: March (2018). DOI: 10.14356/kona.2019008.

Appendices

Appendix A

DOPC Bilayer Structures

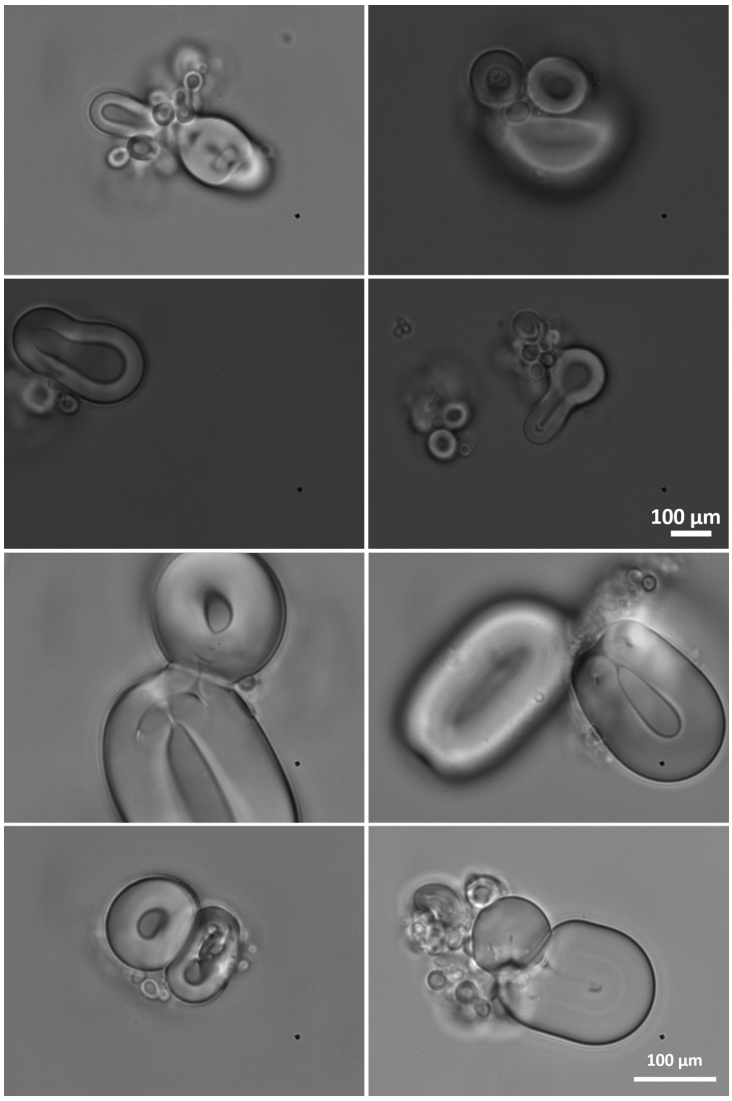

Figure A1: Images from optical microscopy, where dried DOPC was hydrated with PBS. The pictures show toroidal and donuts shape, made of bilayers. DOPC has ($S < 1$) a cylinder shape.

Appendix B

Dry-Etched Silicon Structure With Rectangular Pattern

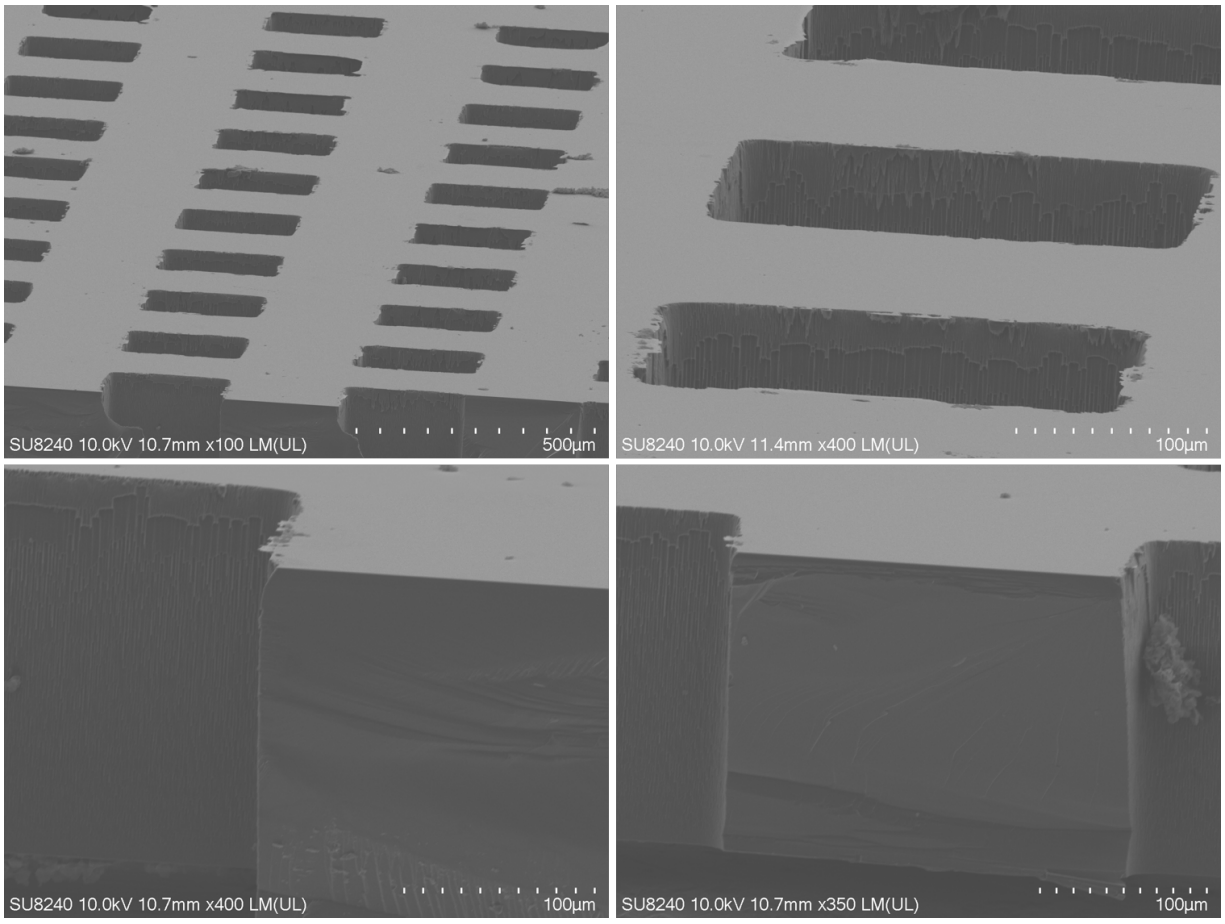

Figure B1: SEM SU8240 images of a dry-etched silicon structure, with rectangular pattern, obtained using photolitography.

Appendix C

Freeze-Thaw Cycles

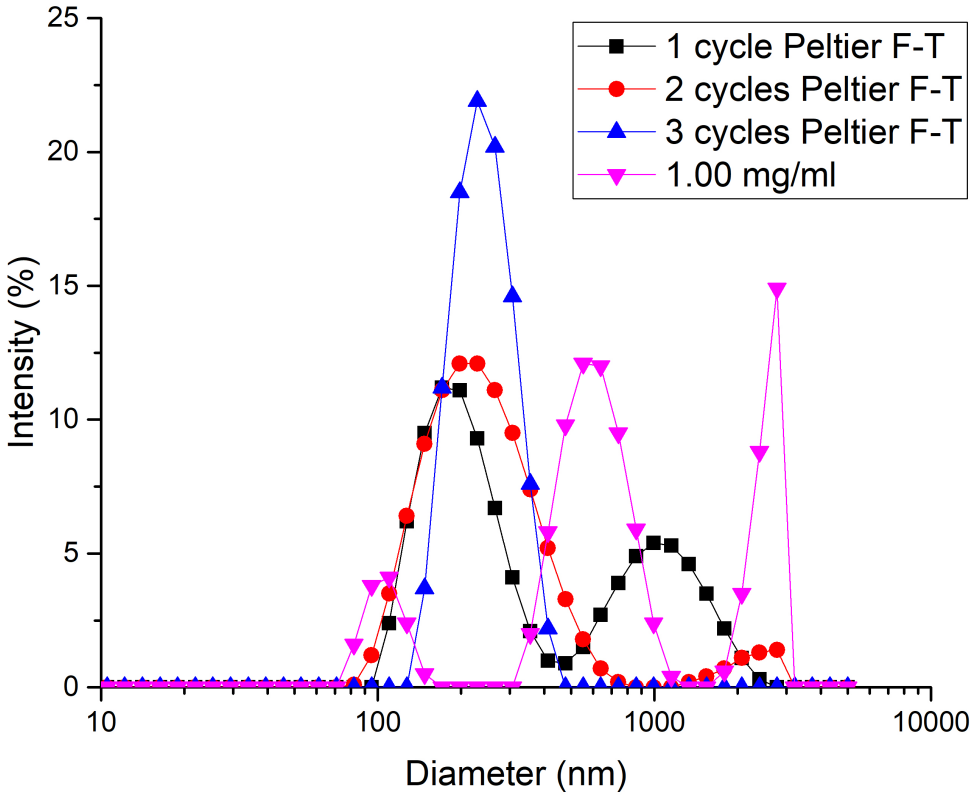

Figure C1: Freeze-thaw cycles. MLVs are rapidly frozen (pink line) at -80°C and thawed in a water bath at 37°C. This process is repeated at least 3 cycles (1 cycle = black line, 2 cycles = red line and 3 cycles = blue line). During freeze-thawing, rapidly-forming ice crystal disrupts the structure of MLVs, leading to the formation of liposomes

Displacement

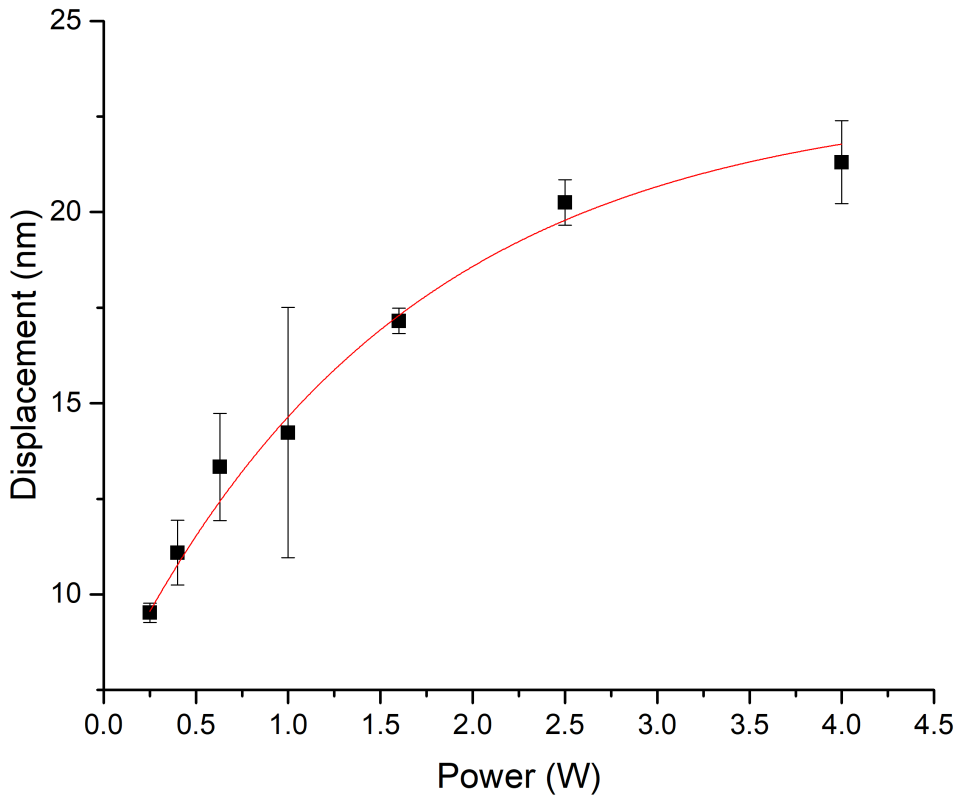

Figure C2: Displacement measurements using a laser doppler vibrometer. The graph shows the increase in displacement with the power increase. The displacement seems to reach the saturation around 4-5 W.

Appendix D

TEM Negative Staining of SAW-Formed Liposomes

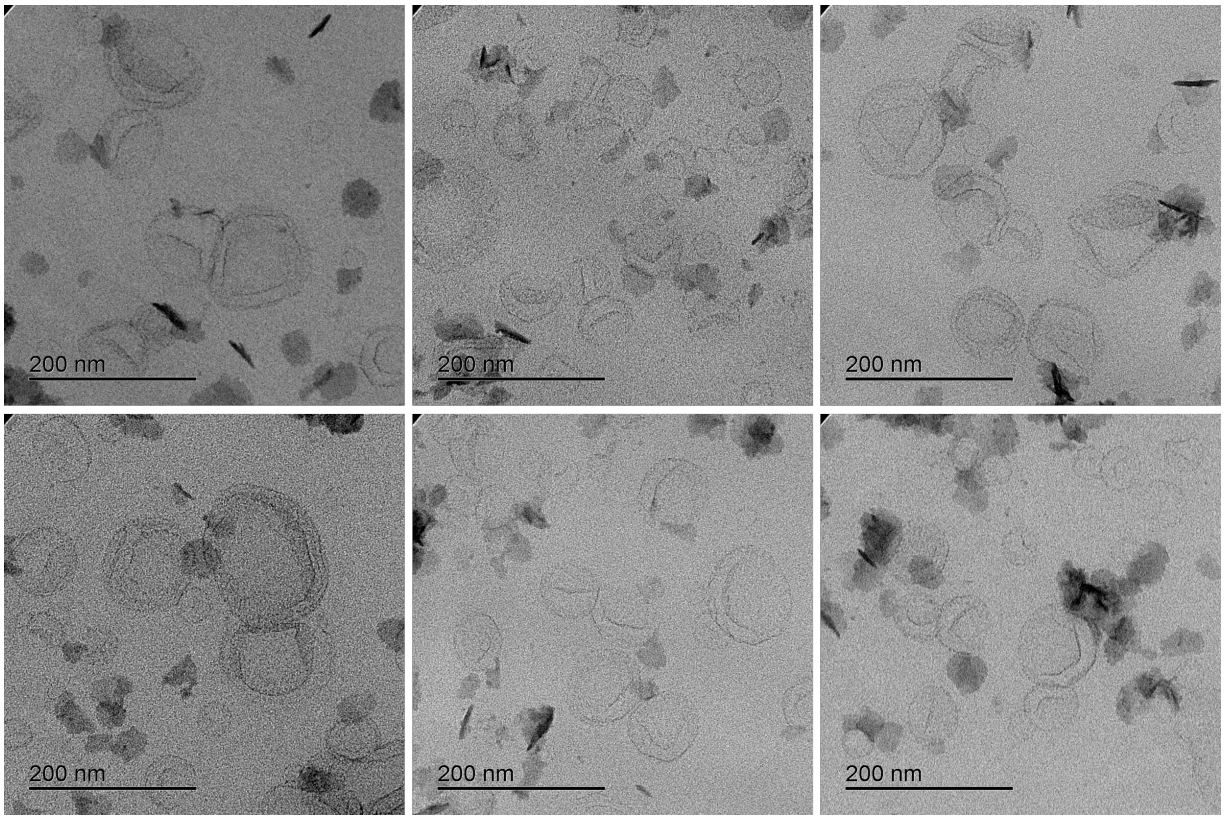

Figure D1: TEM negative staining was used with 2% MethylCellulose/Uranyl Acetate (pH 7) as a negative stain, in order to visualise SAW-formed liposomes.

Cryo-TEM of SAW-Formed Liposomes

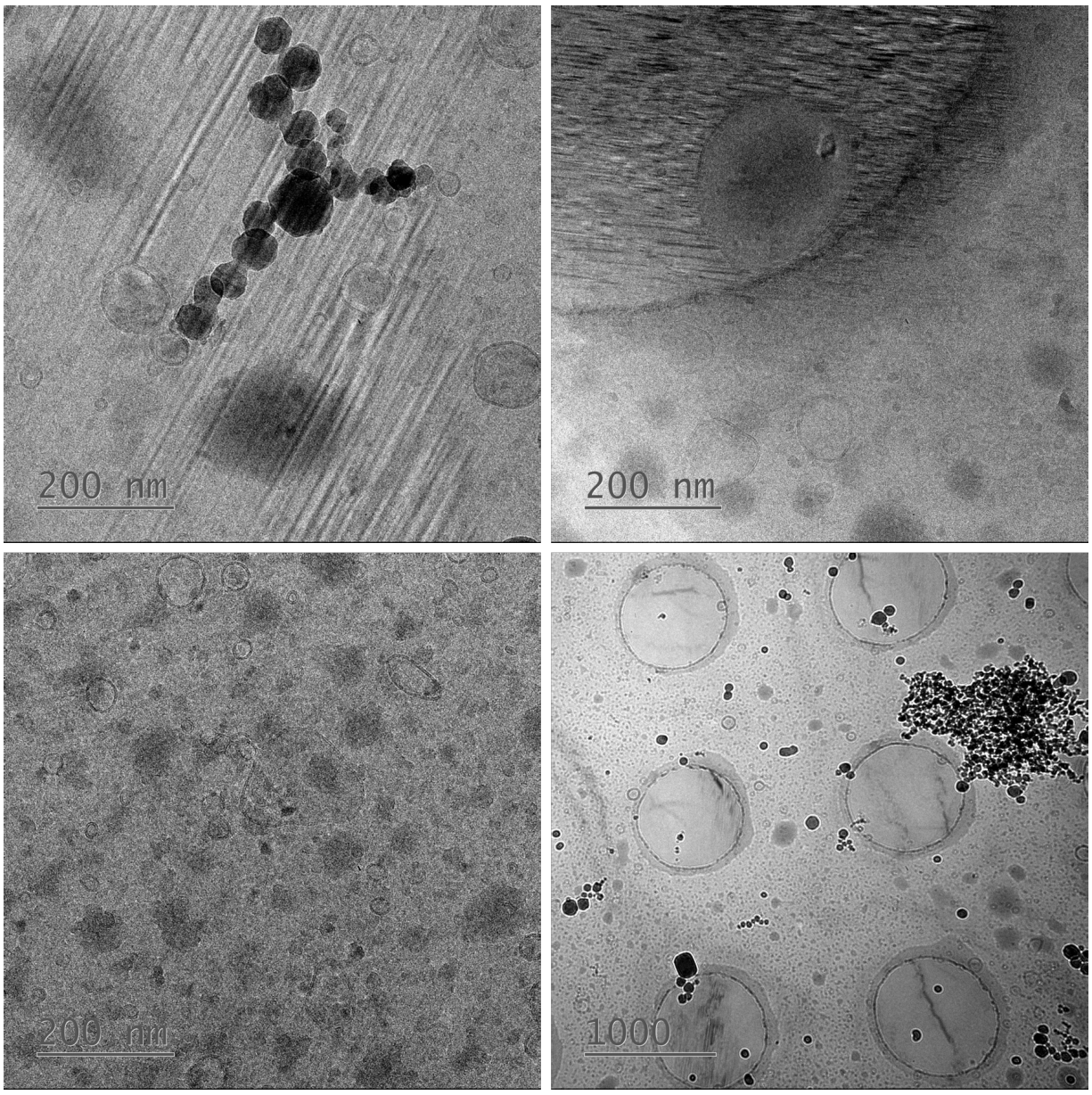

Figure D2: Cryo-TEM was carried out in order to have a better resolution of SAW-formed liposomes. Unilamellar vesicles were obtained after the SAW nebulisation using a silicon chip with 300 µm cavities. Using cryo-TEM it was possible to visualise the number of lamellae of the vesicles.

Appendix E - The University of Hong Kong

HS-DNA Purification Protocol

1. 40 mL, 3 M sodium acetate, adjusted pH 5.2
2. 24 mg HS-DNA for 48 eppendorf in 24 mL of ultrapure water.(DNA powder 4C)
3. 40 mL of ethanol are chilled at 4C for 30 min
4. Add 500 µl of HS-DNA and 50 µl of NaOAc
5. Vortex
6. Add 900 µl of ethanol
7. Vortex
8. Left tube in freezer (-20°C for at least 30 min)
9. Centrifuge the tubes at 13000 rpm at 4°C for 15 min
10. Remove and discard supernatant
11. Add 500 µl of 70% chilled ethanol in each tube and shake tube
12. = repeat 9, 10, 11 (at room T)
13. Centrifuge at 13,000 rpm at room T for 15 min
14. = repeat 10.
15. Air dry sample overnight (ensure tubes are fully dried)
16. Resuspend each sample in 200 µl of DIW/ or TAE buffer
17. Combine 6 tubes of sample into one. Take 1.2 mL sample in 1.5 mL centrifuge tube
18. Plate reader TAKE3 nucleic acid quantification
19. 2 µl sample and pure water
20. Run blank
21. Load sample and run

Agarose Gel electrophoresis Raw Images

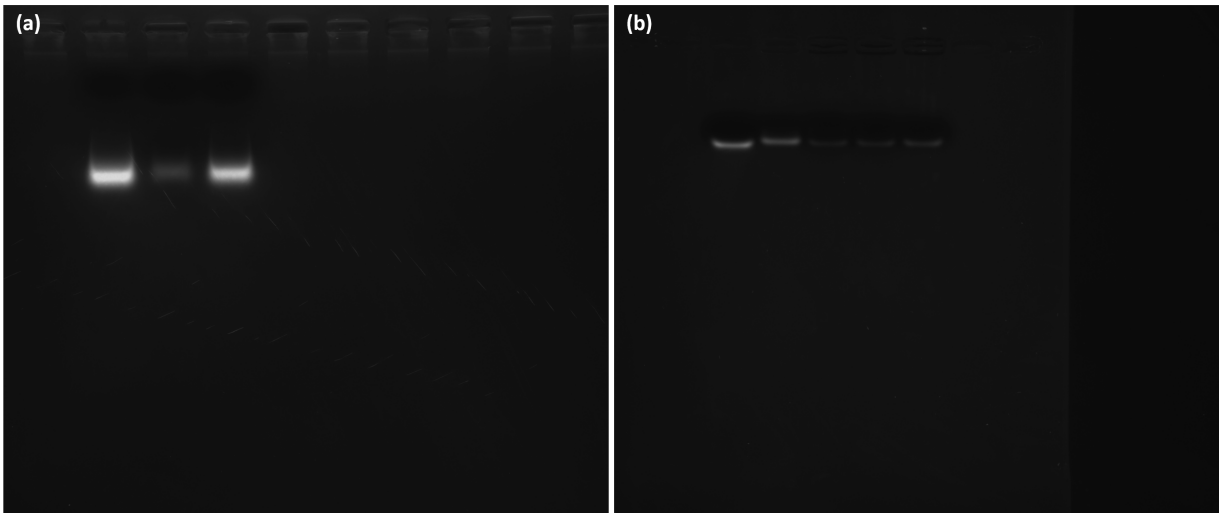

Figure E1: Agarose gel electrophoresis of : (a) Sample before and after nebulisation (See Chapter 6), (b) lipid:siRNA different ratios

MTT Citotoxiciy Assay: Only Lipids

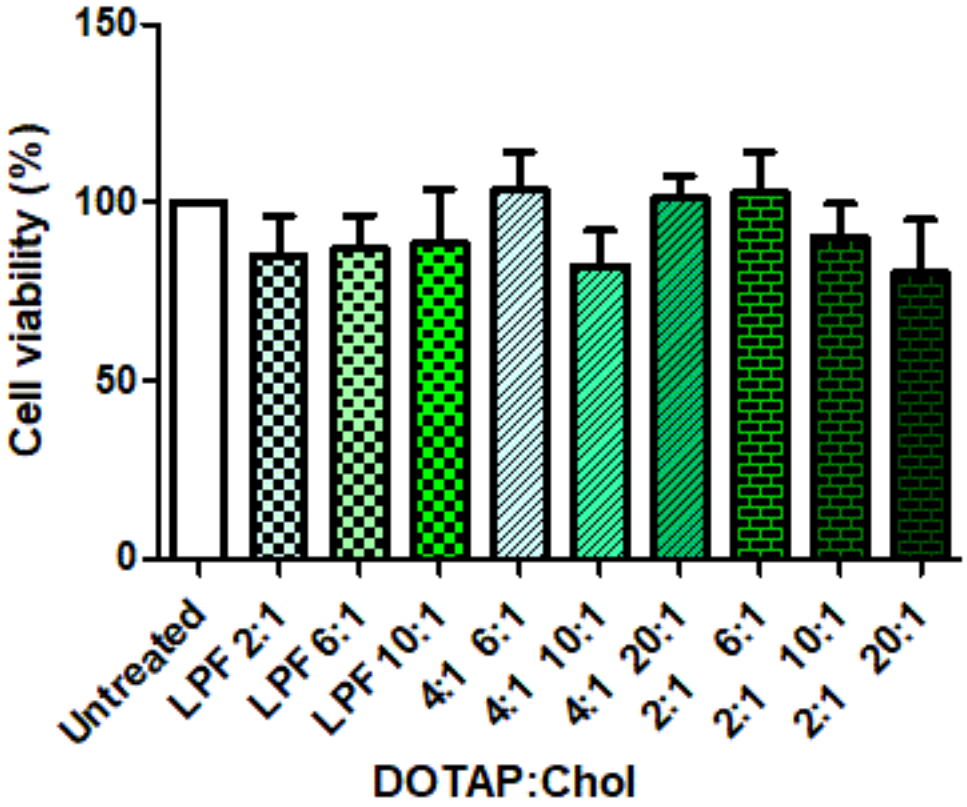

Figure E2: A549 cells were seeded in a 96-well plate. 24 h post-transfection, lipid vesicles made of DOTAP:Chol were added to cells in order to test their toxicity. After 4 h, MTT solution (0.8 mg/ml) was added to the cells. After 2 h, the formazan precipitate was dissolved in 100 µl isopropanol and the absorbance was measured at $\lambda = 595$ nm. The graph shows the mean of three measurements and the error bars represent the SD.

Western Blot Raw Images

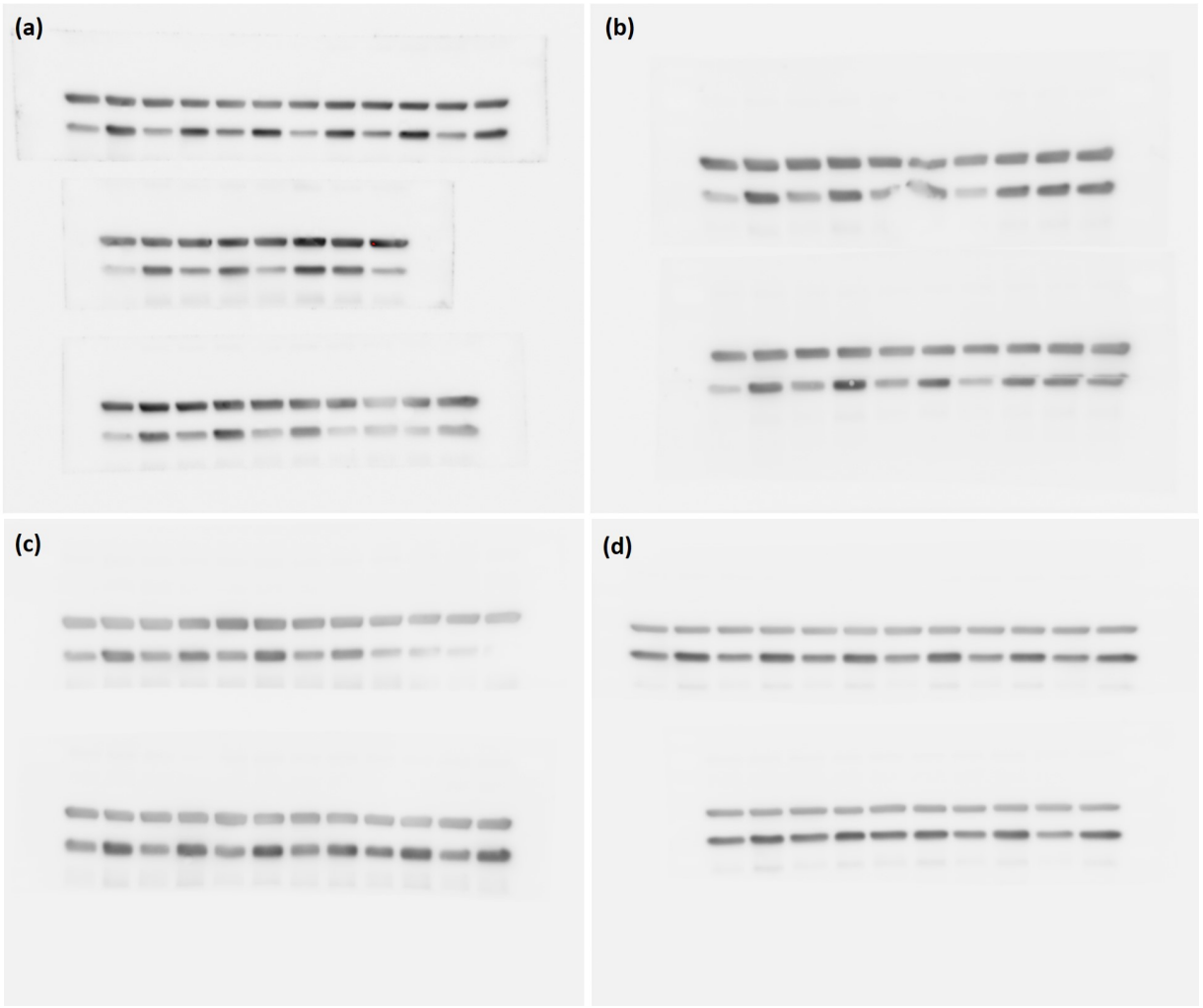

Figure E3: (a), (c), (d) Raw images of different ratio of lipid and GAPDH siRNA complex (values shown in Chapter 6). (b) Raw image of the samples after SAW nebulisation of GAPDH siRNA and MLVs mixture. Comparison between SAW-based and standard transfection method showed a 50% knockdown of the gene. Gel pictures in Chapter 6 were cropped from these raw pictures.

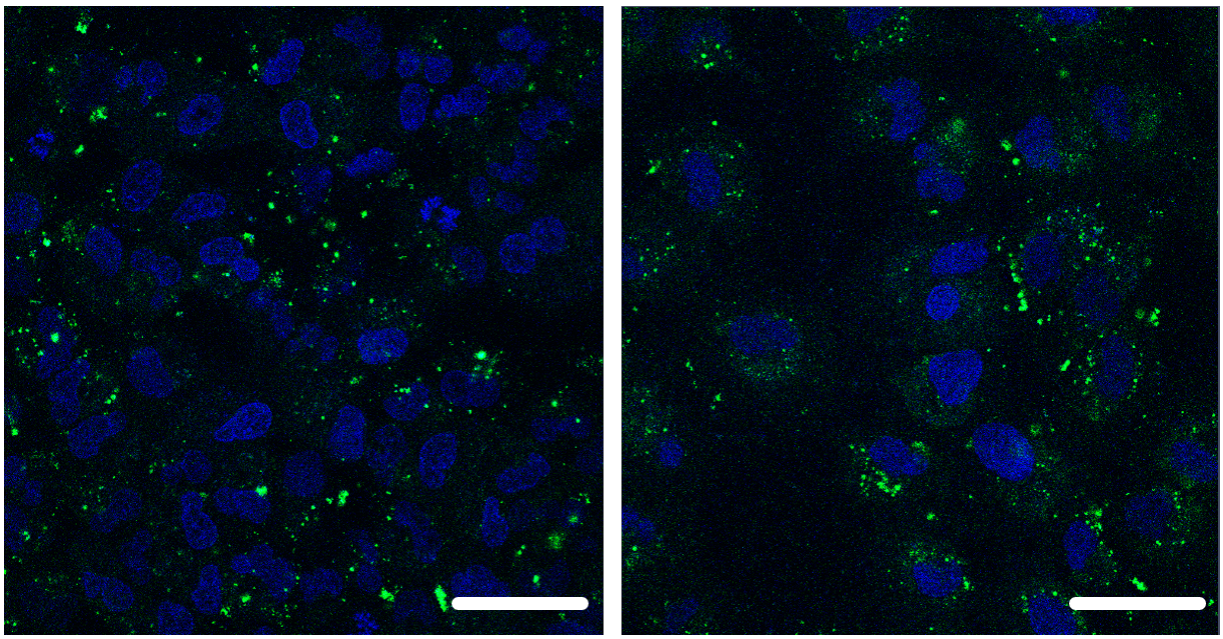

SAW Transfection

Figure E4: Confocal Images of A549 cells at 4 h post-transfection. Cell were transfected by SAW transfection. A lipid-siRNA mixture identical to that used for standard transfection was used, made of DOTAP-cholesterol (4:1) in 5% glucose, with a lipid-siRNA ratio of 6:1. Regarding SAW transfection, a total volume of 200 µl solution was nebulised for 2 min. siRNA (green) was labelled; the nuclei (blue) were stained with Hoechst. High cellular uptake resulted from SAW transfection, showing that lipid vesicles were formed during SAW nebulisation that were able to act as siRNA carriers. Scale bar 40 µm.